



5-2003

## **In-line measurement of additive and pigment loadings in molten polymer systems by fiber optic spectroscopy**

Erik C. Nielsen

Follow this and additional works at: [https://trace.tennessee.edu/utk\\_graddiss](https://trace.tennessee.edu/utk_graddiss)

---

### **Recommended Citation**

Nielsen, Erik C., "In-line measurement of additive and pigment loadings in molten polymer systems by fiber optic spectroscopy. " PhD diss., University of Tennessee, 2003.  
[https://trace.tennessee.edu/utk\\_graddiss/5164](https://trace.tennessee.edu/utk_graddiss/5164)

This Dissertation is brought to you for free and open access by the Graduate School at TRACE: Tennessee Research and Creative Exchange. It has been accepted for inclusion in Doctoral Dissertations by an authorized administrator of TRACE: Tennessee Research and Creative Exchange. For more information, please contact [trace@utk.edu](mailto:trace@utk.edu).

To the Graduate Council:

I am submitting herewith a dissertation written by Erik C. Nielsen entitled "In-line measurement of additive and pigment loadings in molten polymer systems by fiber optic spectroscopy." I have examined the final electronic copy of this dissertation for form and content and recommend that it be accepted in partial fulfillment of the requirements for the degree of Doctor of Philosophy, with a major in Chemical Engineering.

Marion Hansen, Major Professor

We have read this dissertation and recommend its acceptance:

Accepted for the Council:

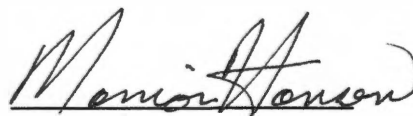
Carolyn R. Hodges

Vice Provost and Dean of the Graduate School

(Original signatures are on file with official student records.)

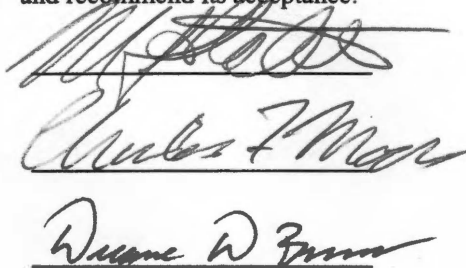
To the Graduate Council:

I am submitting herewith a dissertation written by Erik Christian Nielsen entitled "In-line Measurement of Additive and Pigment Loadings in Molten Polymer Systems by Fiber Optic Spectroscopy." I have examined the final paper copy of this dissertation for form and content and recommend that it be accepted in partial fulfillment of the requirements for the degree of Doctor of Philosophy, with a major in Chemical Engineering.

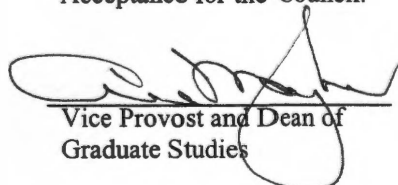


Marion Hansen, Major Professor

We have read this dissertation  
and recommend its acceptance:



Acceptance for the Council:



Vice Provost and Dean of  
Graduate Studies

Thesis  
2003b  
.N54

*[Faint, illegible handwritten text]*

*[Faint, illegible handwritten text]*

*[Faint, illegible handwritten text]*

**IN-LINE MEASUREMENT OF ADDITIVE AND PIGMENT LOADINGS IN MOLTEN  
POLYMER SYSTEMS BY FIBER OPTIC SPECTROSCOPY**

A Dissertation

Presented for

**Doctor of Philosophy**

Degree

**University of Tennessee, Knoxville**

**Erik C. Nielsen**

May 2003

## ACKNOWLEDGEMENTS

I would like to express my appreciation for the guidance and encouragement provided by my research advisor, Prof. Marion G. Hansen during the course of this endeavor. I have learned a considerable amount in the field of polymer processing during numerous discussions. I would like to also thank my other dissertation committee members. Prof. Tsewei Wang provided insight to both chemometrics and statistical analysis. Prof. Duane Bruns assisted in the process control aspects of this study. Professors H. Dudley Dewhirst and Michael Stahl who managed to relate the business world with traditional chemical engineering subjects.

I would also like to acknowledge the support of my colleagues at the University of Tennessee, Knoxville for countless hours of discussion for the preparation of this body of work. In particular, Bhushan Deshpande, Jigui Li, and Mani Dahmdhere provided instrument and computer time as well as moral support to allow this project to be completed.

I owe a debt of gratitude to my colleagues at the Clinton facility of Techmer PM. In particular, I would like to thank John Scott for technical support for the additives project, Brian West for support during the pigment project, Abe Mor for overall project guidance, Sy Commanday and John Greenep for advice in the color matching field.

Lastly, I owe my greatest debt to my family and friends without whose patience, love and encouragement, this work would never have been completed.

## ABSTRACT

The purpose of this project is the further development of in-line spectroscopic measurements for molten polymer systems. There are two main focuses: development of an online technique for the determination of concentration of ultraviolet stabilizers and antioxidant additives in polypropylene at orders of magnitude higher than those previously studied, and the development of a practical on-line color measurement technique. The additive project is an extension of the work completed by Dr. Marion Hansen and graduate students at the Measurement and Control Engineering Center located at the University of Tennessee, Knoxville. The color measurement technique is novel in its approach.

Quality control is one of the most important factors in plastics compounding. Compounding companies engage in the production of additive and color concentrates to be further diluted (or "let-down") by their customers. The end products are usually plastic pellets to be used in molding, film manufacturing, or fiber production. The end concentrations of additives and pigments in these end products are usually less than 1% and more often in the 100-200 ppm region. These low concentrations mandate the knowledge of the actual concentrations of pigments and additives contained in the concentrate.

Current quality control methods are predominantly off-line techniques. Most companies employ a method where a small sample is obtained from the production area and taken to a quality control analytic laboratory, where it is tested for additive concentration and/or color. Depending on the size and capacity of the facility, a large quantity of off specification material can be produced. Off-line techniques also have a given lag period before changes to the operating conditions can be made. The development of on-line measurement techniques not only provides a real time indication of the operating conditions, but is the fundamental element missing in the development of a real time, feed-back control system of the manufacturing process. The development of fiber optic cable allowed for traditional laboratory techniques to be applied in the production area of chemical processing facilities. The use of this type of cable has allowed the development of online techniques using near infrared (NIR), Fourier transform infrared (FTIR), ultraviolet (UV), and Raman spectroscopy.

The additives objective of this project is to look at several of the most commonly used UV-stabilizer and antioxidant additives in the polyolefin fiber industry. The objective is to determine a

spectroscopic technique or combination of techniques to determine the amount of these additives contained in the sample. Research will also be conducted to investigate the effect of additive loading on the rheological properties of the polymer. These results are correlated back to the spectroscopic data to develop an on-line measurement of the viscosity or melt index of the material. The sample additives are compounded with an unmodified polypropylene resin. Research is focused at determining the best spectroscopic technique utilizing NIR or UV methods as well as the optimal mathematical regression to provide the most accurate measurement of the additive concentration.

The color objectives of this project are to look at several commonly used pigments in the plastics industry and also develop a spectroscopic technique to determine the pigment concentration. The actual measurement of color is impossible. It is the final customer that determines whether the material is the correct color for their product. There are several methods to determine color numbers currently that aid color matching. These numbers, however, are determined using a flat plaque and the final pigment loading, not the actual concentrated material. If the pigment is treated like another additive, it is possible to correlate the specification material to the color standard. Once the correct pigment loading is established, online measurement will indicate off specification material. This project will also investigate the different spectroscopic techniques currently available to determine the optimum method for measuring concentration, as well as the proper mathematical regression technique for the most accurate concentration measurements.



## TABLE OF CONTENTS

CHAPTER	PAGE
1. INTRODUCTION	1
2. NIR SPECTROSCOPY	4
2.1 FUNDAMENTALS OF NIR SPECTROSCOPY	4
2.2 BAND ASSIGNMENT IN NIR	12
2.3 APPLICATIONS RELATED TO POLYMER PROCESSING	13
3. UV SPECTROSCOPY	18
3.1 FUNDAMENTALS OF UV SPECTROSCOPY	18
3.2 BAND ASSIGNMENT IN UV SPECTROSCOPY	23
3.3 APPLICATIONS RELATED TO POLYMER PROCESSING	26
4. RAMAN SPECTROSCOPY	29
4.1 FUNDAMENTALS OF RAMAN SPECTROSCOPY	29
4.2 BAND ASSIGNMENT IN RAMAN SPECTROSCOPY	32
4.3 APPLICATIONS RELATED TO POLYMER PROCESSING	33
5. COLOR TECHNOLOGY AND ANALYSIS TECHNIQUES	37
5.1 PRINCIPLES OF COLOR TECHNOLOGY	37
5.2 COLORANTS	46
5.3 COLOR AND COLOR DIFFERENCE MEASUREMENT	47
5.4 QUANTITATIVE DATA ANALYSIS	49
5.4.1 Data Analysis	49
5.4.2 Preprocessing	51
5.4.3 Model Estimation	54
5.4.4 Model Validation	62
5.4.5 Prediction	64
5.4.6 Prediction Validation	64
5.4.7 Summary	65

6.	RESEARCH OBJECTIVES	66
6.1	PROBLEM STATEMENT	66
6.1.1	Estimation of Additive Concentrations in Polypropylene During Extrusion	67
6.1.2	Estimation of Pigment Concentrations in Polypropylene During Extrusion	68
6.1.3	Monitoring the Effects of Pigment Loadings on Rheological Properties of Polypropylene During Extrusion	69
6.1.4	Feasibility of Simultaneous In-Line Monitoring of Pigment and Additive Concentrations in Polypropylene During Extrusion	70
7.	EXPERIMENTAL SETUP	71
8.	ESTIMATION OF ADDITIVE CONTENT IN POLYMER MELTS	85
8.1	THEORY	85
8.2	EXPERIMENTAL	88
8.3	SPECTROSCOPIC RESULTS	95
8.3.1	Preliminary FTIR Studies	95
8.3.2	UV Spectroscopy Studies	100
8.3.3	NIR Spectroscopy Studies	135
8.4	EXPERIMENTAL LIMITATIONS	164
8.5	CONCLUSIONS	168
9.	ESTIMATION OF PIGMENT CONTENT IN POLYMER MELTS	172
9.1	THEORY	172
9.2	EXPERIMENTAL	173
9.3	SPECTROSCOPIC RESULTS	175
9.4	EXPERIMENTAL LIMITATIONS	212
9.5	CONCLUSIONS	212
10.	ESTIMATION OF PIGMENT DISPERSION IN POLYMER MELTS	214
10.1	THEORY	214
10.2	EXPERIMENTAL	219
10.3	MICROSCOPIC AND SPECTROSCOPIC RESULTS	221

10.4 EXPERIMENTAL LIMITATIONS	234
10.5 CONCLUSIONS	237
11. COMPLEX VISCOSITY MEASUREMENTS OF POLYMER MELTS	239
11.1 THEORY	239
11.2 EXPERIMENTAL	242
11.3 RESULTS AND DISCUSSION	243
11.4 EXPERIMENTAL LIMITATIONS	262
11.5 CONCLUSIONS	269
12. CONCLUSIONS AND FUTURE WORK	270
REFERENCES	276
VITA	285

## LIST OF TABLES

<b>Table</b>		<b>Page</b>
2.1	Location of the infrared region in the electromagnetic spectrum	5
2.2	Spectroscopic characteristics and corresponding regions	6
2.3	Brief overview of NIR absorption frequency locations	14
3.1	Electronic band assignment for the UV region for representative organic bonds	25
4.1	Brief overview of Raman scattering band locations	34
8.1	Antioxidants used in polypropylene study	89
8.2	Ultraviolet stabilizers used in polypropylene study	90
8.3	Formulations utilized in initial online UV and NIR spectroscopy	105
8.4	Optimized PLS Model Summary for AO's UV Data	133
8.5	Optimized PLS Error Summary for AO's UV Data	133
8.6	Optimized PLS Model Summary for UV's UV Data	134
8.7	Optimized PLS Error Summary for UV's UV Data	134
8.8	Comparisons of Spectroscopic Effectiveness	142
8.9	Error Summary for AO-2 PLS	151
8.10	Optimized PLS Model Summary for AO's NIR Data	152
8.11	Optimized PLS Error Summary for AO's NIR Data	152
8.12	Optimized PLS Model Summary for UV's NIR Data	162
8.13	Optimized PLS Error Summary for UV's NIR Data	162
8.14	Differences in SEC based on wavelength range for UV-6 in polyethylene	163
9.1	Diazo condensation and phthalocyanine pigments used in polypropylene	174
9.2	Formulations utilized in initial online UV and NIR spectroscopy	176
9.3	PLS models for various NIR regions for 1-5% C-1 in polypropylene	187
9.4	PLS models for various NIR regions for 1-5% C-5 in polypropylene	203
9.5	PLS model for strength values for 1-5% C-5 in polypropylene	211
11.1	Overall variance explained by PLS analysis of complex viscosity matrix	265

11.2	Melt index values for AO-2 in polypropylene	267
11.3	PLS regression model information for AO-2 melt index	267

## LIST OF FIGURES

<b>Figure</b>		<b>Page</b>
2.1	Potential energy diagram of the vibrational modes of a harmonic oscillator and an anharmonic oscillator	10
5.1	Spectral power distributions of blackbodies with color temperatures of 2854K and 6500K	39
5.2	Dimensions of the surface-color-perception solid for the Munsell System	42
5.3	The tristimulus values of the equal energy spectrum colors	44
5.4	Spectral curves required to calculate CIE tristimulus values $X$ , $Y$ , and $Z$	45
7.1	Schematic of the experimental setup of in-line FTNIR spectroscopy of molten polypropylene	72
7.2	Detailed schematic of a variable path length flow cell	73
7.3	Schematic representation design of Sensotron transmission fiber optic probe	74
7.4	Composite design of Sensotron transmission fiber optic probes	75
7.5	Schematic of the in-line monitoring of molten polymers using UV spectroscopy	77
7.6	Schematic of the in-line monitoring of molten polymers using UV spectroscopy with a bifurcated fiberoptic cable	78
7.7	Composite schematic of the University of Tennessee, Knoxville designed UV probe	79
7.8	Schematic of the in-line monitoring of molten polymers using Raman spectroscopy	81
7.9	Schematic of industrial flow cell for 1" Killion operation	82
7.10	Schematic representation of experimental setup for rheological measurements using a Rheometrics Dynamic Stress Rheometer	84
8.1	Chemical structures of antioxidants AO1- AO3 used in this study	91
8.2	Chemical structures of antioxidants AO4 - AO5 used in this study	92
8.3	Chemical structures of ultraviolet stabilizers UV1 - UV5 used in this study	93
8.4	Chemical structures of ultraviolet stabilizers UV6 - UV7 used in this study	94
8.5	Relative absorbance FTIR spectra for sample UV-1	96
8.6	Detailed FTIR spectra for sample UV-1 in the 1075 to 1125 $\text{cm}^{-1}$ region	97
8.7	Relative absorbance FTIR spectra for sample AO-2	98
8.8	Detailed FTIR spectra for sample AO-2 in the 480 to 515 $\text{cm}^{-1}$ region	99

8.9	Optical efficiency of UV fiber optic cables	101
8.10	Optical efficiency of on line UV spectrometer measured on air samples	102
8.11	UV absorbance spectra of polypropylene in the 200 to 800 nm range	104
8.12	Detailed UV spectra for sample AO-1 in the 200 to 800 nm region	108
8.13	Detailed UV spectra for sample AO-2 in the 380 to 800 nm region	109
8.14	Detailed UV spectra for sample AO-3 in the 360 to 800 nm region	110
8.15	Detailed UV spectra for sample AO-4 in the 400 to 790 nm region	111
8.16	Detailed UV spectra for sample AO-5 in the 405 to 800 nm region	112
8.17	Detailed UV spectra for sample UV-1 in the 420 to 800 nm region	113
8.18	Detailed UV spectra for sample UV-2 in the 390 to 800 nm region	114
8.19	Detailed UV spectra for sample UV-3 in the 200 to 800 nm region	115
8.20	Detailed UV spectra for sample UV-4 in the 300 to 800 nm region	116
8.21	Detailed UV spectra for sample UV-5 in the 200 to 800 nm region	117
8.22	Detailed UV spectra for sample UV-6 in the 200 to 800 nm region	119
8.23	Detailed UV spectra for sample UV-7 in the 200 to 800 nm region	120
8.24	Flow chart for prediction of additive concentrations	121
8.25	UV absorbance spectra of AO3 (1 <sup>st</sup> derivative)	124
8.26	SEV values for AO3 PLS model based on 1 <sup>st</sup> derivative UV data	125
8.27	Loadings plot for AO3 PLS model	126
8.28	Predictive versus measured plot for AO3 PLS model	127
8.29	Visible absorbance spectra of UV5 (1 <sup>st</sup> derivative)	129
8.30	Scores plot for UV5 PLS 2 factor model	130
8.31	Regression vector plot for UV5 PLS model	131
8.32	Optical efficiency of NIR fiber optic cables (Transmission versus Wavelength)	136
8.33	Optical efficiency of NIR probe (Transmission versus Wavelength)	138
8.34	Optical efficiency of NIR system (Transmission versus Wavelength)	139
8.35	NIR Spectra of Polypropylene (Absorbance versus Wavelength)	140

8.36	NIR absorbance spectra of AO2 (1 <sup>st</sup> derivative)	143
8.37	SEV values for AO2 PLS model	144
8.38	Scores plot for AO2 PLS model	145
8.39	Loadings plot for AO2 1 factor PLS model	146
8.40	Predictive versus measured plot for AO2 PLS model	147
8.41	Regression vector plot for AO2 PLS model	149
8.42	Reconstructed absorbance data from AO2 PLS model (1 <sup>st</sup> derivative)	150
8.43	NIR absorbance spectra of UV2 (1 <sup>st</sup> derivative)	154
8.44	SEV values for UV2 PLS model	155
8.45	Scores plot for UV2 PLS model	156
8.46	Loadings plot for UV2 PLS model	157
8.47	Predictive versus measured plot for UV2 PLS model	158
8.48	Regression vector plot for UV2 PLS model	159
8.49	Reconstructed absorbance data from UV2 PLS model (1 <sup>st</sup> derivative)	160
8.50	Real time prediction for UV-1 using on-line NIR spectroscopy (6, 18, 24, and 12%)	165
8.51	Real time prediction for UV-2 using on-line NIR spectroscopy (12.5, 20, and 17.5%)	166
8.52	Real time prediction for AO-2 using on-line NIR spectroscopy (10, 8, and 16%)	167
9.1	Chemical structures of pigments C-1 - C3 used in this study	177
9.2	Chemical structures of pigments C-4 - C-5 used in this study	178
9.3	FTIR spectra for sample C-1	179
9.4	Detailed FTIR spectra for sample C-1 in the 480 to 775 cm <sup>-1</sup> region	180
9.5	Detailed UV absorbance spectra for sample C-1 in the 200 to 800 nm region	182
9.6	Detailed UV absorbance spectra for sample C-2 in the 200 to 800 nm region	183
9.7	Detailed UV absorbance spectra for sample C-3 in the 200 to 800 nm region	184
9.8	Detailed UV absorbance spectra for sample C-4 in the 200 to 800 nm region	185
9.9	Detailed UV absorbance spectra for sample C-5 in the 200 to 800 nm region	186
9.10	NIR absorbance spectra for sample C-1 in the 1200 to 2200 nm region	188



9.11	NIR absorbance spectra for sample C-2 in the 1200 to 2200 nm region	189
9.12	NIR absorbance spectra for sample C-3 in the 1200 to 2200 nm region	190
9.13	NIR absorbance spectra for sample C-4 in the 1200 to 2200 nm region	191
9.14	NIR absorbance spectra for sample C-5 in the 1200 to 2200 nm region	192
9.15	First derivative absorbance data for C-1 NIR spectra for 70-112 nm for 1-5%	193
9.16	First derivative absorbance data for C-1 NIR spectra for 1660-1900 nm for 1, 2 and 5%	194
9.17	Scores plot for C-1 PLS model based on 1660 to 1900 nm for 1-5%	195
9.18	Loadings plot for C-1 PLS model based on 1660 to 1900 nm for 1-5%	196
9.19	Scores plot for C-1 PLS model based on 1340 to 1424 nm for 1-5%	197
9.20	Loadings plot for C-1 PLS model based on 1340 to 1424 nm for 1-5%	198
9.21	Predicted versus measured plot for C-1 PLS mode based on 1660 to 1900 nm for 1-5%	199
9.22	Regression vector plot for C-1 PLS model mode based on 1660 to 1900 nm for 1-5%	200
9.23	Reconstructed absorbance data from C-1 PLS model based on 1660 to 1900 nm for 1, 2, and 5%	201
9.24	First derivative NIR absorbance spectra for 1, 2, and 5% C-5 in polypropylene 1660 to 1720 nm	204
9.25	SEV values for 1-5% C-5 in polypropylene 1660 to 1720 nm	205
9.26	Scores plot for PLS model for 1-5% C-5 in polypropylene 1660 to 1720 nm	206
9.27	Loadings plot for PLS model for 1-5% C-5 in polypropylene 1660 to 1720 nm	207
9.28	Predicted versus measured plot for PLS model for 1-5% C-5 in polypropylene 1660 to 1720 nm	208
9.29	Regression vector plot for PLS model for 1-5% C-5 in polypropylene 1660 to 1720 nm	209
9.30	Reconstructed absorbance data from PLS model for 1, 2, and 5% C-5 in polypropylene 1660 to 1720 nm	210
10.1	Schematic of confocal laser scanning microscopy principal	217
10.2	Schematic of data generation for confocal laser scanning microscopy	218
10.3	Physical layout of confocal laser scanning microscopy used in this study	220
10.4	FTIR spectra of blown film of C-3 in polyethylene, background film and agglomerate	222

10.5	Detailed FTIR spectra of blown film of C-3 in polyethylene, background film and agglomerate for the 2250 to 2500 $\text{cm}^{-1}$ region	223
10.6	CLSM micrograph of C-2 at 0.15% loading in polypropylene	224
10.7	CLSM micrograph of C-2 at 0.3% loading in polypropylene	225
10.8	CLSM micrograph of C-2 at 1.2% loading in polypropylene	226
10.9	CLSM micrograph of C-2 at 3.0% loading in polypropylene	227
10.10	Blown film sample of two step dispersion process	229
10.11	Blown film sample of pellet melter dispersion process	230
10.12	Blown film sample of Brabender dispersion process	231
10.13	CLSM micrograph of cromo yellow (C-1, dry color, single screw extrusion)	232
10.14	CLSM micrograph of diazo condensate yellow (C-5, two step dispersion)	233
10.15	CLSM micrograph of cromo red (C-2, intensive mixing, twin screw extrusion)	235
10.16	CLSM micrograph of phthalo blue red shade (C-3, dry color, twin screw extrusion)	236
11.1	Schematic of an ASTM standardized melt index (MI) measurement apparatus	240
11.2	Complex viscosity measurements of UV-4 in PP at 230 °C and strain rate of 2500 $\text{dyne/cm}^2$	244
11.3	Complex viscosity measurements of UV 7 in PP at 230 °C and strain rate of 2500 $\text{dyne/cm}^2$ .	245
11.4	Complex viscosity measurements of UV 1 in PP at 230 °C and strain rate of 2500 $\text{dyne/cm}^2$	246
11.5	Complex viscosity measurements of UV 2 in PP at 230 °C and strain rate of 2500 $\text{dyne/cm}^2$ .	247
11.6	Complex viscosity measurements of UV 6 in PP at 230 °C and strain rate of 2500 $\text{dyne/cm}^2$ .	248
11.7	Complex viscosity measurements of UV 3 in PP at 230 °C and strain rate of 2500 $\text{dyne/cm}^2$ .	249
11.8	Complex viscosity measurements of UV 5 in PP at 230 °C and strain rate of 2500 $\text{dyne/cm}^2$ .	250
11.9	Complex viscosity measurements of AO 4 in PP at 230 °C and strain rate of 2500 $\text{dyne/cm}^2$ .	252
11.10	Complex viscosity measurements of AO 5 in PP at 230 °C and strain rate of 2500 $\text{dyne/cm}^2$ .	253

11.11	Complex viscosity measurements of AO 1 in PP at 230 °C and strain rate of 2500 dyne/cm <sup>2</sup>	254
11.12	Complex viscosity measurements of AO 3 in PP at 230 °C and strain rate of 2500 dyne/cm <sup>2</sup> .	255
11.13	Complex viscosity measurements of AO 2 in PP at 230 °C and strain rate of 2500 dyne/cm <sup>2</sup>	256
11.14	Complex viscosity measurements of C-1 in PP at 230 °C and strain rate of 2500 dyne/cm <sup>2</sup> .	257
11.15	Complex viscosity measurements of C-5 in PP at 230 °C and strain rate of 2500 dyne/cm <sup>2</sup> .	258
11.16	Complex viscosity measurements of C-2 in PP at 230 °C and strain rate of 2500 dyne/cm <sup>2</sup> .	259
11.17	Complex viscosity measurements of C-3 in PP at 230 °C and strain rate of 2500 dyne/cm <sup>2</sup>	260
11.18	Complex viscosity measurements of C-4 in PP at 230 °C and strain rate of 2500 dyne/cm <sup>2</sup> .	261
11.19	Scores plot for PLS regression of AO-2 complex viscosity at 0.1 rad/s	263
11.20	Loadings plot for PLS regression of AO-2 complex viscosity at 0.1 rad/s	264
11.21	SEV values for PLS model	266
11.22	Real time prediction of melt index of AO-2 using on-line spectroscopy	268

## NOMENCLATURE

Symbol	Abbreviation	Description
$\alpha$		Matrix of regression coefficients, obtained from PLS regression
$\beta$		Regression coefficient vectors, obtained from PLS regression
$\Delta E_m$		Energy change, [J]
$\Delta v$		Change in vibrational quantum number
$\Delta j$		Change in rotational quantum number
$\phi$		Phase angle
$\eta_0$		Zero shear viscosity, [Pa.s]
$ \eta^*(\omega) $		Complex viscosity, expressed as a function of $\omega$ , [Pa.s]
$\mu$		Reduced mass of two atoms
$\nu$		Frequency of radiation
$\Sigma$		Diagonal matrix with singular values as diagonal elements
$\sigma$		Singular value
$\omega$		Angular frequency, [rad/s]
<b>A</b>		Absorbance
<b>a</b>		Absorbivity of a chemical species, in Beer-Lambert's law
<i>a</i>		CIE Lab red/green factor
<i>a</i>		Berry-Fox exponent
<b>B</b>		Matrix of regression coefficients, obtained from PLS regression
<i>b</i>		CIE Lab yellow/blue factor
<b>C</b>		Concentration matrix
<b>C*</b>		CIE Lab hue
<i>c</i>		Concentration in Beer-Lambert's law
$d_{ab}$		Euclidean Distance between any two samples
$d_{max}$		Maximum inter-sample distance within a given cluster

<b>E</b>	Residuals matrix, obtained from PCA, PCR, or PLS analysis
$E_p$	Energy of a photon, [J]
<b>EVA</b>	Ethylene-vinyl acetate copolymer
<b>F</b>	Residuals matrix, obtained from PLS analysis
$f$	Effective rank of X
$G'(\omega)$	Storage modulus, expressed as a function of $\omega$ , [Pa]
$G''(\omega)$	Loss modulus, expressed as a function of $\omega$ , [Pa]
$h$	Plank's constant
$h^o$	CIELab chroma
<b>I</b>	Intensity of radiation
$I_o$	Intensity of radiation incident on sample
$j$	Index
<b>K</b>	Absorbance matrix of pure analytes
<b>K</b>	Number of nearest neighbors in KNN validation
$k$	1. Force constant of a harmonic oscillator 2. Index
$L$	CIELab lightness factor
$l$	Optical path length in Beer-Lambert's law
<b>LAS</b>	Leave-a-sample cross-validation approach
<b>LDL</b>	Lower detection limit
<b>MD</b>	Mahalanobis distance
<b>MI</b>	Melt Flow Index, [g/10 min]
<b>MIR</b>	Mid-infrared
$\overline{M}_w$	Weight average molecular weight of the polymer [g/mol]
<b>MWD</b>	Molecular weight distribution of the polymer
$m$	1. Mass of a molecule 2. Index, number of rows in a matrix

NC	Number of samples in a calibration set
NP	Number of samples in a prediction set
NIR	1. Near-infrared 2. Used as a subscript to denote results from regression with NIR data
NV	Number of samples in a validation set
$n$	1. Discrete energy level quantum level 2. Index, number of columns in a matrix
$p$	Index
PCA	1. Principal component analysis 2. Used as a subscript to denote results from PCA analysis
PCR	Principal component regression
PE	Polyethylene
PLS	Partial least squares
PLS-1	PLS regression of one dependent variable
PLS-2	PLS regression of multiple Y data
PP	Polypropylene
PRESS	Predicted residual sum of squares
$r$	Correlation coefficient
reg	Used as a subscript to denote a regenerated matrix, after PCA analysis
SEC	Standard error of calibration
SEP	Standard error of prediction
SVD	Singular value decomposition of a matrix
$s$	Similarity distance
T	Scores matrix
T	1. Transmittance 2. Used as a superscript
$t$	Score vector, column of matrix T
U	Scores matrix or left singular vectors, obtained from SVD of a matrix
$U_q$	Potential energy

UDL	Upper detection limit
UV	Ultraviolet
$u$	Vector of matrix U
V	Right singular vectors, obtained from SVD
VA	Vinyl acetate comonomer, in EVA copolymer
W	Matrix containing loading weights, obtained from PLS regression
X	NIR absorbance data matrix
$X$	CIE tristimulus value
$\bar{x}$	CIE standard observer tristimulus value
$X_e$	Anharmonicity constant
$x$	Displacement for a Hookean spring
$x$	Independent variable vector
Y	Rheology data matrix
$Y$	CIE tristimulus value
$\bar{y}$	CIE standard observer tristimulus value
$Y_e$	Anharmonicity constant
$y$	Vector, column of Y
Z	CIE tristimulus value
$\bar{z}$	CIE standard observer tristimulus value
$\wedge$	Symbol used to denote fitted values of variables, obtained from regression

## CHAPTER 1

### INTRODUCTION

Although polymeric materials have only been introduced in the last one hundred years, their usefulness to mankind is remarkable. Polymers have appeared in numerous consumer and industrial applications. Everything from common items such as plastic bottles to precision components destined for space applications have come about from the use of these materials. These applications arise from polymers unique properties such as flexibility, economy, lightweight and others [1]. Due to the wide range of applications that these materials are used in, customers have a variety of individual requirements that a manufacturer must be able to meet.

Since the advent of polymers being used for commercial applications, the use of additives and colorants has been important. Adding color to a material has been a practice since the beginning of recorded history. Dyes and pigments have been included in fabrics, paper, inks, paints, and a wide variety of other items for thousands of years. It is only natural that their use in plastics has evolved. Along the same lines, additives have also been compounded with resins to give the final product the desired characteristics. These additives can usually be characterized into such groups as anti-fog, antioxidants, anti-stats, clarifying, fillers, lubricants, and UV stabilizing agents as well as countless other specialty chemicals.

There are several current useful analytic techniques for determining the properties of polymers. Some spectroscopic techniques include: infrared (IR), ultraviolet (UV), and Raman as well as nuclear magnetic resonance (NMR) for the determination of structural, composition and crystallinity properties. X-ray diffraction is used for the determination of crystallinity and thermal analysis for the determination of melting and glass transition temperatures. Rheological measurements are made for determining mechanical properties, and gel permeation chromatography is used to determine average molecular weight and distribution. Each of these techniques provides useful information related to the properties of the polymer, but they are off line techniques that are time consuming in measurements and sample preparation time. For the average polymer manufacturing facility, off specification material production can be enormous due to this delay time. Some of the properties that are determined using these techniques are crucial to the



production of high quality material. In the standard polymer unit operations such as extrusion, blow molding, fiber spinning, and injection molding, analytic techniques with no sample preparation time and minimal sampling time, would greatly reduce waste and off specification material resulting in a greater efficiency of the facility. If properly implemented, the results of these analyses can be used as measurements in a robust feedback control system for the unit operation.

In recent years, the use of fiber-optic near infrared (NIR) spectroscopy has been pursued in academia and industry as an alternative to the more time consuming destructive analytical techniques. Its development was chosen because it allows for a rapid, non-destructive analysis in real time. The preparation of samples for this technique requires little or no effort making the procedure simple. Combining the use of fiber optics and rugged mathematical analysis, NIR spectroscopy has succeeded as a useful technique in remote process monitoring and control for traditional chemical and polymer processes [2-7].

NIR spectroscopy's success is the result of the speed at which information about the system can be obtained. Several research investigations have been completed. They include the development of fiber optics for the study of polymer melts [1, 8, 9], composition measurements [10, 11], and chemical property measurements [12]. The focus of these studies has been on measurements of the chemical composition, and properties related to the composition, such as density and viscosity. Some of the work has been done at high and low additive concentrations, but none have looked at pigment loading. The underlying theme of this work is related to the fiber industry and the effect of additives and pigments on polypropylene. The aim of this dissertation project is to develop a practical and efficient instrumental technique for measurement of additive and pigment concentration for polypropylene compounding suitable for the manufacturing environment. Since no one technique is perfect for all polymer systems, NIR, UV and Raman spectroscopy will be investigated for all sample sets.

The layout of this work is as follows. Chapter 2 will provide an overview of NIR spectroscopy, investigating both the theory and practical applications relating to spectral information obtained by this technique. Chapters 3 and 4 will follow this layout as well, but focus on UV and Raman spectroscopy, respectively. Chapter 5 will provide an overview of industrial color technology at the development of

pigment usage as well as current measurement techniques as related to the polymer industry, and review the mathematical relationships suitable for quantitative analysis and regression techniques. The specific objectives of the current research are outlined in Chapter 6. A detailed description of the experimental system used for this project's work is presented in Chapter 7. Chapter 8 will address the objectives related to measuring additive content in polymer systems. Chapters 9 and 10 will address the issue of pigment loading and dispersion respectively in polymer systems. Chapter 11 will focus on the issue of pigment and additive effects on complex viscosity. Conclusions from the above studies as well as proposed future work will be discussed in Chapter 12.

## CHAPTER 2

### NIR SPECTROSCOPY

#### INTRODUCTION

The electromagnetic spectrum is made up of vibrations ranging from several meters (radio waves) to less than 0.01 nm (gamma rays) in wavelength. These vibrations are the result of several types of different phenomena occurring simultaneously. Some of these phenomena include spin orientations in a magnetic field, molecular rotations, molecular vibrations, electronic transitions, nuclear transitions, *et cetera* can occur. The occurrence of a vibrational mode in a particular wavelength region of the electromagnetic spectrum is dependent on the type of molecular structure. A schematic of the electromagnetic spectrum is given in Table 2.1 [13]. This figure highlights the locations of the NIR wavelength region of 700-2,500 nm relative to the mid-infrared region of 2,500-25,000 nm. Spectral signatures in the IR and NIR can be attributed to molecular vibrations. Table 2.2 describes spectroscopic characteristics and corresponding regions [14, 15]. Infrared spectroscopy is usually divided into three sections, near, mid, and far, depending on wavelength. While the information obtained from these regions corresponds to different molecular information, the physics behind the principles are similar.

#### 2.1 FUNDAMENTALS OF NIR SPECTRA

Organic matter is composed of atoms that combine together using covalent and electrovalent bonds to form molecules. The nature of these bonds creates the situation where the bond will vibrate with a characteristic frequency. Without any external excitation, this bond will be in its normal mode of vibration, or its ground state. Normal or fundamental mode frequencies will typically correspond to wavelengths in the infrared region of the electromagnetic spectrum. When these bonds are excited by an external source, such as radiation, the potential exists for an energy change to occur. This energy change will occur if the bond is capable of accepting the energy based on quantum mechanics. The energy of a photon (unit of radiation,  $E_p$ ) is related to the wavelength that it is emitted by:

$$E_p = h\nu \tag{2.1}$$

where:

$h$  = Planck's constant

Table 2.1 Location of the infrared (IR) region in the electromagnetic spectrum

<b>Spectrum of Electromagnetic Radiation</b>				
<b>Region</b>	<b>Wavelength (Angstroms)</b>	<b>Wavelength (centimeters)</b>	<b>Frequency (Hz)</b>	<b>Energy (eV)</b>
Radio	> 10 <sup>9</sup>	> 10	< 3 × 10 <sup>9</sup>	< 10 <sup>-5</sup>
Microwave	10 <sup>9</sup> - 10 <sup>6</sup>	10 - 0.01	3 × 10 <sup>9</sup> - 3 × 10 <sup>12</sup>	10 <sup>-5</sup> - 0.01
Infrared	10 <sup>6</sup> - 7000	0.01 - 7 × 10 <sup>-5</sup>	3 × 10 <sup>12</sup> - 4.3 × 10 <sup>14</sup>	0.01 - 2
Visible	7000 - 4000	7 × 10 <sup>-5</sup> - 4 × 10 <sup>-5</sup>	4.3 × 10 <sup>14</sup> - 7.5 × 10 <sup>14</sup>	36925
Ultraviolet	4000 - 10	4 × 10 <sup>-5</sup> - 10 <sup>-7</sup>	7.5 × 10 <sup>14</sup> - 3 × 10 <sup>17</sup>	3 - 10 <sup>3</sup>
X-Rays	10 - 0.1	10 <sup>-7</sup> - 10 <sup>-9</sup>	3 × 10 <sup>17</sup> - 3 × 10 <sup>19</sup>	10 <sup>3</sup> - 10 <sup>5</sup>
Gamma Rays	< 0.1	< 10 <sup>-9</sup>	> 3 × 10 <sup>19</sup>	> 10 <sup>5</sup>

Table 2.2 Spectroscopic characteristics and corresponding regions [14, 15]

Region	Wavelength (nm)	Characteristic Measured
Ultraviolet (UV)	190-360	Transitions of delocalized Pi electrons
Visible	360-780	Electronic transitions, color measurements
Near Infrared (NIR)	480-2,500	Overtone and combinations bands of fundamental molecular vibrations
Middle Infrared (MIR)	2,500-40,000	Fundamental molecular vibration: stretching, bending, wagging and scissoring
Far Infrared (FIR)	$4 \times 10^4$ - $10^6$	Molecular rotation

$\nu$  = frequency of radiation

The energy of a photon is absorbed by the molecules and will cause an increase in the electronic, rotational, or vibrational energy of the molecule by an amount  $\Delta E_m$  [16]. Molecules can only absorb photons if the energy contained in the photon will allow the molecule to be excited to the next higher energy level, due to quantum mechanical behavior. These quantum energy changes can manifest themselves as vibrational changes ( $\Delta\nu$ ) or rotational changes ( $\Delta j$ ) [13,17]. In either case, the molecular motion of the molecule will change.

Fundamental absorption is defined as when the molecule is excited from its ground state to the next highest energy state allowed ( $\nu_{ij1}$ ). If the molecule absorbs any additional photons while it is at a higher energy state, these absorptions are defined as overtones [18]. As higher energy states are achieved, the intensity of the overtones will become progressively weaker, with the first energy level's intensity lower than the fundamental absorption. This makes practical sense, in that the gap between the ground state and the fundamental absorption state is the largest that the molecule can attain. Sufficiently higher levels of absorption will cause the bond to fracture.

When a photon excites two or more vibrational modes in a simultaneous manner, a combination band is formed. This phenomenon is more of a function of the distance between atoms, rather than their energy level differences. This occurs when the energy of the photon allows for a more complicated vibration to occur within the molecule. Fundamental vibrations are typically found in the mid-infrared region (2,500 nm to 10,000 nm). Generally, the first and second overtones occur at approximately one half and one third the fundamental absorption frequency. This leads to the majority of overtones and combination bands occurring in the NIR region. This phenomenon leads to broad overlapping of the absorption bands, which is why NIR is considered to have less resolution than MIR spectroscopy [3,4].

When molecules absorb infrared radiation, the bond's vibration can be modeled simply as a simple harmonic oscillator. Assuming that the molecule will exhibit this harmonicity, the fundamental frequency of that bond can be calculated. The potential energy for this vibration,  $U_q$ , is given by Hooke's Law [3-4,16,19] has the form

$$U_q = -kx^2 \quad (2.2)$$

where

$k$  = force constant

$x$  = displacement

The frequency of an oscillator,  $\nu$ , is given by

$$\nu = \frac{1}{2\pi} \sqrt{\frac{k}{\mu}} \quad (2.3)$$

where

$\mu$  = reduced mass of the atoms.

The reduced mass is defined as

$$\mu = \frac{m_1 m_2}{m_1 + m_2} \quad (2.4)$$

where  $m_1$  and  $m_2$  are the individual masses of the molecules. This equation is most correct for diatomic molecules and works well as an approximation for two atoms in a polyatomic molecule. Due to quantum mechanical restraints, the energy is restricted to discrete levels. A two-particle system's energy of vibration can be defined as

$$E_n = \left(n + \frac{1}{2}\right) \frac{h}{2\pi} \sqrt{\frac{k}{\mu}} \quad (2.5)$$

where

$E_n$  = energy level of a discrete quantum number

$n$  = the vibrational quantum number

Quantum mechanics preclude energy transitions between more than one energy level. The separation energy between each level is given as

$$\Delta E = E_n - E_{n-1} = h\nu(n - (n-1)) = h\nu \quad (2.6)$$

A representation of the ideal potential energy for this oscillator behavior is shown in Figure 2.1. For this case, there will not be an associated NIR spectrum due to the lack of overtones. This type of behavior would be spectroscopically active in other regions.

The ideal harmonic oscillator model fails at high rates of molecular vibration. At these high energy levels, the molecule is unable to return to an equilibrium position causing dissociation. This will lead to asymmetry of the potential energy curve. This behavior can be accounted for in the model with the addition of higher order terms. These terms are added because the energy levels will not be equally spaced due to deviations from ideal behavior.

$$E_n = \left(n + \frac{1}{2}\right)h\nu - \left(n + \frac{1}{2}\right)^2 h\nu X_e + \left(n + \frac{1}{2}\right)^3 h\nu Y_e + \dots \quad (2.7)$$

where

$X_e$  = second order anharmonicity constant

$Y_e$  = third order anharmonicity constant

Because of the anharmonic nature of these oscillations, energy transitions that would be initially been disallowed by quantum mechanics between two or three energy levels are now possible. Ignoring higher order terms, the new levels will occur at

$$\Delta E = E_n - E_{n-1} = (1 - 2nX_e)h\nu \quad (2.8)$$

This shows that the overtones will not occur at multiples of the fundamental frequency, but rather at an amount that varies with  $X_e$ . Since the probability of a transition between higher energy levels is reduced with increasing  $n$ , the magnitude of combination and overtone bands will be orders of magnitude less than the fundamental absorption [3-4,16,19]. The overall energy of a molecule can be defined as the sum of the energies from the displacement of the molecule, and the changes in energy states from the molecule interacting with electromagnetic radiation. These include electronic, vibrational and rotational changes.

The sum can be represented as

$$E_{tot} = E_{trans} + E_{elect} + E_{vib} + E_{rot} \quad (2.9)$$



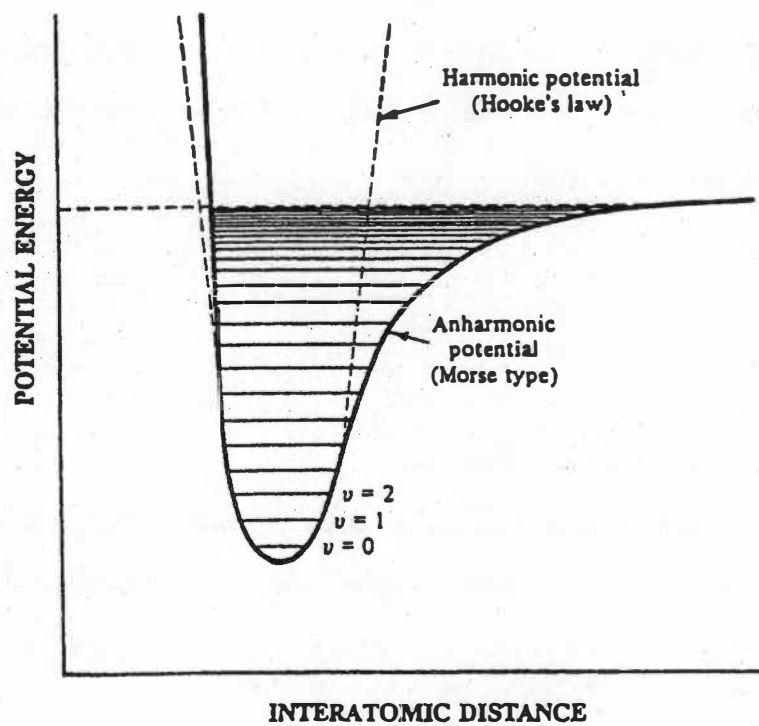


Figure 2.1 Potential energy diagram of the vibrational modes of a harmonic oscillator and an anharmonic oscillator  
 [Source: E. W. Ciurczak, *Handbook of Near-Infrared Analysis*, D.A. Burns and E. W. Ciurczak, Eds. (Marcel Dekker, Inc. New York, 1992).]

The rotational magnitude term will be much less than the vibrational energy term. The effect of the rotational term is really only found in gases [3]. It should also be noted that not all modes of vibration would be active in the NIR spectrum. Group frequencies are the key to spectral interpretation for chemical structure and functionality.

Because most practical applications of this technique will be focused on more complicated systems than just diatomic molecules, some sense of the normal modes of vibration for polyatomic molecules must be stated. The fundamental theory as presented will still apply. The number of degrees of freedom in three-dimensional space can determine these modes. These are determined by

$$\text{Number of normal modes (linear molecule)} = 3N - 5 \quad (2.10)$$

$$\text{Number of normal modes (linear molecule)} = 3N - 6 \quad (2.11)$$

where  $N$  is the number of atoms in the molecule. From these equations, it would be assumed that NIR spectral would be extremely complicated, but this is found not to be the case. Most of the resulting vibrations degenerate resulting in much fewer vibrations than would be expected. Most of the fundamental vibrations will be in terms of bending and stretching of bonds. The spectra will be complicated by the formation of overtone bands for most complicated organic species.

There are several phenomena that can affect the formation of overtones in the NIR spectra. One of these phenomenons that can affect the overtones and combination bands is hydrogen bonding. A hydrogen bond occurs when the  $s$ -orbital of a hydrogen atom in a donor group, overlaps with a  $p$ -orbital from an acceptor atom. The bond will affect the force constant and therefore change the frequency of the oscillation. Usually, this behavior presents itself with three distinct characteristics. These are a decrease in the band frequency, an increase in band width, and an overall decrease in intensity [20].

Fermi resonance has also been found to affect the NIR spectra [4, 13]. This occurs when two simultaneous vibrations occur at similar bond geometry and at the same wavelength. This situation results in accidental degeneracy in which several energy levels have the same energy. The NIR spectrum will show a split at that wavelength in that one vibration will move slightly up and one down at equal amounts. This behavior is most frequently observed with alkanes containing the C-H bending vibration and the C-H stretching vibration.

Dipole moments can also interfere with the NIR spectra. When atoms of unequal charge are bonded, a local electrical field is developed. This field will interact with any incident electromagnetic radiation and will result in an absorption band being formed. The more unevenly the charge is distributed, the stronger the interaction will become [20].

In summary, NIR spectroscopy will result in broad, diffuse absorptions. It is a weak phenomenon when compared with MIR and IR spectroscopy, and the spectra generated will not contain detailed structural information. A NIR spectrum will be reflective of the chemical properties of the sample of interest, but these will be limited to broad interpretation. It is a useful technique for quantitatively determining compositions.

## 2.2 BAND ASSIGNMENT IN NIR

To determine the chemical composition of a species using NIR spectroscopy, an understanding of the functionalities of the chemical constituents that make up the spectra is required. Due to the wide presence of combination and overtone bands in this region, it is impossible to assign bands based entirely on quantum mechanical calculations [21]. Quantum mechanics does provide the basis for band assignment, provided that information on the energy transitions is understood. The location of the absorption band is indicative of the type of chemical bond involved. Band assignments have been heavily studied in the literature [22, 25]. The most predominate bands in the NIR region are those due to C-H, O-H, and N-H bonds.

The methylene bond (C-H) has a spectral response due to a stretching vibration in the 1,600 to 1,800 nm region for the first overtone and the second overtones are located in the 1,150 to 1,250 nm region. Combination bands are evident in the 2,000 to 2,400 nm range. Aromatic hydrocarbons have been shown to absorb at lower wavelengths than aliphatic hydrocarbons with the first overtone usually seen around 1,685 nm and the second one at 1,143 nm. The methylene first overtone stretch band in olefins has been observed at 1,620 nm for terminal groups and has a combination band at 2,100 nm. It is also possible to identify configurational isomers, such as the *cis* configuration bands observed at 1,680 and 1,180 nm [22,24].

Since the structure of most polymers is a hydrocarbon-based composition, this spectroscopic technique allows for widespread use in investigating resin systems. Because each type of carbon-hydrogen

bond has its own spectral signature, it is possible to measure reaction conversion via spectroscopy. An example of this is the study of co-monomer ratio in EVA during manufacturing [25].

Alcohols and phenols have been shown to have their first overtones around 1,400 nm, second overtones around 1,000 nm, and combination overtones at 2,000 nm due to O-H stretching. Goddu completed a comprehensive study of the effects of hydrogen bonding, and integrated absorptivities [26]. The NIR region has been widely utilized for investigation of water content in materials [27]. The O-H stretch in water has its first overtone at 1,440 nm, the second overtone at 960 nm, and a combination band at 1,940 nm. Moisture is a tightly controlled product specification due to processing implications.

Primary amines have been shown to have their first overtone at 1,500 nm and combination band at 2,000 nm for the N-H stretch and NH<sub>2</sub> bonding. Spectral effects due to symmetry are weak for these compounds. Secondary amines have stretching bands around 2,900 nm and the first overtone stretch at 1,500 nm. While primary and secondary amines have recognizable bands in the NIR region, tertiary bands have been found not to have strong spectral signatures in this region. There is also spectroscopic evidence that *cis* and *trans* isomers can be identified due to the presence of doublets in the spectra. Several in depth studies have been completed in the identification of these bands [28, 29]. Table 2.3 presents a brief overview of NIR absorption band locations [21-22, 24].

### **2.3 APPLICATIONS RELATED TO POLYMER PROCESSING**

Research into the field of NIR spectroscopy has included many studies that have direct applications related to the processing of polymeric materials. This research has been aided by the development of instrumentation, chemometric tools, and the employment of fiber optics for on-line measurements. Studies have identified such applications as product purity, moisture content, reaction completion, and contamination, as well as physical property determination, in vast fields covering every aspect of the chemical process industry. This method of spectroscopy has shown to have beneficial applications.

Comparisons have been made [30] in the literature between mid-IR and NIR techniques to show the benefits of the latter. Bunding Lee conducted a comprehensive study of both techniques and has written extensively on the subject. Several comparisons have been published directly related to the Table

Table 2.3 Brief overview of NIR absorption frequency locations [21-22, 24]

Type of compound	Spectroscopic response (nm)
Aliphatic C-H vibrational stretch	1 <sup>st</sup> overtone: 1,600-1,800 2 <sup>nd</sup> overtone: 1,150-1,250 Combination band: 2,000-4,000
Aromatic C-H vibrational stretch	1 <sup>st</sup> overtone: 1,685 2 <sup>nd</sup> overtone: 1,245 Combination band: 2,145-2,460
Olefinic C-H vibrational stretch	1 <sup>st</sup> overtone: 1,645-1,675 Combination band: 2,150-4,190
Amine N-H vibrational stretch	1 <sup>st</sup> overtone: 1,500 Combination band: 2,000
Alcohol and phenolic O-H vibrational stretch	1 <sup>st</sup> overtone: 1,400 2 <sup>nd</sup> overtone: 1,000 Combination band: 2,000
Aqueous O-H vibrational stretch	1 <sup>st</sup> overtone: 1,440 2 <sup>nd</sup> overtone: 960 Combination band: 2,000

polymer processing industry, including measurement of copolymer ratios [31] and determination of the hydroxyl number in polyesters [32].

Several comprehensive review papers [18, 28, 30, 67] have appeared recently in the literature. Initial uses of NIR spectroscopy were limited to qualitative work in determining peak assignments of organic chemicals, rather than attempting to apply the technique towards quantitative assessment [2]. An early paper that had a direct impact on the polymer processing industry was that of Grieve and Doepken [33] who attempted to measure acrylonitrile-butadiene-styrene (ABS) content in polyvinyl-chloride (PVC) products. Spectra with known ABS concentrations were generated and unknown samples were compared to this control set.

The work conducted by Takeuchi *et al.* [34] investigated the use of NIR spectroscopy to describe the composition of ethylene-propylene copolymers. The group studied various rubbers, HDPE, and LDPE polymers as well as combinations of each. Without using elaborate mathematical manipulation, calibration curves were developed that allowed measurement of the homopolymers from correlations of the ethylene-propylene polymers (at 2,466 nm) and random copolymers and blends (at 2,310 nm).

Crandall *et al.* [29] investigated the use of NIR spectroscopy to measure the progress of amidization and imidization processes occurring in a polyamic-acid system. This group identified a combination band at 1,950 nm and another absorption band at 2,300 nm and were able to characterize the curing of the polymer. From these techniques, the group was able to report the effects of temperature and concentration on the curing reaction. Later work directed by Crandall [35] investigated the step growth of the polymer chain in resin systems including polyesters, polyamides and urea-formaldehyde polymers. NIR spectroscopy was conducted on melts, films and solutions. The group was able to measure the reaction progress using the change of intensities of the C-H and N-H overtones and the O-H vibrational band.

Kirkbright and Menon [36] attempted to determine the levels of vinyl acetate in a polyvinyl acetate/polyvinyl chloride copolymer. Utilizing the first stretching C-H overtone band and the combination band, they were able to measure the ratio of vinyl acetate and the particle size in the resin system. This work also reported that particle size was inversely proportional to specular reflectance. Driver's group [37]

described a spectroscopy technique to determine the levels of additives in powders and slurries. Siesler utilized the fact that additives can be discriminated in the NIR spectra [38] in an attempt to measure the presence of two unique antioxidants simultaneously. Spatafore's group [39] measured concentrations of antioxidant and stabilizing compounds in polyolefins. Using a baseline shift technique, Batra *et al.* [40] was able to characterize the loading of titanium dioxide in polyethylene terephthalate extrusion.

The first attempt at on-line fiber optic NIR spectroscopy was conducted by Schirmer [41]. This work investigated the use of fiber optic probes inserted into a polymer melt stream to measure vinyl acetate concentrations in a polyethylene vinyl acetate copolymer. The proof of concept for real time instrumentation via a spectroscopic technique was shown in this work. Farquharson *et al.* [42] extended this idea and demonstrated the use of FTNIR for a similar application. Huehne [43] and Eisenreich [44] demonstrated an NIR instrument to monitor the properties of polypropylene and polyvinyl chloride.

Development in the area of fiber optic probes was conducted by several research initiatives. Khettry [9] developed an initial system for remote on-line spectroscopy of molten polymer systems. Griesser and Sahagen [45] demonstrated that the use of silicon on sapphire coating technology enabled higher temperature and pressure operating conditions to be achieved. Vedula [2] was able to refine these probes and measure erucamide concentrations in polyethylene vinyl acetate copolymers. Further work by Li [46] allowed for a tunable fiber optic probe that could be used to optimize the quantity of light entering the detector. The use of this probe design allowed for the measurement of various polymer additives at low concentrations.

The chemical analysis of polymer pellets and films was reported by Weyer [18]. Utilizing reflectance NIR spectroscopy, measurement of methyl ethyl ketone concentrations in acrylic resins and distinguishing mixtures of structurally similar polymers was demonstrated.

The dissertation work and subsequent publications by Miller [27, 28, 47] compiled significant work on the use of chemometric techniques in conjunction with NIR spectroscopy. The use of chemometric techniques was further refined by the dissertation work of Vedula [2]. Utilizing chemometric techniques, a correlation between the NIR spectra and the complex viscosity of a flowing polymer stream was obtained.

NIR spectroscopy for in-line composition measurement has been the focus of several research projects. Systems studied include physical blends of polymers and copolymer ratios [48, 49]. Industrially important physical properties have been determined using these techniques as well. Included in this group are melt index, complex viscosity, yellowness index, reaction progression, and chemical interactions. Hammond reported an in-line technique for the determination of moisture content [50].

Nondestructive testing utilizing NIR spectroscopy has also been the technique of choice for measuring blend ratios of various polymer combinations [51]. Miller [52] investigated a system of high density and low density polyethylene and laminated polyethylene, polyamide and ethylene vinyl alcohols for food packaging. The laminates study demonstrated a technique for path length correction in dealing with varying film thickness.

Dissertation work conducted by Li [46] investigated the use of NIR spectroscopy to measure additive levels in polyethylene and polypropylene. Tinuvin<sup>®</sup> 770 was shown to have an absorption band at 1,520 to 1,560 nm in polypropylene. Given this information, a PLS model was constructed and able to predict the loading of this additive for a range of 0-2,000 ppm. Erucamide was shown to have potential to be measured in the NIR region when used as an additive in polyethylene. Two absorbance bands were identified due to the  $-NH_2$  stretching at 1,440 to 1,500 nm and the combination band resulting from  $-NH_2$  stretching and bending at 1,930 to 1,990 nm. From these insights, it was possible to construct a prediction model using PLS for a range of 25 to 5,000 ppm.

As has been demonstrated in the literature, the use of NIR spectroscopy has been developed to a point where on-line remote measurement is a practical option to current off-line techniques. Bouveresse *et al.* [53] reviewed the standardization of NIR instrumentation. It should be stressed, however, that each polymeric processing operation has a different characteristic set of information and techniques must be developed and refined for each case.



## CHAPTER 3

### UV SPECTROSCOPY

#### INTRODUCTION

Ultraviolet spectroscopy is an analytic technique designed to study the rotational and vibrational energies of molecules. Molecules in the sample are stimulated by light containing high levels of UV radiation. Depending on the bond configuration and functional groups present, the molecule will absorb a fraction of the incident radiation and transmit the remainder [19]. By investigating the wavelengths of the absorbed light, it is possible to derive an understanding of the chemical structure of the sample. The UV region lies in the 150 to 400 nm range of the electromagnetic spectrum. This region corresponds to the electrical transitions of de-localized Pi electrons [21]. UV spectroscopy has been utilized for wide variety applications in the monitoring of polymer properties.

#### 3.1 FUNDAMENTALS OF UV SPECTROSCOPY

Ultraviolet and visible spectroscopies are universal chemical analytical techniques for a variety of reasons. Many compounds have spectroscopic responses in these wavelength regions. These techniques are available at a low cost and provide sensitive and selective data on the chemical components of the sample of interest. The results of such experiments are also relatively easy to interpret. UV spectroscopy has been shown to be useful in the wavelength region of 150 to 400 nm of the electromagnetic spectrum [54-57].

UV absorption is the result of an electronic rearrangement of the atoms or molecules contained in the sample. The sample will absorb radiation if the wavelength of the incident light corresponds to an electrical site change allowed by Planck's law. Emission is the reverse of this process, when an excited molecule emits an amount of radiation that allows the molecule to return to ground state.

When radiation interacts with matter, a number of processes can occur, including reflection, scattering, absorbance, fluorescence/phosphorescence (absorption and reemission), and photochemical reaction (absorbance and bond breaking). In general, when measuring UV-visible spectra, absorbance is the only preferred form. Because light is a form of energy, absorption of light by matter causes the energy

content of the molecules (or atoms) to increase. The total potential energy of a molecule generally is represented as the sum of its electronic, vibrational, and rotational energies:

$$E_{total} = E_{elect} + E_{vibr} + E_{rot} \quad (3.1)$$

The amount of energy a molecule possesses in each form is not a continuum but a series of discrete levels or states. The differences in energy among the different states are in the order:

$$E_{elect} > E_{vibr} > E_{rot} \quad (3.2)$$

In some molecules and atoms, photons of UV and visible light have enough energy to cause transitions between the different electronic energy levels. The wavelength of light absorbed is that having the energy required to move an electron from a lower energy level to a higher energy level.

If a spectrum is expressed as absorbance ( $A$ ) as a function of wavelength ( $\lambda$ ), the derivative spectra are:

$$\text{Zero order: } A = f(\lambda) \quad (3.3)$$

$$\text{First order: } \frac{dA}{d\lambda} = f'(\lambda) \quad (3.4)$$

$$\text{Second order: } \frac{d^2 A}{d\lambda^2} = f''(\lambda) \quad (3.5)$$

The derivative spectra are always more complex than the zero-order spectrum. The first derivative is the rate of change of absorbance against wavelength. It starts and finishes at zero, passing through zero at the same wavelength as  $\lambda_{max}$  of the absorbance band. This derivative has a positive and a negative band with maximum and minimum at the same wavelengths as the inflection points in the absorbance band. This bipolar function is characteristic of all odd-order derivatives.

The most distinctive feature of the second-order derivative is a negative band with minimum at the same wavelength as the maximum on the zero-order band. This derivative also shows two positive satellite bands on either side of the main band. The fourth derivative shows a positive band with a maximum at the same wavelength as the maximum on the zero order band. Even-order derivatives show a negative or positive band with minimum or maximum at the same wavelength as  $\lambda_{max}$  on the absorbance band.

Optical, electronic, and mathematical methods all can be used to generate derivative spectra. Although optical and electronic techniques formed the basis of early UV-visible spectroscopy, these have been largely superseded by mathematical methods.

The absorption intensity is dependent on the concentration of the absorbing species concentration in the sample,  $c$ , and the path length of the radiation through the sample,  $l$ . The molar extinction coefficient,  $\epsilon$ , is defined by Beer-Lambert's law [16] as

$$\epsilon = \frac{1}{cl} \log_{10} \frac{I_0}{I} \quad (3.6)$$

or

$$A = a c l \quad (3.7)$$

where

A = absorbance

a = absorptivity at a particular wavelength

l = optical path length in the measurement volume

c = concentration of the absorbing chemical

Equation 3.7 states that in the absence of interactions among absorbing molecules, the absorbance at a particular wavelength is linearly related to concentration. The absorptivity value is a characteristic of the species, and is also a function of processing conditions, such as temperature, pressure and others.

Transmittance, T, is calculated from the intensity of light incident on the sample ( $I_0$ ), and the intensity of light after it passes through the sample (I), by the relation:

$$T = (I/I_0) * 100\% \quad (3.8)$$

The absorbance is related to transmittance by the expression:

$$A = \log_{10}(1/T) \quad (3.9)$$

Usually, transmittance spectra are collected for melts and solutions. This quantity is used to measure the efficiency of the absorbing species. For quantitative analysis, the extinction coefficient is chosen at the wavelength of maximum absorbance. The larger the extinction coefficient is, the more dependent on the

detection method the results will be. Samples that absorb in the UV region fit this description more than those in the visible region.

The extinction coefficient ( $\epsilon$ ) is characteristic of a given substance under a precisely defined set of conditions, such as wavelength, solvent, and temperature. In practice, the measured extinction coefficient also depends partially on the characteristics of the instrument used. For these reasons, predetermined values for the extinction coefficient usually are not used for quantitative analysis. Instead, a calibration or working curve for the substance to be analyzed is constructed using one or more standard solutions with known concentrations of the analyte. For electronic transitions, the difference in energy between ground and excited states is relatively large. Therefore, at room temperature, it is highly likely that all molecules are in the electronic ground state. Absorption and return to ground state are fast processes, and equilibrium is reached very quickly. Thus, absorption of UV-visible light is quantitatively highly accurate. The simple linear relationship between absorbance and concentration and the relative ease of measurement of UV-visible light have made UV-visible spectroscopy the basis for thousands of quantitative analytical methods.

Assuming Beer's law is obeyed for the zero-order spectrum, a similar linear relationship exists between concentration and amplitude for all orders of derivative spectra:

$$\text{Zero order: } A = \epsilon c l \quad (3.10)$$

$$\text{First derivative: } \frac{dA}{d\lambda} = \frac{d\epsilon}{d\lambda} cl \quad (3.11)$$

$$\text{n}^{\text{th}} \text{ derivative: } \frac{d^n A}{d\lambda^n} = \frac{d^n \epsilon}{d\lambda^n} cl \quad (3.12)$$

at  $\lambda$ , where  $A$  is absorbance,  $\epsilon$  is the extinction coefficient,  $l$  is the sample path length, and  $c$  is the sample concentration.

To calculate the derivative at a particular wavelength ( $\lambda$ ), a window of  $\pm n$  data points is selected, and a polynomial

$$A_\lambda = a_0 + a_1\lambda + \dots + a_n\lambda^n$$

is fitted by the least squares method. The coefficients  $a_0 \dots a_n$  at each wavelength are the derivative values, where  $a_1$  is the first derivative,  $a_2$  is the second derivative, and so on. Savitzky and Golay [21] developed a highly efficient method to perform the calculations that is the basis of the derivatization algorithm in most commercial instruments.

This method also smooths the data. If the polynomial order ( $l$ ) is less than the number of data points ( $2n+1$ ) in the window, the polynomial generally cannot pass through all data points. Thus the least squares fit gives a smoothed approximation to the original data points. Although transforming a UV-visible spectrum to its first or a higher derivative usually yields a more complex profile than the zero-order spectrum the intrinsic information content is not increased. In fact, it is decreased by the loss of lower-order data such as constant offset factors.

For single-component quantification, the selection of wavelengths is more difficult with derivative spectra than with absorbance spectra since both positive and negative peaks are present. The even-order derivatives have a peak maximum or minimum at the same  $\lambda_{\max}$  as the absorbance spectrum, but for the odd-order derivatives, this wavelength is a zero-crossing point. Taking the difference between the highest maximum and the lowest minimum gives the best signal to noise ratio but may result in increased sensitivity to interference from other components.

UV spectroscopy can be explained by a simplified quantum mechanical treatment [19]. A molecule in a ground state,  $G$ , has total energy  $E(G)$  and can be described by a wave function  $\Psi(G)$ . Upon absorption, the molecule will be excited to a higher state  $S$ . The change in energy for this transition is

$$E(S) = E(G) + \Delta E \quad (3.13)$$

with

$$\Delta E = h\nu \quad (3.14)$$

The requirement for this transition to occur is that the two states ( $G$  and  $S$ ) must be coupled by the electric dipole ( $er$ ) of the incident radiation. Ideally, the spectral response would show up as a sharp peak whose width was equal to the result from the Heisenberg uncertainty principle. This is not the case in practical applications because even though the stimulating radiation is greater than the absorption, there is still a coupling effect that will occur. A similar derivation as was done in Chapter 2 can be done to explain the modes of vibration that can occur utilizing UV spectroscopy. At higher temperatures, the absorption bands will become even smoother in nature because there are higher population levels at each electronic state [58].

There are several transitions that are observed using spectroscopy that would seem to be disallowed following classical molecular orbital theory. The three transitions that are allowed in spectroscopy are (1) the change in angular momentum  $\Delta L=0$  or  $\pm 1$ , (2) there are no change in the spin orientation of the electrons, and (3) the product of the group representations of the two states and the electric dipole vector are symmetrical. The first rule rarely comes into play since most coupled states are within one unit of angular momentum of each other. The second rule is the spin forbidden rule. A transition such as this will always have a lower intensity than a spin allowed transition because of the energy required to change the spin direction. Group theory can be used to explain the third rule [59]. It is necessary to force the representation of the electric dipole vector and the excited state to be identical for ground states, which are symmetrical. There are forbidden transitions that do not follow this rule. They occur from the molecule not totally conforming to the rules regarding transition changes. A molecule can convert some energy into static contributions, which are not temperature dependent, and vibrational contributions, which are dependent on temperature.

### 3.2 BAND ASSIGNMENT IN UV SPECTROSCOPY

Band assignment in the ultraviolet region follows the same systematic methodology as those in the NIR region. Bonding for non-aromatic organic compounds involve the combination of *s* and *p* electrons to produce molecular orbitals [60]. The population of the resulting orbital levels is highly dependent on the molecule in question. The transitions that can occur are limited to the various  $\sigma$  and  $\pi$  orbitals in the molecule. The lowest energy transition will occur from an electron being excited from the non-bonding orbital to the  $\pi^*$  anti-bonding level ( $n \rightarrow \pi^*$ ). These transitions are detectable in the 250 to 600 nm region. The next highest energy transformations are either  $n \rightarrow \sigma^*$  or  $\pi \rightarrow \pi^*$ . These transitions occur around 250 nm. The highest level that are measurable in the UV region involve  $\sigma \rightarrow \sigma^*$  which occur at approximately 130 nm. The intensity of the transition is proportional to the energy level.

Aromatic compounds exhibit similar behavior to those previously described with a few exceptions. Benzene appears as two bands at 256 nm and 204 nm. These transitions are symmetry forbidden, but occur due to static and vibronic distortions. Comparing higher order acenes, the trend is to

red shift the bands and increase the intensities. A table presenting a brief overview of UV absorption bands is shown in Table 3.1 [19].

UV-visible spectra generally show only a few broad absorbance bands. Compared with techniques such as infrared spectroscopy, which produces many narrow bands, UV-visible spectroscopy provides a limited amount of qualitative information. Most absorption by organic compounds results from the presence of  $\pi$  (that is, unsaturated) bonds. A chromophore is a molecular group usually containing a  $\pi$  bond. When inserted into a saturated hydrocarbon (which exhibits no UV-visible absorbance spectrum), it produces a compound with absorption between 185 and 1000 nm.

The presence of an absorbance band at a particular wavelength often is a good indicator of the presence of a chromophore. However, the position of the absorbance maximum is not fixed but depends partially on the molecular environment of the chromophore and on the solvent in which the sample may be dissolved. Other parameters, such as pH and temperature, also may cause changes in both the intensity and the wavelength of the absorbance maxima, but ionic surfactants such as sodium alkyl benzenesulphonates do. Freitag [68] reported a method to measure the presence of the hindered amine light stabilizer Chimassorb<sup>®</sup> 944. This technique involved refluxing a small sample of polymeric material in decalin. The procedure for this method is rather involved and requires numerous additions be made to the analytic sample and then analyzing the resulting mixture with UV spectroscopy. The absorbance of Chimassorb<sup>®</sup> 944 was shown to occur at 245 nm.

Conjugating the double bond with additional double bonds increases both the intensity and the wavelength of the absorption band. For some molecular systems, such as conjugated hydrocarbons or carotenoids, the relationship between intensity and wavelength has been systematically investigated. Transition metal ions also have electronic energy levels that cause absorption of 400–700 nm in the visible region. Although UV-visible spectra do not enable absolute identification of an unknown, they frequently are used to confirm the identity of a substance through comparison of the measured spectrum with a reference spectrum.

Table 3.1 Electronic band assignment for the UV region for representative organic bonds [19]

Type of compound	Band	Frequency range (nm)
Acetylide	-C≡C-	175-180
Aldehyde	-CHO	210
Amine	-NH <sub>2</sub>	195
Carboxyl	-COOH	200-210
Ester	-COOR	205
Ether	-O-	185
Ethylene	-C=C-	190
Nitrile	-C≡N	160
Benzene	C <sub>6</sub> H <sub>6</sub>	222 275 312



### 3.3 APPLICATIONS RELATED TO POLYMER PROCESSING

Since ultraviolet spectroscopy has existed for a number of years, a considerable amount of work has been done searching for applications related to the polymer processing industry. Johnson [61] conducted a detailed review of detectors of ultraviolet applications. Keough [62] compiled a comprehensive overview of various UV sources currently used in instrumentation.

Sung [63, 64] investigated the use of UV spectroscopy to measure the curing reactions of epoxy resins. This work demonstrated that transmission techniques are valid only for thin samples and that reflectance measurements can be conducted for different system geometry. The determination of reaction completion was accomplished by using both intrinsic and extrinsic probe molecules.

Until recently, the chemical analysis techniques used in the determination of additive concentrations in polymer systems have been well-defined extraction techniques. These are quite accurate but rather time consuming [65]. Measurements of additive concentrations as an off-line technique have been shown in the literature. The comprehensive UV spectra of phenolic antioxidants and UV absorbers were presented by Scholl [66]. Newton [65] investigated combinations of polymer additives using UV spectroscopic techniques in chloroform. He conducted this work to get a basic understanding to discriminate among additive combinations. Newton also utilized UV spectroscopy to gain an understanding of alkyphenol ethoxylate surfactant in polytetrafluoroethylene based on methodology developed by Epton [67]. An absorbance band for this additive was identified at 275 nm. It was demonstrated in this work that anionic surfactants do not interfere with the UV absorption in this system,

Spatagore *et al* [69] determined antioxidant levels in combination with light stabilizers in polymer systems. Yang [70] investigated antioxidant levels in PP and showed temperature dependence of the absorbance at elevated temperatures. Schirmer [71-73] demonstrated the measurement of additives in high density polyethylene during an extrusion process. Other reviews of UV spectroscopy and chemical methods for the analysis of additives in polymer systems were conducted by Crompton [74] and Haslam *et al* [76].

Anseth *et al.* [76] attempted to characterize the free-volume distributions during multifunctional monomer polymerizations using ultraviolet spectroscopy. The group identified that the *cis* and *trans* conformations of the polymer backbone were spectroscopically different and they were able to measure the isomerization rate for the conversion. These experiments were unique in that the spectroscopic measurements were conducted *in situ* and in real time. Photochromic probes [77] were developed specifically to make these measurements.

Dissertation work by Li [46] presented significant work utilizing UV spectroscopy for the determination of additive levels in both polypropylene and polyethylene as an in-line real time technique. Studies conducted in polypropylene were centered around Tinuvin<sup>®</sup> 770 (ultraviolet stabilizer). An absorbance band was identified at 270 nm that was used to measure the loading of the additive. This band corresponds to the  $n \rightarrow \pi^*$  excitation of the C=O bond in the carbonyl group. Li also looked at the absorbance at 230 and 270 nm that was attributed to sodium stearate (process aid). No significant spectral changes occurred with concentration differences and the group was unable to construct a calibration model.

Li also investigated Irganox<sup>®</sup> 1076 (primary antioxidant), Irgafos<sup>®</sup> 168 (secondary antioxidant), Tinuvin<sup>®</sup> 622 (ultraviolet stabilizer), erucamide (slip agent), and Armostat<sup>®</sup> 310 (antistat agent). While these additives were shown not to have strong spectral responses in the NIR region, individual additive loadings were measurable. Maximum absorbances at 270 nm and 285 nm were observed for Irganox<sup>®</sup> 1076 and Irgafos<sup>®</sup> 168. This band arises from a  $\pi \rightarrow \pi^*$  transition in benzene chromophores with conjugated structures. The observable difference results from the side groups present in the molecules. The other additives were shown to have absorbances below 260 nm. Li was able to construct PLS prediction models for all five additives. The models for Irganox<sup>®</sup> 1076 and Irgafos<sup>®</sup> 168 were for a concentration range of 0 to 1000 ppm with a standard error of prediction of 40 ppm. Predictions of the other three additives were not as good due to the overlaps in the observable spectra. Errors in prediction of multiple additives were in the 11 to 14% range. Although this high a level of error would be unacceptable in a commercial environment, it was shown that a spectroscopic model could be constructed to measure the overall additive loading of these three individual components.

From a review of the literature, it is obvious that ultraviolet spectroscopy is a useful tool in the characterization of polymer systems. Hunt [65] stated that UV spectroscopy is limited in the applications that it has been found useful, but he was referring to analytic chemical techniques as opposed to the online measurement of practical systems. In the applications that it is being used for, however, its use has been shown to be more than sufficient. The ability to measure additive concentrations at low levels and the extent of development of the fundamental spectroscopic technique make it an ideal choice for instrumentation in an industrial setting. For these reasons, the screening of the technique for new applications is well justified.

## CHAPTER 4

### RAMAN SPECTROSCOPY

#### INTRODUCTION

Raman spectroscopy is a technique of vibrational spectroscopy [19, 21, 78, 79]. The energy levels of molecules are explored by investigating the frequencies present in the radiation scattered by the molecules. The shifts in frequency of the scattered radiation from the incident radiation are quite small, thus requiring the use of monochromatic light in order to make practical observations. The intensity of the scattered radiation is also quite low, requiring high intensity stimulating radiation to be used. These experimental concerns are both overcome with the use of lasers. Raman spectroscopy has been developed as a practical instrumental technique for some applications in the polymer process industry.

#### 4.1 FUNDAMENTALS OF RAMAN SPECTROSCOPY

The Raman effect was first observed in 1928 by Raman [80, 81], after being predicted in 1923 by Smekal [82]. Early experiments utilized highly focused sunlight and required sample exposure times of up to 24 hours. These experiments relied on the observer characterizing the color changes of the sample, usually 600 ml of a liquid. Major improvements were made to this technology in 1952 with the introduction of the Toronto arc source [19]. This high intensity light source allowed for a stronger response from the sample and shorter experiment times. The multi-chromatic nature of the light still limited the observed effect as well as the amount of light that could be used to excite the sample. The appearance of lasers in the field in the early 1960's allowed for Raman spectroscopy to be conducted on increasingly smaller samples in non-traditional testing environments with reliable results.

When light with a high enough energy is shined onto a molecule, vibrations of that molecule can be excited, meaning that the molecule is promoted to a state of higher energy in which its vibrational amplitude is increased. Both infrared and Raman spectroscopy operate with the vibrational properties of molecules as the basis of operation, and make up the major portion of vibrational spectroscopy.

Vibrational spectra are usually measured by two very different techniques: infrared spectroscopy and Raman spectroscopy. In IR spectroscopy, light of many different frequencies is passed through a sample and the intensity of the transmitted light is measured at each frequency. At frequencies

corresponding to vibrational energies of the sample, some light is absorbed and less light is transmitted than at frequencies which do not correspond to vibrational energies of the molecule. By measuring the transmittance, or the ratio of the light passing through the sample to the light passing through a reference cell, an infrared spectrum is produced.

In contrast, transmitted light is not observed in Raman Spectroscopy. Instead, the light scattered by the sample is of interest. Monochromatic light, or light of a single frequency, must be used for Raman scattering. Ordinarily, when light of frequency  $\nu_0$  is shined through a homogeneous solution, most of the light will pass directly through the sample. However, some of the light with about 1/1000 of the incident intensity is scattered in all directions and can be seen from the side of the sample. When the light scattered is the same intensity as the incident ( $\nu_0$ ), the phenomenon is called Rayleigh scattering [21].

Some of the scattered light does not the same frequency as the incident. Instead, this light has frequencies  $\nu_i$  such that

$$\Delta E = h|\nu_0 - \nu_i| \quad (4.1)$$

corresponds to energies that are absorbed by the sample and the value  $|\nu_0 - \nu_i|$  is an infrared (vibrational) frequency. The process that produces light of frequency other than  $\nu_0$  is called Raman scattering [79]. When the frequency of the scattered light is less than the incident frequency, the light is called Stokes radiation. The frequency that is greater than the incident frequency is called anti-Stokes radiation.

To gain a more complete understanding, it is important to understand the concept behind dipole moments. If two particles with charges  $+e$  and  $-e$  are separated by a distance  $r$ , the permanent electric dipole moment  $m$  is given by

$$m = er \quad (4.2)$$

For example, heteronuclear diatomic molecules must have a permanent electric dipole moment since one atom will be more electronegative than the other, and homonuclear diatomic molecules cannot have a permanent dipole moment since both nuclei attract equally.

For a heteronuclear diatomic molecule vibrating at a particular frequency, the molecular dipole moment also oscillates about its equilibrium value as the two atoms move back and forth. This oscillating dipole can absorb energy from an oscillating electric field only if the field also oscillates at the same

frequency. The absorption of energy from the light wave by the oscillating permanent dipole is a molecular explanation of IR spectroscopy.

If a molecule is placed in an electric field,

$$E = E_0 \cos(2\pi n_{ex} t) \quad (4.3)$$

where  $E_0$  is the amplitude of the wave, and  $n_{ex}$  is the frequency of the radiation, a dipole moment  $m$  is induced in the molecule because the nuclei are attracted toward the negative pole of the field, and the electrons are attracted the opposite direction. The induced dipole is proportional to the field strength by

$$m = aE \quad (4.4)$$

where the proportionality constant  $a$  is called the polarizability of the molecule. All atoms and molecules have a non-zero polarizability even if they have no permanent dipole moment.

In order to be Raman active, the polarizability of a bond must vary as a function of the distance between nuclei according to the equation

$$a = a_0 + (r - r_{eq})(da/dr) \quad (4.5)$$

After some algebra, the expression for the induced dipole  $m$  turns out to be

$$m = a_0 E_0 \cos(2\pi n_{ex} t) + (E_0/2) r_m (da/dr) \cos[2\pi(n_{ex} - n_v) t] + (E_0/2) r_m (da/dr) \cos[2\pi(n_{ex} + n_v) t] \quad (4.6)$$

where  $r_m$  is the maximum internuclear separation relative to the equilibrium position, and  $n_v$  is the frequency of the vibration. The first term in the equation above represents Rayleigh scattering, which occurs at the excitation frequency  $n_{ex}$ . The second and third terms correspond to the Stokes and anti-Stokes frequencies of  $n_{ex} - n_v$  and  $n_{ex} + n_v$ . The energy shifts seen in Raman should be the same as the energies of its IR absorption bands, provided that the bonds studied are both IR and Raman active.

The differences that separate IR and Raman spectroscopy come from processes that are mechanistically different [83]. For IR absorption, the vibrational mode of the molecule must have a change in dipole moment or charge distribution while Raman involves a temporary distortion of the electrons around a molecular bond, followed by reemission of the radiation as the bond returns to its normal state. When the molecule is distorted, it is defined as being polarized, meaning that it develops momentarily an induced dipole that disappears upon relaxation and reemission.

Raman samples can be prepared in the liquid, solid, or gas form. Because sensitivity to water interference is minimal, a common method of sampling liquid samples is using an ordinary glass melting-point capillary. In addition, narrow band-pass interference filters transmit a single line from the laser source and rejects over 99.9% of other lines, making the laser is easy to focus on a small sample area. Thus, small samples can be used, even when diluted significantly in water [19].

Problems with concentration and detection limits are not terribly common in solid samples since they are usually studied directly. Weak scatterers such as dilute gases can be placed between mirrors of the laser source creating enhanced excitation power. Interference in Raman spectra does not usually come from equipment or sample medium. Because Raman spectroscopy is insensitive to interference by glass, the use of common glass lenses, mirrors, windows and other optical equipment is negligible. And, as mentioned above, Raman scattering has a low sensitivity to water. Both of these qualities make Raman a very appealing form of scientific study.

One type of interference that is very evident in Raman methods is fluorescence-producing excited electronic energy states. Intensity of Raman scattering varies as the fourth power of the laser frequency, making Raman lines produced with argon and krypton lasers (high frequency, short wavelength) very intense. The tradeoff is that fluorescence is often seen in compounds with these lasers. Instead, diode (782 or 830 nm) and Nd/YAG (yttrium-aluminum-garnet) lasers are becoming more popular because they do not have the power to produce fluorescence-producing excited energy states [83].

## 4.2 BAND ASSIGNMENT IN RAMAN SPECTROSCOPY

Raman scattering allows for molecular identification due to several distinct spectral features. Unlike NIR spectroscopy [85], Raman techniques investigate vibrations from relatively non-polar bonds with symmetrical charge distributions. Vibrations from bonds such as  $-C=C-$ ,  $-C\equiv C-$ ,  $-C\equiv N-$ ,  $-C=S-$ ,  $-C-S-$ ,  $-S-S-$ ,  $-N=N-$ , and  $-S-H$  are particularly visible via this spectroscopic technique. Raman is also capable of observing low frequency vibrations. Spectral information is also obtainable within 20 to 50  $\text{cm}^{-1}$  of the excitation radiation. This region is located in the far-infrared area where important metal bonding vibrations occur in organic materials. Vibrations from short hydrocarbon chains and small rings occur in the 800 to 1,500  $\text{cm}^{-1}$  region. Aromatic compounds exhibit a strong band and 1,600  $\text{cm}^{-1}$ . An  $-S-S-$  bond

gives a band at  $500\text{ cm}^{-1}$ , a -C-S- will be visible at  $650\text{ cm}^{-1}$ , and a -S-H- bond stretch will yield a intense band at  $2,500\text{ cm}^{-1}$ . A more comprehensive listing of Raman scattering bands is presented in Table 4.1[21].

Raman spectroscopy is useful for compounds in which the IR stretching frequencies for N-H and C-H bonds are hidden by O-H absorption [86]. O-H bands are weak in Raman, but the N-H and C-H have moderate intensities. Raman has also proved useful for identification of substituent groups of aromatic rings. Although there are similarities between IR and Raman spectroscopy, some absorptions are more intense in one technique over the other.

#### 4.3 APPLICATIONS RELATED TO POLYMER PROCESSING

Raman spectroscopy has only come into its own recently for polymer processing applications. The technique is not nearly as developed as ultraviolet or infrared spectroscopy mainly because of its more recent introduction to the scientific community. Early experiments into the field were conducted to understand the chemistry and physics behind the technique and then later to develop band assignments and gather fundamental knowledge of the limitations of the method.

Raman has been shown to be a powerful tool in the characterization of polymer systems. Several studies have investigated bulk and surface contamination [87, 88], fiber analysis [88, 89], laminated surface properties [88, 92], and compositional and morphological characterizations [87, 88]. Several studies have also centered around systems that have been historically more difficult to study [88, 89]. Most of these studies couple Raman spectroscopy with other techniques to confirm the spectroscopic data [88, 89].

The monitoring of reaction progression using Raman and IR techniques have been demonstrated in the literature. Bulk conversion of styrene has been the focus of work by Chu *et al.* [93, 94] and Gulari *et al.* [95] as has been methyl methacrylate polymerization. *In situ* Raman spectroscopy [96] was used to investigate microemulsion polymerization of these monomers. The monitoring of the reaction was accomplished by measurement of the peak at  $1,600$  to  $1,650\text{ cm}^{-1}$  that comes from the aliphatic -C=C- peak. This bond disappears during consumption of the monomer.

Considerable polymerization monitoring work has been conducted on the polymerization of hexachlorocyclotriphosphazene [97, 98]. This reaction is the precursor to polyorganophosphazenes. Work conducted has investigated the thermal, melt [97] and solution [98] polymerization. This work is unique in



Table 4.1 Brief overview of Raman scattering band locations

Band	Type of Compound	Frequency Range (cm <sup>-1</sup> )	Intensity
C-H	Alkanes	2,850-2,970	Strong
		1,340-1,470	Strong
C-H	Alkenes	3,010-3,100	Strong
C-H	Alkynes	3,300	Weak
C-H	Aromatics	3,100-3,300	Strong
		690-900	Medium
O-H	Monomeric alcohols and phenols	3,500-3,650	Weak
N-H	Amines, amides	3,300-3,500	Medium
C=C	Alkenes	1,610-1,680	Strong
C≡C	Alkynes	2,100-2,280	Strong
C-N	Amides, amines	1,180-1,360	Strong
C≡N	Nitriles	2,210-2,280	Medium
C-O	Alcohols, ethers, esters	1,050-1,300	Weak
C=O	Aldehydes, ketones, esters	1,670-1,760	Strong
C-C	Aliphatic chains	250-400	Strong

that is utilizes a combined Raman and laser light scattering apparatus and the measurements are conducted on-line.

Raman spectroscopy has also been used to study and characterize the degradation of polymers [99, 100]. The technique has been shown to be useful for polyene characterization [99]. Degradation of polyvinyl chloride has been widely studied [100]. The mechanism for degradation is known and the combination of the mechanism and the monitoring technique allows for a more complete measurement of the degradation during early stages to be monitored. Natural weathering [101] and chemically initiated degradation [102] are just two mechanisms that can be monitored using this technology. Polyacrylonitrile, which is a precursor to the production of carbon fibers, has been investigated by Raman spectroscopy for the measurement of graphitisation levels [103-106].

Raman spectroscopy has also shown usefulness in the determination of morphological properties of polymers. The technique has been used to quantify levels of *cis* and *trans* isomers in polyisoprene [107]. It has also shown use in the determination of crystallization levels in polyvinyl chloride [108]. In this study, several spectral indicators for tacticity were also found. The authors stress the use of deconvolution techniques in their work for this application because of the number of overlapping spectra in the region of interest [109].

Process monitoring applications have appeared utilizing Raman spectroscopy. Cakmak *et al.* [110] described a system to measure the crystallinity of low density polyethylene. Williams *et al.* [111] developed methodology that allows the measurement of polyethylene density and crystallinity using PLS regression.

Polarized Raman spectroscopy's usefulness has also been shown for polymer applications. Insight to the entanglement of melts during extrusion was effectively demonstrated by Archer [112]. This work was centered around the -C-C- and -C-H stretching vibrations in the molecules. Archer [113] later investigated block copolymer orientation. Work was also conducted in observing orientation of polypropylene during extrusion by Hanna [114]. Mikio [115] conducted the first injection molding studies using Raman spectroscopy to gain insight to the molecular orientation during this operation. It was shown by Chai [116] that the population of *trans* -C-C- bonds is proportional to the shear on the polymer. The

undertaking of the determination of polymer orientation is not a simple and straightforward task. For work involving the orientation, Raman is the preferred technique because the sample thickness is not an issue, unlike the other techniques used [117, 118]. It is important for the sample to have good optical quantities to eliminate scrambling of the response signal. Scherer [119] described in detail the experimental requirements for accurate measurement of these properties.

Work by Strolb and Hagerdorn [120] used Raman spectroscopy demonstrated the ability to measure the level of crystallization in polyethylene. It should be stressed that techniques such as vibrational spectroscopy, differential scanning calorimetry, X-ray and density measure different properties so true measurement of crystallinity by spectroscopy will be slightly different than results of the other methods [121].

Almo [122] was able to demonstrate molecular weight effects on melting and orientation of random copolymer ethylene. Crystal features were compared with the results from x-ray diffraction. Several other investigations [123-125] probed the molecular orientation of polymer molecules with this technique of spectroscopy. Other demonstrated capabilities [126-128] include measurement of phase transitions and estimation of chemical composition.

Another application of Raman spectroscopy has been the determination of biaxial orientation of polymer systems. Several studies [129-130] have been conducted on the orientation of polyethylene terephthalate. Using the techniques reported in the literature, Chalmers *et al.* [48] attempted to predict the orientation during the blow molding of PET in the production of soft drink bottles.

Raman spectroscopy has demonstrated its usefulness as a technique in the characterization of polymer systems. The addition of Raman data to typical NIR spectroscopy has greatly enhanced the understanding of fundamental behavior and interactions of practical polymeric materials. Since the technique is still in the development state, more applications will eventually be reported in the scientific literature.

## CHAPTER 5

### COLOR TECHNOLOGY AND ANALYSIS TECHNIQUES

#### INTRODUCTION

Besides meeting all chemical and structural composition requirements, color is the most important feature of most polymer products. The use of pigments dates back to the earliest record of human activity [132]. As polymer processing and engineering has developed, a transfer of color technology from such fields as textiles, printing ink, paper and cosmetics has occurred [133]. The characterization and control of a product's color has only been of scientific interest since early twentieth century. The quantitative measurement of color has always been hampered by the fact that color is subjective in the evaluation of appearance and each observer will view it in a slightly different manner. The effects of this can be reduced by the use of standardized testing methods, which will allow for a corrected comparison between standard and sample.

#### 5.1 PRINCIPLES OF COLOR TECHNOLOGY

Color has many definitions. It can mean a certain type of light, its effect on the human eye, or the result of this effect in the mind of the observer [134]. Most importantly, color is what is seen.

Traditionally, questions regarding color have only had qualitative answers based on skills and memory from a trained color matcher. The advent of increased computing power and color measurement have allowed for objective answers to be given. The existence of color is dependent on three components: a light source, an illuminated object, and an observer or detector to perceive the color.

The light source can be any object that reflects or radiates light. A very important type of light source is the blackbody radiation source [135]. A blackbody is an object whose spectral power distribution is dependent only on its temperature and not its composition. The temperature of a blackbody is called its color temperature. Most practical or naturally occurring light sources are not blackbodies. Arc lamps typically emit light at a few specified wavelengths and not over a spectrum. These wavelengths are characteristic of the material used. Several standard light sources have been defined by the International Commission on Illumination (Commission Internationale de l'Éclairage, or CIE) [136]. The three originally defined light sources are the CIE A, B, and C sources. Source A is a tungsten-filament lamp operating at a

color temperature of 2854 K which has the same properties of an incandescent light bulb. The spectral power distribution of this source is shown in Figure 5.1 [134]. Sources B and C are derived from Source A by the use of filters. Source B has a color temperature of 4800 K and is an approximation of noon sunlight and Source C has a color temperature of 6500 K which approximates average daylight. It should be pointed out that a source is a real light that can be turned on and off whereas an illuminant is defined as a spectral power distribution and it may or may not be possible to construct a source representing it.

Most non-blackbody sources can be described by the color temperature of the blackbody source that they most closely approximate. This temperature is called the correlated color temperature. However, most of these sources do not have spectral distributions that are similar to a blackbody source. Most will have skewed or cyclical distributions. This observation was first made by Grassman [137] and influences the appearance of color from reflected or transmitted light.

When light strikes an object several different phenomena can occur. Transmission occurs when the light travels through an object essentially unaffected if the material is transparent. If the material is colorless, all the light except that which is reflected at the surfaces will be transmitted. This reflection, as well as any scattering that may occur is the result of any changes in refractive index at the interface of the two materials. The refractive index is a measure of the speed of light in a material relative to the speed of light in air. At every interface, a small quantity of light will be reflected unless the light strikes the surface at a normal incidence.

In addition to transmittance, the light may be absorbed by the material. If the object absorbs some of the light, it appears to be colored and transparent. If all the light is absorbed, the object will appear black and opaque. Transmittance will be discussed later with the introduction of the Beer-Lambert law.

Scattering is the third phenomena that can occur when light strikes an object. This happens when some light is absorbed and re-emitted at the same wavelength but in a different direction. When enough scattering occurs, light becomes diffusely reflected from the surface. If only part of the light travelling through the object is scattered and the remainder transmitted, the part is considered translucent. Scattering is caused by light striking small particles in the material whose refractive index is different from the surrounding medium. The amount of light scattered is proportional to the difference in the two indices.

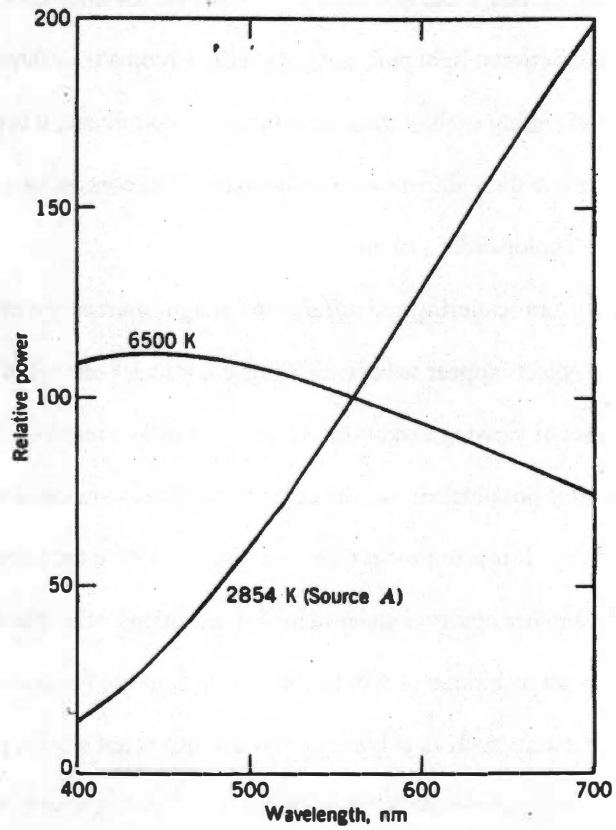


Figure 5.1 Spectral power distributions of blackbodies with color temperatures of 2854K and 6500K  
 [Source: F. W. Billmeyer, M. Saltzman, *Principles of Color Technology*, 2<sup>nd</sup> Ed. (Wiley, New York, 1981).]

Scattering is also proportional to the particle size; very small particles scatter very little light. From this, it is evident that pigment particles should have a larger difference of refractive indices from the medium to have better color properties at lower concentrations.

Color can be described by three separate parameters: hue, lightness, and chroma (colorfulness). Hue is the range of actual colors (green, blue, red, etc...). Lightness is the difference from light to dark across a single color (difference between light pink and dark red). Chroma is difference in saturation of a color (varying levels of gray). Treating each of these quantities as a coordinate, it is possible to describe the color of an object as a point in a three dimensional color space. The concept of a color space was used for the formation of the Munsell color-order system.

One interesting effect from scattering and differences in light sources is metamerism. Metamerism occurs when two objects appear to have the same color under one set of viewing conditions, but are different with another set of viewing conditions. This happens as a result of the materials having two different spectral curves. It is possible for two materials to have the same color space coordinates, but different spectral response curves. It is also possible for two objects to have the same color for one observer, but not the same for another observer under identical conditions. This phenomenon is known as observer metamerism. The easiest technique to avoid metamerism is to use the same pigments in both objects. When dealing with materials such as polymers or paints, this is not always possible.

There are several different color-order systems or color spaces that have been developed. Systems have been derived based on actual physical samples and some have not. Those based on actual samples are the most common systems. Wyszecki and Judd [138] have produced more complete collections. Collections of physical samples have been cataloged in a wide variety of methods, from random atlases to semi-ordered arrays. These catalogs are usually produced for the different colors for a specific product. They are fundamentally lacking in that they provide no description for intermediate colors. In industries such as printing and ink, colored samples are usually produced by combining several high chroma colorants together with varying amounts of black, white and grays. These systems do allow for interpolation for intermediary colors. Another system of color cataloging is the result of color mixing laws. One of the

more famous of these systems is the Ostwald [139] system. This technique used the combination of colored lights to quantify a sample color.

The best industry color-order system that has been utilized is the Munsell System shown in Figure 5.2 [134]. This system is based on the principle that samples are placed at equal visual perception differences and provides for a system for describing all possible colors in terms of Munsell Hue, Munsell Value and Munsell Chroma. The samples are arranged in planes of constant hue and Munsell Value in the vertical direction and Munsell Chroma in the horizontal direction. Rather than using XYZ coordinates, the Munsell system uses letters and numbers to denote a particular color in color space. The first number and letter combination represents the Munsell Hue. It is developed by equal spacing of the five major colors (red, yellow, green, blue, and purple) and the five adjacent pairs (e.g. green-yellow). The hue spectrum is divided into 100 equal sections. The Munsell Chroma and Value are written as a fraction. The Munsell system is accepted by industry for many reasons. First, its conformance to equal visual perception has become a benchmark for all color systems. Secondly, the system is not based on any particular pigment set and thus any conceivable color can be placed in it. The third advantage of this system is that the samples that are prepared are done so with extremely close tolerances. The major disadvantage of the Munsell System is that pigment composition is not stated so metameric pairs can be produced. Another disadvantage of the system is that the differences between the sample plaques are still quite large.

Several other methods of describing the color space exist, but it wasn't until the CIE system was introduced that any level of standardization existed in the industry. This is the system that is most commonly used with any instrumentation application. The system is similar to methods previously discussed, but it introduced the concepts of standard illuminant and standard observer. The standard illuminants were specified as Sources A, B, and C in 1931 as previously described [136]. There were additions made in 1965 when supplementary sources [136] were added that more closely simulated daylight. The "1931 meeting" also defined a group of standard observers whose color vision was representative of the average population with normal color vision. This standard defined a particular set of tristimulus values of the spectrum colors for a particular set of red, green, and blue primaries. This system had a disadvantage in that there were negative values across the spectrum range. A mathematical



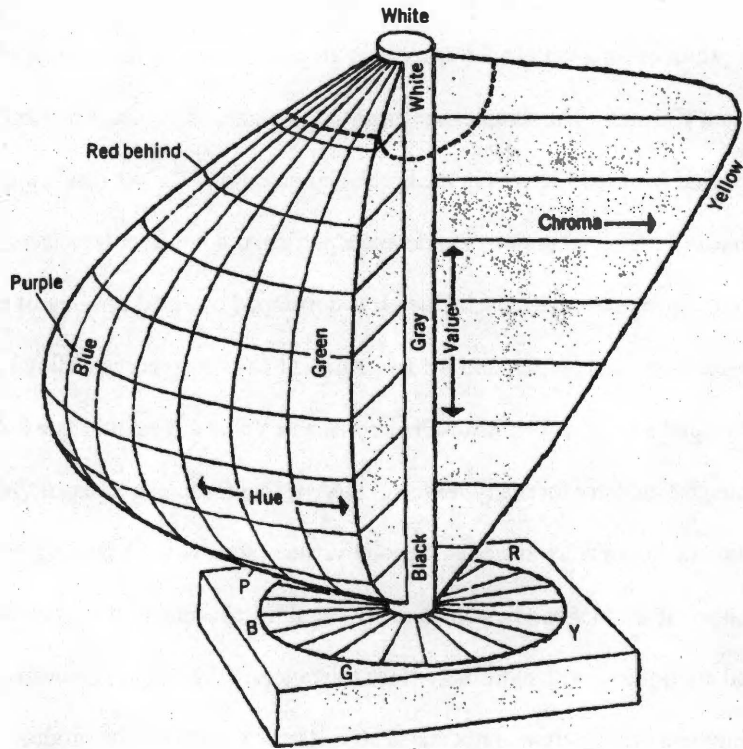


Figure 5.2 Dimensions of the surface-color-perception solid for the Munsell System  
 [Source: F. W. Billmeyer, M. Saltzman, *Principles of Color Technology*, 2<sup>nd</sup> Ed. (Wiley, New York, 1981).]

transformation was defined when the standard was adopted to eliminate this issue. This equal energy transformation for the standard observer functions is shown in Figure 5.3 [134]. The observer was adjusted again in 1965 to allow for a wider field of view for more practical color measurement.

The results of interest using this system are the tristimulus values  $X$ ,  $Y$ , and  $Z$ . These values are obtained by the product of the relative power of the illuminant, the reflectance of the sample, and the standard observer functions. These can be expressed as:

$$X = k \int PR\bar{x}d\lambda \quad (5.1)$$

$$Y = k \int PR\bar{y}d\lambda \quad (5.2)$$

$$Z = k \int PR\bar{z}d\lambda \quad (5.3)$$

where

$$k = \frac{100}{\int P\bar{y}d\lambda} \quad (5.4)$$

and  $P$ ,  $R$ ,  $\bar{x}$ ,  $\bar{y}$ , and  $\bar{z}$  are all functions of the wavelength  $\lambda$  with  $P$  as the power of the light source and  $R$  being the reflectance [134]. A graphical representation of this process is shown in Figure 5.4. A value of  $Y = 100$  is assigned for a perfect white object reflecting 100% at all wavelengths. Color as described by the CIE can be plotted on a chromaticity diagram. Most commonly, the color is plotted in the  $x, y$  plane. For the complete color spectrum, the resulting color space is similar in shape to a football.

Due to the non-linear nature of this color space, several attempts have been made to project it into a different space whose coordinates are easier to manipulate. Some of these attempts have tried to force the color space to be more uniform. This concept has yet to be perfected, but some approximations have greatly improved color measurement for products where color uniformity is critical. The most successful of these is the Hunter  $L, a, b$  space. It represented the introduction of opponent color scales. This approach was recommended by the CIE in 1976 [140] and was given the name CIELab. In CIELab,  $L$  is lightness,  $a$  is the difference between red (positive) and green (negative) and  $b$  is the difference between yellow (positive) and blue (negative). The color space can be obtained from the CIE values by the following:

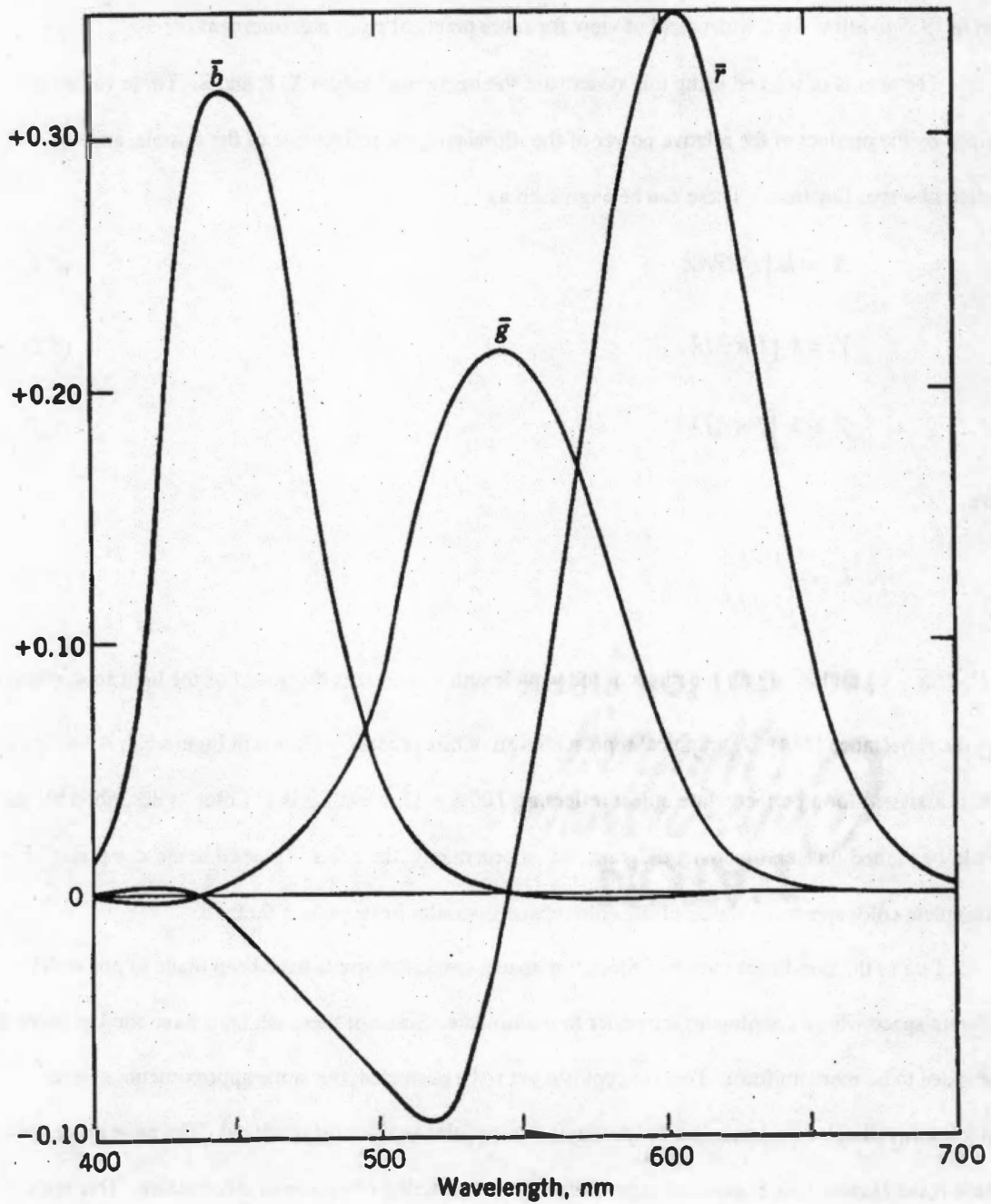


Figure 5.3 The tristimulus values of the equal energy spectrum colors  
 [Source: F. W. Billmeyer, M. Saltzman, *Principles of Color Technology*, 2<sup>nd</sup> Ed. (Wiley, New York, 1981).]

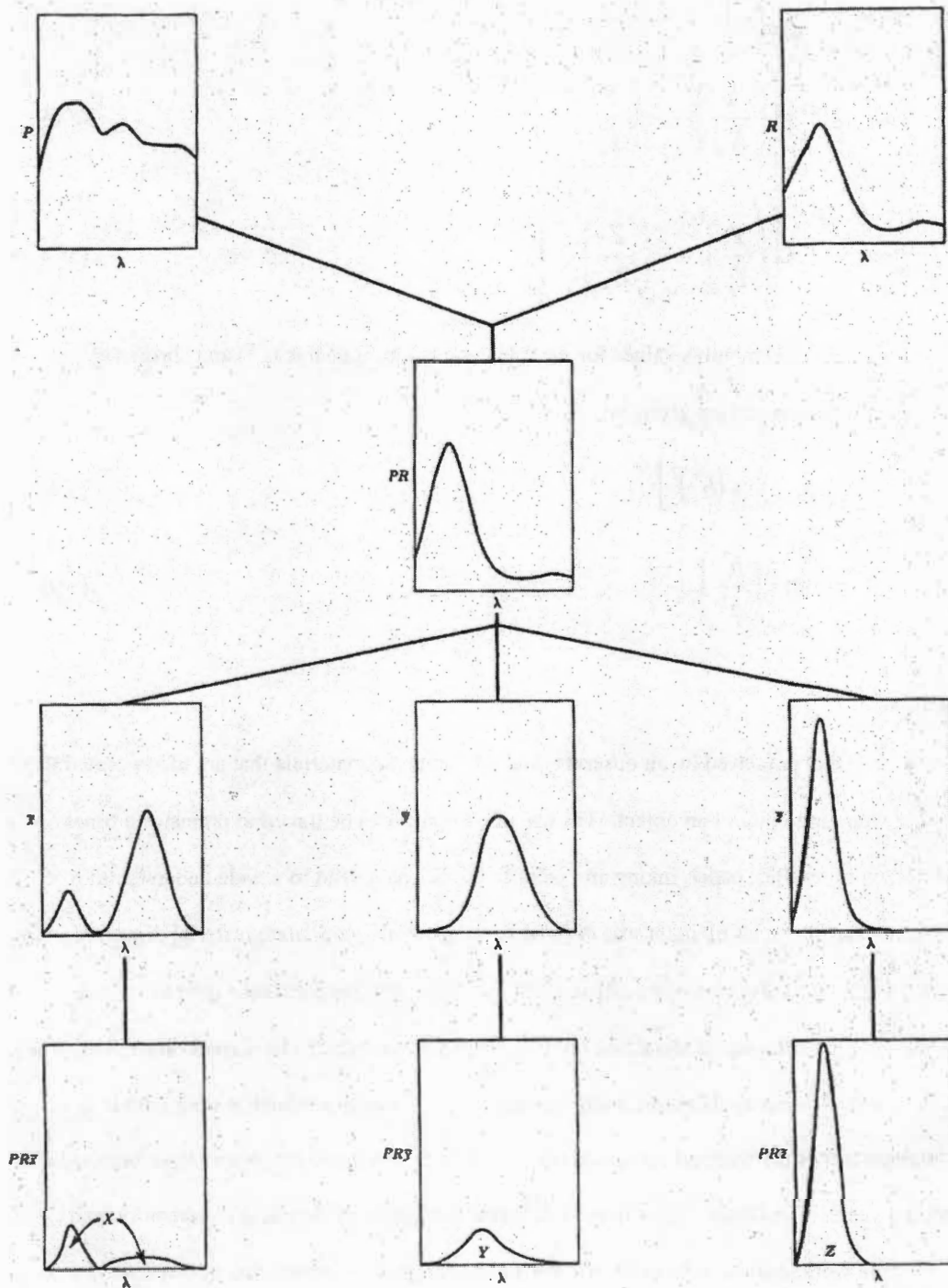


Figure 5.4 Spectral curves required to calculate CIE tristimulus values  $X$ ,  $Y$ , and  $Z$   
 [Source: F. W. Billmeyer, M. Saltzman, *Principles of Color Technology*,  
 2<sup>nd</sup> Ed. (Wiley, New York, 1981).]

$$L^* = 116 \left[ \frac{Y}{Y_n} \right]^{1/3} - 16 \quad (5.5)$$

$$a^* = 500 \left[ \left( \frac{X}{X_n} \right)^{1/3} - \left( \frac{Y}{Y_n} \right)^{1/3} \right] \quad (5.6)$$

$$b^* = 200 \left[ \left( \frac{Y}{Y_n} \right)^{1/3} - \left( \frac{Z}{Z_n} \right)^{1/3} \right] \quad (5.7)$$

where  $X_n$ ,  $Y_n$ , and  $Z_n$  are the tristimulus values for the reference white. The hue ( $C^\circ$ ) and chroma ( $h^\circ$ ) functions for the CIELAB system are given as:

$$C^\circ = \left[ (a^*)^2 + (b^*)^2 \right]^{1/2} \quad (5.8)$$

$$h^\circ = \tan^{-1} \left( \frac{b^*}{a^*} \right) \quad (5.9)$$

## 5.2 COLORANTS

Color is an effect perceived by an observer, and colorants are materials that are incorporated that have the effect of changing color of an object. The use of colorants can be traced to prehistoric times [132]. Development of textiles, paper, inking and paint industries have lead to a wide understanding of pigment and dye technologies. A pigment was defined as an insoluble particulate material dispersed in the medium it colored whereas a dye was originally defined as a water soluble substance used to color a material from an aqueous solution. It should be obvious that a colorant can fit both roles dependent on the application. For most polymer applications, pigments are utilized. Cases in which the pigment becomes soluble and migrates out of the material are called bleeds. A wide variety of substances have been used as colorants over the years. The *Colour Index* lists 31 different categories of chemical composition and summarizes multiple works that have been done in the field of organic pigments and a complete background is not necessary here [141].

When trying to match a manufactured part to a reference color, the most efficient way is to use the same colorants in both materials. This will guarantee that the manufactured part will have the same

spectral response as the standard under all light conditions. Problems arise when the same pigments can not be used due to issues such as chemical instability, thermal instability, solubility concerns, particle size and cost. Applications such as injection molding or cast film do not require high performance pigments since the observer will be seeing more bulk material which will increase the hiding power of the pigment. Film applications require more pigment dispersion to get the proper colorant dispersion. Depending on the application, hiding power is also required, such as for medical waste containers. Fiber applications have the most stringent requirements on pigments. The size of the individual fiber mandates that the pigment be well dispersed in the material. Large agglomerates of pigment will cause a weakness in the fiber, which could cause it to break during spinning operations. Requirements such as these will limit the color matcher's palette of possible pigments to use.

Proper pigment dispersion is the key to proper polymer coloring. Improper dispersion will result in agglomerate formation which reduces color strength. This can be compensated for by increasing the pigment loading, but this directly affects cost. A large number of agglomerates in the molten stream can lead to several processing problems such as screen blockage and produce rough surfaces on the finished part. Pigments range widely on ease of dispersibility. Large particle size materials, such as titanium dioxide, are easiest to handle. In general, inorganic pigments have larger particle sizes, but are not quite as easy to disperse as titanium dioxide. Organic pigments are usually the most difficult to disperse [133]. Some can be dry blended before compounding, but most require more intensive preparation before processing. Organic pigments are light and fluffy as well as carry electrostatic charges. Smaller particle size offers greater coloring strength, but the specific gravity can lead to metering and weighing problems. Many organic pigments are used as color concentrates in which the final processing step involves the addition of resin. These color concentrates improve the final product quality control in that the end manufacturer does not have to contend with variations in a dry color dispersion product.

### **5.3 COLOR AND COLOR DIFFERENCE MEASUREMENT**

As has been pointed out, the color of an object is dependent on the spectral distribution of the light source, the spectral transmittance or reflectance of the surface of the object, and the spectral response curve of the eye. Color measurement is done off-line and in most polymer processing plants, in a different resin

system than the actual part. Color measurement can be done on injection molded chips, blown film, or spun fibers. For applications where color is not tightly controlled, it is common to manufacture a chip or blow film in polyethylene and refer it to a standard. This will give a relatively good indication if the pigment loading is correct. These analytical steps take approximately 20 minutes to give an adequate answer. The addition of the fiber-spinning step for polypropylene products can add an additional 10 minutes to the sample time.

The CIE tristimulus values are obtained from spectrophotometric data for the product of the spectral reflectance of the sample, the relative spectral power of the illuminant, and the tristimulus value of the spectrum colors defining the CIE standard observer at each wavelength. These products are known as weighting factors and the technique is referred to as the weighted-ordinate method. With the exception of fluorescent materials, the nature and spectral power distribution of the source are of little importance for the calculation of tristimulus values. The only requirements are that the source is stable and emits sufficient power at each wavelength in the visible region. With the advent of more powerful computing capabilities, the accuracy in the measurement of the color is actually greater than the color difference in the materials. Color differences are only meaningful to the first decimal place as there is no visual difference beyond that point. As with the human eye, the phenomenon of instrument metamerism also exists. It is most common among dark and highly saturated samples. Due to this fact and also that all instrument manufacturers use different techniques for the optical measurements, color measurements should never be treated as exact numbers.

The ideal end result for color measurement should be a set of numbers that quantify the difference between the sample and the reference. There have been many color measurement techniques reported, unfortunately, conversion between different techniques is almost impossible. Current recommendations originate from the 1976 CIE meeting [142]. Most polymer products utilize the CIELab color difference equation.

$$\Delta E_{ab}^* = \left[ (\Delta L^*)^2 + (\Delta a^*)^2 + (\Delta b^*)^2 \right]^{1/2} \quad (5.10)$$

Substituting for hue, lightness, and chroma the difference is given by

$$\Delta E_{ab}^* = \left[ (\Delta H_{ab}^*)^2 + (\Delta L^*)^2 + (\Delta C_{ab}^*)^2 \right]^{1/2} \quad (5.11)$$

where the individual terms are defined in equations 5.5 through 5.9. These equations have been shown not to reproduce the Munsell color spacing well. The final judgement on whether or not a sample is within specifications will always be a visual comparison test.

#### 5.4 QUANTITATIVE DATA ANALYSIS

For an analytic technique to reach industry in any successful manner, it must be a robust technique that is relatively simple to perform, yet deliver useful information in a timely manner. Spectral measurements contain inordinate amounts of chemical and physical information. This makes practical interpretation of the data rather difficult. With recent advances in both physical equipment and computing power, a surge of research activity has occurred in these fields. The use of chemometrics, the use of mathematics and statistics on chemical data, has also made employment of industrial spectroscopic techniques feasible. Chemometrics is used to develop a correlation between experimental spectral data and a property of interest.

The data contained in the spectral curves are highly interrelated, and the essential information is contained in only a few redefined variables based on the physical system. The goal of any regression analysis is to develop a calibration model, which correlates information contained within a set of measurements to one or more properties of the sample. Multivariate regression techniques are particularly useful for calibration models because of the increased precision gained from using multiple channels of data.

There are six steps to the effective analysis of an analytical problem using chemometrics. These include data examination, preprocessing, model generation, model examination, prediction, and examination of the results.

##### 5.4.1 Data Analysis

The first step is to visually examine the data. This is done to identify any obvious errors in the data collection. Some of these include negative values, inappropriate clustering, or spread. The most common way to perform this analysis is to plot the data as it was originally collected. Errors can occur on



both the measurement side of the experiment, and the characteristic side. Mathematical manipulation of the data will only lead to meaningful results if the data itself is free of errors.

Outlying replicates must be eliminated to prevent their effect on any mathematical manipulation later in the process. One method proposed by Cochran [155], involves a univariate test method to compare the variance between several replicates and the sum of the variances. The sum of the variances for each of the samples is computed, and then each is ranked on the variability associated with that sample. If the variance exceeds a critical value, then that sample is assumed to contain one or more outlying replicate.

Principle component analysis (PCA) is a technique that can be used for preliminary data analysis. In this method, a new set of variables (eigenvectors or factors) are constructed that are linear combinations of those in the original data set, or the measured variables (spectra) are converted into new ones (scores on latent variables). These eigenvectors can be visualized as new axis within the data that are orthogonal to each other. The axes created from this technique are created in relative order of the amount of variance that each accounts for, i.e. the first eigenvector will account for the most variance in the data set. This analysis is designed to provide the best view of the variability in the data set. This will allow for the observation of natural clustering in the data set, the identification of outliers, and the dimensionality of the data to be determined.

Let  $X$  be a matrix of the data collected. PCA's goal is to find a new set of coordinates to project this data containing orthogonal axes. Using matrix decomposition, this  $X$  matrix can be written as a product of two matrices.

$$X = T L^T \quad (5.12)$$

Where  $T$  is the scores matrix and  $L$  is the loadings matrix. The new factors need to each be a linear combination of the original variables. How much each variable contributes to each factor direction is the information contained in the loading. High loadings for certain original variables on a particular eigenvector mean that these variables are important in the development of the new variable on that principal component. There are any number of sets of factor axes in which the axes are orthogonal, but PCA attempts to find the factors which capture to the highest level of variance in the data.

The first factors will account for the most amount of variance in the data, meaning that subsequent factors will model only a small portion of it. These later factors can be omitted without significantly affecting the ability of the new factors to generate the original data within some error,  $\epsilon$ .

$$\mathbf{X} = \mathbf{T}_k \mathbf{L}_k^T + \epsilon \quad (5.13)$$

With the proper choice of  $k$ , the magnitude of the data size can be dramatically reduced. The set of  $k$  factors after the data has been reduced are called the principal factors or components. One way to select  $k$  is to observe the eigenvalue (variance captured) and determine at which principal component the value reaches a constant value. This occurs when all relevant information is explained without including variation due to random errors, such as noise.

There are two main advantages from this decomposition. The first is that the new variables are orthogonal, which allows inversion of the matrix required in multiple linear regression (MLR) to be simple, unlike the normal case where all of the spectroscopic variables are highly correlated. Also, since the first new principal components account for the majority of the variance, and therefore meaningful information in the original data, the later ones must only account for noise and can be eliminated from further evaluations.

#### 5.4.2 Preprocessing

Once the data has been reviewed, it should be preprocessed as needed. The main goal of preprocessing or signal processing is to remove part of the noise present in the data, or eliminate some sources of variation, including background effects. Random or systematic noise can hide variations within the data set. There are several techniques that can be used to preprocess the data. Normalization is performed by dividing each variable by a constant. Normalizing to the unit area is called the 1-norm and defined as:

$$1 - norm = \sum_{j=1}^{n \text{ var } x} |x_j| \quad (5.12)$$

for all values ( $j$ ) of the vector  $\mathbf{x}$ . This is done to remove systematic variation within the data. The result of this manipulation is the maximum sum for the columns in the matrix with the result being a scalar.

Normalizing to the unit length (2-norm) is achieved by taking the square root of the sum of the squares.

$$2 - norm = \sqrt{\sum_{j=1}^{n \text{ var } i} |x_j^2|} \quad (5.13)$$

This manipulation forces the data range to be between 0 and 1, allowing for more straightforward statistical manipulation of the data. Preprocessing of the data set can also include sample weighting. In this process, each element in the data set is multiplied by a constant. This technique is similar to normalization, but different in the constants used. This is used when there may be differences in the way that the sample sets were collected to give more weight to those that are deemed more reliable.

Another method of preprocessing is smoothing. Smoothing is designed to reduce the amount of random noise in a data set in order to increase the signal to noise ratio. The underlying principle of this technique is that the noise will be at a higher frequency than the signal of interest. Smoothing can be visualized as a way to determine the value of interest at point  $j$  by utilizing the values surrounding that point. There are several ways to accomplish this. Mean smoothing refers to reducing the number of variables in the data set by averaging all of the points in a particular window  $n$  and performing this process for  $n$  times in the data set. A running mean smoothing is similar, but is done by moving the point being averaged along the entire data set, rather than after each  $n^{\text{th}}$  point. Smoothing can also be accomplished by using a running median smoother, which uses the same methodology as the running mean smoother, but the median value is used instead of the mean. This helps reduce the number of spikes that appear in the data set. A simple method of smoothing is simply to perform repeated measurement of the spectrum. In this way, the signal to noise ratio increases with the square root of the number of scans. With the speed of most spectroscopic systems, this is a relatively quick method. Other techniques include using a polynomial smoother or a Fourier filter smoother. Regardless of which smoothing technique is chosen, the result is a data set that contains few points, but at a cost of a reduction in resolution.

Baseline correction is the third major technique of data preprocessing. The main goal of this mathematical manipulation is the reduction of low frequency noise in the data set. These variation characteristics cannot be removed by signal averaging techniques. The most commonly used technique is to take the derivative of the data with respect to the independent variable. This is useful when the baseline may not be obvious in the data, or are inconsistent with each other. The more the data is processed in this

manner, the higher order terms in the baseline will be removed. Other techniques for baseline correction include explicit modeling, where the baseline is described as a function of the independent variable, and running difference equations, which are approximations to taking the 1<sup>st</sup> derivative of the data.

The third major area of preprocessing is manipulation of the variables. Mean centering is one of the major ways that this can be accomplished. This technique involves subtracting the mean of the variable vector from all of its elements. This removes the mean sample vector from all of the sample vectors from the beginning of the data analysis. This allows the regression to be performed on the differences in the spectral data, not the absolute values, and will eliminate the constant term from the model. Data sets that include an intercept should be treated this way. If its use is valid, the resulting regression models should be compared to models generated using non-mean centered data and should show a reduction in the amounts of error.

The variables in the sample set can also be preprocessed using a weighting function. A priori weighting is used if sufficient information is known about the past performance of the system. Variable selection sets the weight of some of the data to zero, if the non-zero values contain enough information to build a mathematical model. For example, in spectroscopy, variable selection is used to reduce the size of the data in regions where there would not be a meaningful spectroscopic response, due to the underlying chemistry not being active in this region. Variance scaling is used where the data is skewed due to the units. In this technique, each variable element is divided by its standard deviation to remove the weighting that is imposed due to the scale of the variable. Autoscaling the data will account for an intercept in the calibration model and remove differences in units between variables. Autoscaling consists of dividing each element in a column centered table (i.e. the difference of the value and the mean) by its standard deviation. This results in each column having a variance of one. This technique can be applied to give an indication about the relative importance of the variables, but this technique is typically not applied to spectroscopic data since it can inflate the noise in baseline regions.

In the case of very similar spectra, differentiation can help to identify differences in the spectra. By taking the second derivative of the data, one is able to remove constant and linear effects in the background simultaneously. Second derivative methods also create an inverse at the location of the

original peak. The drawback of differentiation techniques is that they decrease the signal to noise ratio, by increasing the noise. For this reason, if differentiation is chosen as a preprocessing method, it must be performed after smoothing of the data. Another disadvantage is that the calibration model may not be able to account for instrumental changes such as wavelength shifts, and require the modeling process to be repeated.

Preprocessing should be done as an approach to maximize the validity of the resulting models. Choices as to which technique to start with can be made with the knowledge of the behavior of the system of interest. For spectroscopic data, mean centering and the derivative techniques are used most commonly in order to eliminate baseline effects and ensure that the model is built to capture the differences in the spectra. For NIR data, variation between spectra is the result of three sources: non-specific scattering of the radiation at the surface of the particles, variable spectral path length through the sample, and the chemical composition of the sample. The main goal is to obtain the calibration from only the last source of variability. The best preprocessing method will be the one that will lead to the development of a robust model with the best predictive ability.

#### **5.4.3 Model Estimation**

The next step in the chemometric process is the development of a predictive model. A calibration model, or primary measurement, consists of a mathematical model relating an instrument's spectral output to the properties of the sample. For example, spectra from various chemical concentrations of samples in the calibration set are mathematically correlated to the actual chemical concentrations in the sample. Prediction is the use of this model to predict the sample's properties from the instrument's output of process samples. In order to construct this model, the instrument's responses of samples whose concentration levels are known are used to establish a mathematical relationship describing the property. The methodology used for building this model will depend greatly on the instrumental response used.

In some measurement systems, one instrument response can be attributed solely to the concentration of a single chemical component. This type of analysis is univariate calibration. In spectroscopy, the data that is contained in the spectra are related to the concentrations of the multiple chemical species present in the sample of interest. Because of the nature of the data sets, a multivariate

calibration models will have to be constructed. Multivariate techniques are used when the univariate technique will not adequately model the data. Multivariate techniques have four main advantages over a univariate technique. These include: simultaneous multiple component analysis, redundant measurements can increase the precision in prediction, redundant measurements can help identify fault detection, and the techniques can be used to replace traditional measurements.

Multivariate analysis can be divided into two main types, classical least squares (CLS) and inverse least squares (ILS). The choice of which technique to use is based on what is initially known about the characteristics of the system. For example, CLS is a valid technique when all of the analytes are known and that the pure spectra can be obtained directly. This method is useful for relatively simple systems that have responses that are dependant only on changes of concentration and do not contain responses that interfere with one another.

There are two main types of CLS that can be performed on spectral data, direct and indirect. Direct CLS is used where the analytes can be measured independently as pure samples. Indirect CLS is a technique to be employed where the analytes cannot be measured separately, and consists of a mathematical routine to obtain the pure spectra from the mixture's spectra. Both of these techniques require that all of the analytes of the system are known.

CLS is used in systems where there is a linear relationship between the measurement vectors and the concentration. As an example, consider Beer's law. If the path length is held constant, the product of the path length and the absorbivity can be rewritten as sensitivity ( $s$ ). If the law holds at multiple wavelengths, the absorbance at multiple wavelengths can be written as

$$A = cs \tag{5.14}$$

where  $A$  is the spectral response of the analyte at multiple wavelengths,  $c$  is the concentration and  $s$  is product of the absorbivity and the path length for multiple wavelengths, i.e. Beer's law for multiple wavelengths. CLS also requires the concept of superposition, or that the total instrument response is equal to the sum of the response from the individual components. This means that the concentrations can be written as elements of a vector quantity and the above equation can be rewritten as

$$A = cS \tag{5.15}$$

where  $\mathbf{S}$  is now the vector sensitivity at multiple wavelengths. This indicates that the mixtures response can be written as a superposition of the pure component spectra. The CLS model is then constructed by finding all of the spectra for the pure analytes to form  $\mathbf{S}$ . To use this as a prediction, the absorbance for the mixture  $\mathbf{A}$  is known and the  $\mathbf{S}$  matrix can be constructed. Equation (5.15) can be solved for  $\mathbf{c}$ :

$$\mathbf{A} = \mathbf{cS} \quad (5.16)$$

$$\mathbf{AS}^T = \mathbf{cSS}^T \quad (5.17)$$

$$\mathbf{AS}^T(\mathbf{SS}^T)^{-1} = \mathbf{c}(\mathbf{SS}^T)(\mathbf{SS}^T)^{-1} \quad (5.18)$$

$$\mathbf{AS}^T(\mathbf{SS}^T)^{-1} = \hat{\mathbf{c}} \quad (5.19)$$

where  $\hat{\mathbf{c}}$  is the estimated concentration.  $\mathbf{SS}^T$  is not always invertable and a substitution can be made in equation (5.19) to eliminate this problem.

$$\mathbf{AS}^\dagger = \hat{\mathbf{c}} \quad (5.20)$$

where  $\mathbf{S}^\dagger$  is the pseudo-inverse of  $\mathbf{S}$ , where the pseudo inverse is the generalization of the inverse for any matrix.

$$\mathbf{A}^+ = (\mathbf{A}^T\mathbf{A})^{-1}\mathbf{A}^T \quad (5.21)$$

This matrix can be used to predict the concentrations of all analytes.

To gain some measure of the model's fit to the spectral data, residuals can be calculated. The residual is the component of the mixture spectra that cannot be described using a model constructed from pure spectra. To calculate this, first a reconstructed mixture spectrum is generated using the estimated concentration and the substituting matrix  $\mathbf{S}$ .

$$\hat{\mathbf{A}} = \hat{\mathbf{c}}\mathbf{S} \quad (5.22)$$

The residual is the difference between this quantity and the measured absorbance.

$$\mathbf{Residual} (\mathbf{R}) = \mathbf{A} - \hat{\mathbf{A}} = \mathbf{r} - \hat{\mathbf{c}}\mathbf{S} \quad (5.23)$$

The closer this vector is to zero, the better the model, because the difference of  $\mathbf{c}$  and  $\hat{\mathbf{c}}$  is an indication of how close the created model fits the actual data. So long as the three assumptions are valid (known pure spectra, linearity, and linear additivity), calibration is as straightforward as obtaining the spectra of the pure components.

Indirect CLS is used when the pure spectra are not known directly, but estimated from mixture spectra. To perform this, several mixture spectra need to be collected using experimental design with known concentrations ( $\mathbf{c}$ ). The mixture spectra ( $\mathbf{A}$ ) are related to the desired pure spectra ( $\mathbf{S}$ ) by

$$\mathbf{A} = \mathbf{cS} \quad (5.24)$$

With known quantities for  $\mathbf{A}$  and  $\mathbf{c}$ , the goal of obtaining the pure spectra can be estimated using

$$(\mathbf{c}^T \mathbf{c})^{-1} \mathbf{c}^T \mathbf{R} = \hat{\mathbf{S}} \quad (5.25)$$

Designed experiments must be used so that  $\mathbf{c}^T \mathbf{c}$  exists.

For cases where the system of interest is more complex or not all of the analytes are known, an inverse calibration technique must be used. These techniques do not require that the spectra of the pure analytes are measured. Three main inverse techniques exist. These include MLR, PCR, and PLS. By the very nature of the measurement problem with spectroscopy, it can be seen that multivariate analysis must be used, but the choice of technique is also dependant on the data.

All three of these techniques are similar in how the measurement and the concentrations are modeled. The concentration ( $\mathbf{c}$ ) is treated as a function of the responses where  $\mathbf{b}$  is the unknown.

$$\mathbf{c} = \mathbf{Ab} \quad (5.26)$$

While this equation looks very similar to the approach taken in CLS, the techniques used are different. In this case, the concentration is presented as a weighted sum of responses, whereas the CLS model is a linear combination of the pure spectra. The regression coefficients can be estimated as

$$\hat{\mathbf{b}} = (\mathbf{A}^T \mathbf{A})^{-1} \mathbf{R}^T \mathbf{c} \quad (5.27)$$

The quantity  $(\mathbf{A}^T \mathbf{A})^{-1} \mathbf{A}^T$  can be expressed as  $\mathbf{A}^\dagger$ , the pseudo-inverse of  $\mathbf{A}$ . With this transformation, equation (5.27) can be rewritten as

$$\hat{\mathbf{b}} = \mathbf{A}^\dagger \mathbf{c} \quad (5.28)$$

With the unknown sample spectrum ( $a_{unk}$ ) and the regression coefficient, it is possible to estimate the concentration.

$$\hat{\mathbf{c}} = a_{unk} \hat{\mathbf{b}} \quad (5.29)$$



The difference between the three techniques is the way that the transformed pseudo-inverse matrix is calculated [155].

MLR attempts to solve the inversion problem by selecting at least as many variables as there are sources of variation in the system. Typically, this involves choosing a statistical algorithm with underlying assumptions. MLR is beneficial as a modeling technique because it can be used to design simple measurement systems and the resulting models are simple to understand and diagnose. It is weak in several areas. It has limited outlier detection capabilities. There is no straightforward technique for optimal variable selection. It has limited use as a multivariate technique due to the small number of variables used. It is relatively weak for complex systems. The statistical assumptions are not always valid and can be misleading. PCR approaches the model problem by converting the physical variables into principal components that describe the variation in the data.

PLS and PCR are the most widely used techniques in chemometrics. There are two main advantages using this approach over multiple linear regression (MLR) as a result of PLS and PCR being full spectrum techniques. The first is that by using more of the spectrum rather than a stepwise approach, the model will be more sensitive to detecting outliers. The second advantage of the model is it has better signal averaging properties. These two advantages arise from the use of more variables to model the spectral data.

The inverse model can be written as

$$\mathbf{c} = \mathbf{R}\mathbf{b} \tag{5.30}$$

where  $\mathbf{c}$  is a vector (# of samples x 1),  $\mathbf{R}$  is a matrix of measurements (# of samples x # of variables), and  $\mathbf{b}$  contains the model coefficients (# of variables x 1). The problem is solving for  $\mathbf{b}$  is that the matrix  $\mathbf{R}^T\mathbf{R}$  is not invertible. This can be overcome using PCR by creating a matrix  $\mathbf{U}$  with columns that are linear combinations of the original columns in  $\mathbf{A}$ . This matrix will have the same number of rows as  $\mathbf{R}$ , but fewer columns:

$$\mathbf{c} = \mathbf{U}\tilde{\mathbf{b}} \tag{5.31}$$

where  $\tilde{\mathbf{b}}$  is the new regression vector and  $\mathbf{U}^T\mathbf{U}$  is now invertible.

U can be constructed several different ways. PCA is an easy way to find linear combinations of variables that will describe row space variation in R. U will be the scores matrix from PCA. The scores matrix is related to the original matrix R as

$$\mathbf{R} = \mathbf{USV}^T \quad (5.32)$$

where

U = score

V = loadings matrix

S = diagonal matrix of singular values

The scores matrix gives the location of the samples relative to one another in row space. The diagonal elements contain the information of how much variance each of the principal components describes. Due to the orthogonal property ( $\mathbf{V}^T\mathbf{V} = \mathbf{I}$ ), (5.32) can be solved for U as [155]

$$\mathbf{U} = \mathbf{RVS}^{-1} \quad (5.33)$$

Care must be used in selecting the minimum number of principal components so that the inverse is stable. The principal components used are chosen sequentially starting with the one with the highest percentage of variance explained. This equation also demonstrates why the number of columns in the calculation needs to be reduced. U is a function of  $\mathbf{S}^{-1}$ .  $\mathbf{S}^{-1}$  is calculated by taking the inverse of each of the diagonal elements of S.

Given a truncated U matrix, the regression vector b can be solved as

$$\tilde{\mathbf{b}} = \mathbf{U}^T \mathbf{c} \quad (5.34)$$

where the orthonormal property U is used.  $\tilde{\mathbf{b}}$  is the estimate of  $\tilde{\mathbf{b}}$ . The regression vector can then be used to predict the concentration in an unknown sample using a two-step process. First, given the measurement of the unknown ( $\mathbf{r}_{un}$ ) and the V and S from the calibration, the score vector for the unknown is found using (5.33)

$$\mathbf{u}_{un} = \mathbf{r}_{un} \mathbf{VS}^{-1} \quad (5.35)$$

This  $\mathbf{u}_{un}$  and  $\tilde{\mathbf{b}}$  from (5.18) can be used to predict the concentration of the unknown using (5.31)

$$\hat{\mathbf{c}} = \mathbf{u}_{un} \tilde{\mathbf{b}} \quad (5.36)$$

These processes can be combined into one step. If  $u_{un}$  of (5.36) is replaced with the right side of (5.35) then

$$\hat{c} = r_{un} (VS^{-1}\tilde{b}) \quad (5.37)$$

Even though the PCR model is written to relate score vectors to concentration, it is still a linear combination of variables being used to estimate the concentrations.

The difference between PCR and PLS is the way that the linear combinations of variables for the columns of U are chosen. PCR only uses the R matrix to determine the combinations. Concentrations are used in estimating the regression coefficients (5.34), but not in the estimation of U. The disadvantage of this technique is that variation in R is not correlated with the concentrations used in U. If the variation related to the concentrations is small compared to the overall variation, PCR will not find the appropriate linear combinations of variables to model the concentrations. In PLS, the covariance of the concentration measurements is used with the variance in R to calculate the surrogate matrix. PCR's U matrix will be determined independent of the different analytes.

There are several advantages to using PLS and PCR that MLS also has. One, these techniques provide excellent diagnostic tools as will be discussed in model validation. They also account for a large amount of variation within a data set without identifying the source. This allows for implicit modeling if the variation is present in the calibration set. These techniques also use the full spectrum approach allowing for built in redundancies in the model. The limitations of these techniques include the need for many samples to be used in creating the calibration model. Rank determination is not necessarily straightforward. The excellent diagnostic tools require patience in reviewing for inconsistencies.

For the analysis of spectroscopic data containing overlap and combination effects, it can be seen that a univariate technique would not be adequate to build a calibration model. First, there is a great more deal of information contained in a multivariate model. The behavior of the spectral regions of interest is a function of combination bands and overtones in which the different regions of the molecule interact with each other in the spectral response. Because of the behavior of the turbidity in the melt, it would be impossible to obtain the neat spectra of each component and generate a calibration model for the entire concentration range of interest. A technique such as MLS would be easy to model, but does not contain advantages such as signal averaging, and requires too many statistical assumptions that may not be valid for

the data set. MLS is also limited to cases where the number of variables does not exceed the number of samples. This leads to MLS attempting to over fit the data if it contains noise. This leads to the use of PCR and PLS. PLS was chosen in this work because both modeling techniques present similar results, but PLS uses both the  $R$  and the  $c$  matrices to generate the linear combination of variables. This is useful in highly complex spectra.

PLS models the relationship between the independent and dependent variables more closely than PCR and usually requires fewer principal components in creating the calibration model. As was presented, PCR is factor analysis followed by a regression step. While it uses the same inverse least squares approach as MLS, it uses the principal components rather than the original variables. This combines the advantage of using all of the variables, avoids unnecessary noise, and retains the MLR independence of uncalibrated components. Factor analysis reduces error in the independent variables and the regression minimizes errors in the dependent variables.

Multivariate techniques will not only model the measurement of interest, but also the noise contained in the system. Therefore, care must be used in the selection of the model size. Too many variables will cause the model to account for the noise in the sample data set; too few will not allow the model to capture the important characteristics.

Another important aspect is the development of the calibration data set. In classical calibration, the resulting signal is a function of concentration. This signal is subject to noise, but the assumption is made that the concentration is exactly known. In multivariate calibration, the concentrations of all components that influence absorbance in spectroscopy do not have to be known. In this case, the concentration becomes a function of the signal. The resulting regression parameters will be biased as well as the predicted concentrations obtained from this model. However, the resulting predictions will be more precise than those obtained through classical calibration. This is the result of the least squares step involves a minimization of the sum of squares in the direction of concentration, rather than the direction of the signal.

#### 5.4.4 Model Validation

Once the regression of the data has been performed, many software packages will also give diagnostic tools to evaluate the validity of the model. The goal of which is to determine the minimum number of factors required in the model. Too few factors and the model will not accurately represent the information contained in the spectra. Too many factors and the model will try and correlate noise in the model. The range of the calibration model can be divided into several local models rather than one global model to improve the predictive ability of the model. Additionally, because such techniques of PCA and PCR are least squares based models, they are sensitive to the presence of outliers.

A percent variance table can be used to look at the number of factors and ensure that there is decreasing variance with increasing factor number. This will also provide a good place to identify the minimum number of factors to be used in the model. A cumulative value with factor number of the percent variance can explain the total amount of independent data (X block) and dependant data (Y block) variance explained with that number of factors. The variance explained can also be compared to the amount of noise in the data. Most software packages will give both the concentration variance ( $c$ ) and the measured variance ( $R$ ). It is important to determine if the number of factors chosen account for both of these variances.

A plot of the root mean square error of prediction can be used to analyze the model. This function is defined as

$$RMSEP = \sqrt{\frac{\sum_{i=1}^{nsamp} (c_i - \hat{c}_i)^2}{nsamp}} \quad (5.38)$$

If using a cross validation approach, the original calibration data set is divided into calibration and prediction subsets. The roles of each subset are then reversed so that each of the samples in the data set is predicted once. Another technique is leave a sample cross validation in which the data set is divided into  $n-1$  and 1 samples. The  $n-1$  samples are used to build the model and then the left out sample is used for prediction. The process is repeated until each of the samples has been left out once. The error in (5.38) can be plotted against the number of factors until a minimum is found. Ideally, this function will have a

specific minimum, but there can be cases where there is no minimum (where additional factors decrease the RMSEP), or even erratic behavior. The no minimum case is common in spectroscopic studies, in that the RMSEP will continue to decrease, as more factors are included in the model resulting in more variation in the data being accounted for. In this case, the number of factors used is chosen by setting tolerances in the error values of interest. The erratic behavior case suggests that the model was not able to accurately describe the variation in the data set.

The predicted residual sum of squares value (PRESS), the residual error term, can be calculated from

$$\text{PRESS}_j = \sum_{i=1}^N (y_i - \hat{y}_{i,j})^2 \quad (5.39)$$

where

$j$  = number of factors in the model

$y_i$  = actual property value of the  $i$ -th sample

$\hat{y}_{i,j}$  = predicted property of the  $i$ -th sample for a calibration model built with  $j$  factors

$N$  = number of samples used for cross validation.

A PRESS value is plotted against the number of factors used in constructing a given model. The number of factors can be chosen to minimize the PRESS value and this number is used in the final calibration model.

The PRESS value can be converted into units of the measurement. Standard Error of Prediction (SEP) takes into account the number of samples tested, and the Standard Error of Calibration (SEC) takes into account both the number of samples used to make the model, but also the number of factors contained in the model.

Another technique that can be used is a plot of the predicted concentration versus the actual concentration. The ideal behavior would be a line with a slope of one that crosses the y-axis at zero. This plot is also useful for identifying unusual samples in the data set. These outliers would be far away from the line in the plot. This plot should be viewed for bias or lack of fit of the data.

A loadings plot can be constructed to help determine the optimal number of factors to be used in the model. For analysis of spectroscopic data, the number of factors used usually coincides with the

maximum number used before the loading start displaying random behavior. The loadings are also useful in evaluating which variables contribute most to the model. They represent the relative contribution of the variables. Points of interest to investigate are those where the frequency of the loading is much different from the frequency of the original spectra. One use of this information is to find the number of factors at which the loading's behavior becomes random, i.e. the number of factors at which the loadings contain high frequencies.

A plot of the scores can be used to evaluate the effectiveness of the regression model. It can be used to determine the homogeneity of the samples and for identification of outliers. This plot can be analyzed for consistency with what is known about the data set. For example, are the scores constantly increasing as a function of the concentration, which follows the behavior of the concentration in the data set? Analysis of all of these will lead to some indication of the reliability of the regression and an understanding of the spectra.

#### 5.4.5 Prediction

This step in the chemometric process is simply the application of the previously developed model on an unknown sample. The output of this step is the predicted properties of the unknown data set. This is the important application of all of the development work.

#### 5.4.6 Prediction Validation

The best technique for validating the prediction is to plot the measured concentration versus sample number. This plot can then be investigated to see if the concentrations measured are valid in comparison with the range that the values should be in. The spread of the data can also be compared to the error of prediction to determine if the model is accurate.

The residual errors can be statistically averaged to form the standard error of calibration (SEC). The calibration set error is

$$SEC = \sqrt{\frac{\sum_{i=1}^{NC} (y_{i,c} - \hat{y}_{pi,c})^2}{NC - 1}} \quad (5.40)$$

where  $\hat{y}_{pi,c}$  and  $y_{i,c}$  are the predicted and actual properties. The standard error of prediction (SEP) is

$$SEP = \sqrt{\frac{\sum_{i=1}^{NP} (y_{i,p} - \hat{y}_{pi,p})^2}{NP}} \quad (5.41)$$

where  $\hat{y}_{pi,p}$  and  $y_{i,p}$  are the predicted and actual properties in the calibration set. The SEC and SEP values give a reasonable indication of the accuracy of the calibration models. Limits on processing theoretically can be set to within the SEP and SEC values.

#### 5.4.7 Summary

The preceding sections are intended to give an introduction to the accepted mathematics of color and the mechanics of multivariate calibration techniques. The development of a calibration model is not a trivial task, not only due to the complexity of the analysis itself, but the interaction of error and variance within the data set for complicated systems such as spectroscopic data. By understanding the details of the regression techniques and the requirements of the analysis, the proper chemometric tools can be selected for the task. The goal is to identify a method that is suitable for the regression task and ensure that the data is in a manner where no avoidable sources of error or inaccuracy are present in the model.



## CHAPTER 6

### RESEARCH OBJECTIVES

#### INTRODUCTION

The status of on line process measurement and control has changed drastically over the last two decades. As more and more once classified spectroscopic and imaging technologies become available to the general scientific community, numerous applications for the new technologies have been sought out. Spectroscopic techniques are now accepted as a rapid, non-destructive analysis for process monitoring in real time. These techniques have found use in a variety of research and manufacturing applications, such as polymers, textiles, specialty chemicals, pharmaceuticals, and agriculture.

Polymer science has benefited from these advances as well. Work in the last decade has investigated the use of fiber optic technology for the study of molten polymer systems. These include the study of polymer melts [9], real time concentration monitoring [2,10-12], and the measurement of polymer rheology properties [2]. These studies focused on low concentration levels of additives in the melt. While these are important data sets for manufacturers such as resin producers, no work was conducted on highly loaded systems such as those typically found in the production of concentrates. There has also been work in the study of various spectroscopic techniques for the relation of spectroscopic information to physical properties as related to chemical composition. To develop a complete feedback control system for polymer compounding process, the understanding of not only measurement of chemical composition, but also the complex interactions of chemical composition on physical properties must also be obtained. It is the goal of this research undertaking to address these issues as related to process control.

#### 6.1 PROBLEM STATEMENT

The general objectives of the current research can be classified into the following broad categories:

- (1) Estimate concentrations of highly loaded anti-oxidant and ultraviolet stabilizer polymer additives in polypropylene by conducting feasibility studies utilizing fiber optic near infrared, ultra violet, and Raman spectroscopy techniques.

(2) Estimate concentration levels of diazo condensation and phthalocyanine pigment in polypropylene and conducting feasibility studies utilizing fiber optic near infrared, ultra violet, and Raman spectroscopy techniques.

(3) Quantify the effects of pigment concentrations on the rheological properties of polymer melts, and correlate the spectra with the rheological properties of polymer melt.

(4) Perform feasibility studies of simultaneous in-line monitoring of pigment and additive concentrations utilizing fiber optic NIR, UV, and Raman spectroscopy techniques.

The focused work of this dissertation is unique for two main aspects. First, the concentrations of additives and pigments investigated are orders of magnitude higher than those studied in previous research. These levels are typical of practical industrial levels rather than the final end use level. The other unique feature of this work is the development of a flow cell that is compatible with actual production equipment. Prior research utilized bench scale flow cells and inferred that the technique could be scaled up for the manufacturing environment. In this work, the measurements were made on actual manufacturing process equipment in a commercial environment.

#### **6.1.1 Estimation of Additive Concentrations in Polypropylene During Extrusion**

In this research, a systematic approach to the measurement of ultraviolet stabilizers and antioxidant additive concentrations in an in-line polymer extrusion process will be developed using spectroscopic techniques. This technology will utilize the two main on-line spectroscopic techniques (NIR and UV) for feasibility studies for real time measurements. This work will investigate and correlate absorption spectra from the various spectroscopic methods to the actual instantaneous composition during extrusion. Composition has been shown to be heavily correlated to different spectral signatures at different wavelength regions. This work will also look at the various secondary effects that emerge as changes of rheological flow effects during extrusion. These will be presented in a later section.

The monitoring of additive concentrations can be a daunting task for most polymer applications. This work focuses on the compounding industry problem where the additives are being used in the manufacturing of master-batch products, or products with high additive concentrations that will be diluted before production of the final product. The research will focus on two main classes of polymer additives

used in polypropylene fiber production, ultraviolet stabilizers and antioxidant additives. The additives chosen for this study represent the most commonly used additives for this application and all are widely commercially available.

The original contributions in this area of study are two-fold. The first is the measurement of additive concentrations that are several orders of magnitude higher than those that have been studied in prior dissertation research. This work is also focused on not only a new industry, but also using realistic sample sets. By focusing on one of the more difficult sides of the polymer processing industry, the bringing to fruition prior laboratory research is demonstrated.

The second aspect that is original in this work is the development of a commercial grade flow cell. Prior work was focused on a small-scale lab extruder with a throughput on the order of 5 pounds per hour. This research was focused on the thirty to forty pound per hour range on an actual production extruder. This flow cell could be directly attached to even larger processing equipment with no significant modification. The combination of these two factors was designed to demonstrate the practical commercial manufacturing application of these techniques.

### **6.1.2 Estimation of Pigment Concentrations in Polypropylene During Extrusion**

The second focus of this research is similar to the first. Here again, a systematic approach will be made in the measurement of pigment concentration during a polymer extrusion. Traditionally, color is measured using optical equipment on a sample in the final product form, either an injection molded part or a cast or blown film. This part is then placed in either a colorimeter for parts in which color is not critically important or in a spectrophotometer where color is a critical property such as in fiber. Historically, all color measurement has been in the visible region with little significant work being done on spectroscopic measurement to correlate color properties [134].

This research will investigate the feasibility of correlating spectral data with final-part-color properties. It is worth pointing out that the specification of final-part-color is still subjective, but it is necessary to obtain a baseline for employing color control techniques [138]. A methodology is demonstrated which uses this correlation to perform such an analysis. The benefits and disadvantages of

the spectroscopic approaches will be discussed. The research will focus on high performance pigments used in the production of fiber products.

The original contribution of this component of the research is that this type of measurement has not been done before. Prior online spectroscopic research has been focused on low levels of additives for the determination of polymer composition. Pigments are one of the more complicated issues to deal with due to the highly subjective nature of assigning quantitative data to quality measurements. In this work, a practical technique is proposed to treat the pigment concentration as another chemical constituent and determine if real time measurements are feasible. Along with the feasibility of the measurements, the practical limitations of this approach are also discussed.

### **6.1.3 Monitoring the Effects of Pigment Loadings on Rheological Properties of Polypropylene During Extrusion**

This research will focus on the development of a spectroscopic technique to monitor the rheological properties of a polypropylene system during extrusion. The methodology developed correlates the rheological properties of interest with the various absorption spectra. A systematic screening of the three on-line spectroscopic techniques was made and the advantages and disadvantages of each are discussed.

It is a goal of this project to separate the effects of composition and rheology on the spectra. By doing so a separate algorithm can be developed for the in-line monitoring of melt index and complex viscosity. The pigments chosen for this system are high performance pigments for the fiber industry, and are representative of those used for the production of carpet fiber. The concentration ranges chosen represent concentrations typically used in the production of color concentrates by the compounding industry. These loadings are significantly higher than loadings that would be found in a final finished product.

The original contribution to this field is the extension of prior work focused on real time melt index measurements. The measurement of melt index is the only main practical rheological measurement that is reported in quality measurements. The rheology of highly loaded concentrates can greatly change the nature of the rheology due to pigment/additive interactions. By demonstrating that real time

measurements can be made on these systems, a further advantage of the spectroscopic technique is highlighted.

#### **6.1.4 Feasibility of Simultaneous In-line Monitoring of Pigment and Additive Concentrations in Polypropylene During Extrusion**

Only in extremely rare occurrences is a compounded polymer system a binary mixture. Product performance demands mandate that various additives are included to increase the longevity of the final product. Additives are included in product formulation to increase product life, aid in processing, add a physical characteristic (such as flame resistance), or reduce the product cost. All of these requirements must be met with the final product meeting the appearance requirements as well.

This research endeavor investigates the feasibility of simultaneous measurement of additive concentrations and pigment loadings. This is the proof of concept that will allow for practical in-line process monitoring in the compounding field. Results of the three previous sections will be combined to evaluate the instrumentation requirements needed for the development of a robust feedback control system. The product systems chosen for this evaluation are representative of the product formulation supplied to the fiber industry.

As will be discussed, pigment dispersion will play a large factor in this role. Due to the high light scattering associated with highly loaded pigment systems, alternative techniques would have to be developed to gather further information as to the degree of dispersion in the polymer system. The original work in this field was focused on developing the use of confocal laser scanning microscopy for pigment dispersion evaluation. This technique had never been used for this application, and the research was focused on both the feasibility of this technique and the determination of the practical limitations.

## CHAPTER 7

### EXPERIMENTAL SETUP

Figure 7.1 illustrates a schematic of a system for in-line fiber optic spectroscopy of molten polymers during extrusion. Solid polymer pellets are melted by heat and shear in the barrel of a ¼ inch single screw extruder. This extruder has an L/D ratio of 25:1. A stabilized flow is delivered to the variable path length flow cell via a gear pump. Temperature controllers in the extruder allow for a temperature profile that is conducive for homogeneous melting and proper material transfer rates. Temperature in the flow cell is also controlled and can be independently set. A control system is in place that will allow for the temperature and pressure in the cell to be maintained. Dynisco pressure transducers are utilized to measure the upstream and downstream pressure conditions.

Figure 7.2 shows a schematic of the lab scale flow cell, which has ports for the attachment of two fiber optic probes. The flow cell is located downstream of the gear pump and allows for a rectangular flow pattern to be developed. The flow channel has dimensions of 25 mm in width by 9.5 mm high and 18 cm long. Dual transmission fiberoptic probes are used to transmit light through the flow stream. The probes have a housing that was first developed and commercialized by Sensotron, Inc. The optical path length between the probes can be altered by use of ring spacers of different thickness. This path length can be altered from 1.0 to 9.5 mm. The path length is optimized for Beer-Lambert's law so that a linear relationship exists for absorbance to concentration. This has a secondary benefit in that by having lower absorbance, it will have a higher signal to noise ratio. Detailed research was conducted on this probe design by Khettry [9], Vedula [2] and Li [46]. Figures 7.3 and 7.4 present schematic diagrams and the composite housing for this probe design.

The NIR system used for this study consists of an NIR source, two fiberoptic cables, two NIR transmission probes, a flow cell and an NIR detector. The NIR light is produced by the source and is then transmitted through the first fiber to the first transmission probe. The light is then selectively absorbed in the molten polymer stream and collected by the opposite transmission probe. This transmitted light is then transmitted via the other fiberoptic cable to the detector. A Diamond-20<sup>®</sup> FTIR spectrometer produced by

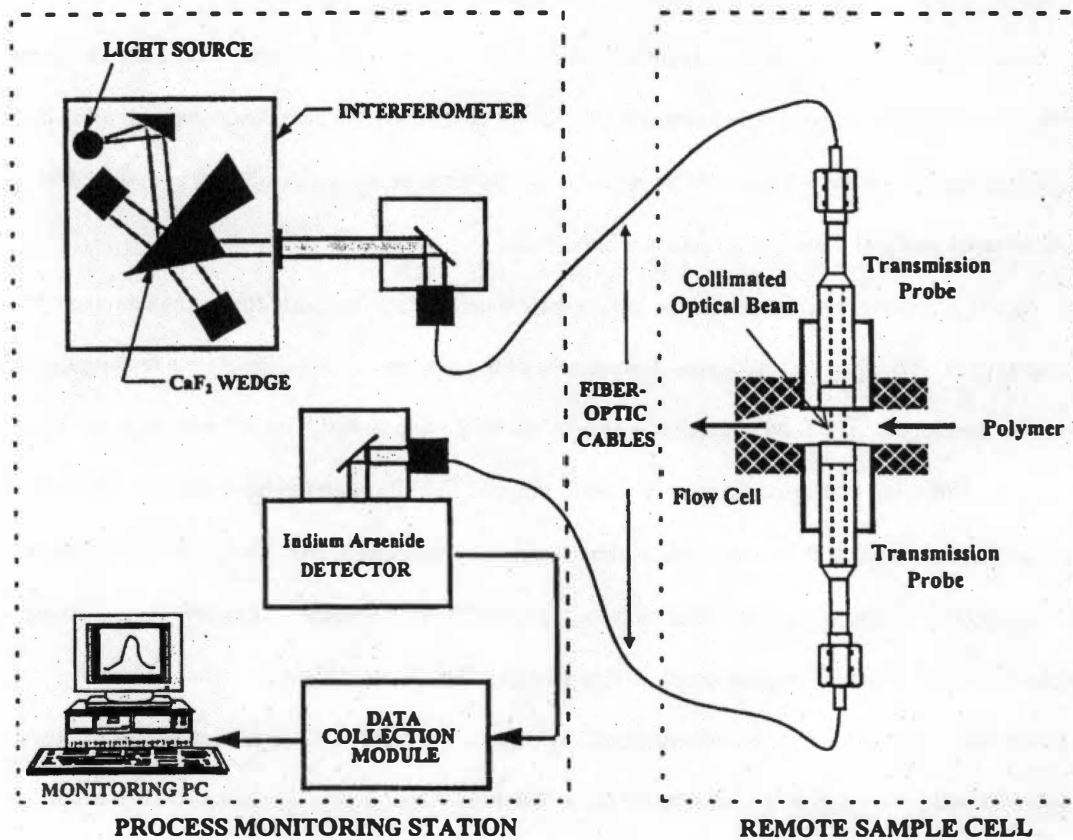


Figure 7.1 Schematic of the experimental setup of in-line FTNIR spectroscopy of molten polypropylene

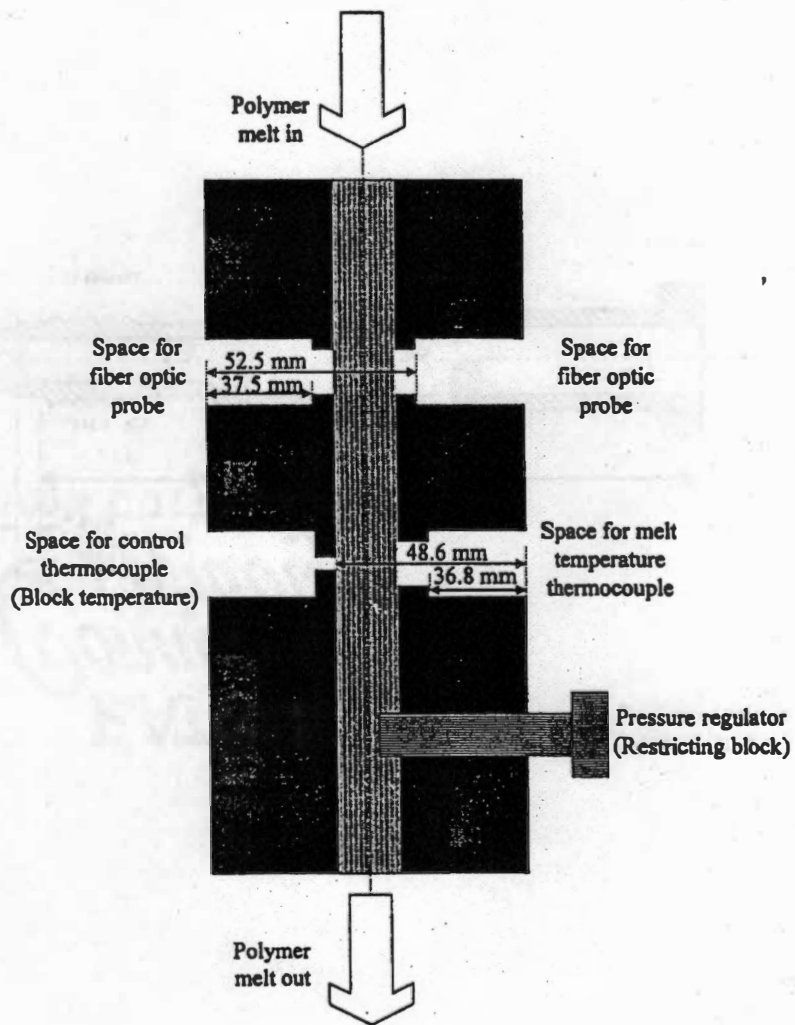


Figure 7.2 Detailed schematic of a variable path length flow cell



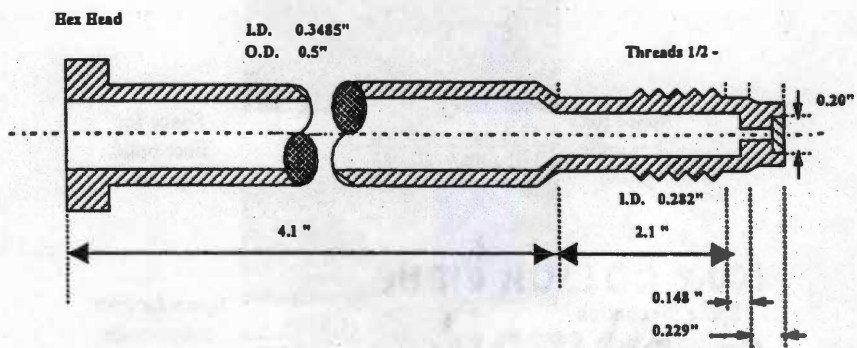
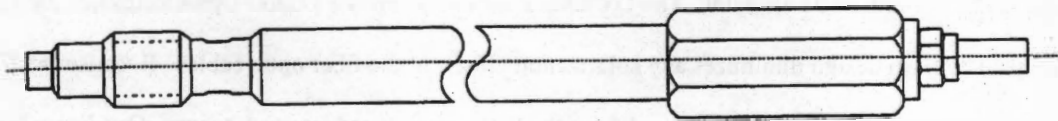


Figure 7.3 Schematic representation design of Sensotron transmission fiber optic probe



**Figure 7.4** Composite design of Sensotron transmission fiber optic probe

Orbital, Inc. is used as the analyzer in this system. The NIR light is produced by a quartz halogen lamp and detected by a indium arsenide detector with a calcium fluoride window.

The interferometer works on the moving wedge principle. The spectral range covered by this setup is  $12,000\text{ cm}^{-1}$  to  $1,200\text{ cm}^{-1}$ . The working range of the instrument is 1200 nm to 2200 nm. The fiber optic cables used have a 500  $\mu\text{m}$  diameter and are produced with high -OH group fused silicon.

Two fiberoptic UV systems were to be used in this research endeavor. The first of which utilized a dispersive spectrometer. In this case it is a Guided wave model 260 spectrometer. The extruder and fiber optic cables are the same as the NIR system. A deuterium lamp is used as a UV light source with a photo multiplier tube as the detector. This detector uses a rotating diffraction grating grooved at 1,200 lines/mm. This allows for a resolution of 0.1 nm. This experimental setup is shown in Figure 7.5.

The second fiberoptic UV system consists of a UV source, a bifurcated fiberoptic cable, two transmission UV probes and a detector. The UV source for this setup is a EG&G Optoelectronics Xenon flash lamp. The flash design minimizes any solarization effects of the fiber optic cables. Because the fiber optic cable is bifurcated, the UV light emitted from the lamp is separated into two beams. One beam is sent to the transmission probe and the other is sent to the detector to be used as a reference beam. The sample beam has a diameter of 600  $\mu\text{m}$  and the reference beam has a diameter of 200  $\mu\text{m}$ . The detector is a 256 pixel diode array. This system is superior to the first in that it has smaller solarization of the fiberoptic cables due to the flash lamp, reduced collection times, and better reproducibility. A schematic of this system is depicted in Figure 7.6. The probes utilized are manufactured by the University of Tennessee, Knoxville [46] and allow for a more collimated beam to be produced. A schematic of this probe design is shown in Figure 7.7. It is separated into two parts, labeled X and Y in the figure. The distance between the fiber optic cable and the lens can be adjusted by rotating the Y piece so that the fiber is at the focal point of the lens. This allows for a stronger collimated beam to be collected by the fiber and transmitted back to the instrument.

The Raman spectroscopy system used in this study consists of a Raman spectrometer, two fiberoptic cables, a fiberoptic probe head and a Dynisco style probe. The Raman spectrometer is a Kaiser Optical System with a charged coupled device detector to measure the intensity of the scattered Raman

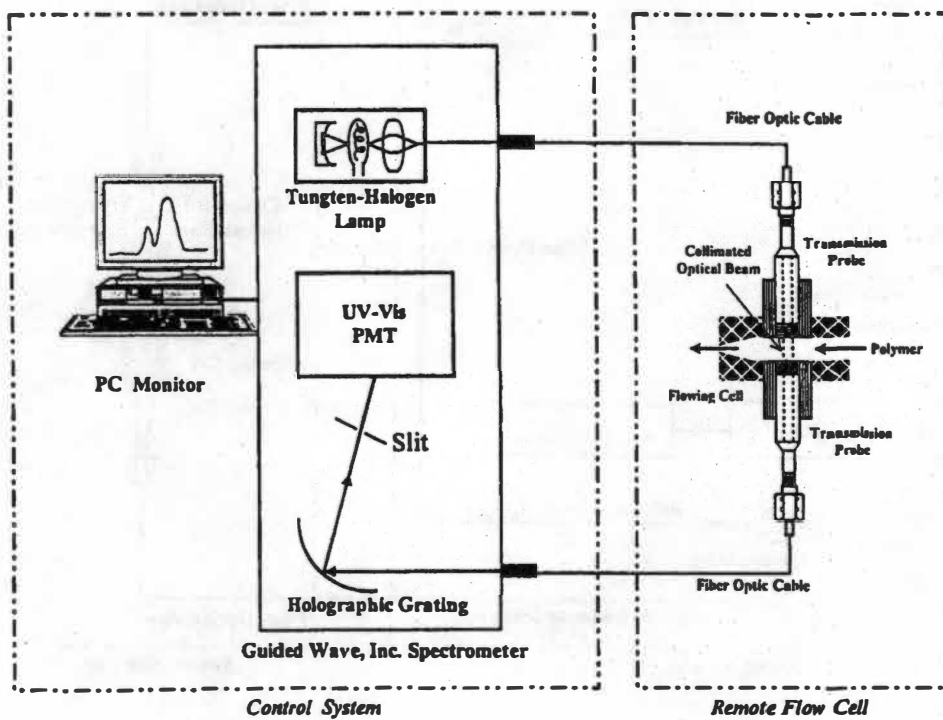


Figure 7.5 Schematic of the in-line monitoring of molten polymers using UV spectroscopy

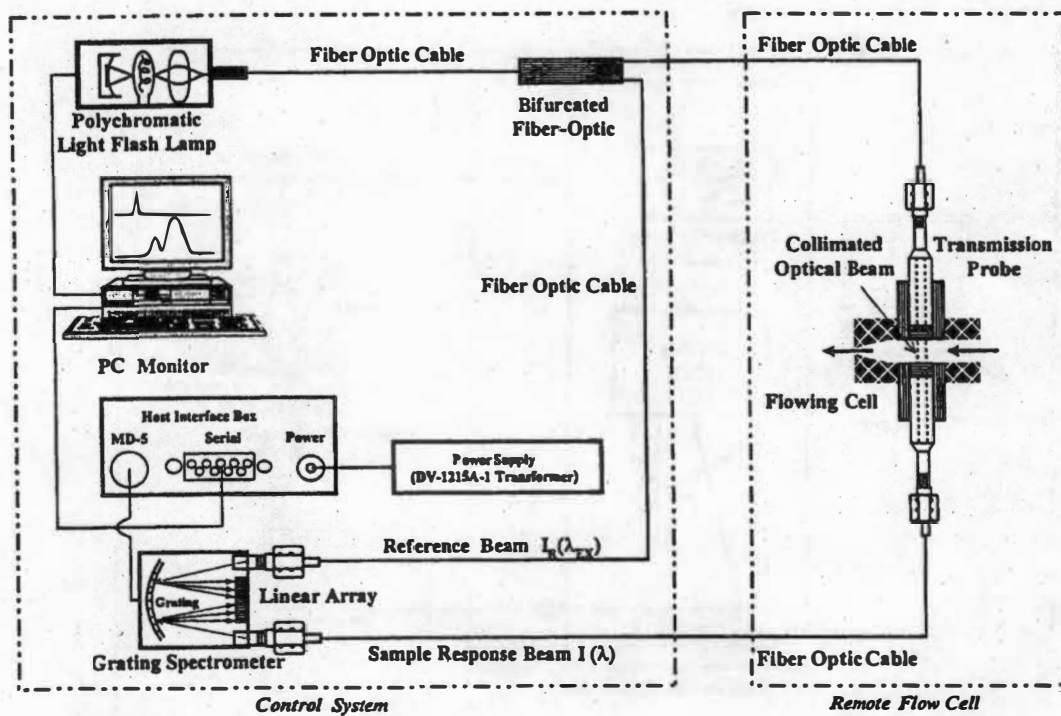


Figure 7.6 Schematic of the in-line monitoring of molten polymers using UV spectroscopy with a bifurcated fiberoptic cable

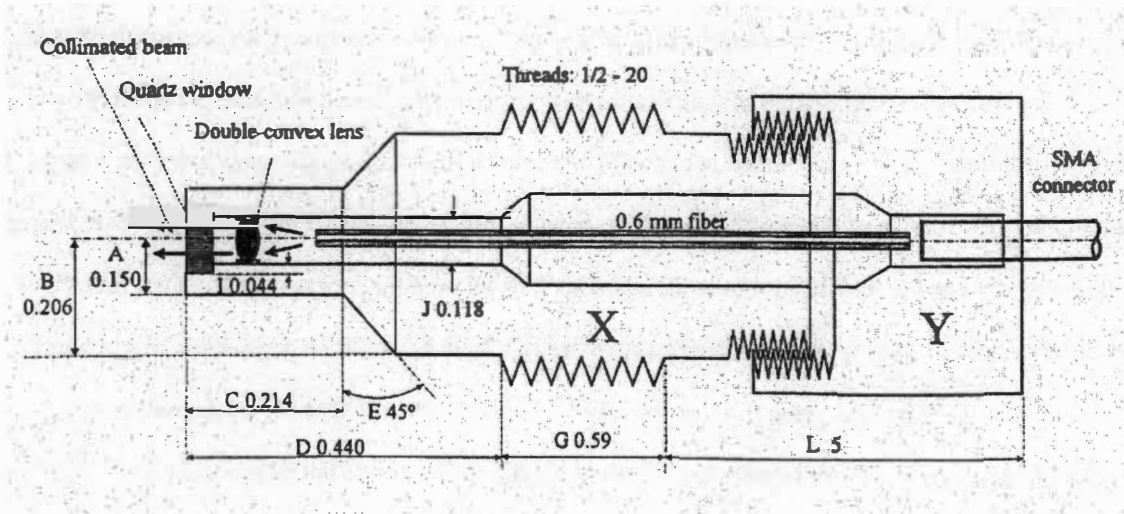


Figure 7.7 Composite schematic of the University of Tennessee, Knoxville designed UV probe

light. The excitation source is a 300 mW external cavity stabilized diode laser operating at 785 nm. The system is attached to the extruder in a similar fashion as the NIR and UV systems. The probe was designed to operate in the 180°-backscatter mode. The input of the collection fiber acts as a confocal aperture to discriminate against out of focus light. Back scattered and Raman emission light are removed from the fiber optic cable by use of a confocal design and a notch filter in the probe head. A diagram of this experimental setup is shown in Figure 7.8.

The manufacturing experimental online system consisted of an on-line NIR spectrometer system developed by Brimrose Corporation of America for this purpose. The device was able to collect spectra from two transmission probes mounted in a modified head of a 1" Killion single screw extruder, with a L/D ratio of 24:1. The design of this novel flow cell is shown in Figure 7.9. Using this design, the path length could be adjusted by turning the probes in the adaptor. This allowed for path lengths from 0.5 mm to 3.0 mm to be evaluated. This system was deemed structurally robust for industrial installation in a polymer processing facility. The fiber optic SMA/probe connections were identified as the weak point in the system, but for a properly maintained extruder operation, these were found not to be an issue.

The design of this flow cell was performed to demonstrate the scale up of prior on-line spectroscopic techniques. This cell is an improvement over prior lab designs for several reasons. The first is that the geometry of the probe location does not interfere with the flow of polymers. This is important to maximize the output flow rate of the extruder. This design does not increase the pressure in the flow cell to values greater than those experienced with the polymer only flowing through the die head. Secondly, the design allows for the flow cell to be easily transferred from extruder to extruder. This allows for flexibility in a manufacturing environment. The simplicity of the design also allows for minimal contamination issues when changing from sample to sample. The relatively low surface area minimizes cross contamination issues. This design also reduces the amount of time needed for thorough cleaning, also allowing for reduction of changeover time. The thermal mass of the flow cell allows for easy temperature control via contact heaters coupled with a thermocouple located in the head of the extruder.

The rheological measurements performed in this study were done using a cone and plate viscometer. This apparatus consists of a flat plate and a cone. The axis of the cone is perpendicular to the

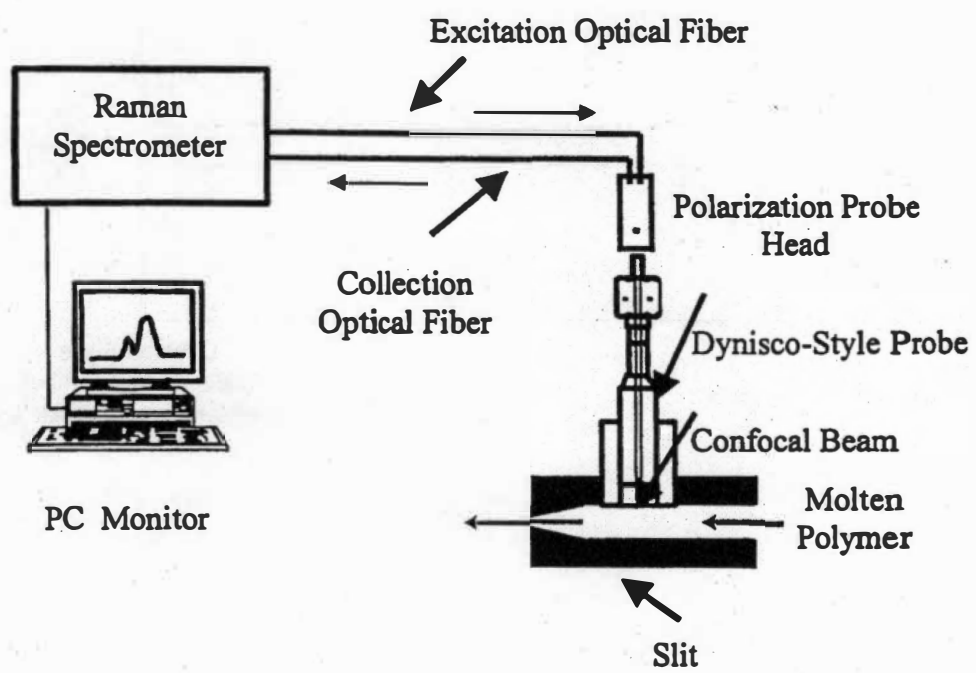


Figure 7.8 Schematic of the in-line monitoring of molten polymers using Raman spectroscopy



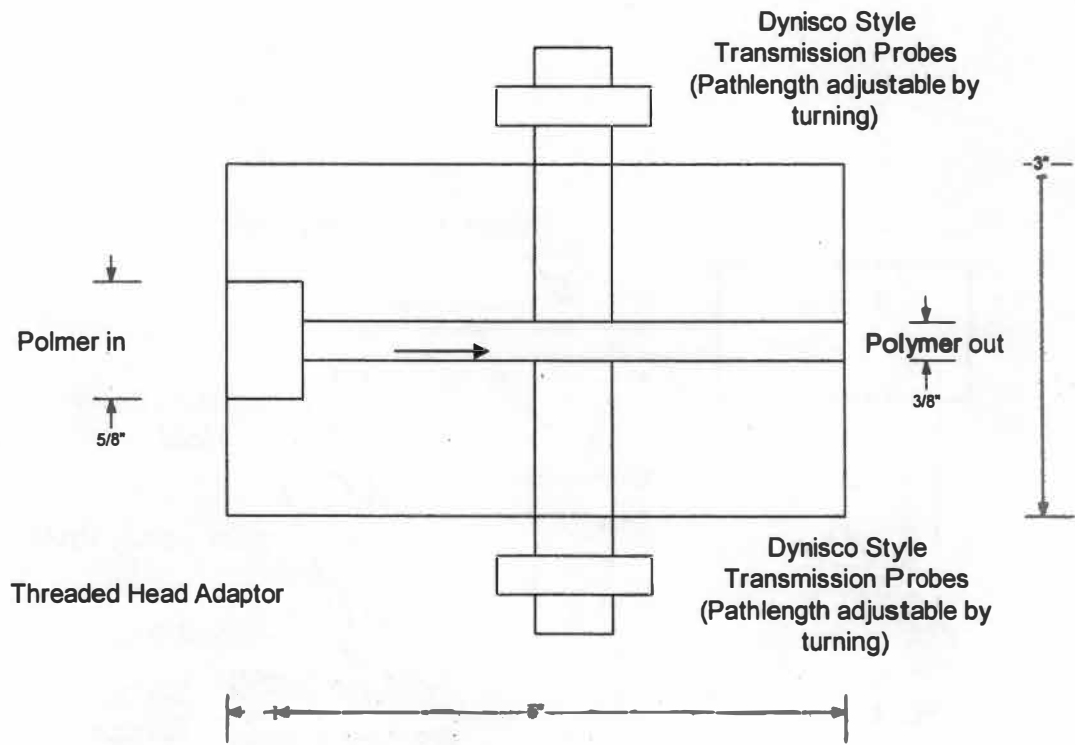
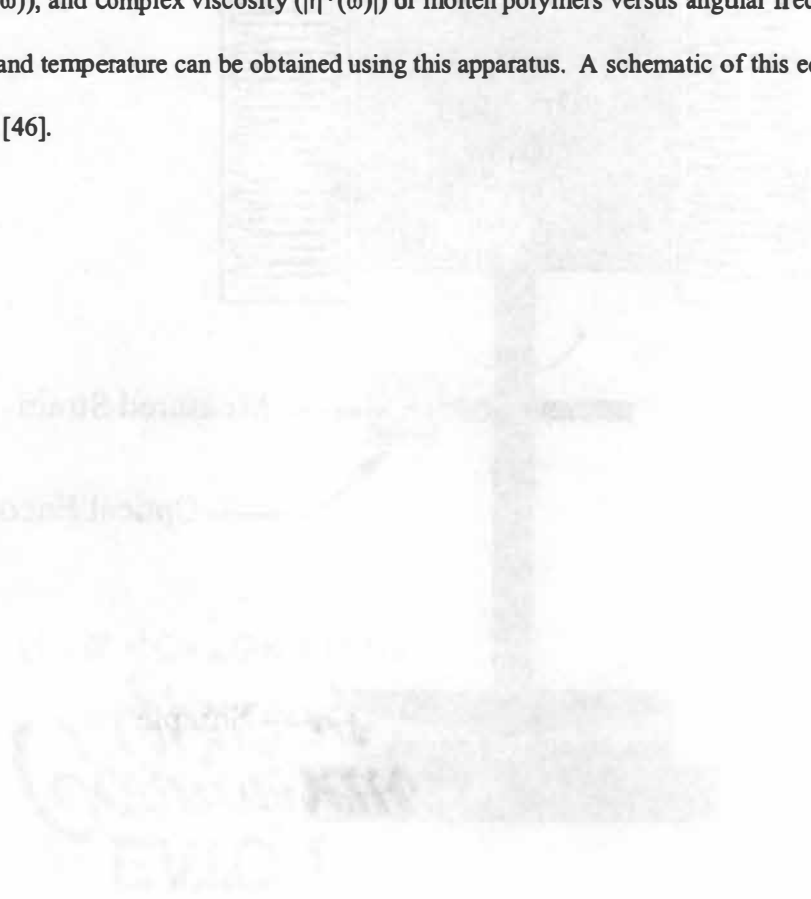


Figure 7.9 Schematic of industrial flow cell for 1" Killion operation

plate and the apex of the cone rests on the surface of the plate. A Rheometrics Dynamic Stress Rheometer with a gap angle of 0.1 radians was used for this study. Information such as storage modulus ( $G'(\omega)$ ), loss modulus ( $G''(\omega)$ ), and complex viscosity ( $|\eta^*(\omega)|$ ) of molten polymers versus angular frequency ( $\omega$ ) under a given stress and temperature can be obtained using this apparatus. A schematic of this equipment is given in Figure 7.10 [46].



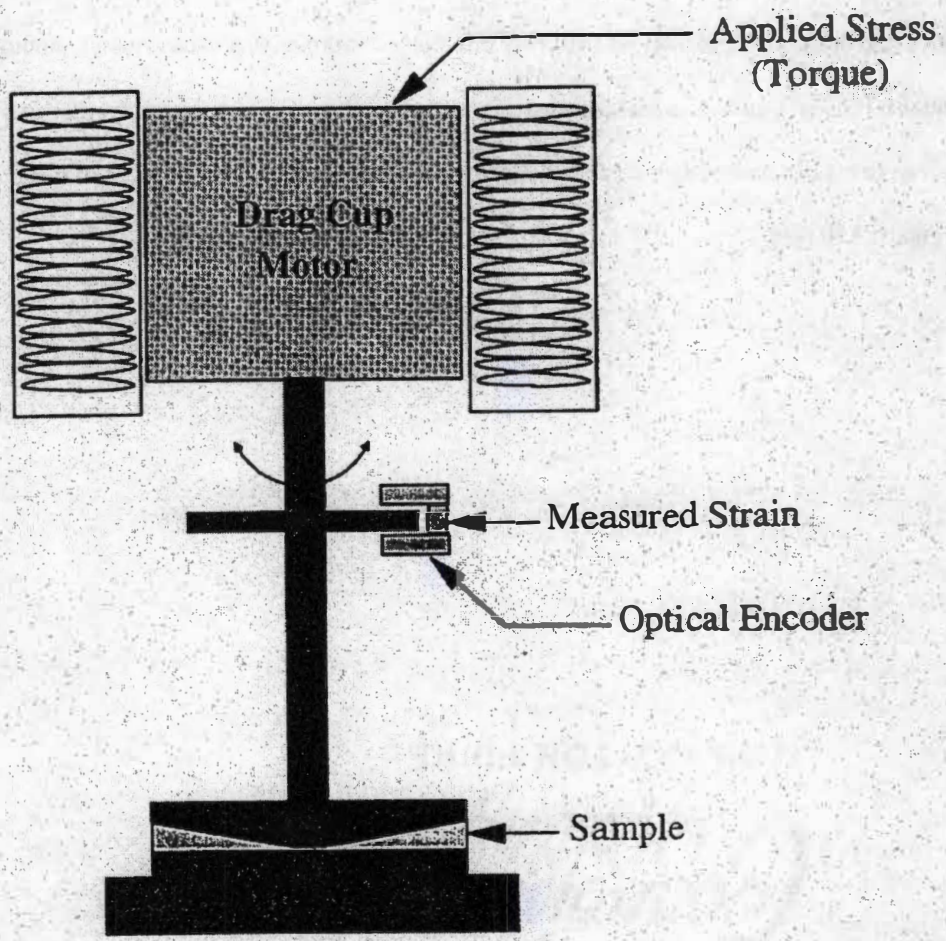


Figure 7.10 Schematic representation of experimental setup for rheological measurements using a Rheometrics Dynamic Stress Rheometer

## CHAPTER 8

### ESTIMATION OF ADDITIVE CONTENT IN POLYMER MELTS

#### INTRODUCTION

Additional components have been added to products to increase performance, add chemical resistance, alter mechanical properties and otherwise improve products from the earliest written history. With very few exceptions, most final polymer products are highly added value products, which meet strict physical and chemical requirements. There are two main additives that are incorporated into polymers in the compounding state to increase the life expectancy of the final product: anti-oxidants and ultraviolet stabilizers. Both of these categories address different requirements forced on the product by the environment.

#### 8.1 THEORY

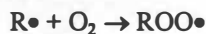
Polyolefins are susceptible to attack by ultraviolet light, oxygen and heat, resulting in the polymer becoming brittle, undergoing a color change and increased product failure [46]. The addition of additives is included to directly counteract these chemical changes. UV stabilizers have been designed to reduce the effects of sunlight on plastic parts. UV radiation can cleave bonds in polymeric materials. This process is referred to as photodegradation. The first step of photodegradation is the absorption of UV light by the polymer.



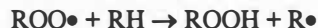
The resulting excited molecule will attempt to reduce its energy level by multiple methods, but the most damaging one is the formation of free radical mechanisms. For example, the excited molecule can break a bond and form a free radical.



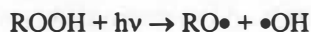
This phenomenon is referred to as photolysis. Once a free radical has been formed, the process of autoxidation can occur.



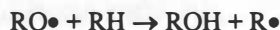
The peroxy radical that is formed in this step is capable of attacking the polymer chain (R-H) via hydrogen abstraction. This results in a hydroperoxide and another free radical being generated.



The hydroperoxide molecule is very susceptible to attack from UV light and will fragment and generate more additional free radicals.



These free radicals can initiate further reactions and continue to propagate through the autoxidation cycle.



It is easy to observe that if the initial free radical is not produced, the rate of polymer oxidation will be significantly reduced.

To combat this situation, two classes of UV stabilizers have been developed. One class was designed so that its molecules would absorb incident radiation rather than the polymer backbone. This class is known as UV absorbers. The second class of additives takes the strategy of not absorbing UV light, but rather inhibiting or controlling the degradation by other means. This class of UV stabilizers is widely varied and is referred to as light stabilizers.

Ultraviolet absorbers screen out incident UV light from attacking the polymer. These compounds do not rapidly degrade and convert the incident radiation to heat via tautomerism (where the two isomers are in equilibrium with each other). This process can be described in simple terms as the formation/destruction of an O-H bond. In this way, only a change of electron configuration in the absorbing species will allow for protection of the polymer matrix. The limitations of this are that the absorption is governed by the absorptivity of the molecule. Beer's Law requires that the absorbing species be in a high enough concentration to effectively filter out the UV light.

The most commonly used class of light stabilizing agents for polyolefin applications are hindered amine light stabilizers (HALS) [165]. Several theories have been submitted to explain their mechanisms for preventing degradation, including energy transfer, free radical termination and peroxide decomposition. HALS exhibit excellent light stabilizing efficiency. Significant levels of stabilization occur at relatively

low levels. Attempts have been made to explain this feature by a cyclical process rather than the stabilizer being consumed in the reaction. These compounds were first introduced to industry in the mid-1970s and have been highly utilized since. Higher molecular weight HALS are used for film and fiber applications where lower molecular weight compounds may be lost due to volatilization and migration during processing, degradation from post production operations, or loss from long term exposure. HALS also have a benefit in that they are relatively colorless when compared to other light stabilizers and easy to handle.

Polymeric materials are also subject to oxidation [165]. The rate of oxidation is dependent on several conditions, such as end use, polymer constituency, and processing considerations. As a result of oxidation, properties of the polymer system can be adversely affected including discoloration, elongation, and loss of physical strength due to embrittlement. Antioxidants are designed to control the molecular weight of the polymer, thereby limiting the changes to the physical properties.

There are two major types of antioxidants commercially available and widely used in the polymer processing industry, primary and secondary antioxidants. Primary antioxidants function as chain terminators. Most of these compounds are sterically hindered phenols. These compounds react rapidly with radicals and are used for scavenging purposes. Secondary antioxidants decompose hydroperoxides. These compounds are typically made of phosphite compounds and thioesters. Secondary antioxidants are most commonly used in conjunction with primary antioxidants for a synergistic effect. From this mechanism, the secondary antioxidants are able to replenish the active sites of the primary antioxidant and allow for an initial lower concentration to be used. Secondary antioxidants have also been shown to work best at higher temperatures due to the kinetics of peroxide formation and are used to provide protection for the polymer and primary antioxidant during processing.

The use of antioxidants when dealing with polypropylene systems is particularly important. Polypropylene contains tertiary carbons as part of the polymer backbone. These carbons are particularly susceptible to chain scission caused by free radicals. Use of a combination of primary and secondary antioxidants has shown to greatly improve the product life of these materials.

## 8.2 EXPERIMENTAL

The samples chosen in this work represent the most commonly used ultraviolet stabilizers, primary antioxidants and secondary antioxidants used in the manufacturing of highly loaded additive concentrates for the fiber industry, particularly the production of bulk continuous filament for carpet applications. This study focused on highly loaded additive products that would be utilized by the end user as a concentrate material. Although these materials are effective at concentrations as low as 500 PPM, it is more economically feasible to produce an concentrate that can be diluted with polypropylene resin immediately before fiber spinning operations. Antioxidants are typically supplied as a concentrate as highly loaded as 25% by mass. Depending on the ultraviolet stabilizer chosen, UV stabilizers are supplied in the 20-50% concentration range. The antioxidants chosen are readily available commercially and are shown in Table 8.1 with the codes that they will be referred to. Likewise, the ultraviolet stabilizers utilized are shown in Table 8.2. The structures of these additives are presented in Figures 8.1 through 8.4.

For these experiments, concentrates with the maximum loading were compounded on 34 mm twin-screw co-rotating extruder with a L/D ratio of 24:1. These samples were compounded with a neat 12-melt index polypropylene. Preliminary experiments investigated ranges of concentrations from 1% additive concentration to the maximum levels that were to be used in this study. The reduction in concentration was achieved by mixing the concentrate with the 12 MI polypropylene in a small 3 to 5 pound lot, followed by then compounding the material on a ¾ inch extruder. Preliminary investigations on two of the samples were conducted by forming thin sheets of material by use of a Carver press. The thickness of these films was 2 mils. The samples were then subjected to standard laboratory FTIR experiments and some distinguishing peaks were identified. These preliminary studies were conducted only for proof of concept of the technique, rather than trying to obtain quantitative information about the concentrations in the films. However, the data collected from these experiments was entered into a proprietary database for use in off line quality control functions.

The samples in the larger data set were studied using both NIR and UV-Vis spectroscopy. Spectra were collected using the spectroscopic systems described in Chapter 7. The flow cell was connected onto the head of the ¾ inch extruder and allowed for the appropriate probes to be inserted into the melt stream.

Table 8.1 Antioxidants used in polypropylene study

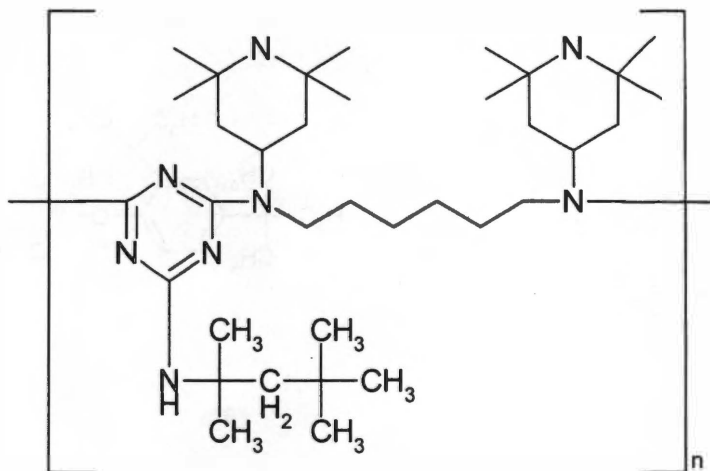
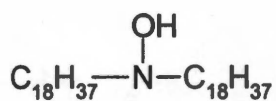
Chemical Name	Code/ CAS Number/ Ratio	Manufacturer/ Trade name	Neat Form/ T <sub>m</sub> (°C)	Final Product Loadings (max)	Concentration Range Studied
bis(Hydrogenated tallow alkyl) amides, oxidized/ Poly[[6-(1,1,3,3-tetramethylbutyl)amino]-s-triazine-2,4-diyl][(2,2,6,6-tetramethyl-4-piperdyl)imono] hexamethylene [(2,2,6,6-tetramethyl-4-piperdyl)imono]	AO-1/ 143925-92-2 70624-18-9 50:50	Ciba/ FS 410 FF	Powder/ 76-186 56-92	20-25	1-25 %
Tris(2,4-di- <i>tert</i> -butylphenyl) phosphite	AO-2/ 31570-04-4	Ciba/ Irgafos <sup>®</sup> 168	Powder/ 181-186	20-25	1-25 %
Tris(4- <i>t</i> -butyl-3-hydroxy-2,6-dimethylbenzyl)-s-triazine-2,4,6-(1H, 3H, 5H) trione	AO-3/ 040601-76-1	Cytec/ Cyanox <sup>®</sup> 1790	Powder/ 145-155	20-25	1-25 %
3,9-bis[2,4-bis(1,1-dimethylethyl)phenoxy]-2,4,8,-10-tetraoxa-3,9-diphosphaspiro{5,5}undecane/2(3H)-benzofuranone, 5,7-bis-(1,1-dimethylethyl)-3-hydroxy- reaction products with (o)-xylene	AO-4/ 026741-53-7, 181314-48-7/ 70:30	Ciba/ Irgafos <sup>®</sup> XP 60	Powder/ 99-124 160-175	20-25	1-25 %
3,9-bis[2,4-bis(1,1-dimethylethyl)phenoxy]-2,4,8,-10-tetraoxa-3,9-diphosphaspiro{5,5}undecane/2(3H)-benzofuranone, 5,7-bis-(1,1-dimethylethyl)-3-hydroxy- reaction products with (o)-xylene/ Tetralis[methylene(3,5-di-( <i>tert</i> )butyl-4-hydroxyhydrocinnamate)] methane	AO-5/ 026741-53-7 181314-48-7 6683-19-8/ 30:20:50	Ciba/ Irganox <sup>®</sup> XP 620	Powder/ 110-122 99-124 160-175	20-25	1-25 %



Table 8.2 Ultraviolet stabilizers used in polypropylene study

Chemical Name	Code/ CAS Number/ Ratio	Manufacturer /Trade Name	Neat Form/ T <sub>m</sub> (°C)	Final Product Loadings (max)	Concentration Range Studied
N,N''-[122-Ethanediy]bis[[[4,6-bis[butyl(1,2,2,6,6-pentamethyl-4-piperidinyl)amino]-1,3,5-triazin-2-yl]imino]-3,1-propanediy]]bis[N'N''-dibutyl-N'N''-bis(1,2,2,6,6-pentamethyl-4-piperidinyl)]-1,3,5-triazine-2,4,6-triamine	UV-1/ 106990-43-6 65447-77-0/ 90:10	Ciba/ Chimassorb® 119	Granular/ 115-150	20 %	1-25 %
2,4-bis(2,4-dimethylphenyl)-6-(2-hydroxy-4-N-octyloxyphenyl)1,3,5-triazine	UV-2/ 2725-22-6	Cytec/ Cyasorb® 1164	Powder/ 88-91	20-25 %	1-25 %
2-(2H-Benzotriazol-2-yl)-4,6-bis(1-methyl-1-phenylethyl) phenol	UV-3/ 70321-86-7	Ciba/ Tinuvin® 234	Flake/ 135-143	20-25 %	1-25 %
Hexane-1,6-diamine, N,N'-bis(-2,2,6,6-tetramethyl-4-piperidinyl)-,2,4-Dichloro-6-(4-morpholinyl)-1,3,5-triazine	UV-4/ 082451-48-7	Cytec/ Cyasorb® 3346	Flake/ 110-130	50 %	1-50%
C <sub>20</sub> -C <sub>24</sub> maleic anhydride products with 2,2,6,6-tetramethyl-4-piperidinamine	UV-5/ 152261-33-1	BASF/ Uvinol® 5050H	Pellet/ 93	50 %	1-50 %
Dimethyl succinate polymer with 4-hydroxy-2,2,6,6-tetramethyl-1-piperidine ethanol /Poly[[6-[(1,1,3,3-tetramethylbutyl)amino]-s-triazine-2,4-diyl][(2,2,6,6-tetramethyl-4-peperdy]amino hexamethylene [(2,2,6,6-tetramethyl-4-piperidyl)imino]]	UV-6/ 65447-77-0 70624-18-9/ 50:50	Ciba/ Tinuvin® 783 FB	Granular/ 55-74 64-140	20-25 %	1-25 %
Poly[[6-[(1,1,3,3-tetramethylbutyl)amino]-s-triazine-2,4-diyl][(2,2,6,6-tetramethyl-4-peperdy]amino hexamethylene [(2,2,6,6-tetramethyl-4-piperidyl)imino]]	UV-7/ 70624-18-9	Ciba/ Chimassorb® 944	Pastel/ 100-135	50 %	1-50 %

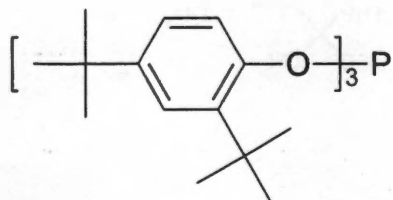
AO-1



50%

50%

AO-2



AO-3

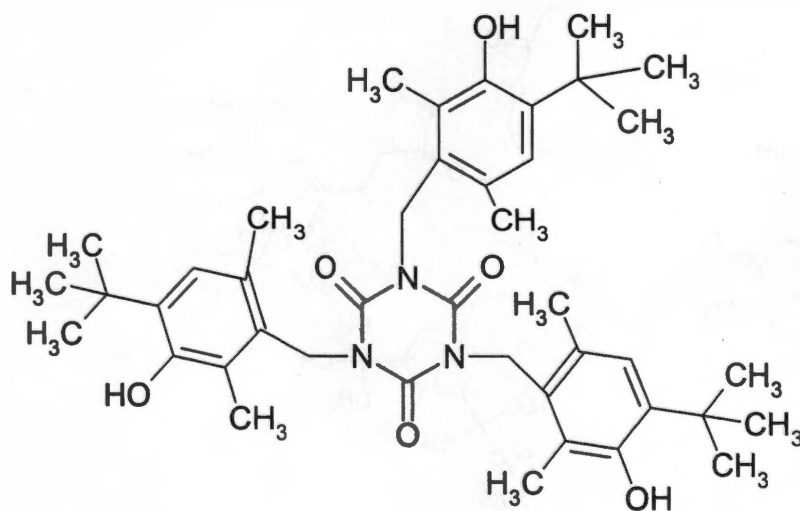
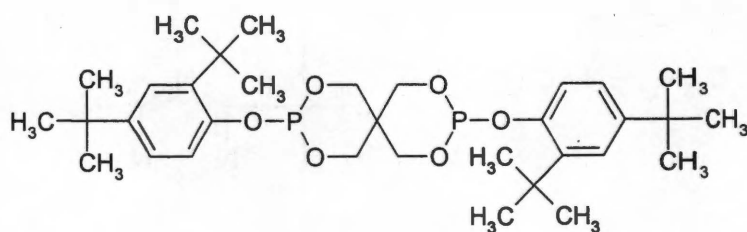
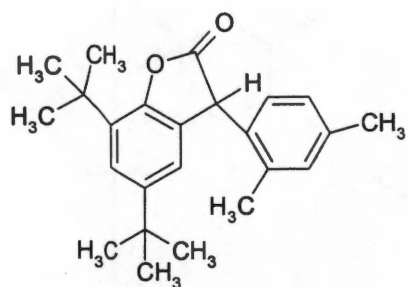


Figure 8.1

Chemical structures of antioxidants AO1 - AO3 used in this study

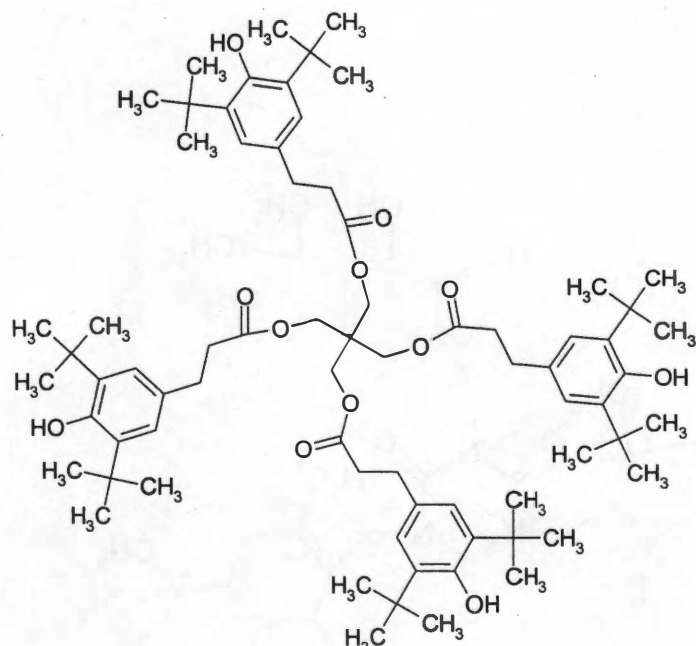
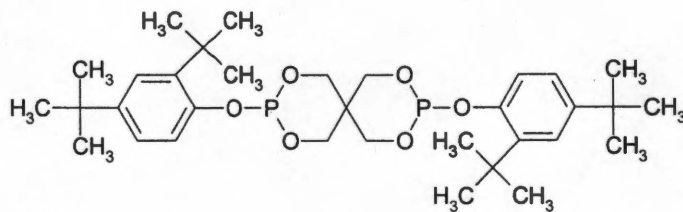
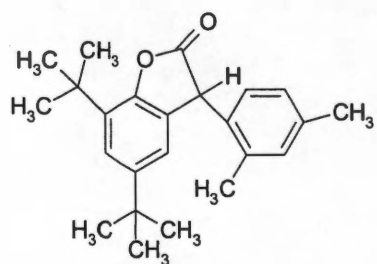
AO-4



70%

30%

AO-5



30%

50%

20%

Figure 8.2 Chemical structures of antioxidants AO-4 - AO5 used in this study

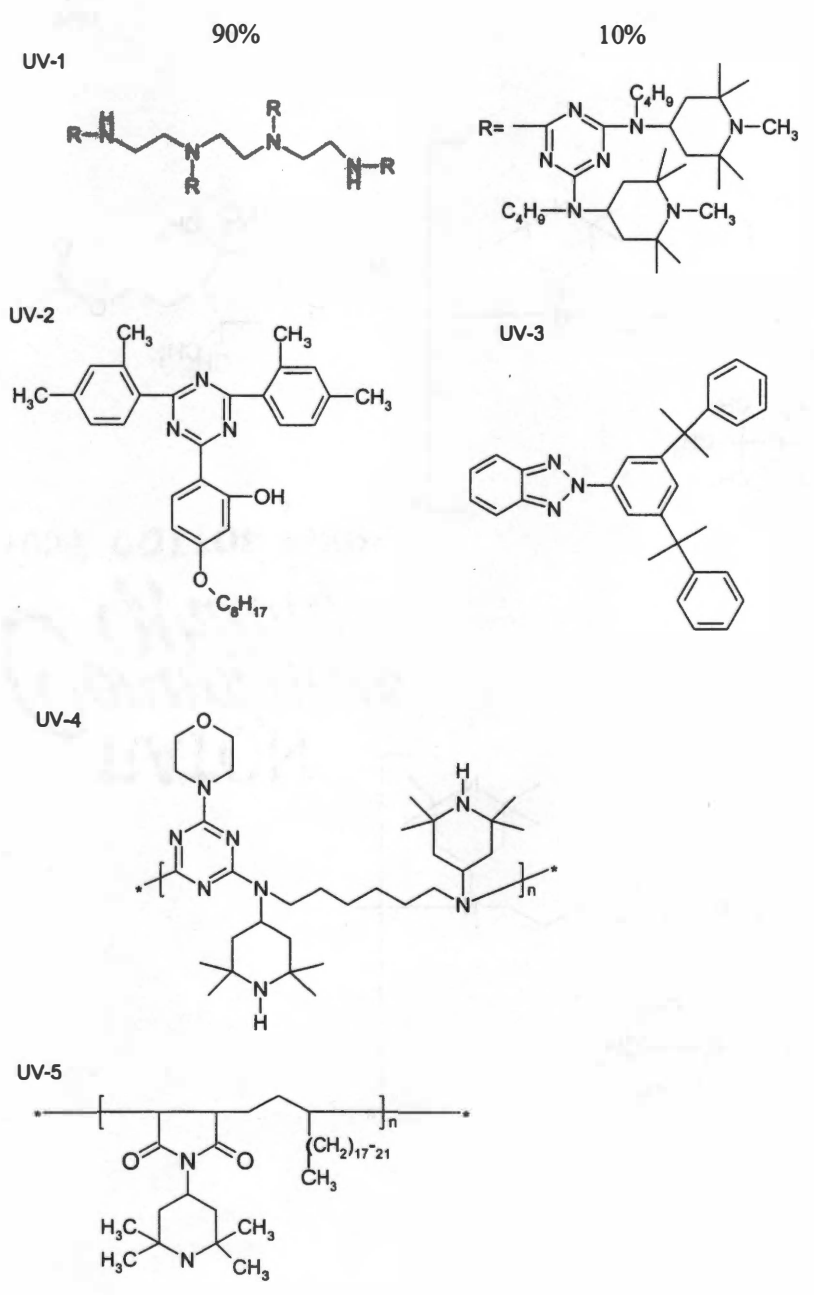


Figure 8.3 Chemical structures of ultraviolet stabilizers UV1 - UV5 used in this study

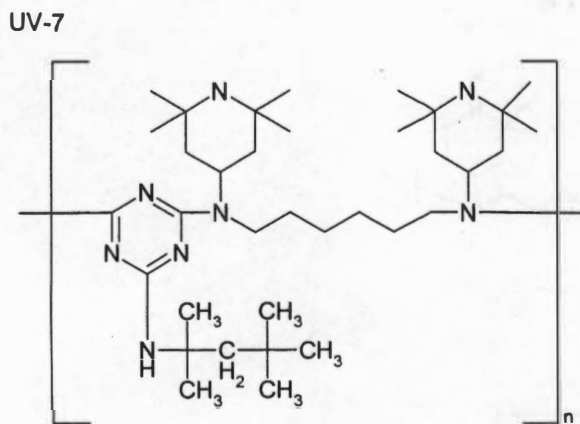
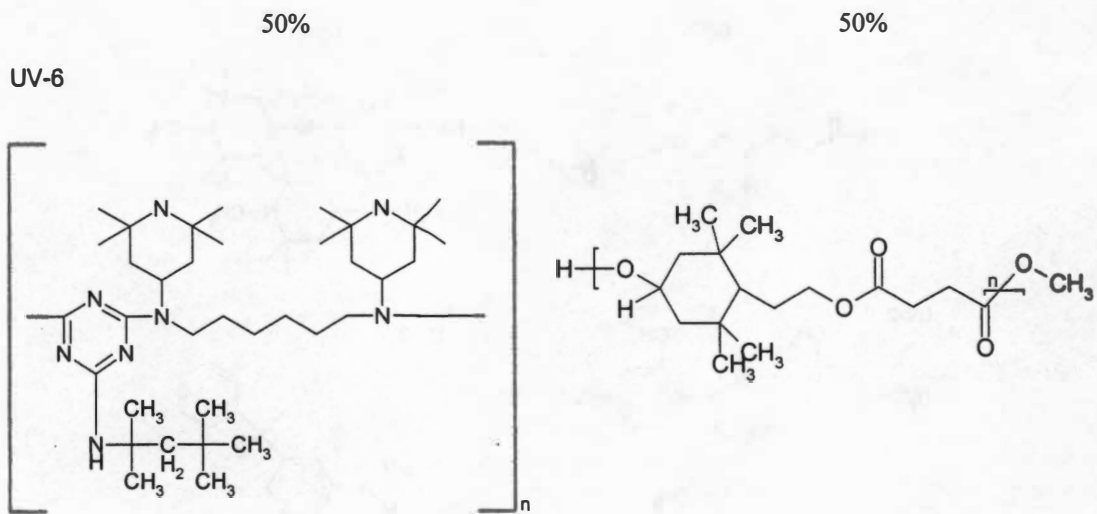


Figure 8.4 Chemical structures of ultraviolet stabilizers UV6 - UV7 used in this study

The samples were prepared in a similar manner to that of the initial FTIR spectra, in that 3 to 5 pound lots were made consisting of a master batch containing the maximum concentration of interest blended with virgin polypropylene resin. This size lot allowed for thirty minutes of data collection. The extruder was purged with a talc concentrate and neat resin between runs. The spectra were then analyzed for significant features that would allow for a spectroscopic analytic technique to be developed to measure the instantaneous additive concentration in the flow cell.

## 8.3 SPECTROSCOPIC RESULTS

### 8.3.1 Preliminary FTIR Studies

Preliminary work was done on AO-2 and UV-1 (see Table 8.1 and 8.2) at concentrations of 1%, 2%, 5%, and 10% in a 2-mil thick polypropylene film. Spectra were collected for these samples using a Nicolet 5DXC FT-IR spectrometer. Several peaks can be identified as suitable for correlating the concentrations and it is common laboratory practice to determine additive concentrations in this manner by regressing the intensity of the spectra as a function of concentration at several chosen wavelengths. The UV-1 sample was found to contain unique characteristic peaks at the following regions: 1575 to 1630  $\text{cm}^{-1}$ , 1230 to 1275  $\text{cm}^{-1}$ , 1075 to 1125  $\text{cm}^{-1}$ , 1020 to 1060  $\text{cm}^{-1}$ , 710 to 740  $\text{cm}^{-1}$ , 610 to 660  $\text{cm}^{-1}$ , and 560 to 595  $\text{cm}^{-1}$ . The relative absorbance results for the entire spectra range are shown in Figure 8.5 with a detailed view of the 1075 to 1125  $\text{cm}^{-1}$  region shown in Figure 8.6. These figures are relative in scale to show the increase in peak intensity with concentration. These trials were done on 2 mil thick film samples and are only for proof of concept purposes. These were done off line in a manner similar to routine quality control techniques and mathematical models for on-line prediction were not constructed for these trials.

The AO-2 sample displayed a similar response as the UV-1 sample. Peaks whose absorbance intensity varied directly proportionally with additive concentration were identified in the following regions: 1580 to 1615  $\text{cm}^{-1}$ , 1265 to 1285  $\text{cm}^{-1}$ , 1205 to 1230  $\text{cm}^{-1}$ , 1060 to 1085  $\text{cm}^{-1}$ , 880 to 915  $\text{cm}^{-1}$ , 675 to 700  $\text{cm}^{-1}$ , 570 to 590  $\text{cm}^{-1}$ , and 480 to 515  $\text{cm}^{-1}$ . The spectroscopic data for the IR region is shown in Figure 8.7 with a detailed view of the 480 to 515  $\text{cm}^{-1}$  peaks shown in Figure 8.8. These trials were also conducted on a 2-mil thick film sample and the absorbencies shown in Figure 8.7 are relative. From the results of these two experiments, it can be seen that the concentration of the additive in polymer will effect the spectra and

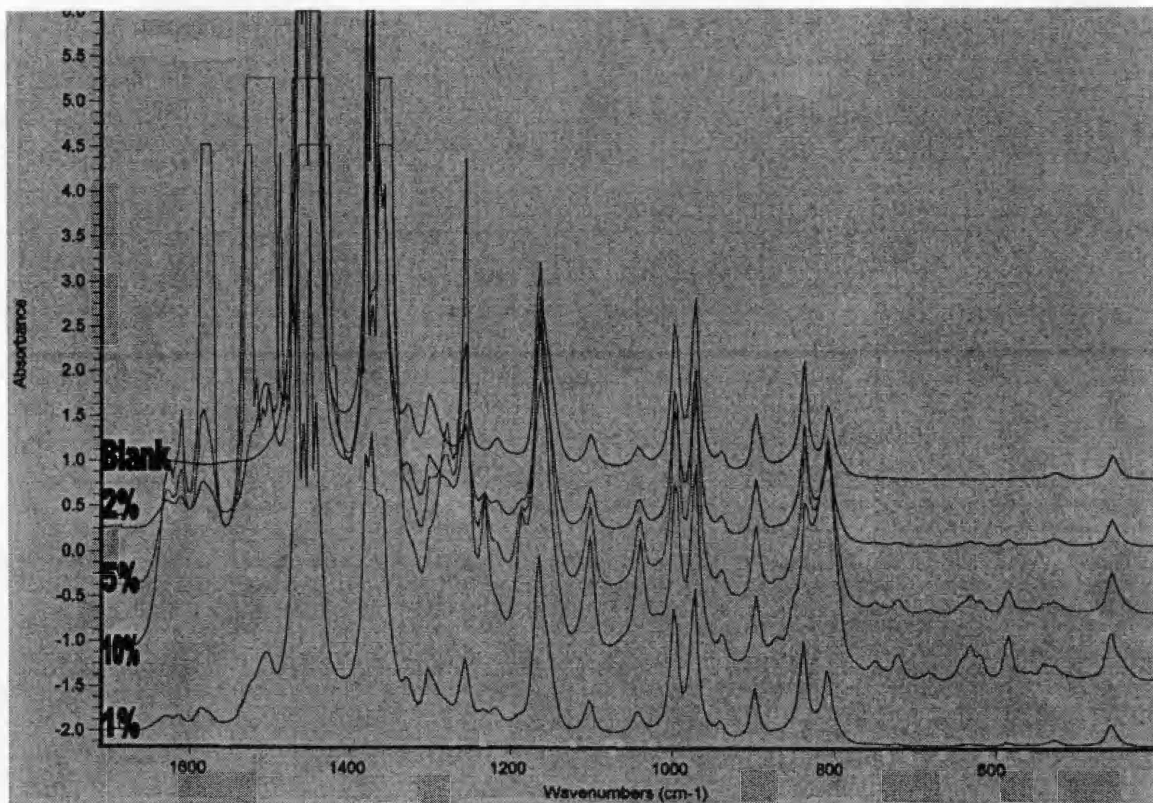


Figure 8.5 Relative absorbance FTIR spectra for sample UV-1 (Note: axis is only relative, not absolute)

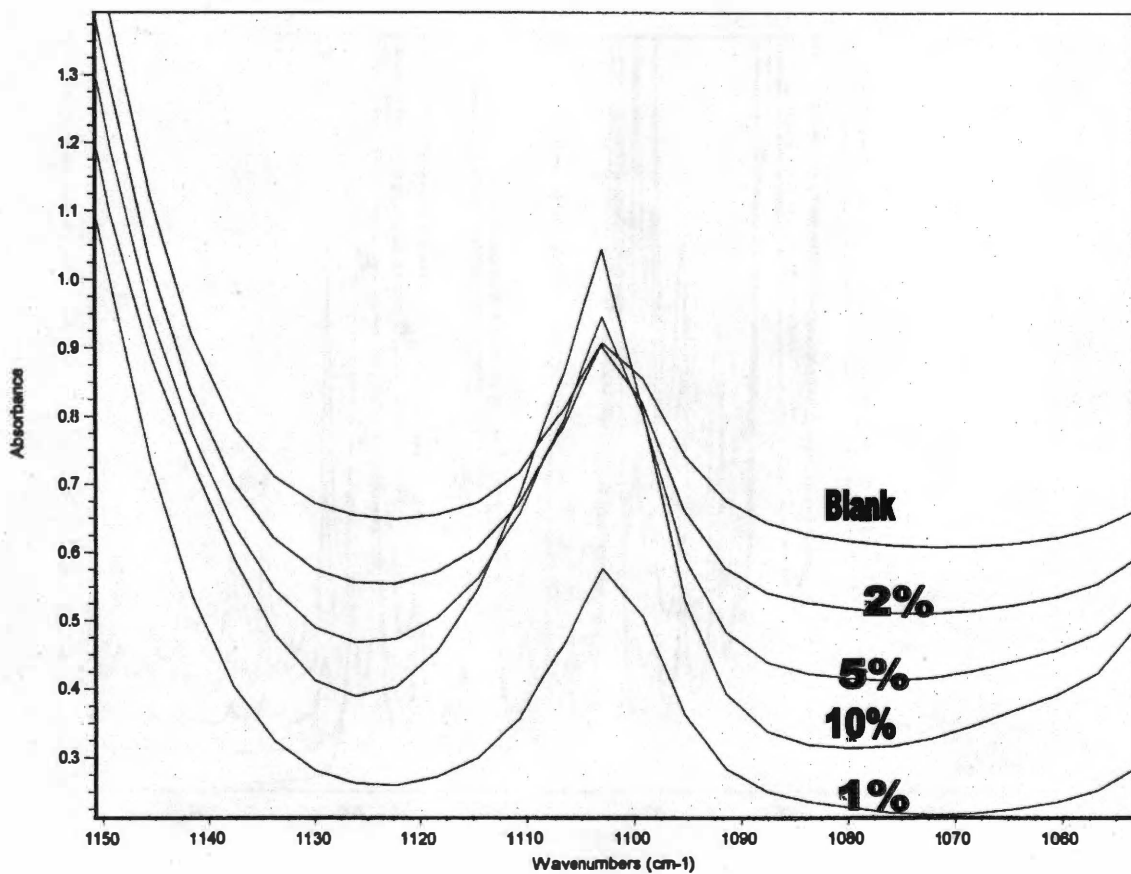


Figure 8.6 Detailed FTIR spectra for sample UV-1 in the 1075 to 1125  $\text{cm}^{-1}$  region (Note: axis is only relative, not absolute)



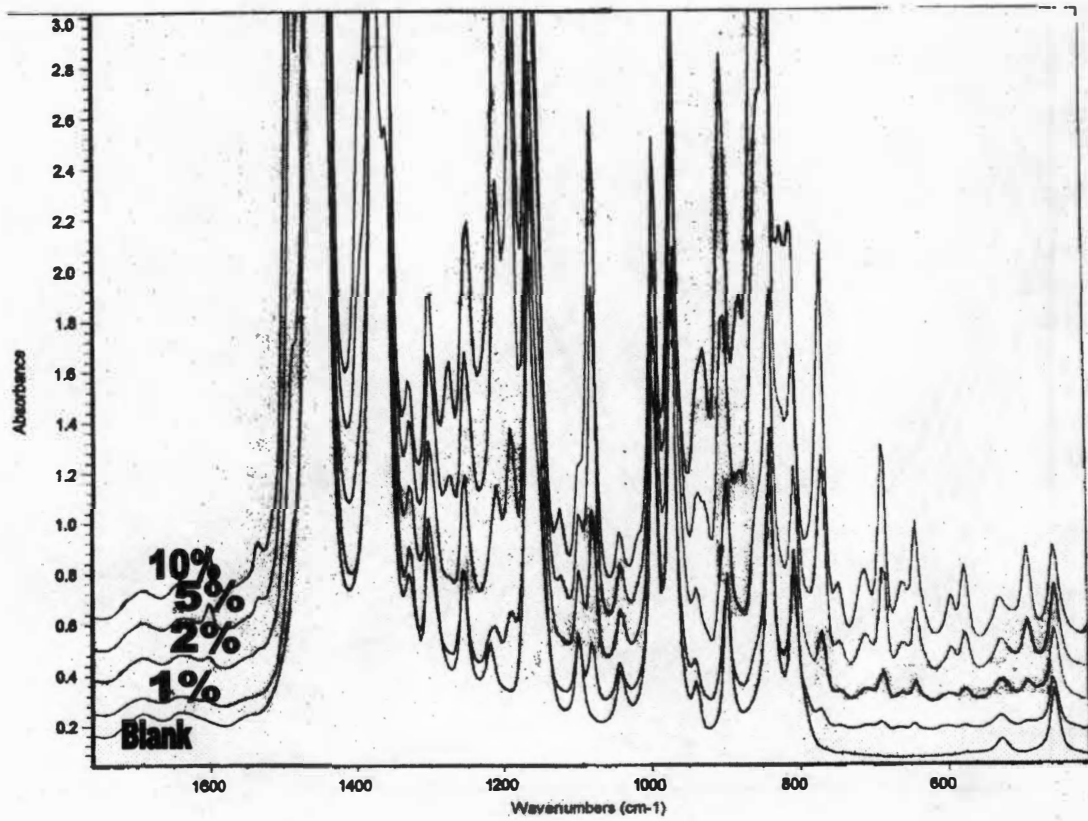


Figure 8.7 Relative absorbance FTIR spectra for sample AO-2 (Note: axis is only relative, not absolute)

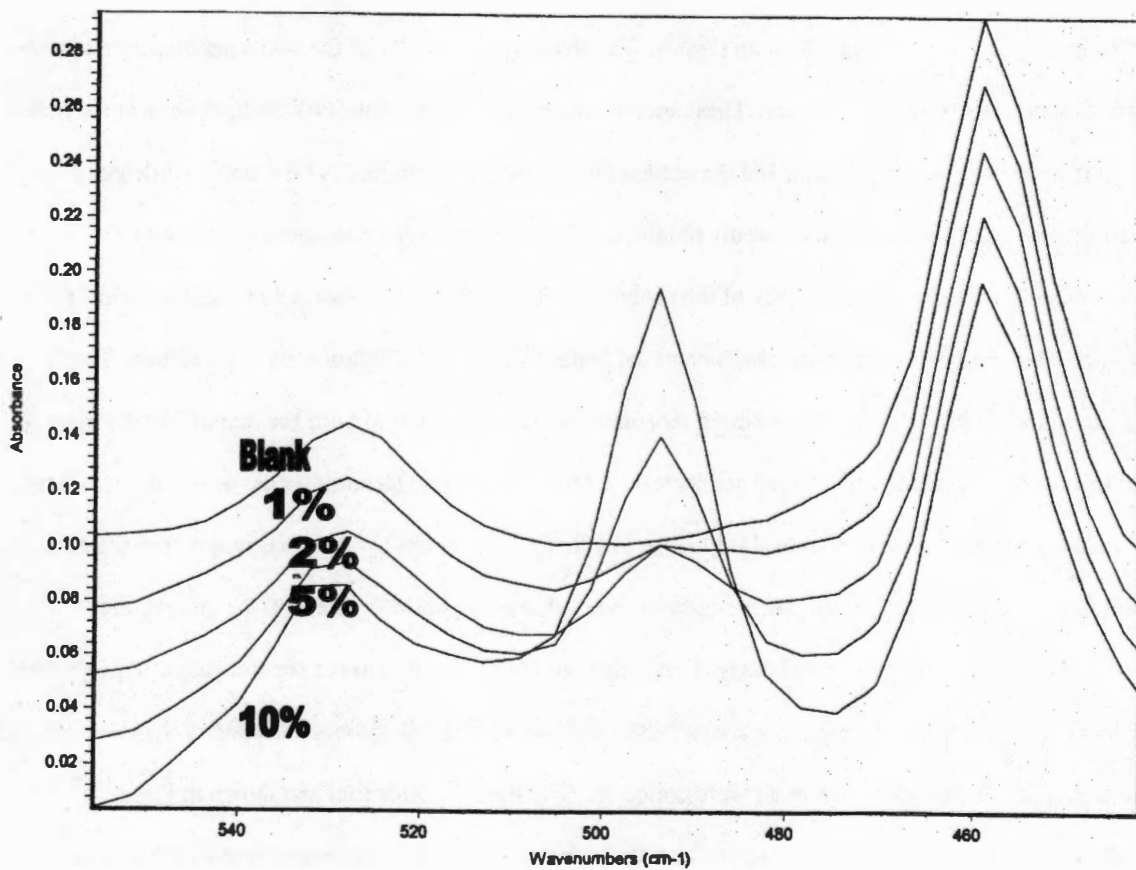


Figure 8.8 Detailed FTIR spectra for sample AO-2 in the 480 to 515 cm<sup>-1</sup> region

allow for an off-line calibration routine to be constructed. These trials were conducted only to demonstrate that there can be multiple regions for concentration measurement, and not to make any quantitative conclusions. The spectra were entered into a proprietary database to be used for both quality control purposes and identification of unknown materials.

### 8.3.2 UV SPECTROSCOPY STUDIES

As was explained in Chapter 7, the UV spectrometer is connected optically to the melt by use of fiber optic cables and two transmission probes. The transmission ability of the total spectroscopic system will be dependant on several factors. These include the emission capabilities of the light source, the optical properties of the fiber optic cables and the optical throughput of the probes. The source and detector performance characteristics are not easily obtained. They are however a constant for a modern spectroscopic system. The efficiency of the probes and the fibers can be obtained by measurement of the transmission ability of each of the components separately and in combination with one another. The fiber's transmission can be individually measured by connecting a single fiber to both the output and the input of the spectrometer using the SMA type connectors. Current fiber optic technology has allowed for cables to be manufactured with transmission ability close to 100% for the entire UV spectral range. For the cables used in this study, the measured transmission for one cable is shown in Figure 8.9. As shown, the transmission for the entire spectral range is very close to 100%. To determine the transmission properties of the entire system, measurements were collected with both of the UV probes installed in the flow cell and the transmission characteristics of air were collected. The results of this trial are shown in Figure 8.10. From these trials, it was seen that transmission through the UV region was approximately 25%. The minimum is between 350 and 425 nm, and then the transmission increases steadily to a maximum transmission of almost 70%. These

For the testing of on-line UV spectroscopy in an industrial setting, an Equitec MPX 2000 spectrometer was attached to a modified die on a 1" Killion single screw extruder. The melt temperature was controlled at 220 °C and a path length of 3.0 mm was used, after tests at several path lengths showed that this value had the least effect on product flow in the flow cell. This was the result of the die holes being approximately 3 mm in diameter and any further reduction will change the flow geometry

### UV Fiber Optic Transmittance

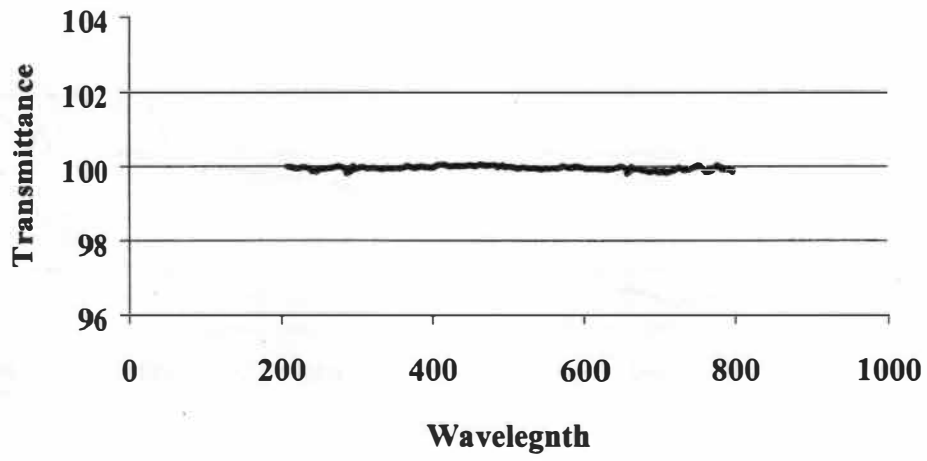


Figure 8.9 Optical efficiency of UV fiber optic cables

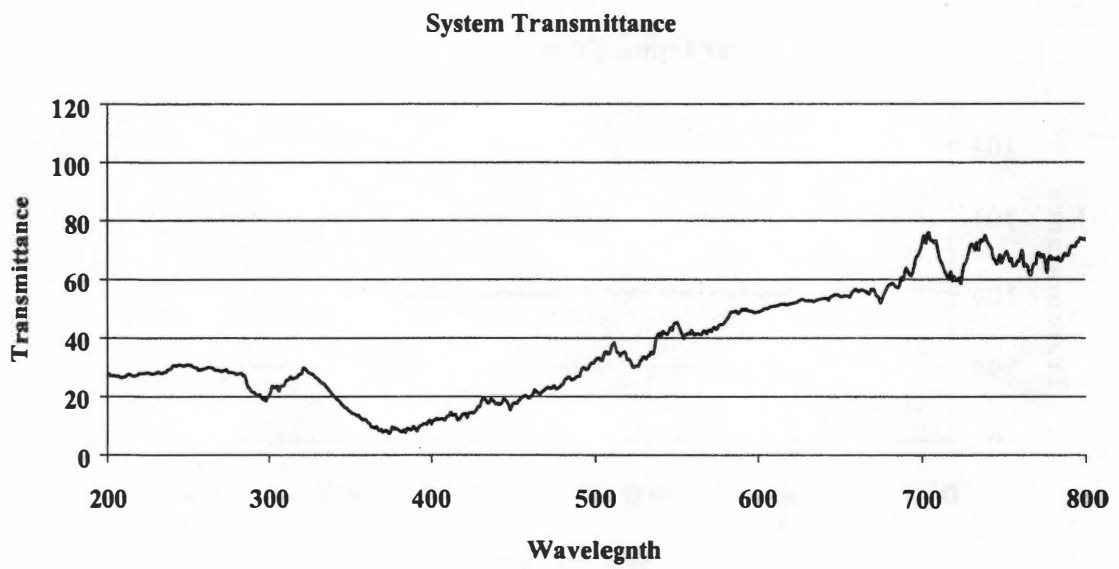


Figure 8.10 Optical efficiency of on line UV spectrometer (fiber optic cables and transmission probes) measured on air samples

within the production cell. Because of the high concentrations of interest, according to Beer's law, the path length should be minimized in order to work in the linear range of the absorbance data. Air was chosen as the reference spectra since the polymer did not have a large spectroscopic response for this technique. This air reference spectrum will be subtracted from collected spectra. This path length also kept the absorbance value below 1.0. The UTK designed UV probes were used for these experiments.

With this setup, transmission spectrum was obtained for neat polypropylene. This spectrum is shown in Figure 8.11. For the UV spectroscopic work, each spectrum was the average of 25 scans, with 3 replicates collected for each measurement. This method allowed for the screening of multiple samples to identify potential peaks and base line shifts that could be used for the in-line measurement of additive loadings. The raw spectroscopic data was then analyzed to determine if UV spectroscopy could be used as a valid measurement technique for that polymeric system. This entailed the collected sample spectra that were obtained first be viewed against the peaks that were present in the analysis of the neat resin, and then identifying peaks that varied with the concentration of the additive.

Another factor that will determine the feasibility of using a spectroscopic technique for in-line concentration measurement is the amount of light that can be transmitted through the chosen path length. For polymer additives, the concentration ranges that can be used are a function of the actual color of the neat additive and the light scattering properties of the resultant mixture. Additives used in polymer processing can be slightly soluble in the polymer matrix depending on their molecular configuration. For most additives, the molten additive must be distributed within the molten polymer. This will result in both regions of both molten polymer and additive on the microscopic level and will increase the light scattering properties of the resultant mixture, thereby decreasing the effectiveness of transmission spectroscopy.

To determine where these scattering problems occur, samples were prepared with concentrations that would be similar to those in commercial use. These concentrations are presented in Table 8.3. Spectra were then collected for each of these formulations and investigated to determine the maximum concentrations that could be used for measurement. The criteria selected included the absorbance values would be 1.0 or below and concentrations where there would not be significant noise from scattering. A detector problem was also identified as a false reading at 660 nm inherent to the instrument.

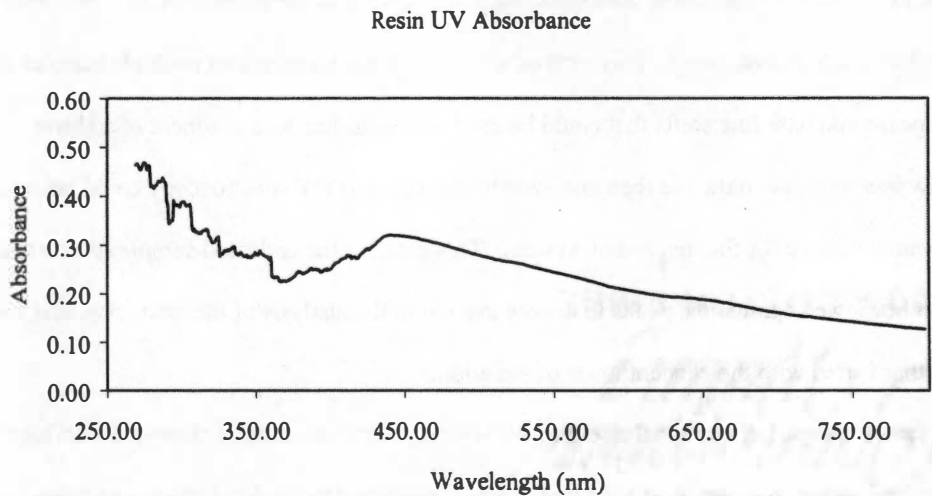


**Figure 8.11** UV absorbance spectra of polypropylene in the 200 to 800 nm range

Table 8.3 Formulations utilized in initial online UV and NIR spectroscopy

<b>Individual additive</b>	<b>1%</b>	<b>2%</b>	<b>5%</b>	<b>10%</b>	<b>15%</b>	<b>20%</b>	<b>25%</b>	<b>30%</b>	<b>40%</b>	<b>50%</b>
<b>AO-1</b>	AO-1a	AO-1b	AO-1c	AO-1d	AO-1e	AO-1f	AO-1g			
<b>AO-2</b>	AO-2a	AO-2b	AO-2c	AO-2d	AO-2e	AO-2f	AO-2g			
<b>AO-3</b>	AO-3a	AO-3b	AO-3c	AO-3d	AO-3e	AO-3f	AO-3g			
<b>AO-4</b>	AO-4a	AO-4b	AO-4c	AO-4d	AO-4e	AO-4f	AO-4g			
<b>AO-5</b>	AO-5a	AO-5b	AO-5c	AO-5d	AO-5e	AO-5f	AO-5g			
<b>UV-1</b>	UV-1a	UV-1b	UV-1c	UV-1d	UV-1e	UV-1f	UV-1g			
<b>UV-2</b>	UV-2a	UV-2b	UV-2c	UV-2d	UV-2e	UV-2f	UV-2g			
<b>UV-3</b>	UV-3a	UV-3b	UV-3c	UV-3d	UV-3e		UV-3f	UV-3g	UV-3h	UV-3i
<b>UV-4</b>	UV-4a	UV-4b	UV-4c	UV-4d	UV-4e	UV-4f	UV-4g			
<b>UV-5</b>	UV-5a	UV-5b	UV-5c	UV-5d	UV-5e		UV-5f	UV-5g	UV-5h	UV-5i
<b>UV-6</b>	UV-6a	UV-6b	UV-6c	UV-6d	UV-6e		UV-6f	UV-6g	UV-6h	UV-6i
<b>UV-7</b>	UV-7a	UV-7b	UV-7c	UV-7d	UV-7e		UV-7f	UV-7g	UV-7h	UV-7i



The sample sets for this project presented some unique challenges in application of spectroscopic techniques. Because of path length limitations, Beer's law may not be applicable for high concentrations due to the scattering of the light. To determine the highest concentration possible for performing multivariate analysis, an iterative technique was required to determine the highest concentrations. The approach was two fold in nature. The first was to collect spectroscopic data for a large concentration range and to visually inspect the resulting spectra. From this analysis, it was possible to identify concentrations where the high concentrations effectively scattered the instrument's light. In these cases, the signal to noise ratio was extremely low and the spectra had no discernable information in the regions of interest based on chemical composition.

The second approach to determining the highest concentration was the generation of calibration models and the analysis of the model diagnostics. In this approach, PLS models were constructed on several regions of the spectra, based on the regions where a response due to the chemical nature of the system would be present. The models were then analyzed with regards to the error levels generated. If the SEC values exceeded 10% of the measurement range, then the model was reconstructed using a lower maximum concentration. For these studies, the concentration chosen was an incremental reduction to gain an understanding of the nature of the system.

Because of the complex nature of the spectra due to the chemical moieties having similar functional groups resulting in overlapping regions, a multivariate approach was needed to model the data. PLS regression was chosen for this approach because it is capable of modeling the dependence of the spectra on the concentration in a more concise manner than MLS would. PLS modeling can also treat data that has more features than objects. This is the case with spectroscopic data. Due to the highly complex relationships embedded in the spectra due to both overlapping regions and the individual molecules containing similar chemical subgroups, PLS can extract the information contained in the spectra and allow the user better understandings of the multilevel relationships. The relationships between the mathematical modeling and the concentration ranges apply whether UV or NIR spectroscopy is used to characterize the system.

For the antioxidant additives, regions were identified that would allow for a mathematical model to be constructed to determine the additive loading. For AO-1 (Figure 8.12), an applicable spectroscopic range of 2-15% loading in the concentrate was found. Higher levels were found to block transmission because of opacity of the melt. A major peak was identified at 400 to 480 nm with a minor peak at 500 to 520 nm. AO-2 (Figure 8.13) was found to have a spectroscopic response for the entire concentration range up to 25% loading in the melt, however, the acquired spectra had a large noise value associated with it even after spectral averaging. AO-3 (Figure 8.14) was found to have a usable range from 1% to 10%, with higher concentrations blocking transmission due to their opacity. This additive had an excellent response at the 370 to 450 nm range. AO-4 (Figure 8.15) was found to only have a working range up to 5% due to the opacity and the natural color of the additive. AO-5 (Figure 8.16) also showed similar behavior to AO-4 in that the material was too opaque for UV measurements above 5% concentration. It should be noted that the scales would not be linear with concentration due to the log function in converting transmission to absorbance. The visible region response results from the natural color.

Noise found in lower wavelength regions that can be attributed to the concentration of the additives in the system and the complication of the 3.0 mm path length. These compounds all contain chemical species that have strong UV spectroscopic responses, as well as scattering the available light due to their turbidity. Wavelengths below 400 nm are more susceptible to this problem, and direct measurement of the concentration using this technique is not feasible.

The testing of the ultraviolet stabilizers was conducted in the same manner as the antioxidants. UV-1 (Figure 8.17) was found to have a suitable spectral range up to 10% loading of the active ingredient. UV-2 (Figure 8.18) exhibited useful spectra for the entire concentration range up to 25% with several peaks located throughout the wavelengths of interest. UV-3 (Figure 8.19) was also found to provide useful data up to 50% in the melt with several peaks throughout the spectral range. UV-4 (Figure 8.20) was found to be very opaque from a turbidity standpoint as to not allowing transmission above a 2%. UV-5 (Figure 8.21) exhibited useful spectra to a concentration of 10%, but higher concentrations resulted in the model containing large error values as a result of turbidity in the high loaded samples from their opacity. Some of this noise can be seen in the 10% curve as a high frequency. This additive did have a unique response

### AO1 UV-Vis Spectra

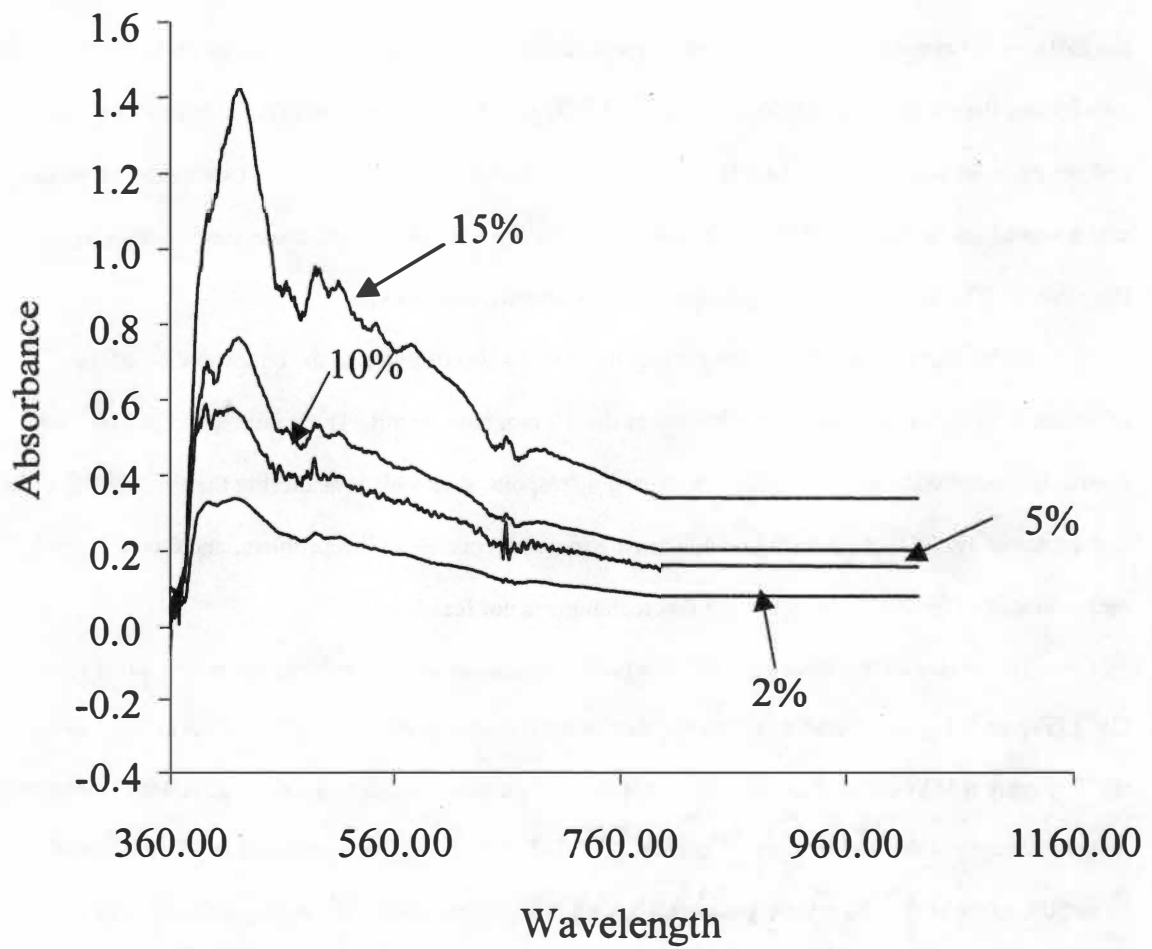


Figure 8.12 Detailed UV spectra for sample AO-1 in the 200 to 800 nm region

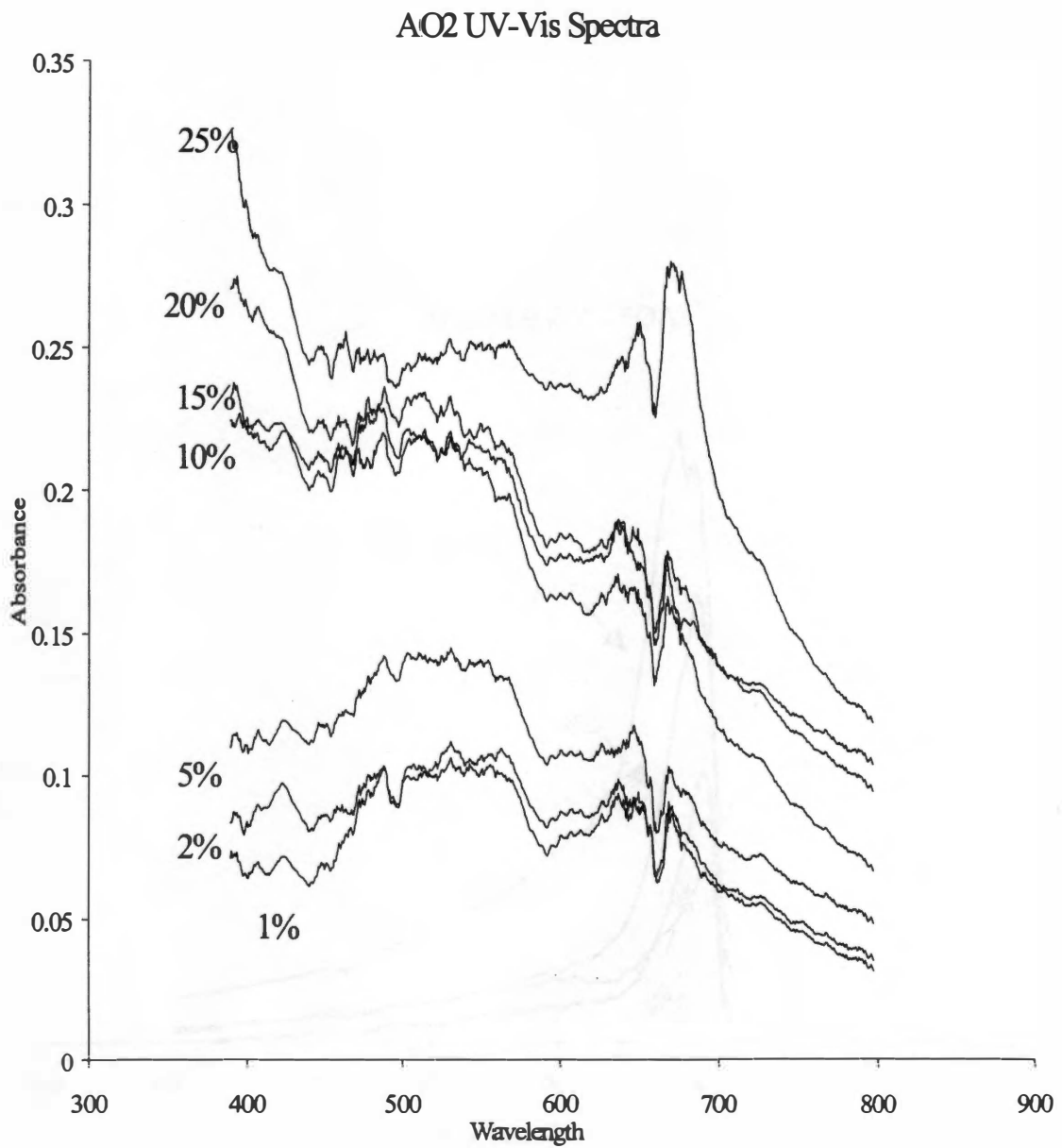


Figure 8.13 Detailed UV spectra for sample AO-2 in the 380 to 800 nm region

### AO3 UV-Vis Spectra

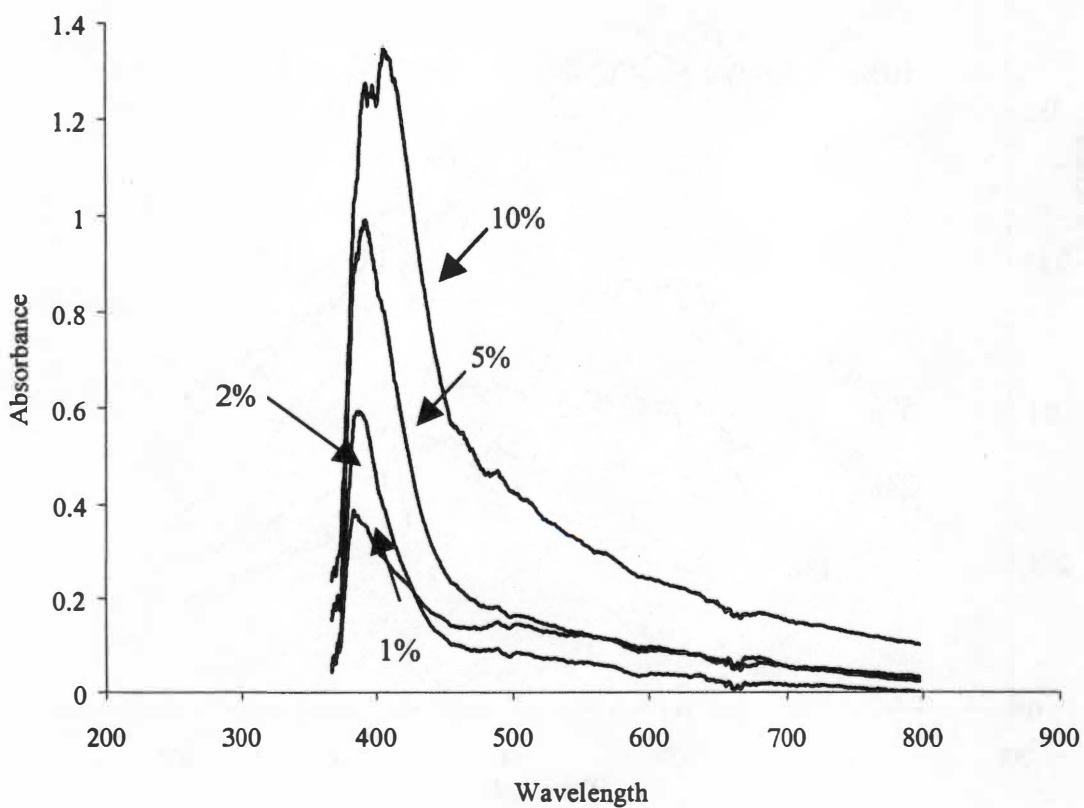


Figure 8.14 Detailed UV spectra for sample AO-3 in the 360 to 800 nm region

AO4 UV-Vis Spectra

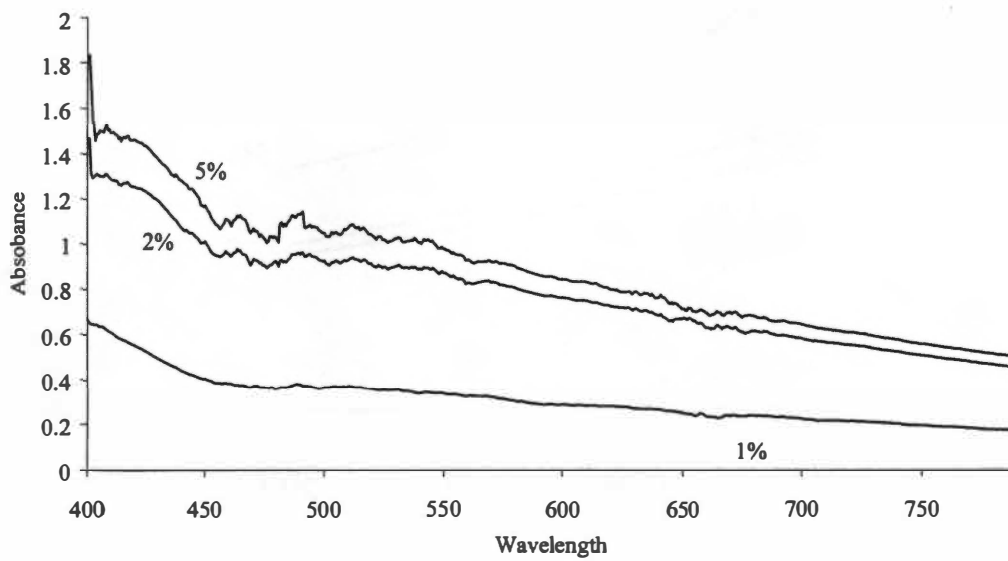


Figure 8.15 Detailed UV spectra for sample AO-4 in the 400 to 790 nm region

### AO5 UV-Vis Spectra

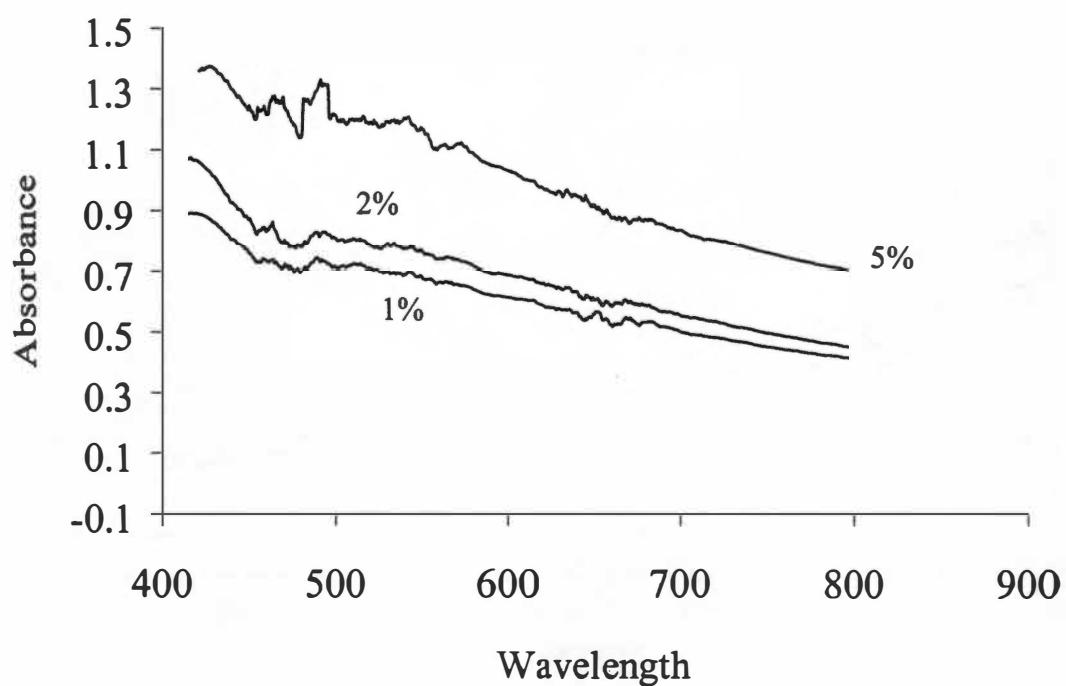


Figure 8.16 Detailed UV spectra for sample AO-5 in the 405 to 800 nm region

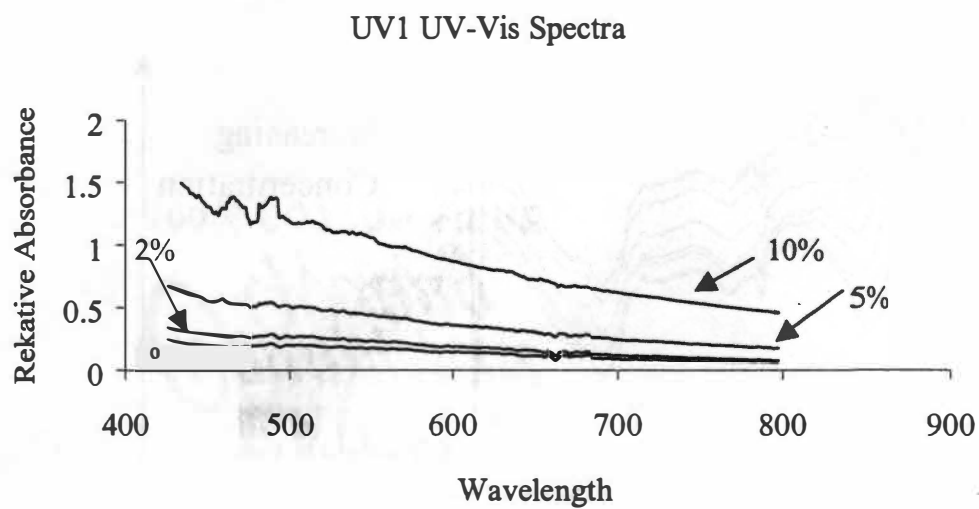


Figure 8.17 Detailed UV spectra for sample UV-1 in the 420 to 800 nm region



### UV2 UV-Vis Spectra

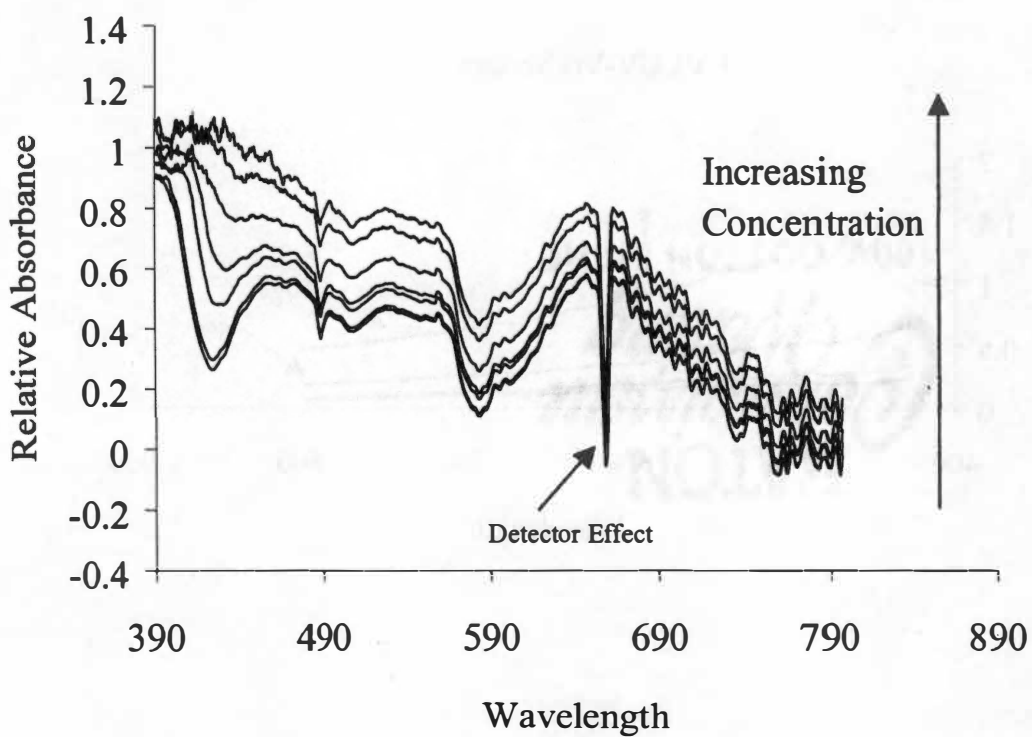


Figure 8.18 Detailed UV spectra for sample UV-2 in the 390 to 800 nm region (1, 2, 5, 10, 15, 20, 25%)

### UV3 UV-Vis Spectra

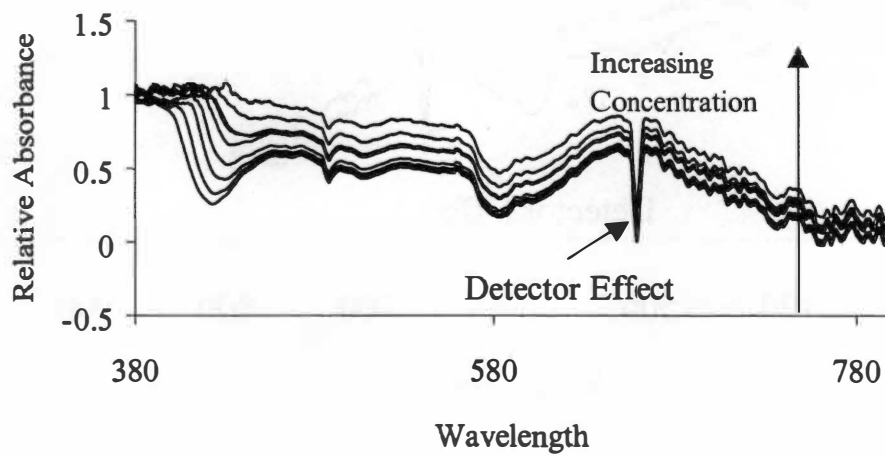


Figure 8.19 Detailed UV spectra for sample UV-3 in the 200 to 800 nm region (1, 2, 5, 10, 15, 25, 30, 40, 50%)

### UV4 UV-Vis Spectra

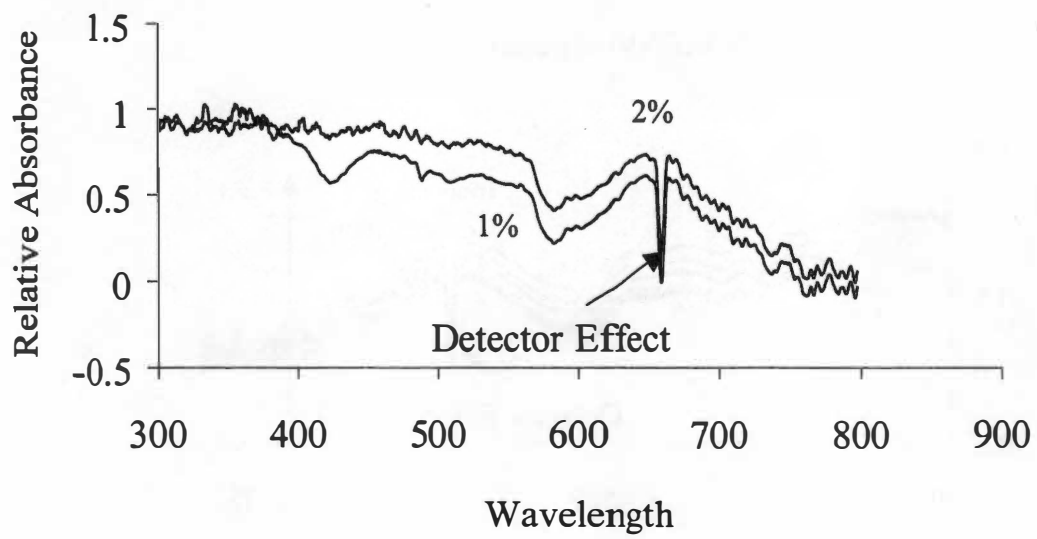


Figure 8.20 Detailed UV spectra for sample UV-4 in the 300 to 800 nm region

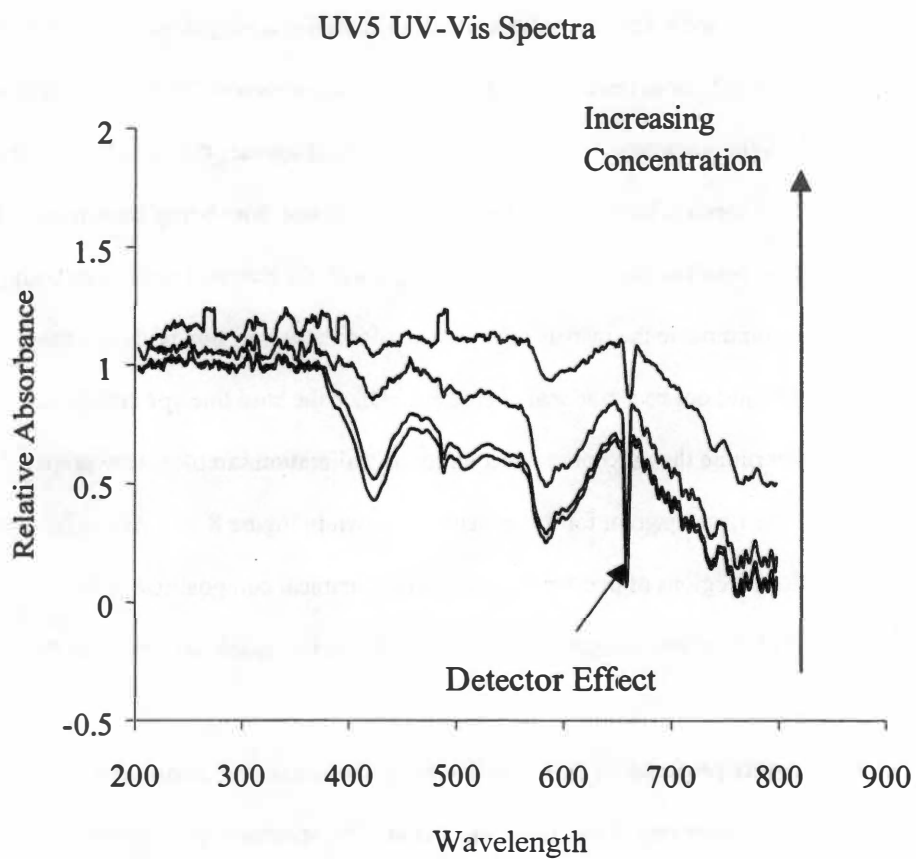


Figure 8.21 Detailed UV spectra for sample UV-5 in the 200 to 800 nm region (1, 2, 5, 10%)

be seen in the figure. UV-6 (Figure 8.22) was found to only have a useful response for concentrations less than 5% because higher concentrations had no transmission spectra, with most of the response being a change in the relative absorbance compared to air. UV-7 (Figure 8.23) was found to be measurable for concentrations less than 10% of the active ingredient with several peaks that could be used for modeling.

The limitations for these measurements can be attributed to the opacity of the melt. This product came out of the extruder with an appearance similar to a TiO<sub>2</sub> concentrate. For highly loaded concentrates, the additive will reach the solubility limit in the molten polymer. Because of this thermodynamic limitation, the additive will be dispersed within the polymer, rather than being totally dissolved. This will cause discrete regions of different indices of refraction and hence the transmission of the exciting light will go to zero at the detector as the light is scattered. The result of this is that it appears that all of the light is being absorbed by the component species, but the light is really being blocked from being transmitted. The light that enters the detector is the result of the interaction of the light with the polymer melt. The path length could be decreased to accommodate the increase in concentration; however, this will limit the throughput of the extruder and would not be a practical alternative. Once the base line spectroscopic measurements were made to determine the maximum concentrations, calibration samples were prepared for development of PLS models. The flow diagram for this process is shown in Figure 8.24. As can be seen in the spectral data, there are multiple regions of overlap because of the chemical composition of the additives. Because of this, it is obvious that univariate analysis would not be capable of modeling the concentration.

Six to twelve samples were prepared for each additive sample with concentrations that could be measured using the UV on-line spectrometer. From these calibration sets, spectroscopic regions were identified where an effect of the concentration of the additive was evident. This usually entailed four or five peaks or regions and the combinations of these. A PLS model was then constructed for each identified region and the error of calibration was investigated along with interpretation of the scores and loadings of the model. The model that gave a low value of SEC, loadings plots that increased with concentration, and review of the predicted versus measured concentrations to identify outlying data was chosen for building in-line measurement models.

### UV6 UV-Vis Spectra

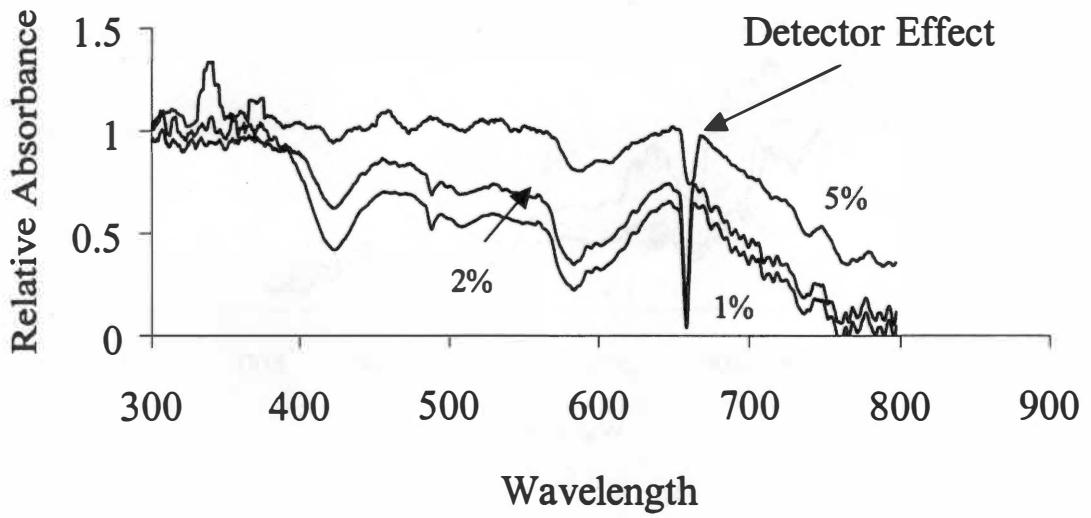


Figure 8.22 Detailed UV spectra for sample UV-6 in the 200 to 800 nm region

### UV7 UV-Vis Spectra

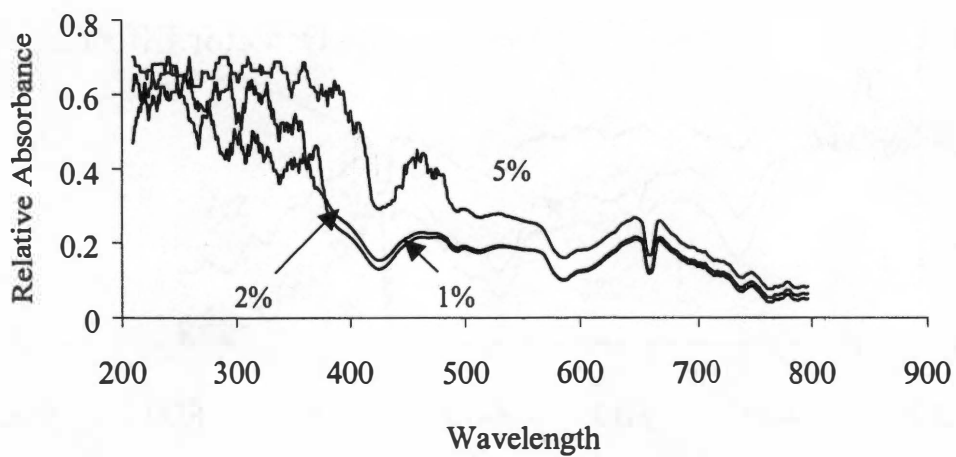


Figure 8.23 Detailed UV spectra for sample UV-7 in the 200 to 800 nm region

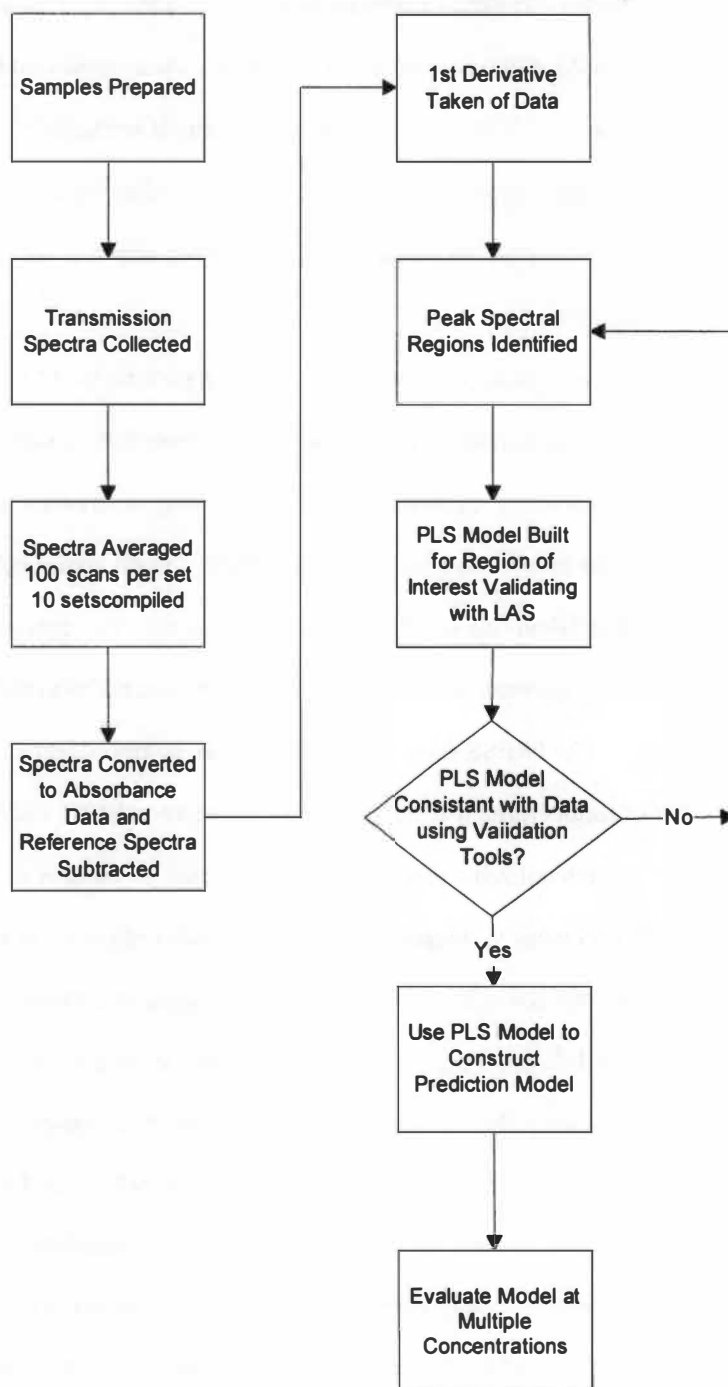


Figure 8.24 Flow chart for prediction of additive concentrations



To build an optimal PLS model, the data was preprocessed by taking the 1<sup>st</sup> derivative of the data. This method is often recommended for performing multivariate regression analysis. This is done because it eliminates any base line variation in the different sample sets. While this does introduce a higher frequency signal to the spectra, the technique is valid if the initial signal to noise ratio is sufficiently high. Mean centering was performed after this step to allow for modeling to be performed on the differences in the spectra, not on the actual value. In taking this approach, the model-building step will account for more of the variation contained within the spectra.

A leave-a-sample (LAS) cross validation technique was used to perform the PLS multivariate analysis and to study the behavior of the calibration model. In the LAS procedure, a sample from the calibration set is left out temporarily from the calibration set. The remaining samples are then used to build a calibration model and to predict the properties of the removed sample. The difference between the actual value and the predicted value is then calculated and designated as the residual. This procedure is repeated until all of the samples have been left out once and all of the residuals are then added to yield the overall residual to yield the PRESS value. The PRESS value is dependant on the number of principal components retained. The optimal number of factors (principal components) was chosen to be the one that minimizes the PRESS factor value. This research utilized a plot of SEC or SEP versus the number of principal components coupled with the PRESS value to determine the optimal number of factors to be used in the models. LAS also allows for determination of the fitness of a linear relationship between the independent and dependent variables in the model. In this way, it will highlight outliers in the sample data set. In a plot of the predicted versus measured values of the data set, if the data is not scattered closely along both sides of a slope of 1 in the plot, then the proposed relationship does not accurately reflect the data contained in the spectra. If there are large outliers in the data set, the model will try and account for these differences and the resultant prediction model will not be used for prediction. The prescreening of the spectra attempted to eliminate outliers. A review of the loading vector will also give some indication as to the validity of the model constructed. The loading vector expresses the relationship between measured variables and principal component axis.

Spectra were collected for samples containing various levels of AO-3 in polypropylene. These spectra were then preprocessed by taking the 1<sup>st</sup> derivative of the spectra using 9 wavelengths, and then the spectra were mean centered. The original spectra for a range of 400 to 500 nm are shown in Figure 8.25. The spectra were arranged in an X matrix containing the UV spectral information and a Y vector containing the concentration information. The spectra were then subjected to a LAS PLS multivariate analysis using Pirouette® software available from Infometrix. The number of factors was chosen to minimize the value of PRESS. For this case, it was found that a minimum PRESS value of 0.225 was obtained using two factors.

It is also possible to find the minimum number of factors where the standard error of validation (SEV) value is minimized. For this data set, the SEV was found to be at a minimum with two factors as well and a value of 0.489 was obtained. A plot of SEV versus factor number is shown in Figure 8.26. The number of factors used needs to be kept to a minimum, because as more factors are introduced, the model is actually accounting for more of the noise in the data, yet still capture the variance in the model due to the chemical composition. The SEC values will also follow this trend and decrease with increasing number of factors.

The first factor was found to account for 99.21%, while the second factor only accounted for 0.77%. From this analysis, one can see that almost all of the variance within the model can be dealt with in two factors. To further examine the properties of the calibration model, the loading vector is also analyzed. Figure 8.27 shows a plot of the two loadings vectors versus wavelength for this data set. The first loading resembles the profile of the spectrum indicating why such a large amount of variance was captured.

Comparing the actual concentration of AO-3 with the predicted value tested the reliability of the calibration model. Figure 8.28 shows the predicted concentrations of AO-3 versus the measured concentrations using a two factor LAS PLS regression model. The correlation coefficient, which is a measure of how the two variables being plotted are associated, was found to have a value of 0.9955 for this example. The range on the correlation coefficient can be from 0 to 1. If  $R^2$  is close to 1.0, there is a high association with the x and y data within the data set. An R value of 0 indicates that there is little

### UV Absorbance Spectra (1st Derivative)

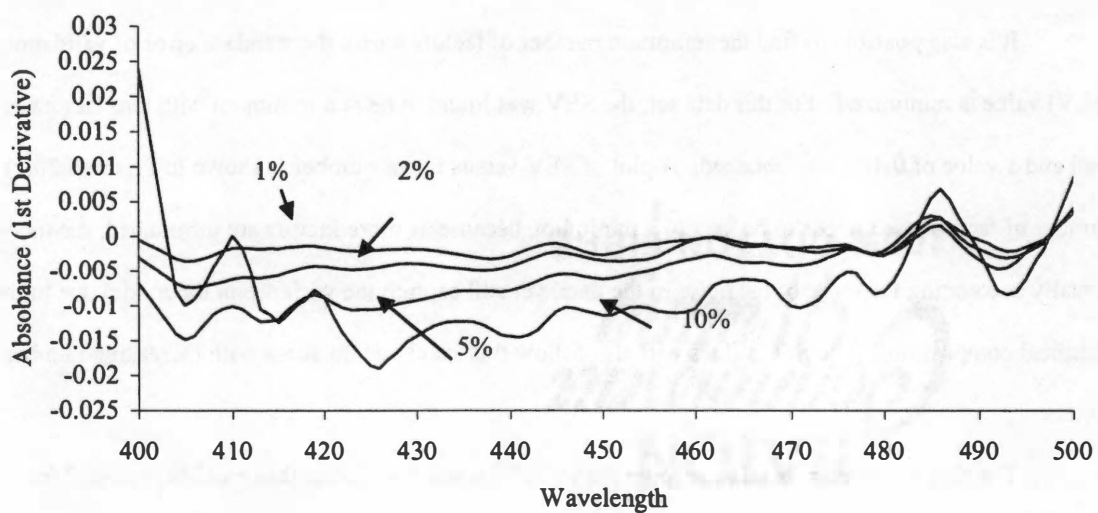


Figure 8.25 UV absorbance spectra of AO3 (1<sup>st</sup> derivative)

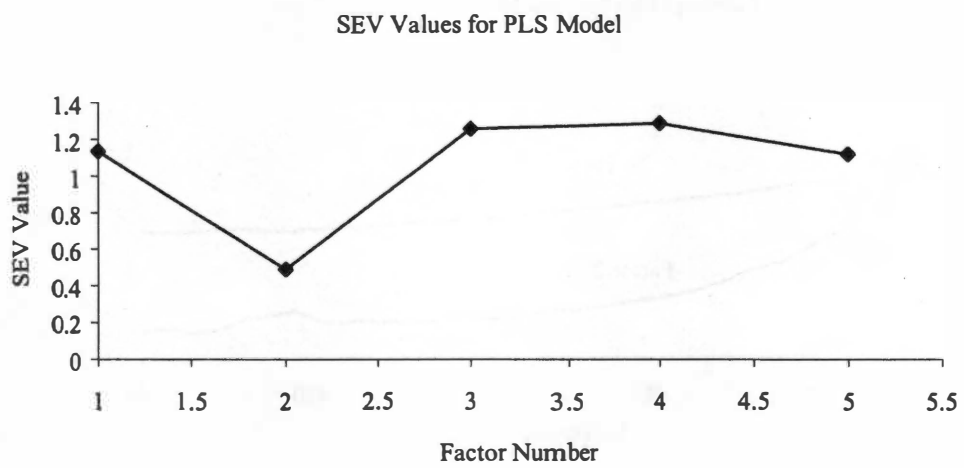
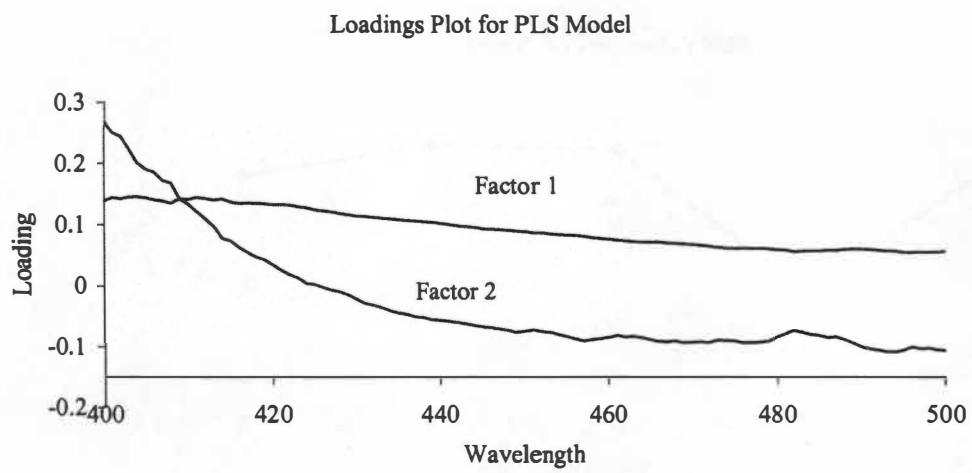


Figure 8.26 SEV values for AO3 PLS model based on 1<sup>st</sup> derivative UV data



**Figure 8.27** Loadings plot for AO3 PLS model

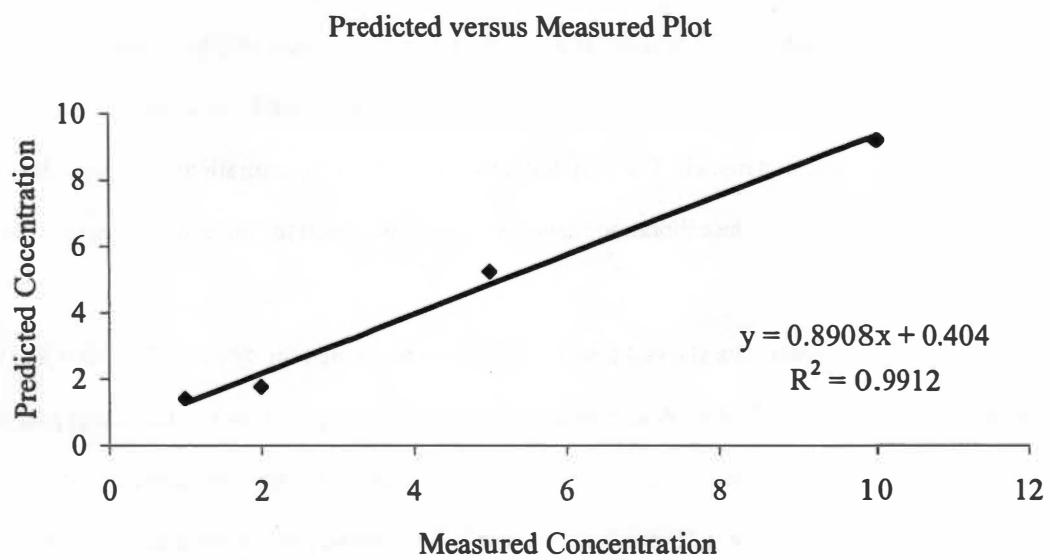


Figure 8.28 Predictive versus measured plot for AO3 PLS model

linear association within the data set. The value for this data set indicates that there is a high degree of linearity within the data around a slope of 0.89.

Inclusion of concentrations higher than 15% greatly added to the error within the calibration model. Using including data collected at 17.5% as the upper concentration limit in a test case, two-factor model was created and the SEV value increased to 1.849, or more than 3 times the error as the first model presented. Because of this result, the 2-factor calibration model chosen was limited to concentrations below 15% of the antioxidant. This approach to determining the upper concentration limit was applied to each of the additive concentration calibration data sets.

UV spectroscopy was also used to build calibration models for UV-5. Following the same procedure outline for AO-3, spectra were collected for a concentration range of 1 to 50% by mass in polypropylene. This trial consisted of 7 concentrations collected over 100 wavelengths. Through investigation of its first derivative spectra, the range of 700 to 800 nm was found to exhibit the best response for building a regression model. The first derivative spectra for concentrations 1-10% in this region are shown in Figure 8.29. The calibration model developed was used for the entire concentration range.

Analysis of the variance data showed that the first factor accounted for 99.86% of the data and the second factor only accounted for 0.14%. A simple way to detect clustering is to look at the scores plot and determine if the scores represent meaningful information, such as do they increase or decrease with concentration. This plot is presented in Figure 8.30. As can be seen in the plot, factor 1 increases with concentration, whereas factor two is approximately zero for all samples.

A further technique to evaluate the regression model is to evaluate the regression coefficient. It contains the coefficients of the calibration model. It is used to identify variables that do not contribute to the prediction. These values will be close to zero. The shape and relative value can be similar to that of the original spectral data in no other analytes show absorbance in the same region [46]. The regression coefficient was plotted versus wavelength and presented in Figure 8.31. As can be seen in the plot, it is not a similar profile as presented in Figure 8.21, indicating that resulting spectra are the result of several

UV5 UV Absorbance Spectra (1st Derivative)  
For 1, 2, 5, and 10%

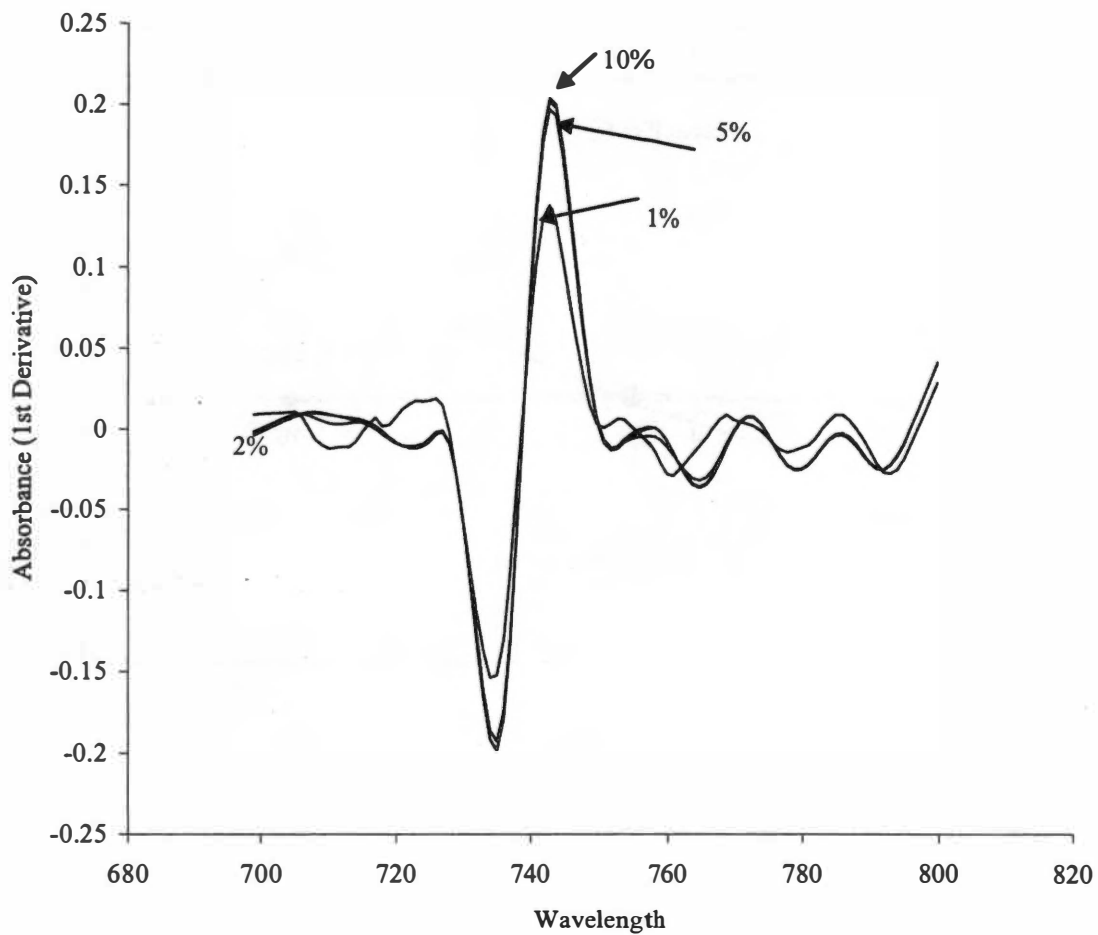


Figure 8.29 Visible absorbance spectra of UV5 (1<sup>st</sup> derivative)



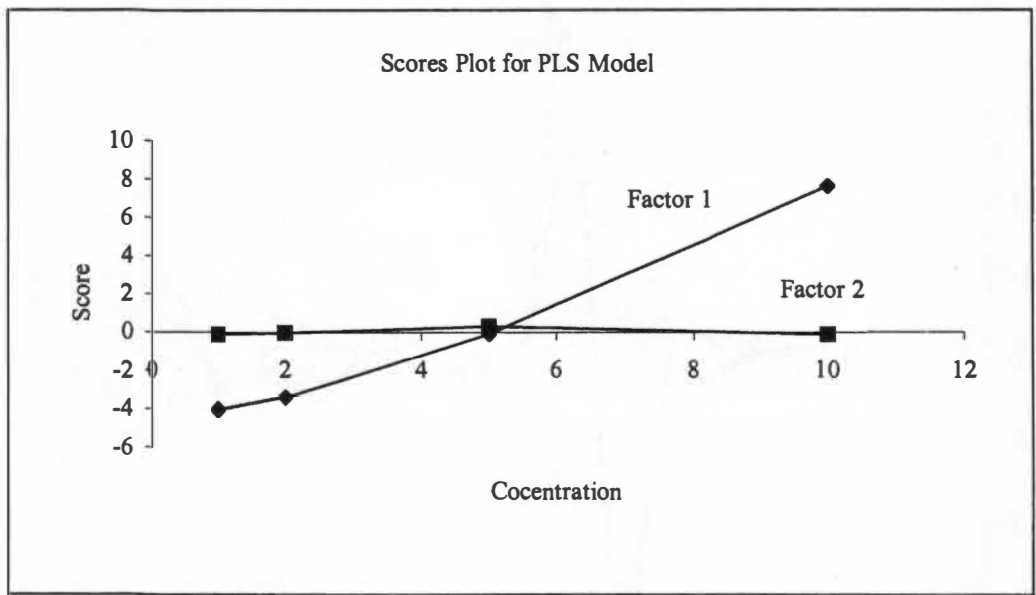


Figure 8.30 Scores plot for UV5 PLS 2 factor model

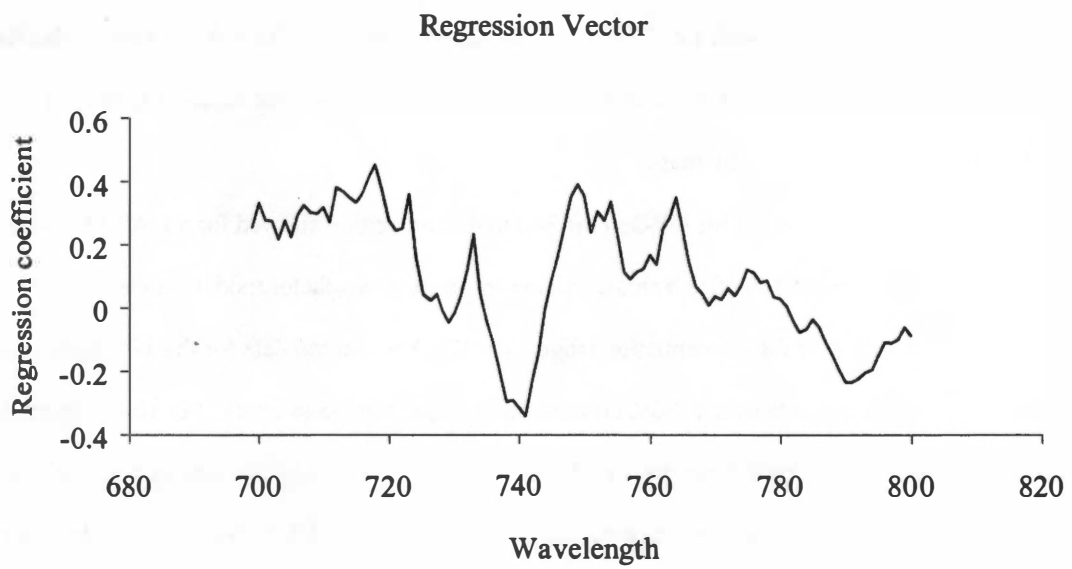


Figure 8.31 Regression vector plot for UV5 PLS model

analytes. Some of the variance in the plot is associated with the regression model also accounting for subsequent minor peaks contained in the original spectra.

PLS regression models were also built for AO-1 for a concentration range of 2-15% (5 samples), UV-2 for a range of 1-15% (5 samples), UV-3 for a range of 1-50% (7 samples), and UV-6 for a concentration range of 1-5% (3 samples). The model for AO-1 was built from the spectra in the 250 to 600 nm range. Using this information, a two-factor model was constructed that gave a SEC value of 1.82 for a concentration range of 2-15%. In this model, it was also discovered that one factor could account for 99.32% of the range. The model built for UV-2 was constructed from the 300 to 400 nm range. This data suggested that a two-factor LAS-PLS regression model could be constructed that resulted in SEC of 0.62 for a concentration range of 1-15% by mass.

The spectral data collected for UV-3 in the 300 to 400 nm region allowed for a LAS-PLS model to be constructed for the range of 1 to 50% by mass. Using this data, a two-factor model was built which resulted in a SEC of 2.55 over the concentration range. The UV-Vis spectral data for the UV-6 additive concentrates was only applicable over a 1-5% concentration range, using 3 samples. For this additive, a one-factor model was built using the spectral data for the 700 to 800 nm range, and resulted in a SEC of 0.06. The summaries of the regressions are presented in Tables 8.4 through 8.7. Based on the development of these regression models, it can be concluded that regression models can be constructed for a limited range of concentrations for commonly used antioxidants and ultraviolet stabilizers. The models chosen had relatively few factors so that the majority of the information could be extracted without attempting to model the gross noise in the system. The inclusion of multiple factors will attempt to model any high frequency noise contained within the spectral data. While the overall variance of the data will be reduced, the model will not be valid for prediction of new samples.

The path length of 3.0 mm limited the use of this spectroscopic technique because of the scattering that occurs due to the high concentrations of the additives at the lower wavelengths. UV spectroscopy is one of the more direct forms of spectroscopy and is based on the absorbance characteristics of individual chemical species. This fact reduces its effectiveness in measuring highly concentrated samples with a

Table 8.4 Optimized PLS Model Summary for AO's UV Data

Sample ID	Concentration Range	Scan Range	Factor	Variance in X Block (%)	Cumulative X Block Variance	Variance in Y Block (%)	Cumulative Variance in Y Block
AO1	2-15%	250-600	1	75.45874	75.45874	99.32902	99.32902
			2	0.488766	75.947506	0.64338	99.97240
AO3	1-10%	400-500	1	35.1772	35.1772	99.21201	99.21201
			2	0.274797	35.4519	0.775024	99.98703

Table 8.5 Optimized PLS Error Summary for AO's UV Data

Sample ID	Factor	SEV	SEC	Press	R <sup>2</sup>
AO1	1	3.531116	2.478435	12.28528	0.935222
	2	1.922876	1.8222	3.320414	0.982913
AO3	1	1.133982	0.623952	0.778633	0.992023
	2	0.489952	0.150102	0.022531	0.99977

Table 8.6 Optimized PLS Model Summary for UV's UV Data

Sample ID	Concentration range	Scan range	Factor	Variance in X Block	Variance in Y Block
UV2	1-15%	300-400	1	77.83733	96.6656
			2	2.353921	2.923317
UV3	1-50%	300-400	1	87.698	90.84179
			2	15.51565	7.509243
UV5	1-50%	700-800	1	86.16102	99.85826
			2	0.120673	0.139857
UV6	1-5%	700-800	1	9.16752	99.93568

Table 8.7 Optimized PLS Error Summary for UV's UV Data

Sample ID	Factor	SEV	SEC	Press	R <sup>2</sup>
UV2	1	1.82723	1.299027	5.062414	0.981378
	2	0.934022	0.621724	0.773082	0.997179
UV3	1	7.578236	6.340733	281.4342	0.94105
	2	3.081588	2.549859	39.0107	0.992038
UV5	1	1.342867	0.543296	0.59034	0.993958
	2	0.721943	0.256525	0.065805	0.999328
UV6	1	0.193542	0.063879	0.00408	0.999765

rather large path length. Beer's law may not apply if there is significant scattering on the light within the sample. Based on these factors, the feasibility of using NIR spectroscopy was also investigated. Also, due to the limited capability in regards to the concentration ranges of the models and the limitation of the spectroscopic technique, the calibration models were not used with prediction sample sets

### 8.3.3 NIR SPECTROSCOPY STUDIES

The on-line NIR spectrometer was used to investigate fresh samples with the same concentrations as those that were used with the UV system. The experimental setup was to have a path length of 3.0 mm between the two transmission probes. This was found to be the minimal path length that would not interfere with the flow of polymer in the production of master batch pellets (i.e. the diameter of the strands). The temperature of the melt in the flow cell was 220 °C, which is consistent with all of the other experiments in this study. The transmission properties for the fiber optic cables that were used in this system are given in Figure 8.32. The transmission was measured by using one fiber connected to both the output and the input of the spectrometer. They were found to have a high throughput for most of the NIR range, with some diminishing performance above 1800 nm that is inherent to the fibers.

NIR spectroscopy was chosen for highly loaded samples to overcome some of the technical difficulties associated with UV spectroscopy. In NIR spectroscopy, the spectra generated are the result of combination effects within the composition matrix. As a result, these responses are much lower in magnitude than those found in alternative spectroscopic techniques. If a technique is developed to maximize the signal to noise ratio (example: taking the 1<sup>st</sup> derivative of the spectra), a multivariate technique can be used to correlate the spectra with the concentration. Multivariate techniques must be used because of the significant overlaps contained within the spectra, as the nature of the NIR spectral response. A univariate method would not be able to adequately describe the concentration information. PLS regression is chosen here for the same reasons that it was applied to the UV spectroscopic data in that it is modeling tool for data sets, which have more features than objects. In other words, data sets that have highly correlated responses that are due to relatively few variables.

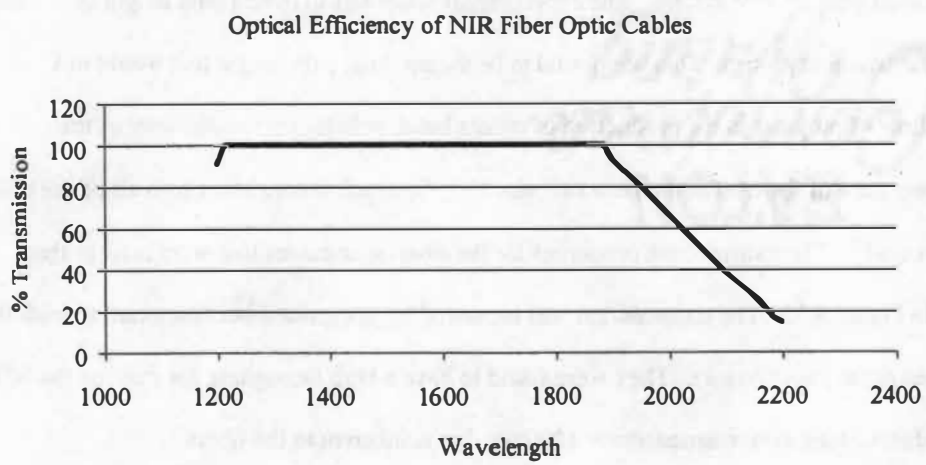


**Figure 8.32**      **Optical efficiency of NIR fiber optic cables (Transmission versus Wavelength)**

The NIR probes were found to have high throughput for this set up and the transmission capability of one setup is given in Figure 8.33. This measurement was obtained by connecting the probe via one fiber optic cable to the instrument and transmitting through the fiber optic connection of the other fiber. The location of the second fiber was done in a manner so that the transmission was maximized. It follows the similar response to the fibers. The transmission capability for the entire system is given in Figure 8.34. This experiment was conducted by connecting the NIR fiber optic cables to the transmission probes and then placing the probes in the flow cell with air in the path length. The system was then tested using neat polypropylene whose absorbance spectra is shown in Figure 8.35. The peaks in this spectrum are from the C-C bond interactions and the spectra compares well with the results in pervious work [46]. From these results, the transmission efficiency was found to be much lower due to the instrument's limitations and the absorbance and scattering of the NIR light by the molten polymer.

Each sample spectrum was collected as an average of 100 scans and 10 replicate spectra were collected, or each spectrum was the average of 1000 scans. The background for all of the NIR measurements was air (Figure 8.34) and the spectrum was subtracted from the collected calibration spectra. Because NIR spectroscopy works primarily on secondary and combination effects, it is expected that more useful data could be collected on polymer systems with higher loadings of additives. Also, because of the combination of various regions containing information about relatively few concentrations, PLS regression was used to model the data.

AO-1, AO2, AO-4 and AO-5 were found to have responses in the NIR region for a concentration range of 1% to 25%. These would be the highest levels found in commercial products. AO-3 showed opacity limitations at concentrations higher than 15% due to the highly opaque nature of the sample that were further magnified by the attempt to model a concentration of 16.5%. For the ultraviolet stabilizers, UV-1 and UV-2 had meaningful spectra for concentrations in the range of 1-25%, and UV-3 and UV-5 could be measured for concentrations up to 50% by weight. The serious limitations came with UV-7 where opacity became an issue above 17.5%, UV-6 at concentrations above 10% and UV-4 at concentrations higher than 5%. The turbidity of these samples was quite high and each had a milky white appearance to the melt. This arose from the high degree of scattering from the sample. Turbidity was the result of the



Optical Efficiency of NIR Probe

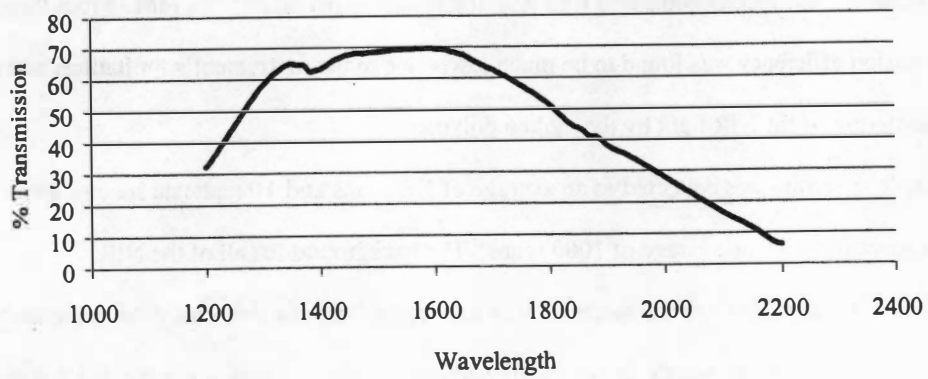


Figure 8.33 Optical efficiency of NIR probe (Transmission versus Wavelength)

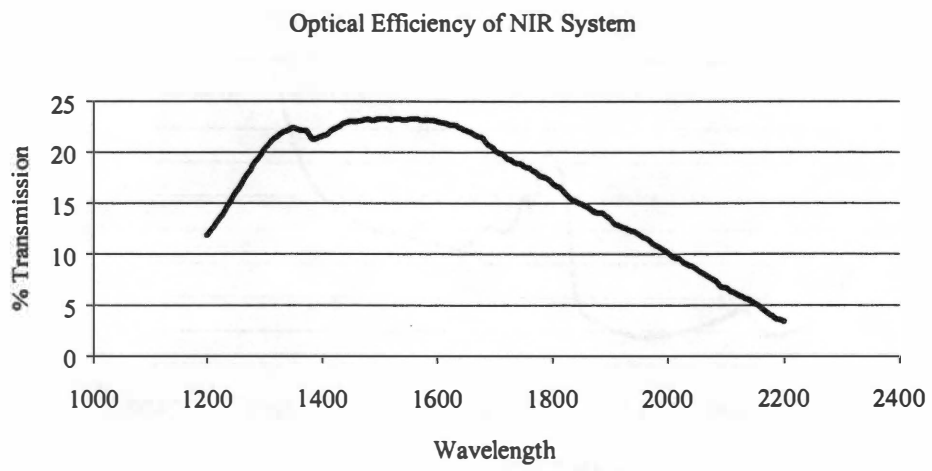


Figure 8.34 Optical efficiency of NIR system (Transmission versus Wavelength)

NIR Spectra of Polypropylene Resin

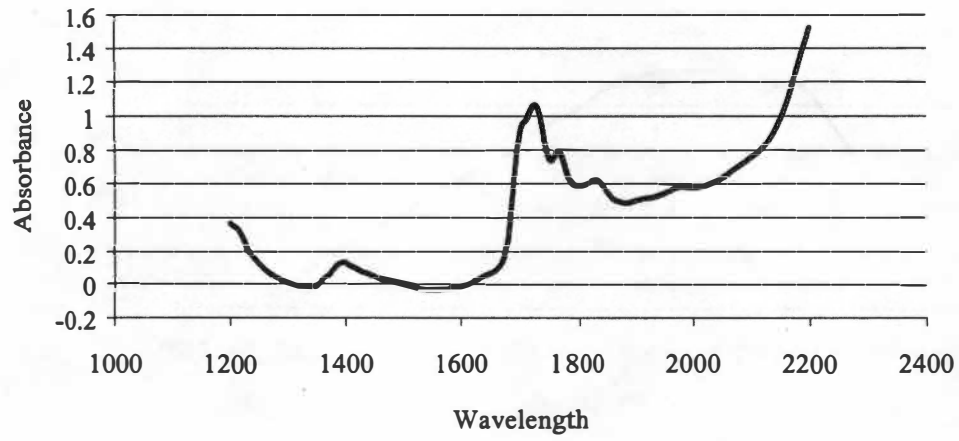


Figure 8.35 NIR Spectra of Polypropylene (Absorbance versus Wavelength)

immiscibility of the two compounds. The melt for highly loaded samples could best be described as an emulsion.

Table 8.8 provides a summary of the concentration limitations of the additives in polypropylene and compares the differences with the two techniques. The optimal models were based on different ranges of spectra as each additive behaved differently and had unique characteristics associated with it. The methodology employed was the same as those for the UV data. AO-1 was found to have the most information in the 1400-1600 nm region. This corresponds to the C-H combination band. Using the spectral information for this region, a two factor PLS model was constructed for a concentration range of this additive at 1-25% by weight in polypropylene and the optimal model was found to have a SEV of 2.28 and a SEC of 1.99. AO-2 had most of its response in the 2040-2200 nm region, which is due to the C-H stretch vibration band combinations. Data analysis on this additive showed that the optimal PLS model was found utilizing a single principle factor with a SEV of 0.91 and a SEC value of 0.85 was obtained for a concentration range of 1-25%. For this data set, the corresponding analysis is shown in Figures 8.39 to 8.45, including the 1<sup>st</sup> derivative spectra, SEV versus number of factors, scores, loadings, regression vector, the predicted versus measured plot and the reconstructed data

Figure 8.36 shows the first derivative NIR spectra for a NIR range of 2040 to 2200 nm for concentrations ranging from 1 to 25% by mass. In this plot, a clear inflection point is evident centered around 2120 nm. Figure 8.37 shows the plot of SEV versus number of factors. In this plot, it is evident that a minimum of the SEV occurs with only one factor. Further justification of this can be seen in an examination of the scores plot as presented in Figure 8.38. In this plot, the scores vector for the first factor follows an increasing trend that corresponds to an increase in concentration. The other scores in the model are all centered on the zero point, which indicates that there are modeling more of the noise in the data and not any true concentration effects.

The model can be tested for reliability by the examination of the actual versus the predicted concentrations from the PLS model. Figure 8.40 shows the predicted concentrations of AO-2 using the one factor PLS model with LAS cross validation. The regression coefficient ( $R^2$ ) between the actual concentration and the measured concentration is 0.994. Since this value is very close to 1.0, the model can

Table 8.8 Comparisons of spectroscopic effectiveness

Sample ID	Range Investigated	UV Effective Range	NIR Effective Range
AO-1	1-25%	2-15%	1-25%
AO-2	1-25%	NA	1-25%
AO-3	1-25%	1-10%	1-25%
AO-4	1-25%	NA	1-25%
AO-5	1-25%	NA	1-25%
UV-1	1-25%	1-10%	1-25%
UV-2	1-25%	1-15%	1-25%
UV-3	1-50%	1-50%	1-50%
UV-4	1-50%	1-2%	1-5%
UV-5	1-50%	1-10%	1-50%
UV-6	1-25%	1-5%	1-10%
UV-7	1-50%	NA	1-17.5%

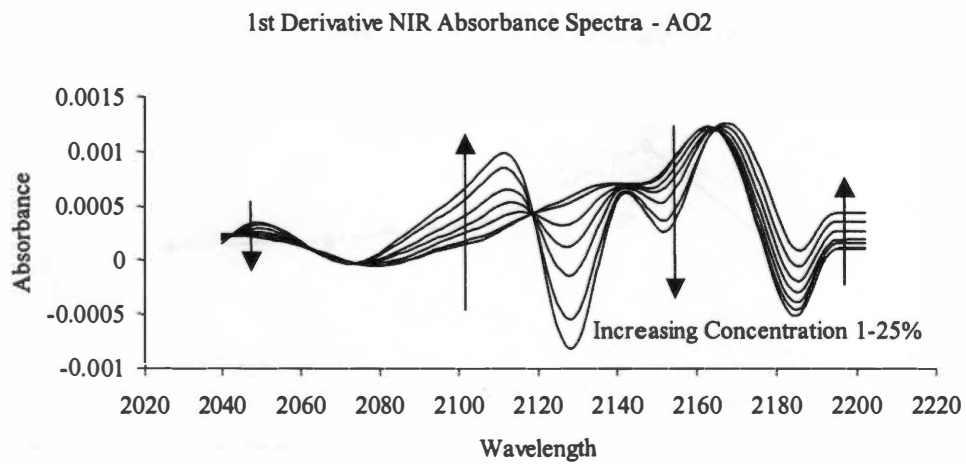
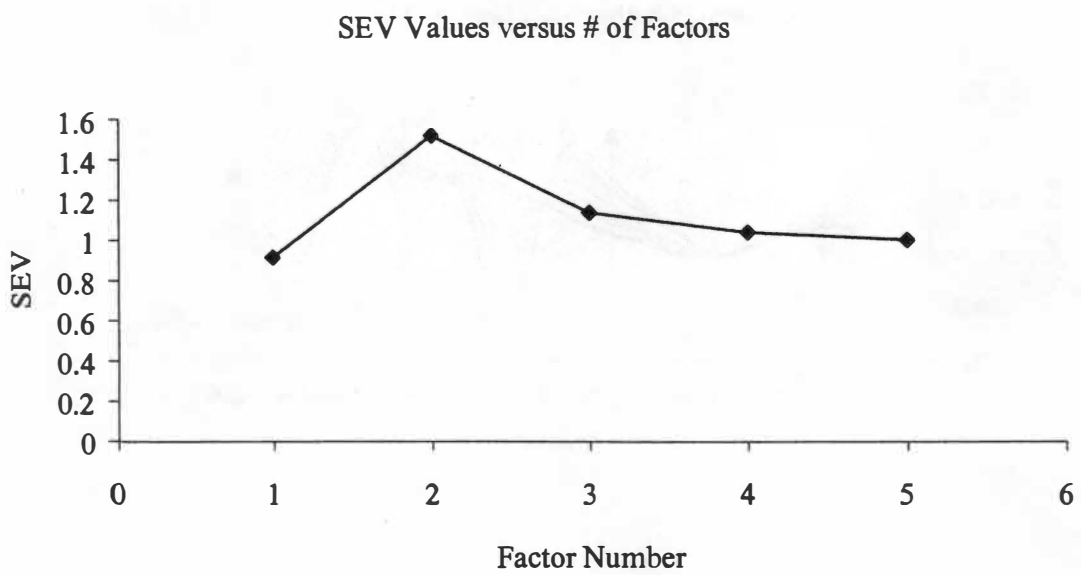


Figure 8.36 NIR absorbance spectra of AO2 (1<sup>st</sup> derivative, 1, 2, 5, 10, 15, 25, 25%)



**Figure 8.37** SEV values for AO2 PLS model

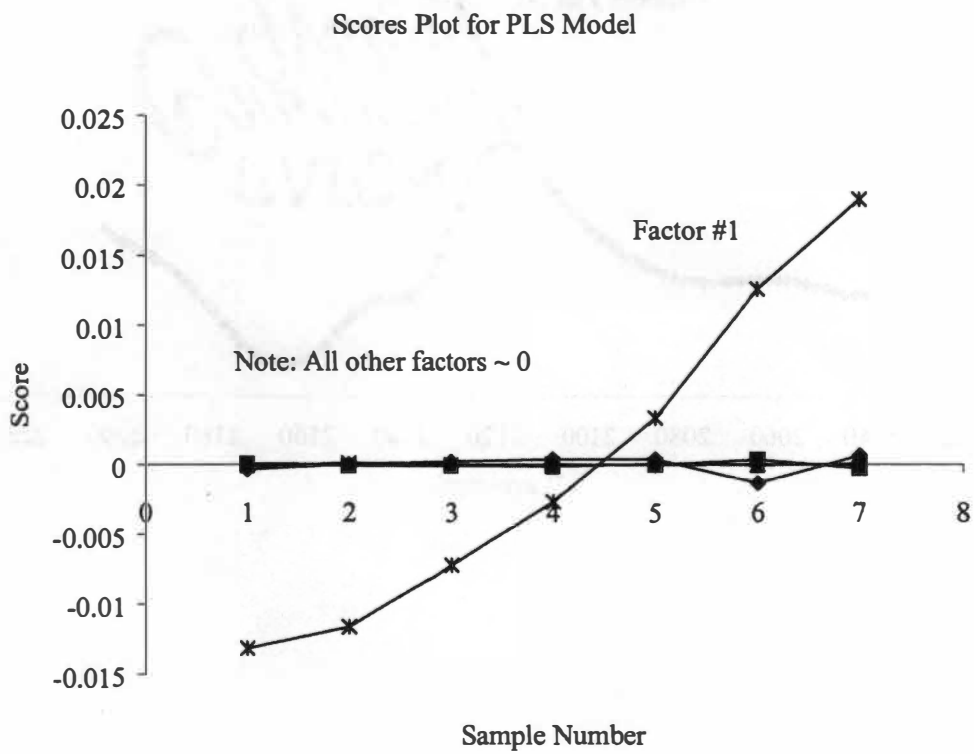


Figure 8.38 Scores plot for AO2 PLS model



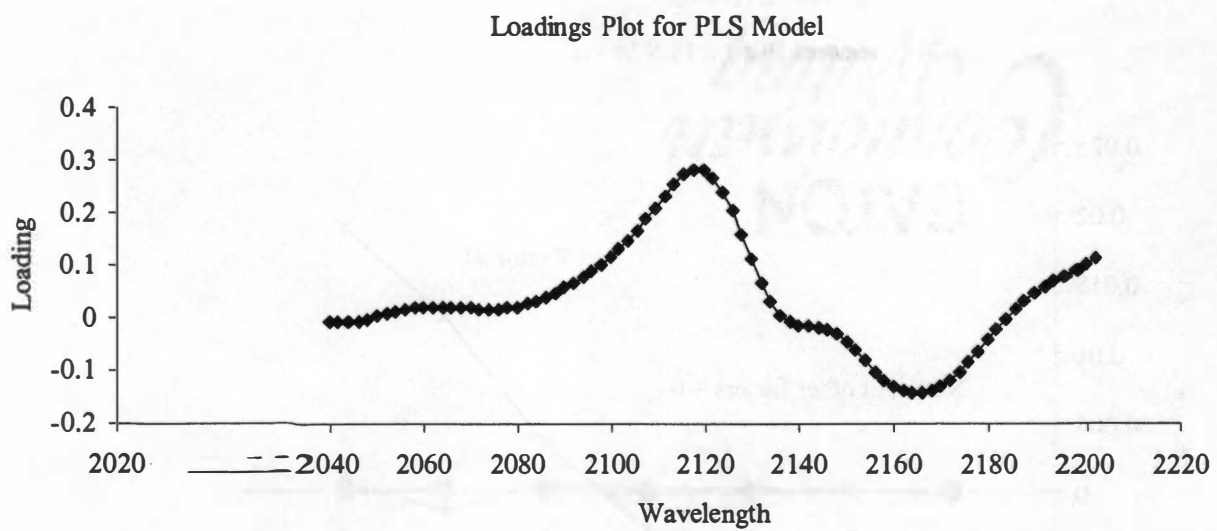


Figure 8.39 Loadings plot for AO2 1 factor PLS model

Predicted versus Measured Concentration AO-2

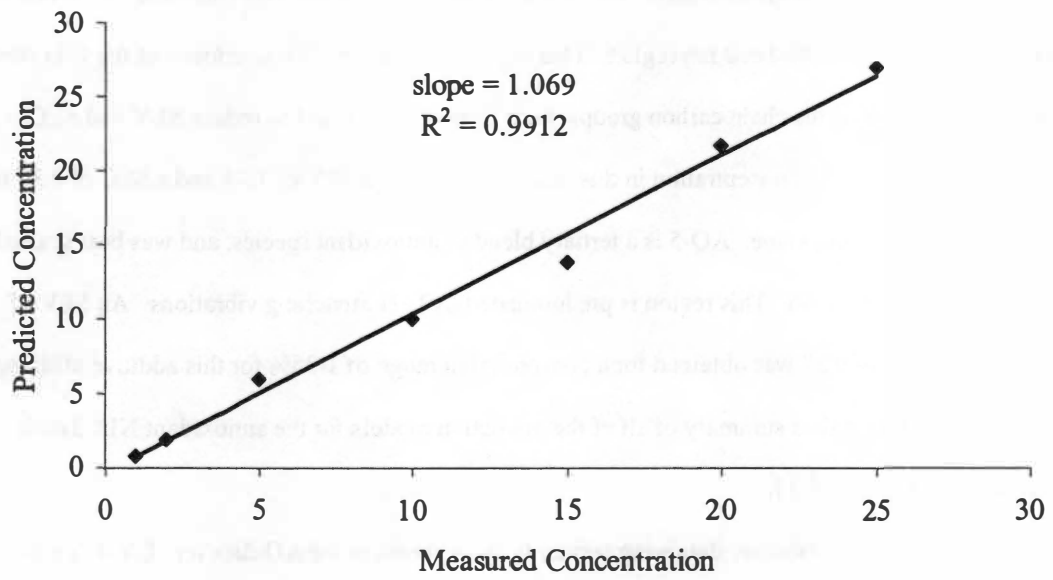


Figure 8.40 Predictive versus measured plot for AO2 PLS model

be deemed reliable. The regression coefficient's profile for this model, Figure 8.41, also follows the spectral profile of the absorbance data and is similar in shape to the plot of the first loading. A final method of reviewing the model is to reconstruct the spectral response from the model. Reconstructed data for the one factor PLS model is presented in Figure 8.42 and has the same behavior as the original spectral data as shown in Figure 8.36. Table 8.9 presents the error values associated with the model, showing that one factor is sufficient to model the data.

AO-3 had most of its response in the 2000-2100 nm region, which includes both the C-H stretch vibration as well as the O-H stretch combination band. The optimal PLS model for this additive was found to be a two-factor model based on this region and resulted in a SEV 3.10 and a SEC value of 1.74. This model could be used for a concentration range of 1 to 15%, as higher concentrations of antioxidant were not miscible with the molten polymer matrix. AO-4 is a blend of two unique molecules and was found to be best modeled using the 1600-1800 nm region. This region includes the first overtones of the C-H stretch for the aromatics as well as the chain carbon groups. Four factors were found to reduce SEV and SEC model was used to predict the concentration in this range and yielded a SEV of 1.74 and a SEC of 0.39 for a range of 1-25% in polypropylene. AO-5 is a tertiary blend of antioxidant species, and was best studied using the 1800-1900 nm region. This region is predominated by C-H stretching vibrations. An SEV of 1.47 with a SEC value of 0.27 was obtained for a concentration range of 1-25% for this additive utilizing a four-factor PLS model. A data summary of all of the prediction models for the antioxidant NIR data is presented in Table 8.10 and 8.11.

The results of UV stabilizer data were similar to those found in the AO data set. UV-1 is a two-component mixture and was found to have the majority of its spectral information in the 1800-1930 nm region. These peaks are the result of C-H stretching in the molecules. From this information, the optimal PLS model was constructed utilizing one principal component and a SEV of 1.68 with a SEC value of 1.17 was obtained for a range of 1-25% additive. UV-2 is an aromatic compound and has the majority of its information in the 2050-2200 nm range. This corresponds to the C-H stretch in aromatic compounds.

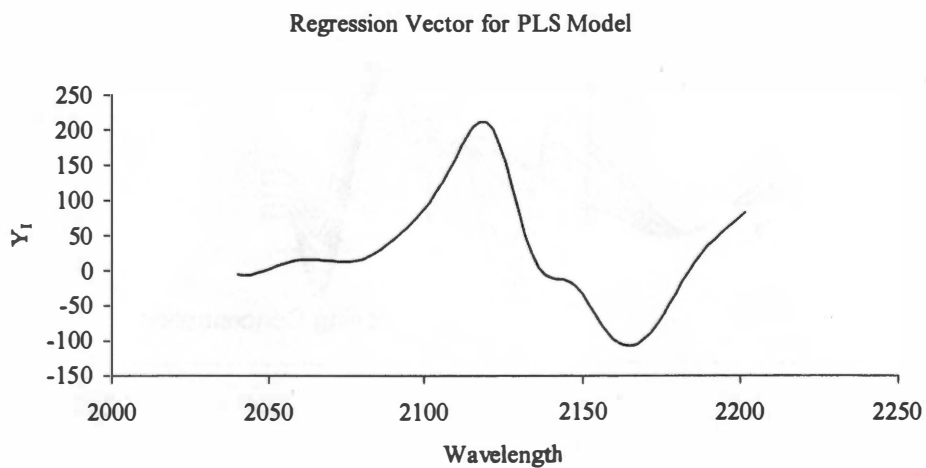


Figure 8.41 Regression vector plot for AO2 PLS model

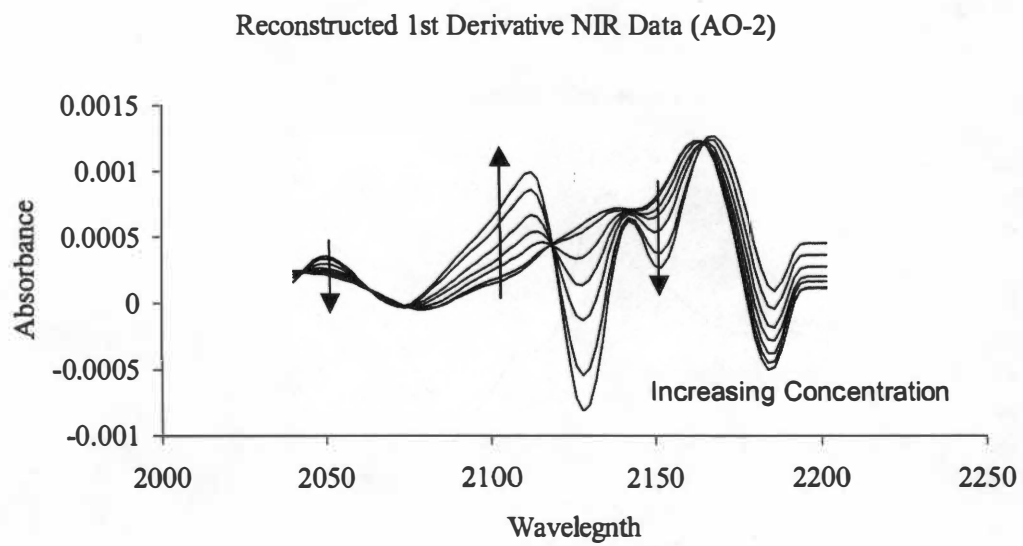


Figure 8.42 Reconstructed absorbance data from AO2 PLS model (1<sup>st</sup> derivative, 1, 2, 5, 10, 15, 20, 25%)

Table 8.9 Error summary for AO-2 PLS Model

Factor	Variance in X Block	SEC	PRESS	R <sup>2</sup>
1	99.66422	0.851156	3.622335	0.996448
2	0.30322	0.857973	2.944471	0.997114
3	0.025488	0.465585	0.650307	0.999363
4	0.002957	0.122291	0.02991	0.999971
5	0.002856	0.0219	0.00048	1

Table 8.10 Optimized PLS Model Summary for AO's NIR Data

Sample ID	Concentration range	Scan range (nm)	Factor	Cumulative Variance in X Block	Variance in Y Block
AO1	1-25%	1400-1600	1	99.75	90.4406
			2	99.97	9.5532
AO2	1-25%	2040-2200	1	99.91	99.6642
AO3	1-15%	2000-2120	1	99.96	89.5347
			2	99.99	10.4333
AO4	1-25%	1600-1800	1	97.62	98.7638
			2	99.98	0.8504
			3	99.99	0.2640
			4	99.9996	0.0905
AO5	1-25%	1800-1900	1	99.92	90.6176
			2	99.99	9.1569
			3	99.9997	0.2154
			4	99.9999	0.0078

Table 8.11 Optimized PLS Error Summary for AO's NIR Data

Sample ID	Factor	SEV	SEC	Press	R <sup>2</sup>
AO1	1	6.4594	4.7072	110.7869	0.8849
	2	2.2802	1.9900	15.8407	0.9844
AO2	1	0.9143	0.8512	3.6223	0.9964
AO3	1	3.7286	3.2684	32.0475	0.8755
	2	3.1017	1.7446	6.0873	0.9776
AO4	1	5.1400	3.9525	62.4904	0.9225
	2	3.5015	1.8496	10.2628	0.9877
	3	2.3294	0.7142	1.0201	0.9988
	4	1.7492	0.3933	0.1547	0.9998
AO5	1	6.5786	5.8635	171.9050	0.8146
	2	2.4161	1.5640	9.7841	0.9904
	3	1.5804	1.0745	3.4633	0.9966
	4	1.4703	0.2738	0.1499	0.9999

UV-2 was found to behave ideally in a spectroscopic sense and a two principal factor PLS model was constructed for a range of 1-25%. This model resulted in a SEV of 0.16 with a SEC value of 0.14. The plots for this additive are shown in Figures 8.43 through 8.49.

Figure 8.43 shows the first derivative spectra for a concentration range of 1-25% UV-3 in polypropylene. As is evident in the plot, there is a well-defined inflection point in the data. Figure 8.44 shows a plot of the SEV values versus the number of factors. The SEV is at a minimum with two factors in the LAS SEV regression model. But when a plot of the scores is analyzed (Figure 8.45), it should be noted that all of the scores are approximately zero with the exception of the score for the first factor. This point is further demonstrated when reviewing the loadings plot for the regression model presented in Figure 8.46. In this plot, the loading for the first score follows the same trend as the original absorbance data. The other loadings have much more variability in them indicating that they are attempting to account for much less variation in the data.

The reliability of the PLS regression model was further examined and tested by comparing the actual concentration of UV-2 and the predicted concentration in the calibration set. Figure 8.47 shows the predicted concentrations of UV-2 using the 1 factor PLS model with LAS cross validation. The correlation coefficient between the actual concentrations and the predicted concentrations in the calibration set is 0.999. As was done in the AO-2 example, Figure 8.48 is a plot of the regression vector. Using the LAS PLS regression model, the original spectra can be reconstructed to determine if the model actually simulates the absorbance spectra. Figure 8.49 demonstrates that the original spectra are indeed modeled correctly with this procedure.

UV-3 is also an aromatic compound, but the best spectral information came from the 1800-1900 nm region, which is a result of N-H stretching in the molecule. A 2-factor PLS model was built on this calibration data and resulted in a SEV of 0.35 with a SEC value of 0.31 for a range of 1-50%.

UV-4 is a high molecular weight stabilizer designed to be more compatible with the polymer system. The best spectral information was found in the 1520-1560 nm region. This comes from the first overtones of the N-H bond. Unfortunately, this additive was also found to be opaque at concentrations



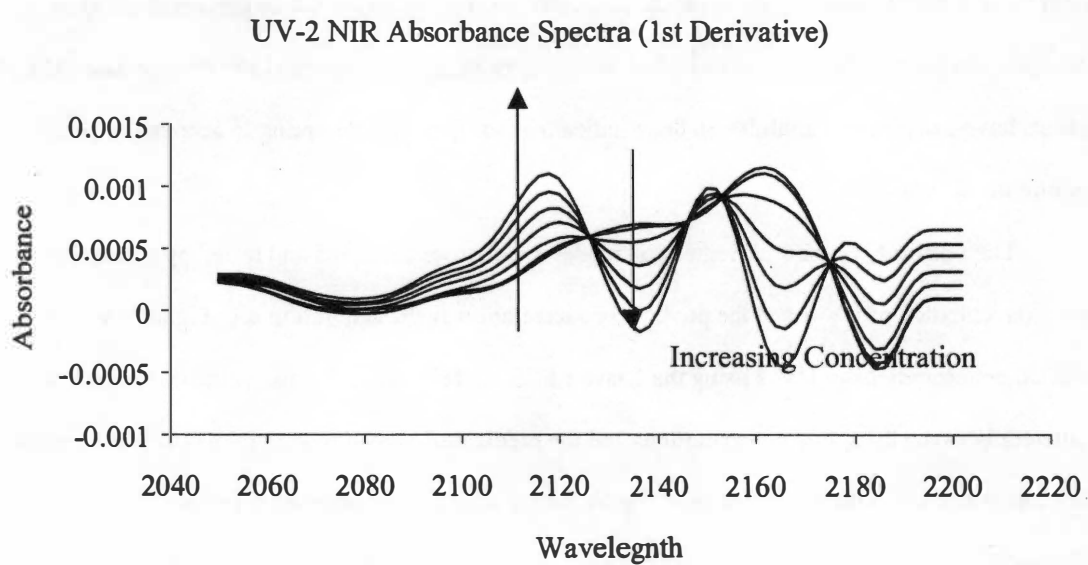


Figure 8.43 NIR absorbance spectra of UV2 (1<sup>st</sup> derivative, 1, 2, 5, 10, 15, 20, 25%)

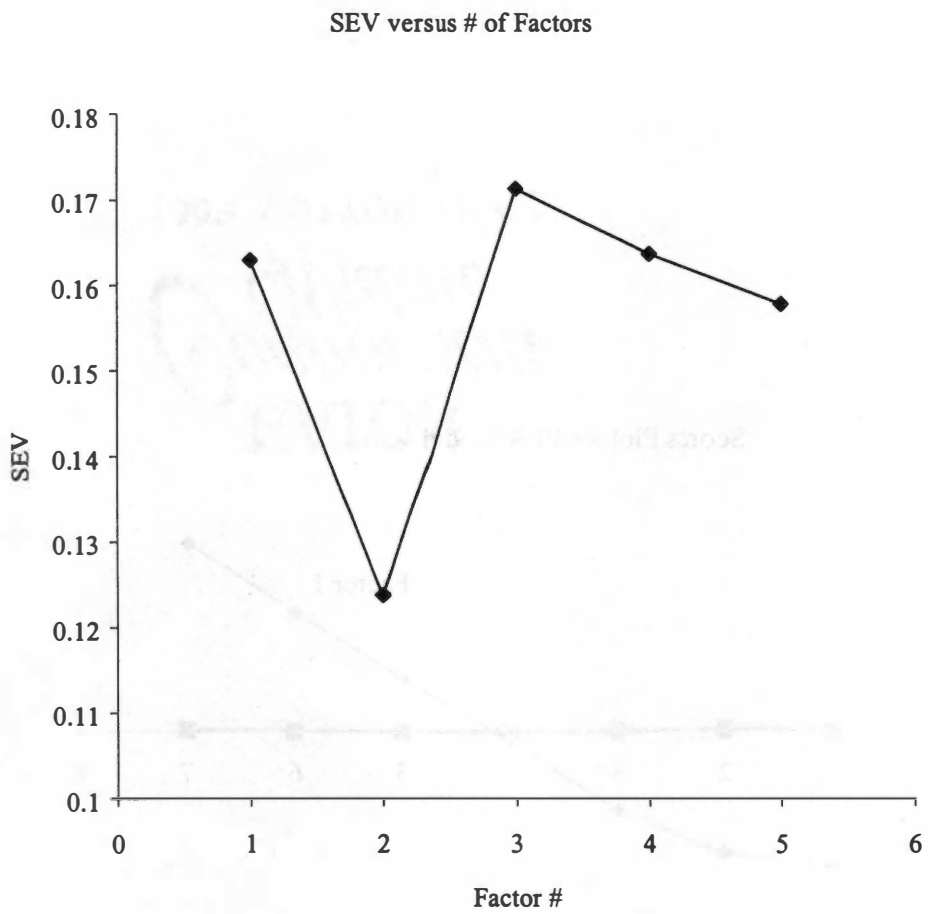


Figure 8.44 SEV values for UV2 PLS model

Scores Plot for PLS Model

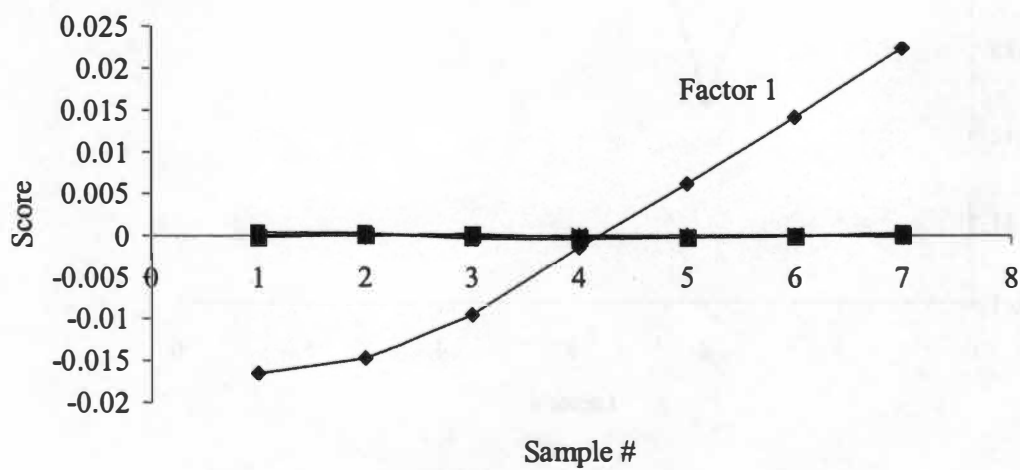


Figure 8.45 Scores plot for UV2 PLS model

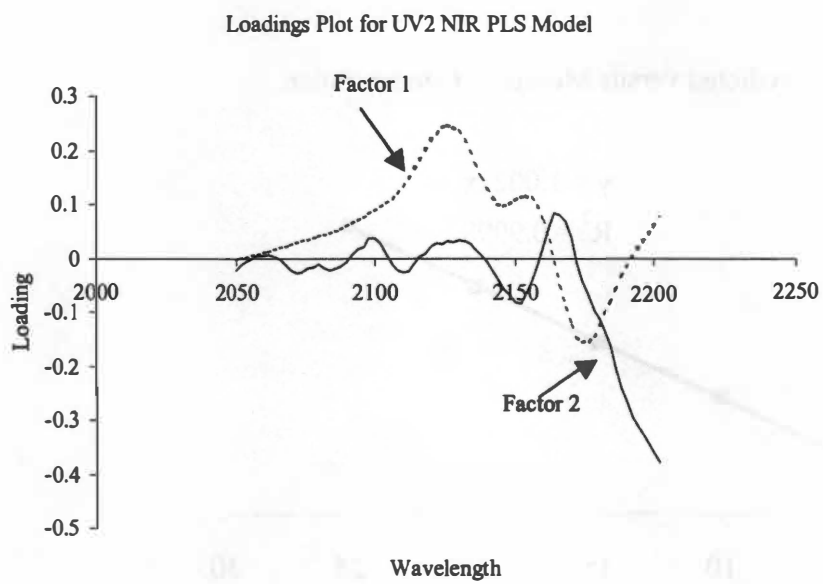


Figure 8.46 Loadings plot for UV2 PLS model

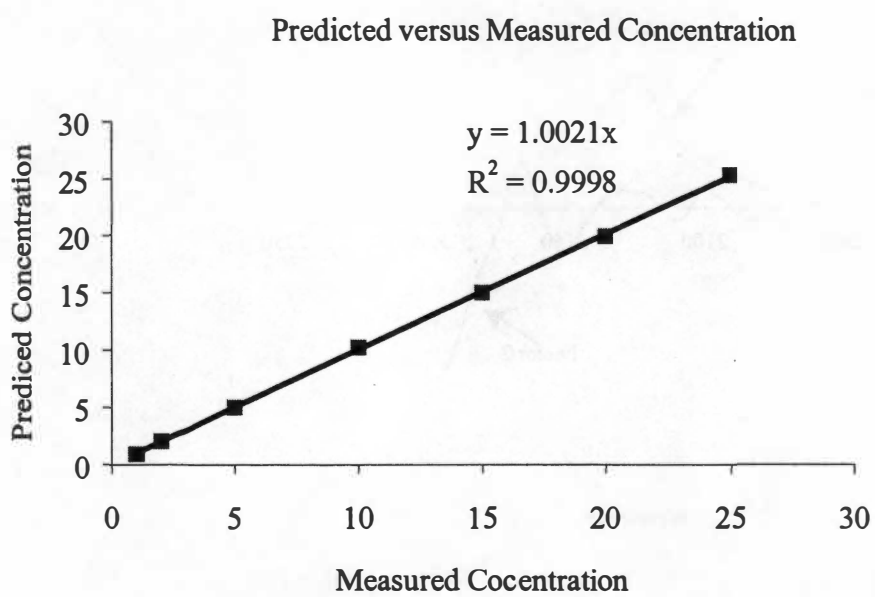


Figure 8.47 Predictive versus measured plot for UV2 PLS model

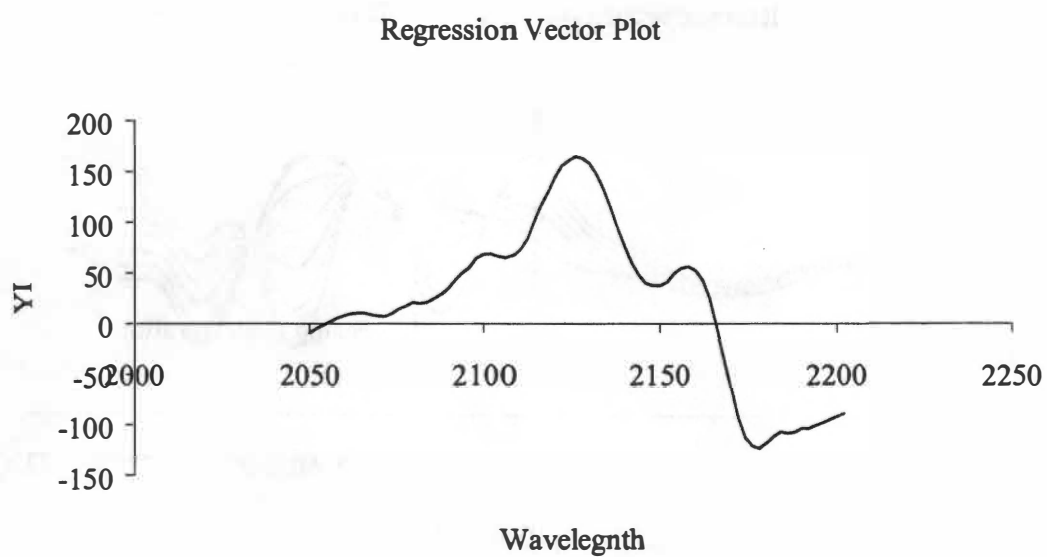


Figure 8.48 Regression vector plot for UV2 PLS model

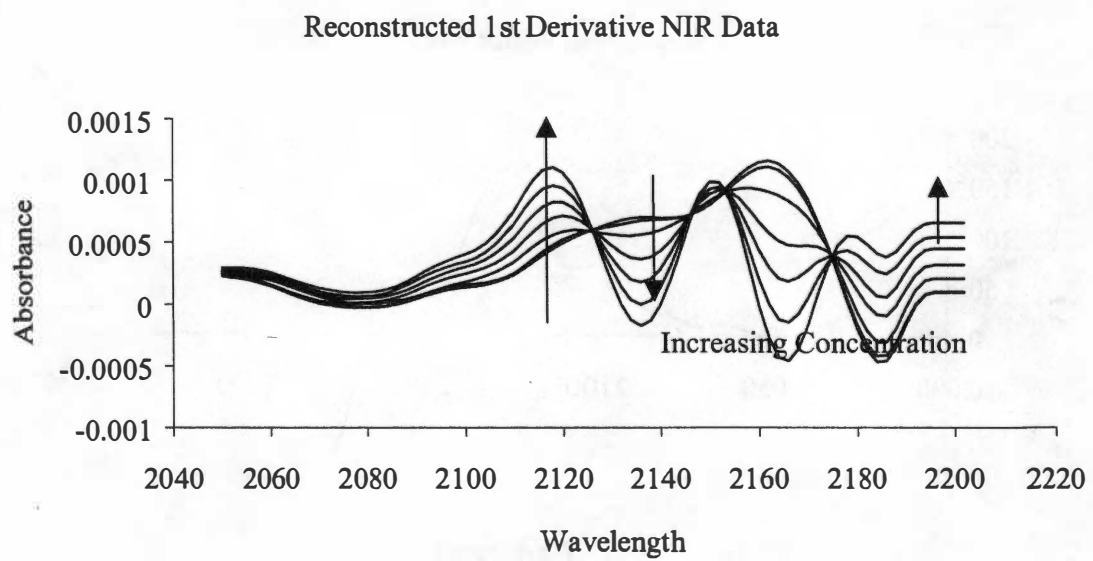


Figure 8.49 Reconstructed absorbance data from UV2 PLS model (1<sup>st</sup> derivative, 1, 2, 5, 10, 15, 20, 25%)

above 5% by weight. A one-factor model was determined to be optimal and had a SEV of 3.05 and a SEC value of 0.56 for a range of 1-5%. UV-5 is also a high molecular weight additive and was found to have the largest response in the 1480-1580 nm region which also corresponds to the N-H stretch first overtone band. Because of the high molecular weight, it was also very soluble in the resin, and a PLS model was constructed for a range of 1-50%. The SEV for this model was found to be 1.14 using 3 principal components. It also resulted in a SEC of 0.36.

UV-6 is a blend of UV-7 with another stabilizer molecule. It was determined that this combination has the best spectral information in the 1600-1800 nm region for 1-10% concentration, which is due to the C-H stretch vibration due to aliphatic hydrocarbons. This combination is only slightly soluble with polypropylene and a 1-factor PLS model was constructed and found to have a SEV value of 3.10% with a SEC value of 1.28%. The UV-7 molecule on its own however, was determined to have the majority of its spectral information in the 2000-2200 nm region, corresponding to the combination bands of the C-H stretch. It was more soluble than the blend found in UV-6 and the applicable spectroscopic range for modeling was increased to 17.5%. Using the spectra available from the calibration data, a two factor PLS model was built and resulted in a SEV of 0.75 with a SEC value of 0.51. The summary of the NIR calibration models for the UV additives is presented in Table 8.12 and 8.13.

To demonstrate the differences that can occur based on which region of the spectra the PLS regression is performed on, a separate experiment using UV-6 in polyethylene was performed. In this set of experimental work, a calibration set of 12 different formulations centered on a 10% +/-2% target concentration had NIR spectra collected and averaged in the same manner as those previously discussed. Different spectral regions were then identified as having unique signals based on concentration. Once these regions were identified, PLS regression models were built for each region and the SEC values were calculated. Table 8.14 shows the difference in SEC that can be obtained. The models varied from one to three principal components, and the resultant SEC values were from 1.52 to 0.87. This demonstrates that care must be used in choosing which spectroscopic information is used for the data analysis.



Table 8.12 Optimized PLS Model Summary for UV's NIR Data

Sample ID	Concentration range	Scan range	Factor	Variance in X Block	Variance in Y Block
UV1	1-25%	1800-1930	1	99.99	99.5336
UV2	1-25%	2050-2200	1	99.87	99.9377
UV3	1-50%	1800-1900	1	99.99	99.6358
			2	100	0.2846
UV4	1-5%	1520-1560	1	99.97	99.7425
UV5	1-50%	1480-1580	1	99.98	92.6023
			2	100	4.1054
			3	100	3.2777
UV6	1-10%	1600-1800	1	99.98	98.2311
UV7	1-17.5%	2000-2200	1	99.98	94.0890
			2	99.99	5.1981

Table 8.13 Optimized PLS Error Summary for UV's NIR Data

Sample ID	Factor	SEV	SEC	Press	R^2
UV1	1	1.6861	1.165832	6.795819	0.993326
UV2	1	0.162928	0.144646	0.104612	0.999898
UV3	1	0.66081	0.556664	2.169127	0.999559
	2	0.346316	0.306848	0.564934	0.999885
UV4	1	3.048836	0.560699	0.314383	0.981695
UV5	1	3.041068	1.92779	14.865491	0.982115
	2	2.836606	0.527343	0.834272	0.999005
	3	1.138286	0.358729	0.257373	0.999693
UV6	1	3.090349	1.282964	3.291992	0.965824
UV7	1	0.960544	0.785833	1.852599	0.993226
	2	0.751823	0.506946	0.513988	0.998125

**Table 8.14** Differences in SEC based on wavelength range for 8 to 12% UV-6 in polyethylene

<b>Model ID</b>	<b>Range (nm)</b>	<b># of Factors</b>	<b>SEC</b>
A	1660-1730	1	1.0706
B	1740-1790	1	1.3499
C	1790-1830	2	1.5164
D	1840-1900	2	0.9627
E	1900-2050	2	1.3179
F	2020-2140	3	0.868

Due to the greater range of concentrations that the NIR instrument was capable of measuring, prediction models were built for the UV data, but calibration work focused entirely on the NIR instrument.

For the use of quality control, the error in the prediction models must be below 0.5% for practical industrial usage. While most of the data that is shown for the NIR models has a SEC below that value, on those that it does not, the technique should not be dismissed. The concentration ranges that these models were constructed on are much greater than what would ever be seen as a process variation. For commercial use, prediction sets would be constructed that are closer to the set value of that particular process. For example, a 20% concentrate would need to have a model that would allow for a range of 14 to 26%. The intent here is to demonstrate the versatility of the technique

Once the PLS model was constructed using the calibration data, it was possible to create a prediction profile using SNAP 2.03 a GUI for building real time prediction models available from Brimrose for support of their instrument. This feature allowed for the development of real time concentration monitoring. Figures 8.50 through 8.52 show the results of this data from real time monitoring. These samples were run at different dates, so there is no ramping between the data sets, i.e. the plot is a merge of three separate data files. For these examples, each data point represents 100 averaged scans, which are then compared with the PLS model. The concentrations that were prepared for these trials were as follows: UV-1 (6%, 18%, 24%, 12%), UV-2 (12.5%, 20%, 17.5%), and AO-2 (10%, 8%, 16%). While there is some variation in the results, the regressed models fit quite well with the target concentrations. The control limits are the set concentration +/- the SEC.

#### **8.4 EXPERIMENTAL LIMITATIONS**

The limitations of the experiments come mainly from the analytical techniques used and the sample preparation. The Nicolet 5DXC FT-IR spectrometer has a working range of 4800 to 400  $\text{cm}^{-1}$ . This particular instrument has been shown to have a slight problem in resolving peaks around 1000  $\text{cm}^{-1}$  using the manufacturer's calibration and validation software. The instrument was within the specifications during these experiments. Problems could have developed during the loading of the instrument. This instrument uses a laser as its light source. While this allows the operator to determine where on the sample the measurements will be made, the spot chosen may not have the exact amount of additive in that small a

### Concentration Prediction Plot

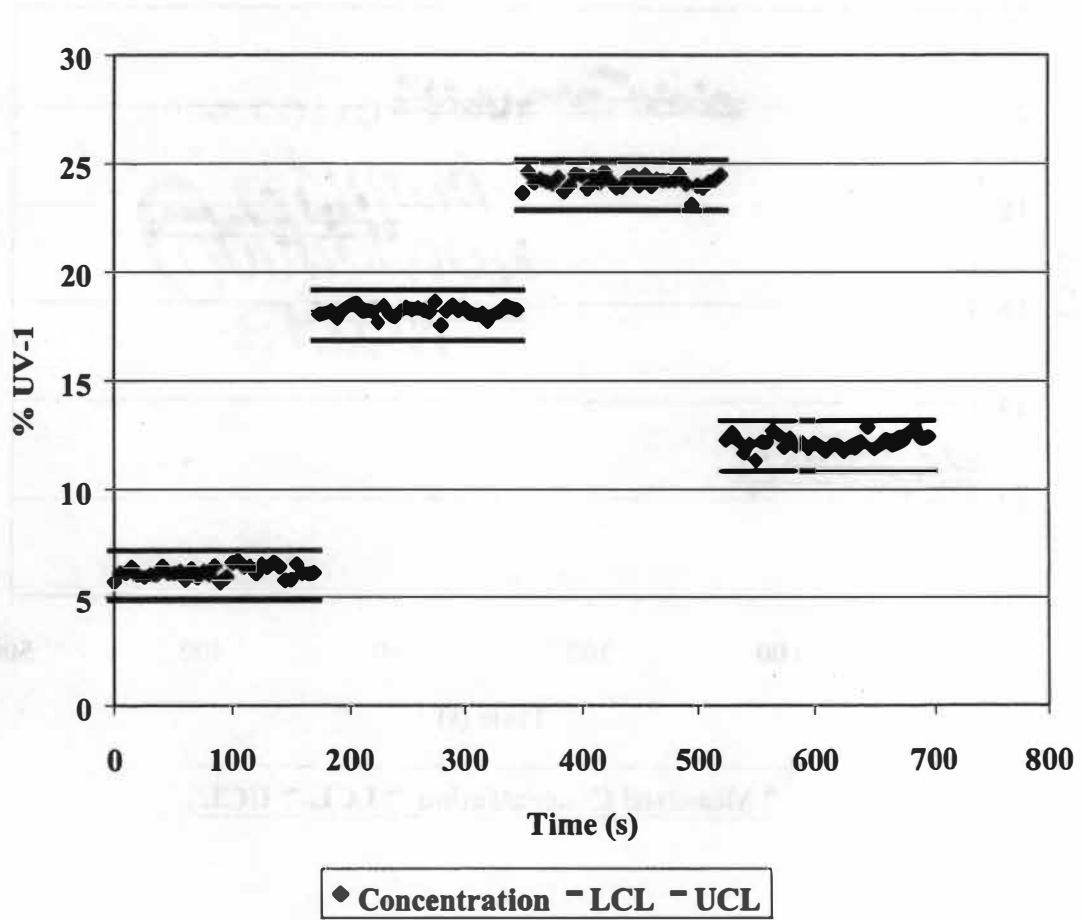


Figure 8.50 Real time prediction for UV-1 using on-line NIR spectroscopy (6, 18, 24, and 12%)

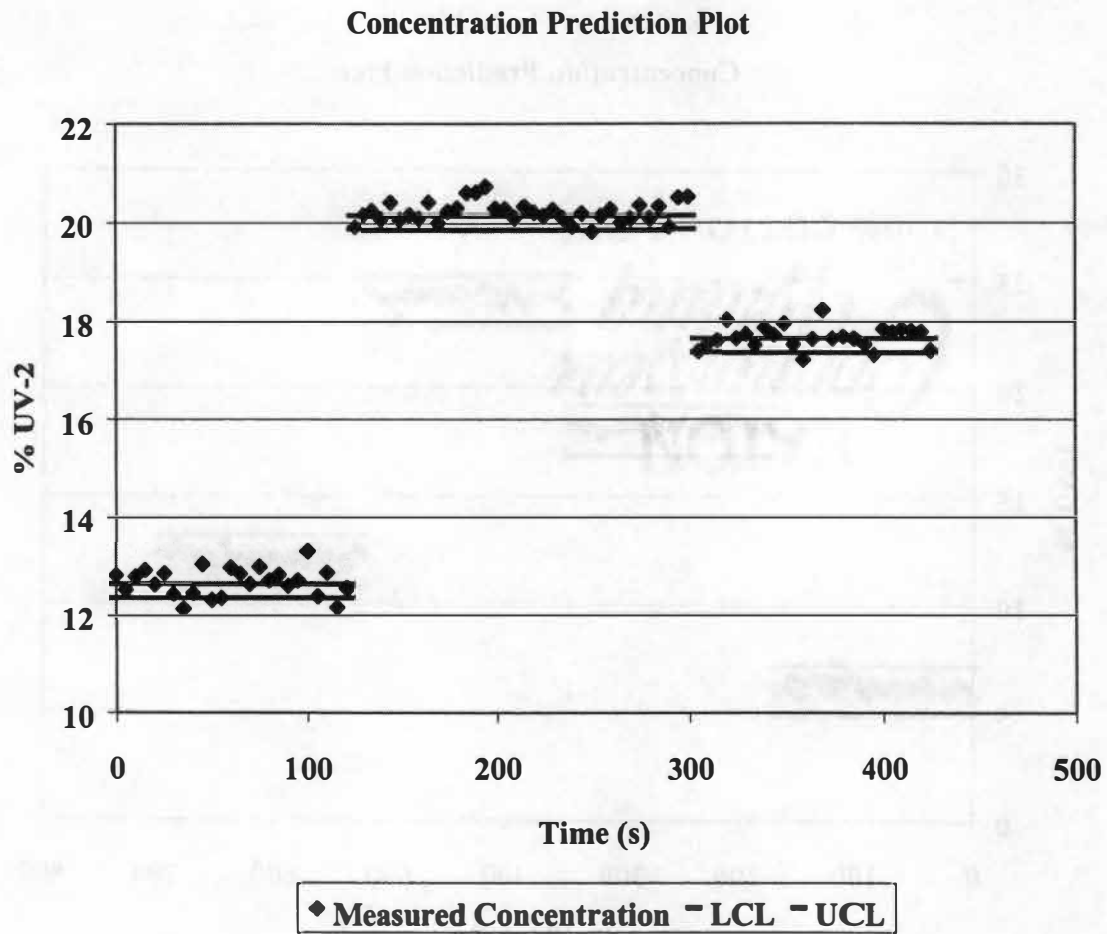


Figure 8.51 Real time prediction for UV-2 using on-line NIR spectroscopy (12.5, 20, and 17.5%)

### Concentration Prediction Plot

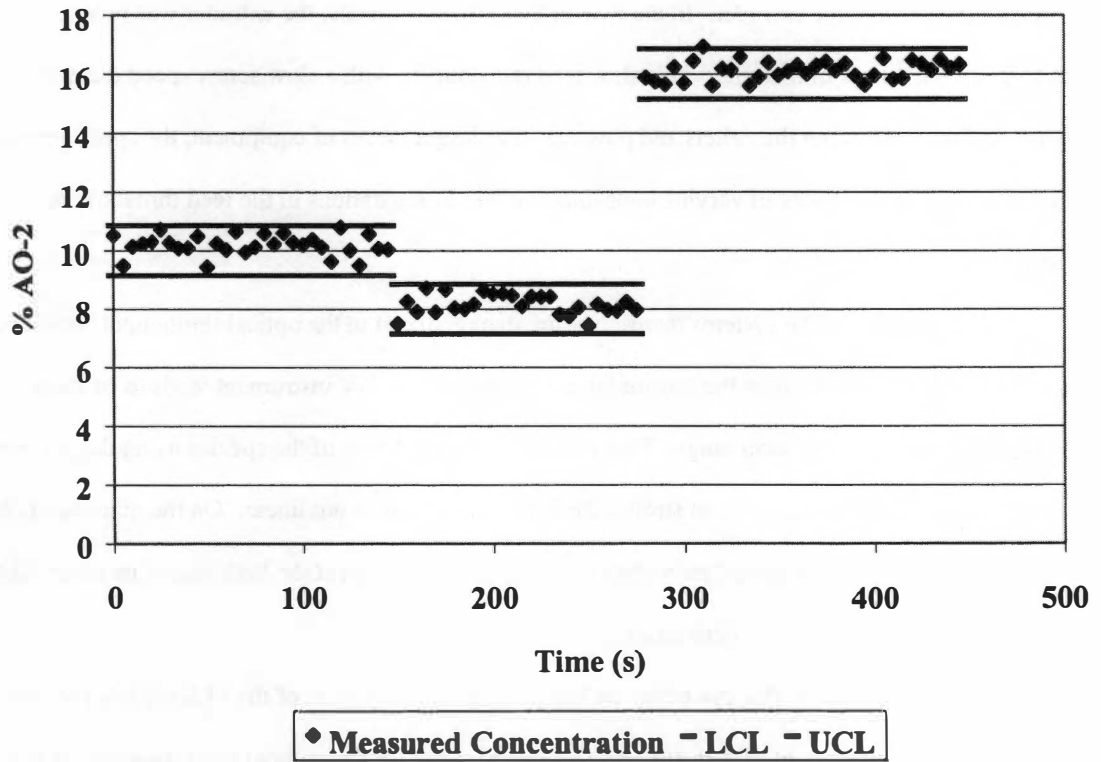


Figure 8.52 Real time prediction for AO-2 using on-line NIR spectroscopy (10, 8, and 16%)

location. This is the reason that multiple spectra are required to make accurate on-line measurements during production of these products.

As was seen in both the calibration trials, the thermodynamic stability of the system will give the concentration range that can be suitably measured. The issue of opacity is one that cannot be avoided in making these measurements. This limitation comes from the light scattering properties of the highly loaded samples. For some cases, this scattering invalidates the use of Beer's law. The other issue is the actual flow of material through the extruder. In the case of these measurements, the extruder was processing about 15 pounds per hour of material. This slow feed rate coupled with a slow screw speed did not allow for much separation between the pellets and powders. For larger pieces of equipment, the spectrometer may be able to identify regions of varying concentration due to separations in the feed throat of the extruder.

The limitations of the systems themselves are demonstrated in the optical throughput shown in Figures 8.10 and 8.37 which show the transmission efficiency. The UV instrument tends to be more limited at the lower end of its scan range. This is due to the absorbance of the species using the 3.0 mm path length. Since the absorbance is so strong, the data in this range is not linear. On the other hand, the NIR instrument has excellent optical properties for most of its range, but at the high end of its range (above 2000 nm), the throughput starts to deteriorate.

The other limitations that can occur are based on the development of the PLS models themselves. There was a significant amount of data analysis that had to occur for the optimal regression model to be chosen. As was shown with the UV-6 polyethylene example, six different regions were investigated to minimize the error in the model using the same calibration spectra. While this does lead to a great error reduction, there is always some doubt as to the "perfect" error minimization in the analysis problem. For most of the models presented, the error is still well below what is accepted or even available in the commercial environment.

## 8.5 CONCLUSIONS

From the preliminary results, it is possible to conclude that detailed information of the additive loadings in polymer samples can be made using spectroscopic techniques. The data generated using FTIR

was used as proof of concept for these measurements with this sample set. The spectra were not regressed to get detailed mathematical models of the concentration, but rather as a visual confirmation of the technique. From the experimental limitations in these experiments, it is a reminder on the benefits of conducting these experiments in a real time practical manufacturing environment. Issues of human error can be greatly reduced by the sheer volume of samples and measurements. Finding regions of the spectra that are useful that are also in the more sensitive can eliminate limitations from the instrument

The detailed study shows that spectroscopic techniques when coupled with a multivariate analysis technique can be used in an on-line manner for monitoring additive concentrations in polymer processing applications. While limited because of the opaque nature of the samples, on-line UV spectroscopy was successfully used for measuring concentrations for commonly used antioxidant stabilizers and most of the common ultraviolet stabilizers for the polypropylene fiber market. These were limited to lower concentrations, but still on the order of those that would be found commercially. The error in the model, would allow for real time process monitoring, but is not the ideal method for use in real time process control with a feed back routine.

Results of the NIR work was much more promising in comparison. Not only was the technique able to expand the range of concentrations for the additives that were modeled using UV spectroscopy, it was able to collect meaningful spectra for the additives that were not able to be modeled using the other technique. For AO-1, the range was expanded from 2 to 15% to 1 to 25%, while the SEV increased slightly from 1.92 to 2.28. The SEC for this model was raised from 1.88 to 1.99. AO-2, which was unable to be measured, using UV spectroscopy, was successfully monitored for a working range of 1-25% with a SEV of 0.91 and a SEC value of 0.85. AO-3, which was limited to a maximum concentration of 10% with a SEV of 0.49 using UV spectroscopy, was expanded to a maximum of 25%, but suffered with a SEV of 3.10. The SEC went from 0.15 to 1.74 as well. This additive showed the complexities associated with spectroscopy for on-line analysis. Even though the accuracy is much better utilizing UV spectroscopy, the range may be limited to a non-commercially viable option. Fortunately, commercially available antioxidant products are typically lower in concentration than ultraviolet stabilizer master batch products. AO-4 and AO-5 were not successfully monitored using UV spectroscopy, but were found to be capable of



being measured for the entire range of interest using the NIR technique. SEV values of 1.74 and 1.47 respectively were obtained from PLS regression of the calibration spectra. The SEC values for these models were 0.39 and 0.27 respectively.

The use of NIR spectroscopy was also found to be more successful for ultraviolet stabilizer type products. Concentrations UV-1 were not able to be measured using UV spectroscopy, but could be measured up to 25% with on-line NIR. UV-2 was increased from a maximum of 15% to 25% and had the SEV drop from 0.93 to 0.16 by using NIR instead of UV. The SEC value also dropped from 0.63 to 0.14 for this set of experiments. UV-3 could be monitored using both techniques for a range 1 to 50% in concentration, but the SEV was 3.08 using UV techniques and only 0.35 using the NIR equivalent. The SEC values were 2.55 for the UV techniques, and 0.30 for the NIR technique. In this example, the use of NIR spectroscopy is by far the method of choice. UV-4 was found to be difficult to monitor using either technique due to its high opacity in the melt. UV-5 was found to be similar to UV-3 in that both techniques were useful for the full concentration range of 1 to 50%. In this case, the UV technique proved superior over the NIR analysis. The SEV was 0.72 versus 1.13 respectively, and SEC values of 0.26 and 0.36 respectively. NIR spectroscopy doubled the monitoring range for UV-6, but the SEV for this model was 3.09 as compared to 0.19 for the UV method. The SEC values were found to be 0.06 for the UV technique and 1.28 for the NIR model. This is another case of range suffering for accuracy. UV-7 was another additive that was not successfully monitored using UV spectroscopy, but was capable of being monitored for a range up to 17.5% using the NIR method with a SEV of 0.75.

Both spectroscopic techniques were found to be durable enough to be used in an industrial environment and did not interfere with the normal operation of the polymer processing equipment. Both systems were also found to be easy to use once all the nuances of their operation were fully understood. The NIR system held the advantage in this regard in that the prediction routines could be built using the software that came with the instrument and did not require any additional mathematical manipulation to be performed to obtain the real time concentration. The results from this study demonstrate the versatility of the use of these on-line systems and serve to counter the concept that these techniques should only be used for low level additive monitoring. The models developed are truly as good as the spectra that they are

derived from, since the mathematical manipulation remains the same. If reasonable spectra can be obtained from the process, then an on-line monitoring technique can be instituted. Taking these factors into account, on-line spectroscopic measurements are feasible for these types of products.

The use of multivariate analysis for these problems is evident. The spectra collected from the various techniques are highly complicated and interrelated. PLS is a useful multivariate analysis tool in that it is capable of handling data that has multiple interacting features from a few concentrations in an iterative manner. The models chosen had relatively few factors as to not increase the amount of noise that was accounted for in the model. The data was mean centered to allow the model to be generated based on the differences in the spectra rather than the trying to model absolute values of absorbance. This was one technique used to maximize the signal to noise ratio.

## CHAPTER 9

### ESTIMATION OF PIGMENT CONTENT IN POLYMER MELTS

#### INTRODUCTION

In addition to performance requirements, many polymeric products have appearance requirements, the most important of which is color. Fiber applications usually are highly value added products of which the color specifications are controlled within tight bounds. Pigment loadings in fiber concentrates are an important parameter and most companies would like to have tighter process control. Utilizing similar techniques used in the measurement of additive levels in molten polymer systems, and quantification of the pigment loading can be obtained.

#### 9.1 THEORY

Since the first use of pigments in prehistoric times, attempts have been made to reproduce specific colors in various products. Organic pigments have been used since the beginning of recorded history with the earliest examples being prehistoric cave paintings utilizing ocher, hematite, brown iron oxide and other mineral based pigments. The first inorganic pigment (Prussian Blue) was not synthesized until 1704 [133]. Cobalt Blue did not appear until another century later. True applied chemistry was not introduced into the field until the advent of scores of pigments in the textile industry around 1900.

Comparison of pigments is highly dependent on particle size distribution. Most modern pigment manufacturers have tight controls set on the size distribution in their products. Due to the crystalline nature of most organic pigments, a distribution of size will always occur. Due to surface energy constraints and the polar nature of some pigments, there is a probability that some pigment particles will re-agglomerate during manufacturing processing. Since several mixing operations have occurred prior to the material being extruded at lower concentrations into the final product, this effect is less evident. It is the goal of color concentrate manufacturers to produce a highly dispersed pigment concentrate requiring the least expensive processing route to achieve their customer's requirements [133].

Diazo condensation pigments are produced by a condensation reaction between two carboxylic monoazo compounds with an aromatic diamine.



These pigments have high molecular weights and exhibit excellent solvent and migration characteristics. They are mainly used in the production of fibers and spin dyeing due to their high heat stability and excellent color properties. The spectral range of these pigments extends from yellow to orange and bluish red to brown. Phthalocyanine pigments are polycyclic compounds that are derived from a phthalocyanine structure. The basic molecule can chelate with many metals, but only copper (II) compounds are currently being utilized. These compounds exhibit excellent chemical and physical properties and are well received in every field using organic pigments. Shades used commercially include a reddish-greenish and bluish to yellowish shades of greens. The latter are the result of chlorine or bromine atoms being introduced to the structure [133].

There are many factors that determine what the final appearance of a product will be. This section of research does not attempt to measure the color of the material during processing conditions. Rather, by taking the simple case and assuming that there are not significant variations in the lot of pigment used, the pigment can be treated as an additive component in the polymer system. By obtaining information regarding the pigment concentration, the correlation to a properly pigmented part can be made with the material that is flowing through the extruder. The more complicated issue of pigment dispersion and the insight of proper appearance are tackled in Chapter 10.

## **9.2 EXPERIMENTAL**

The samples chosen for these experiments represent five common high performance pigments currently utilized by the fiber industry for the manufacturing of various grades of carpet. This study focused on the measurement of highly loaded polypropylene products at concentrations that would typically be supplied to a fiber spinning operation. Immediately prior to the spinning of fibers from this material, these color concentrates would be reduced in concentration with the addition of polypropylene. By supplying the colorant in a highly loaded product, there is a significant reduction in the cost required not only to produce the concentrate, but also a reduction in secondary product handling operations such as shipping. These pigments are typically supplied at the 25% level with the customer reducing the final pigment loading to the 0.05 to 1.5% range. The pigments chosen for this study are shown in Table 9.1.

Table 9.1 Diazo condensation and phthalocyanine pigments used in polypropylene

Pigment Chemical Name	Code/ CAS Number	Pigment Generic Name/ Trade Name	Manufacturer	Form
Benzamide,3,3'-[(2-chloro-5-methyl-1,4-phenyl)bis[imino-(1-acetyl-2-oxo-2,1-ethanediyl)azo]]bis[4-chloro-N-(3-chloro-2-methylphenyl	C-1/ 5580-57-4	Cromo yellow / PY-93	Ciba	Powder
2-Naphthalene carboxamide, N,N'-(2-chloro-1,4-phenylene)-bis-[4-[(2,5-dichlorophenyl)azo]-3-hydroxy	C-2/ 5280-78-4	Cromo red brn / PR-144	Ciba	Powder
Monochloro copper phthalocyanine	C-3/ 147-14-8	Phthalo blue rs / PB-15:1	BASF	Powder
Polychloro copper phthalocyanine	C-4/ 1328-53-6	Phthalo green bs / PG-7	BASF	Powder
Benzamide,3,3'-{2,5-dimethyl-1,4-phenylene}bis{imino(1-acetyl-2-oxo-2,1-ethanediyl)azo} } bis{4-chloro-N-(5-chloro-2-methylphenyl)	C-5/ 5280-80-8	Disazo condensate Ye R / PY-95	Ciba	Powder

For these experiments, the colorant concentrates were compounded at their maximum loadings on a 34 mm twin screw co-rotating extruder with an L/D ratio of 24:1. These samples were compounded with a 12 MI polypropylene containing no additional additive formulations. Preliminary investigations dealt with a range of concentrations from a range of 0.5% to the maximum concentration for each individual pigment as shown in Table 9.2. The reduction in concentration was achieved by mixing the pigment concentrate with additional polypropylene prior to extrusion on the ¾ inch single screw extruder. These samples were then probed using NIR and UV spectroscopy. The generated spectra were examined for characteristic regions that represented measurable properties of the sample to allow for determination of the instantaneous pigment loading in the flow cell.

To gain a more realistic picture of the practical applications of this technology, the pigment master batches were produced using a pre-dispersion pigment concentrate. This source material could include various additives at low levels and different carrier materials. The concentrations of these other components were kept constant throughout the trials, and the peaks of interest were the result of the pigment chemistry and not any other constituents.

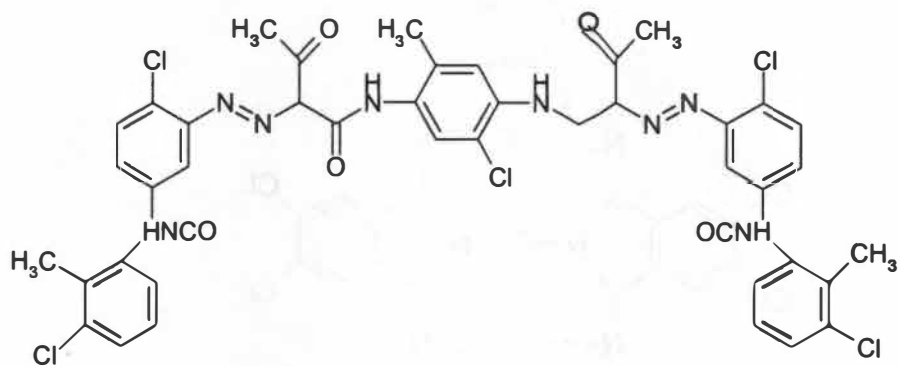
### 9.3 SPECTROSCOPIC RESULTS

Preliminary work was done on C-1 at pigment concentrations of 1%, 2%, 5%, and 10% by mass in polypropylene. Spectra were collected using a Nicolet 5DXC FT-IR spectrometer. Several peaks and regions were identified as peaks whose absorption intensity was directly proportional to pigment concentration in the sample. These regions include 3230 to 3375  $\text{cm}^{-1}$ , 1620 to 1725  $\text{cm}^{-1}$  and 480 to 775  $\text{cm}^{-1}$ . The spectroscopic results for the infrared region are shown in Figure 9.3. More detailed results for the 480 to 775  $\text{cm}^{-1}$  region are shown in Figure 9.4. These spectra show that information related to the concentration of pigment in the polymer can be measured using this off-line spectroscopic technique. These trials were conducted only to demonstrate that there can be multiple regions for concentration measurement, and not to make any quantitative conclusions. The spectra were entered into a proprietary database to be used for both quality control purposes and identification of unknown materials.

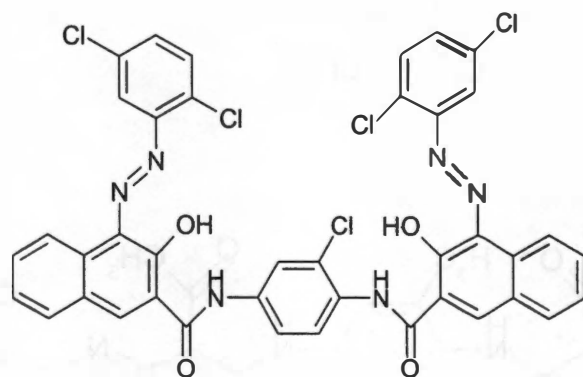
**Table 9.2 Formulations utilized in initial online UV and NIR spectroscopy**

	<b>Range</b>	<b>1%</b>	<b>2%</b>	<b>5%</b>	<b>10%</b>	<b>17.50%</b>	<b>25%</b>	<b>35%</b>
<b>C-1</b>	1-35%	C-1a	C-1b	C-1c	C-1d	C-1e	C-1f	C-1g
<b>C-2</b>	1-35%	C-2a	C-2b	C-2c	C-2d	C-2e	C-2f	C-2g
<b>C-3</b>	1-35%	C-3a	C-3b	C-3c	C-3d	C-3e	C-3f	C-3g
<b>C-4</b>	1-35%	C-4a	C-4b	C-4c	C-4d	C-4e	C-4f	C-4g
<b>C-5</b>	1-35%	C-5a	C-5b	C-5c	C-5d	C-5e	C-5f	C-5g

C-1



C-2



C-3

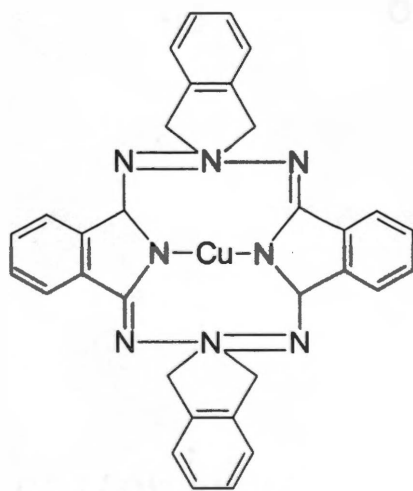
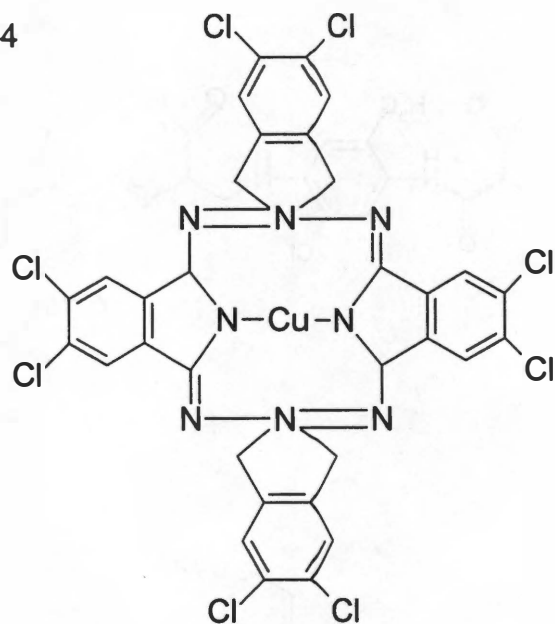


Figure 9.1 Chemical structures of pigments C-1 - C-3 used in this study



C-4



C-5

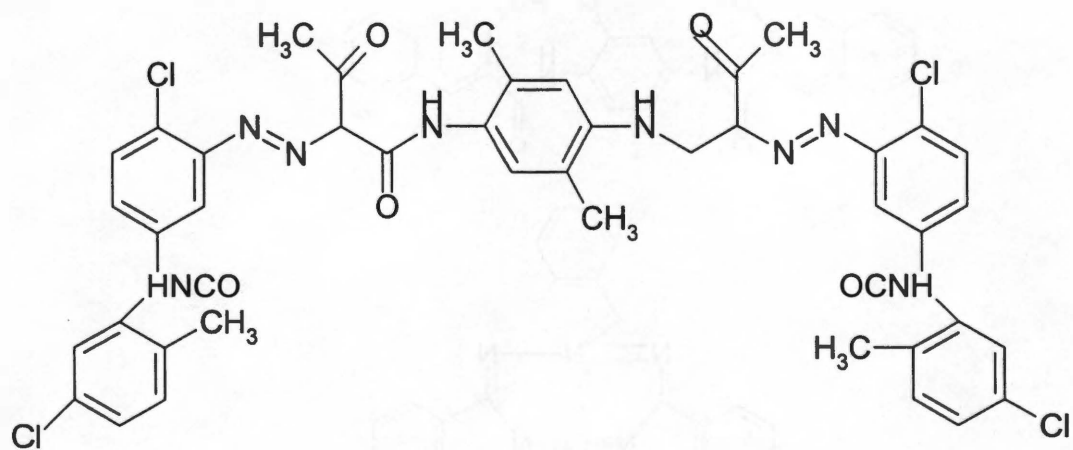


Figure 9.2 Chemical structures of pigments C-4 - C-5 used in this study

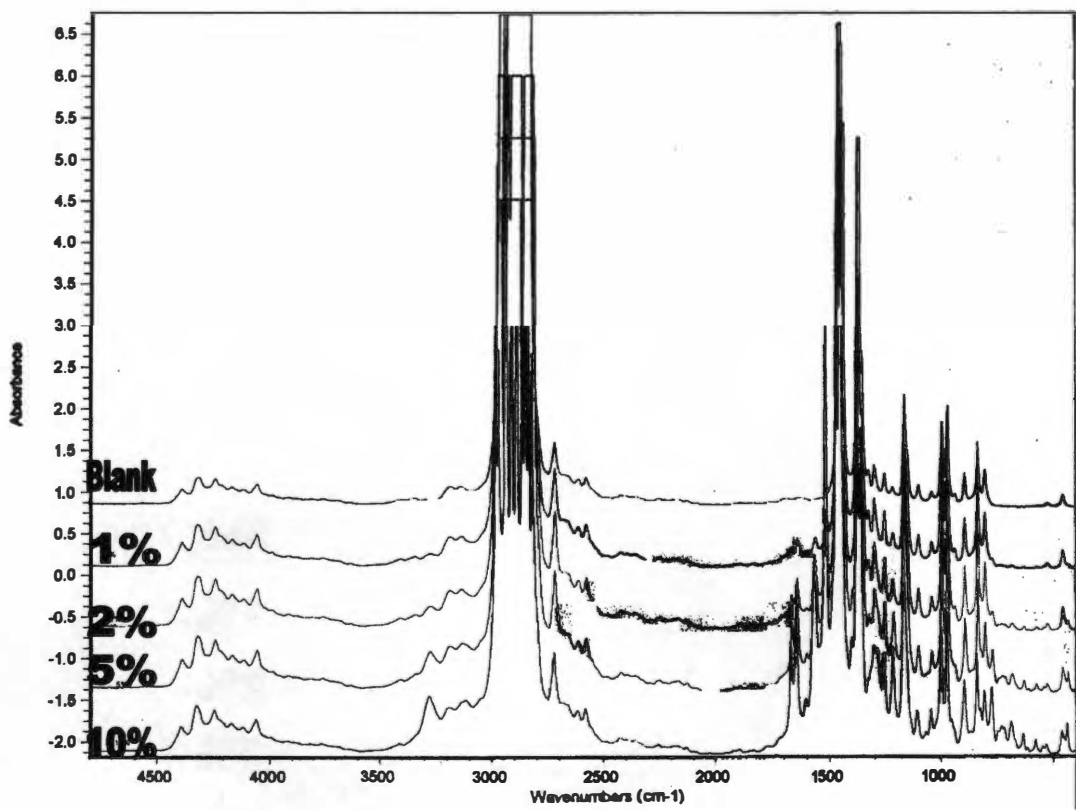


Figure 9.3 FTIR spectra for sample C-1 (Note: axis is only relative, not absolute)

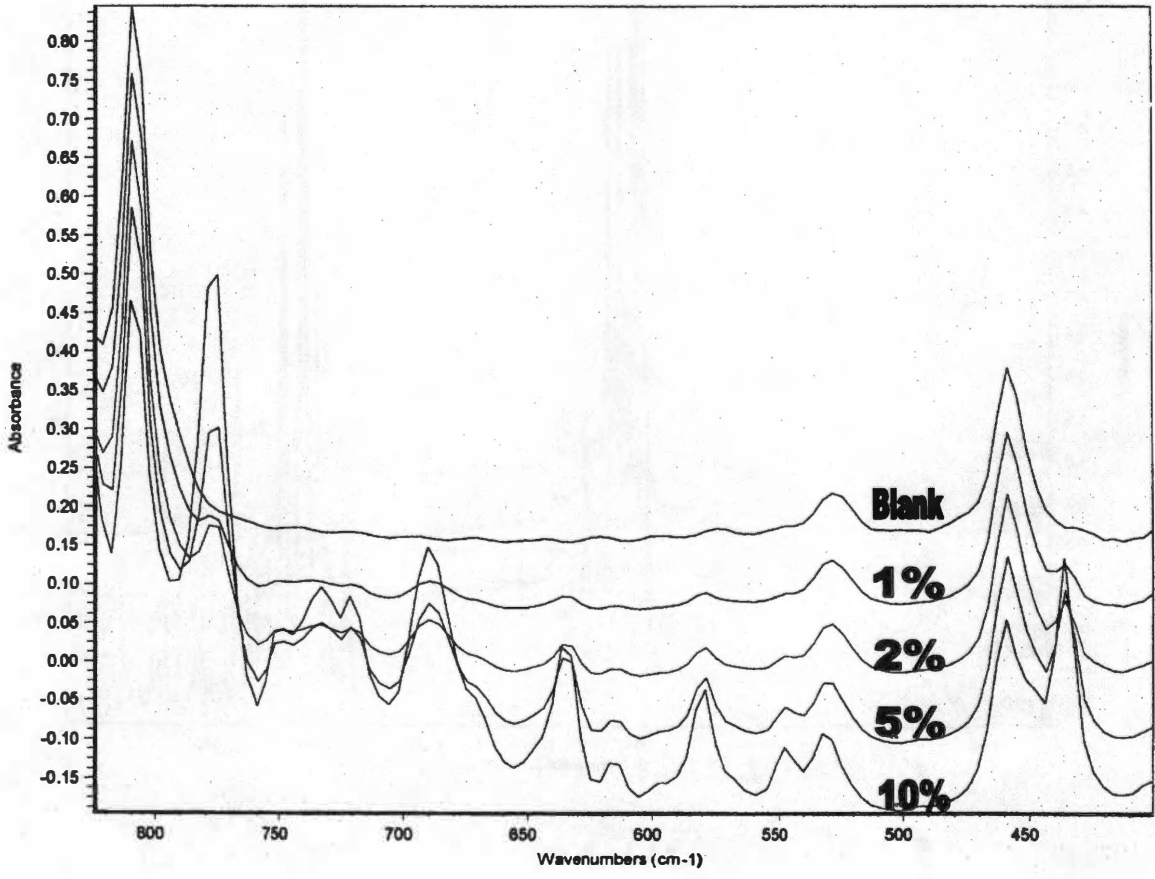


Figure 9.4 Detailed FTIR spectra for sample C-1 in the 480 to 775 cm<sup>-1</sup> region (Note: axis is only relative, not absolute)

Online UV spectroscopy was conducted on all samples for concentration ranges from 1% to 35% by mass using the Equitec MPX 2000 spectrometer. It was found that at these loadings, the sample would absorb almost all of the UV light leaving very little to be transmitted, thereby negating any meaningful data from being produced. These results are shown in Figures 9.5 through 9.9. Some trace of the pigment's reflectance curve can be seen in the data for C-1, C4, and C-5. As is evident in the plots of this spectral data, only noise was measured and not a definitive response due to the structure of the pigment.

The online NIR spectroscopy was better in determining the concentration of pigment but had some of the same problems that were observed with the UV results (Figures 9.10 to 9.14). Using this technique however, it was possible to construct prediction models using the same methodology as explained in Chapter 8 for C-1 and C-5 for concentrations up to 5% (Figures 9.15 to 9.23). While these fall short of those originally anticipated, they correspond to those seen on custom color master batch type products (i.e. matched color rather than a highly loaded single pigment). This capability is meaningful for color products that are commercially available.

From the initial screening data, PLS models were built to determine what type of accuracy could be achieved at low levels. A prediction model was not created due to the limitation of the spectroscopic techniques. Several regions were identified in the spectra of C-1. These were 1340-1424 nm due to C-O stretching, and various peaks in the 1660-1900 nm region due to C-H stretching from various carbon centers. PLS models were built upon this data for each region where there was a spectroscopic response. For the 1340 to 1424 nm region, a two-factor model was built and resulted in 75.4% of the variance accounted for in the first factor and 24.5% in the second factor. Although this model had a PRESS value of only 0.001, other models were found to be more accurate in accounting for the spectra in fewer factors. Investigation of the 1660 to 1900 nm spectra showed that 99.6% of the behavior could be accounted for in only one factor with a SEC value of 0.36. Reducing the range of the spectra to the 1660 to 1720 nm range, a one factor model was built that increased the percent variance accounted for with one factor to 99.9% and the SEC fell slightly to 0.35. This ended up as the most reliable model built for this pigment. Other models were constructed for other areas in the 1660 to 1900 nm range, and are presented in Table 9.3. As can be seen, the majority of the variance in the data can be accounted for in one factor. Also presented to

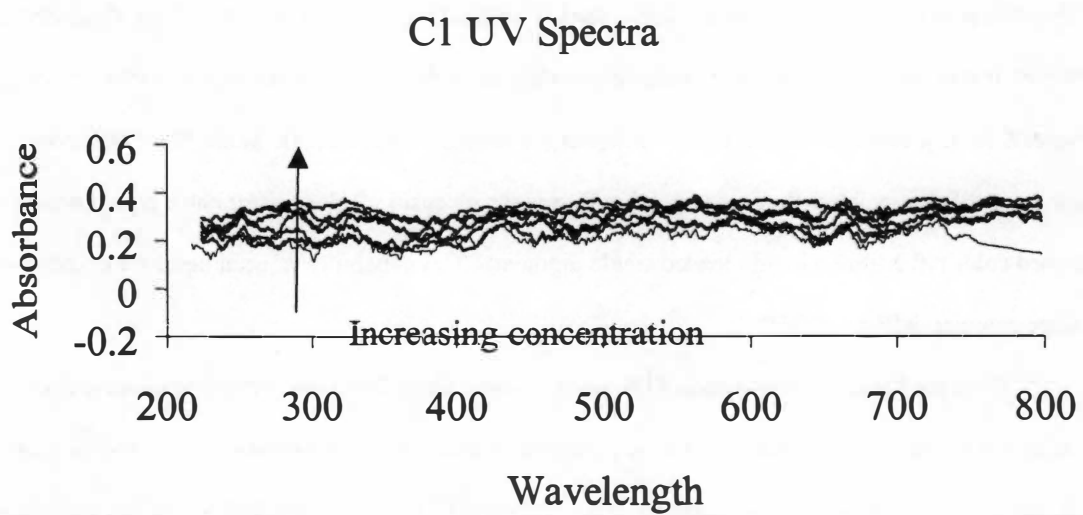


Figure 9.5 Detailed UV absorbance spectra for sample C-1 in the 200 to 800 nm region (1, 2, 5, 10, 17.5, 25, 35%)

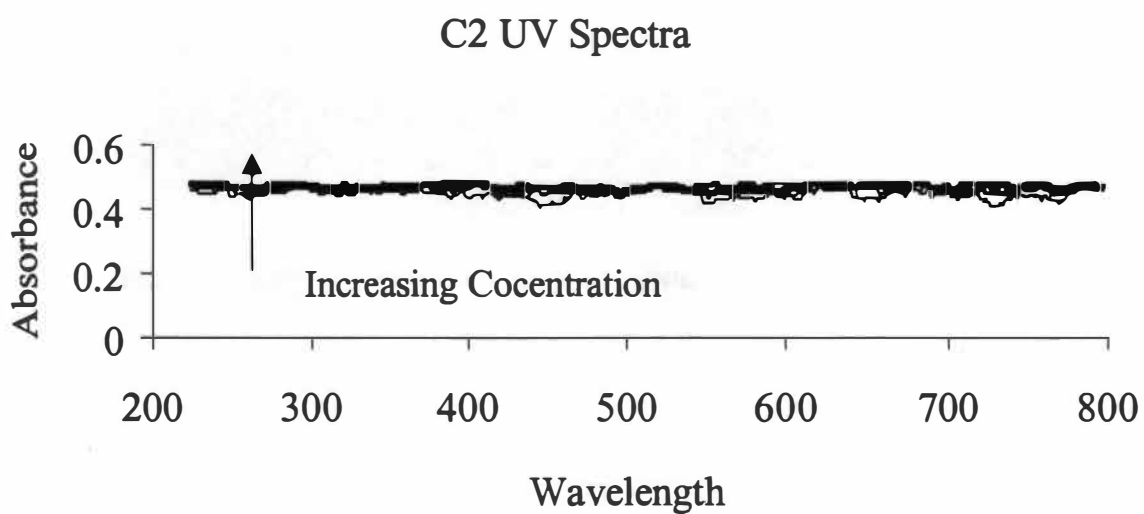


Figure 9.6 Detailed UV absorbance spectra for sample C-2 in the 200 to 800 nm region (1, 2, 5, 10, 17.5, 25, 35%)

### C3 UV Spectra

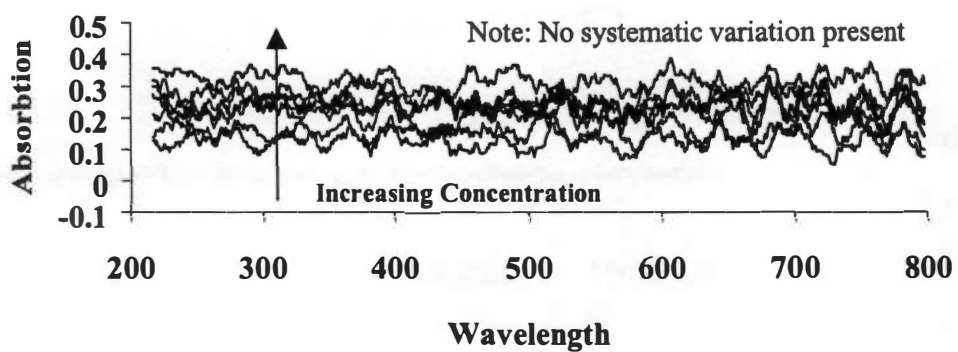


Figure 9.7 Detailed UV absorbance spectra for sample C-3 in the 200 to 800 nm region (1, 2, 5, 10, 17.5, 25, 35%)

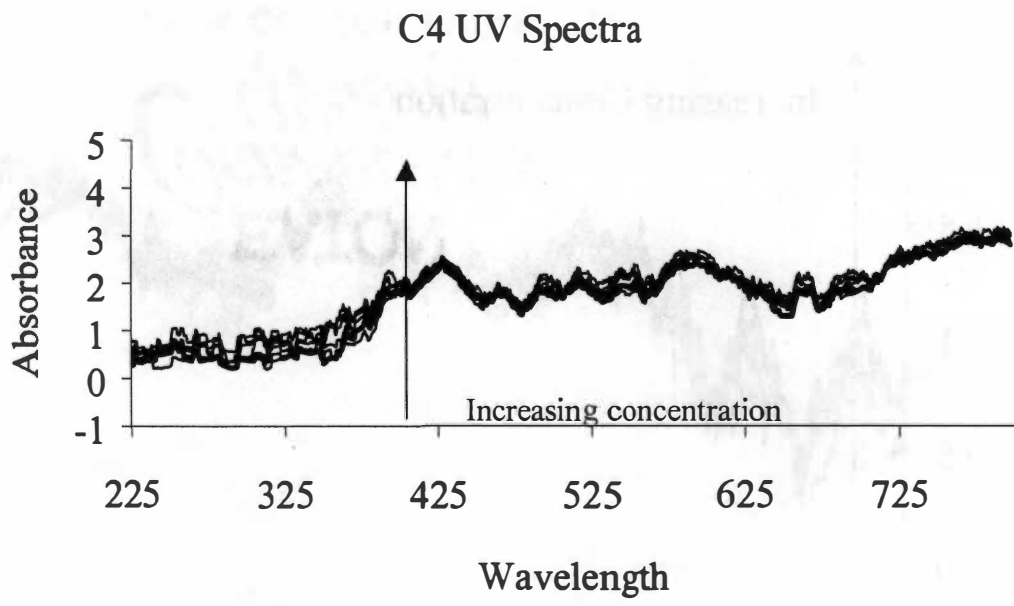


Figure 9.8 Detailed UV absorbance spectra for sample C-4 in the 200 to 800 nm region (1, 2, 5, 10, 17.5, 25, 35%)



### C5 UV Spectra

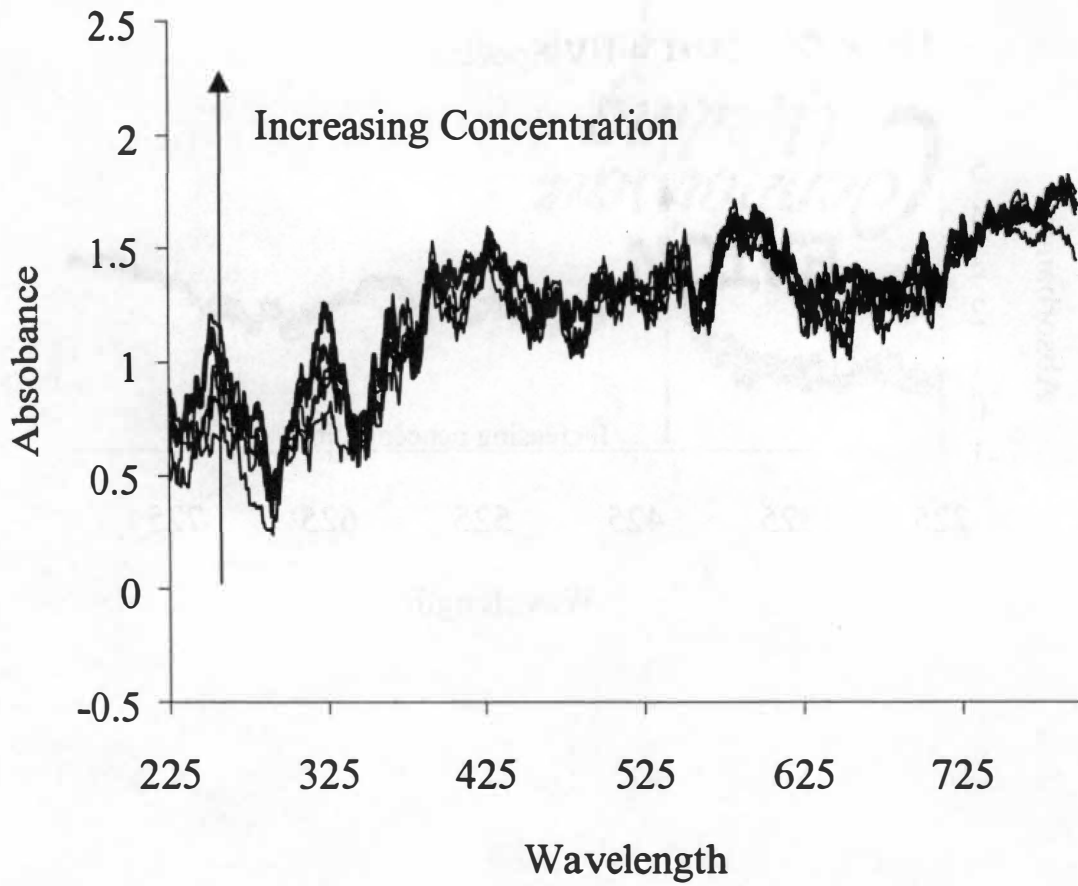


Figure 9.9 Detailed UV absorbance spectra for sample C-5 in the 200 to 800 nm region (1, 2, 5, 10, 17.5, 25, 35%)

Table 9.3 PLS models for various NIR regions for 1-5% C-1 in polypropylene

Range (nm)	# of Factors	Variance	Percent	Cumulative	SEC	Press Cal	r Cal
1340-1424	Factor1	0.000515	75.45283	75.45283	0.034537	0.001193	0.999931
	Factor2	0.000167	24.54717	99.99999	0	0	1
1660-1900	Factor1	0.011214	99.60815	99.60815	0.358792	0.128732	0.992545
	Factor2	0.000044	0.391835	99.99999	0	0	1
1660-1720	Factor1	0.008117	99.90998	99.90998	0.34622	0.119868	0.99306
	Factor2	0.000007	0.090011	99.99999	0	0	1
1720-1770	Factor1	0.00264	99.5249	99.5249	0.4136	0.171065	0.990082
	Factor2	0.000013	0.475094	100	0	0	1
1740-1812	Factor1	0.00231	99.35684	99.35684	0.488161	0.238301	0.986156
	Factor2	0.000015	0.643168	100	0	0	1

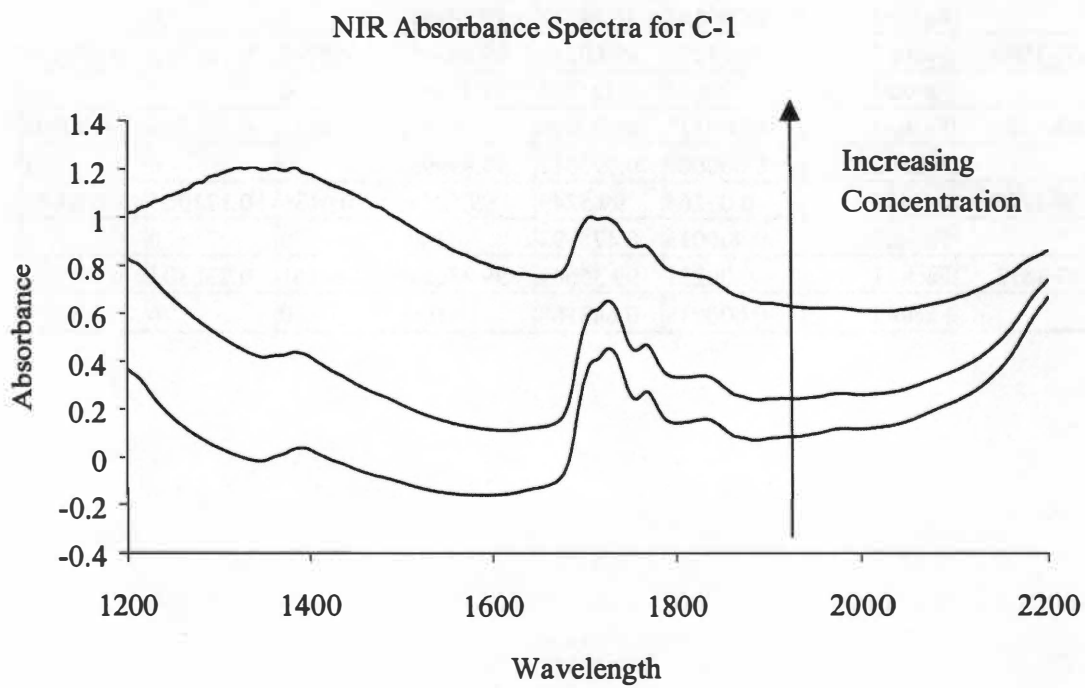


Figure 9.10 NIR absorbance spectra for sample C-1 in the 1200 to 2200 nm region (1, 2, 5%)

### NIR Absorbance Spectra for C-2

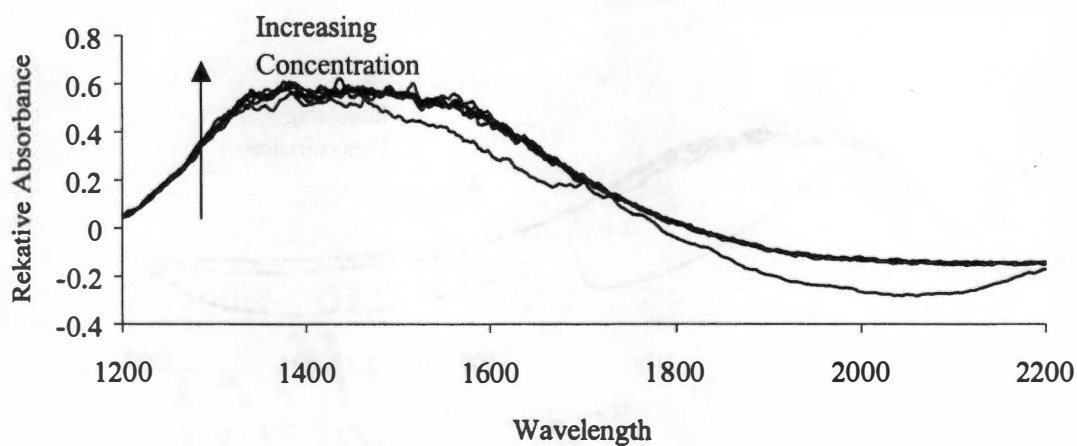


Figure 9.11 NIR absorbance spectra for sample C-2 in the 1200 to 2200 nm region (1, 2, 5, 10, 17.5, 25, 35%)

NIR Absorbance Spectra for C-3

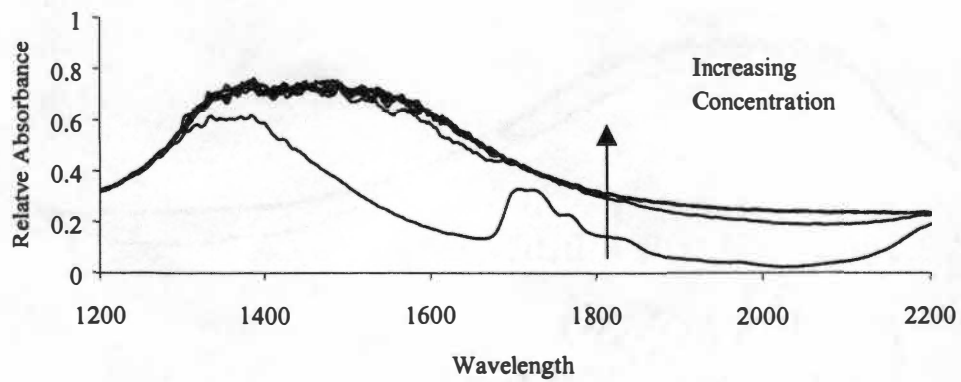


Figure 9.12 NIR absorbance spectra for sample C-3 in the 1200 to 2200 nm region (1, 2, 5, 10, 17.5, 25, 35%)

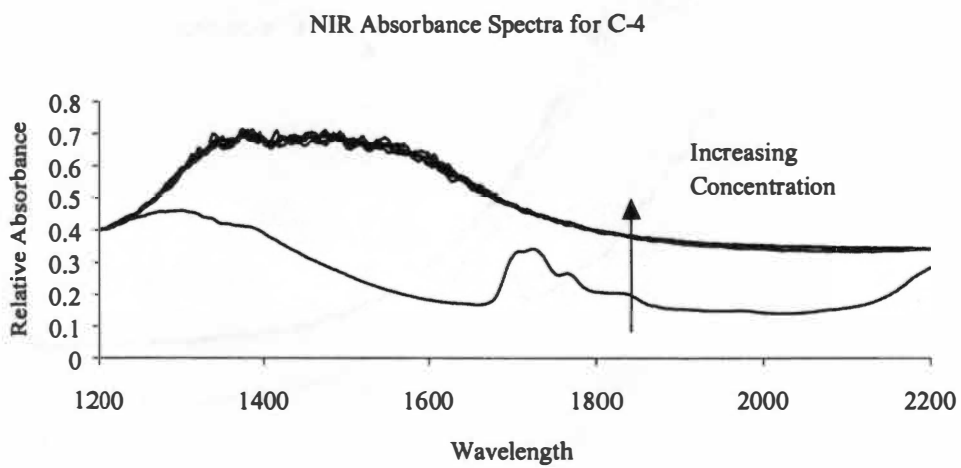


Figure 9.13 NIR absorbance spectra for sample C-4 in the 1200 to 2200 nm region (1, 2, 5, 10, 17.5, 25, 35%)

### NIR Absorbance Spectra for C-5

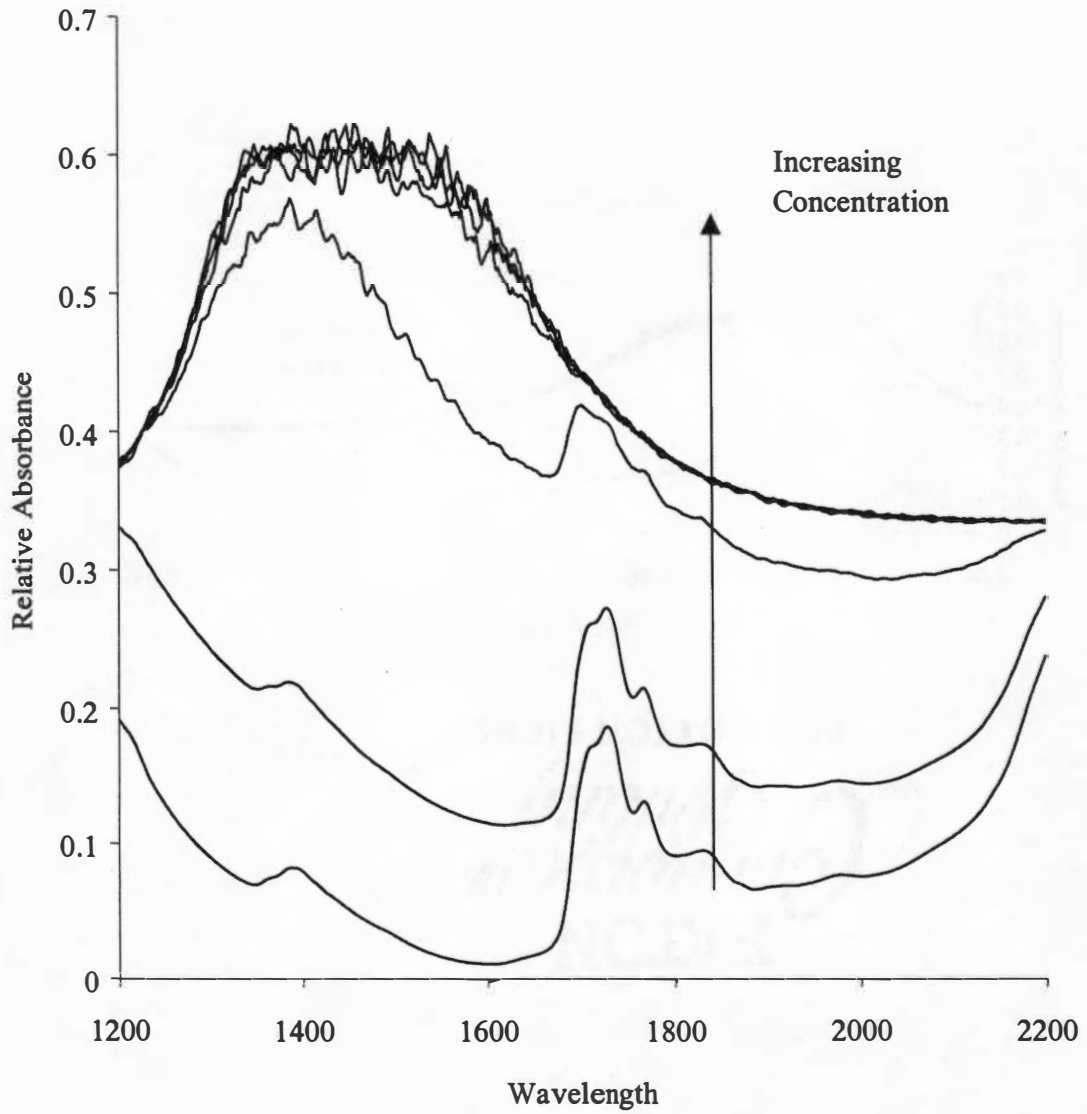


Figure 9.14 NIR absorbance spectra for sample C-5 in the 1200 to 2200 nm region (1, 2, 5, 10, 17.5, 25, 35%)

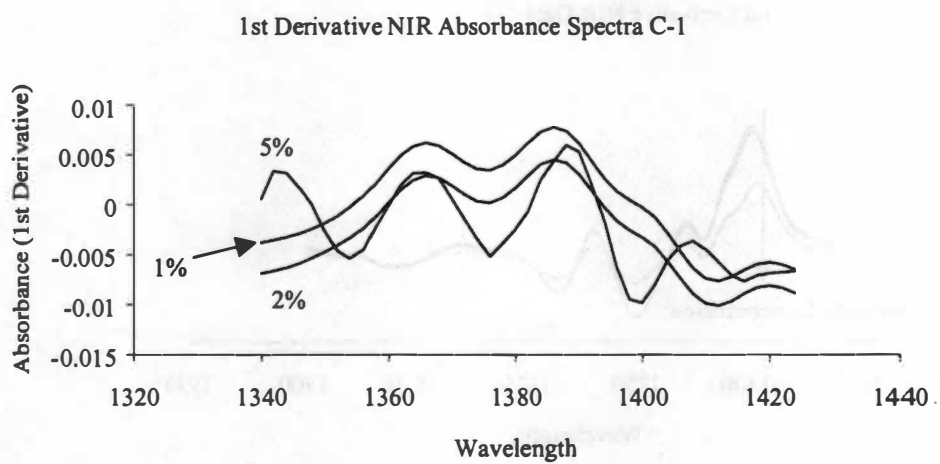


Figure 9.15 First derivative absorbance data for C-1 NIR spectra for 70-112 nm for 1-5%



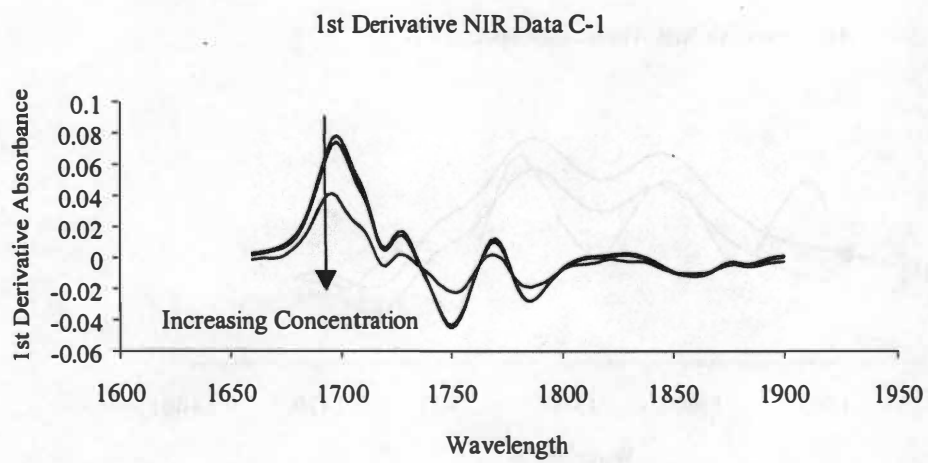


Figure 9.16 First derivative absorbance data for C-1 NIR spectra for 1660-1900 nm for 1, 2 and 5%

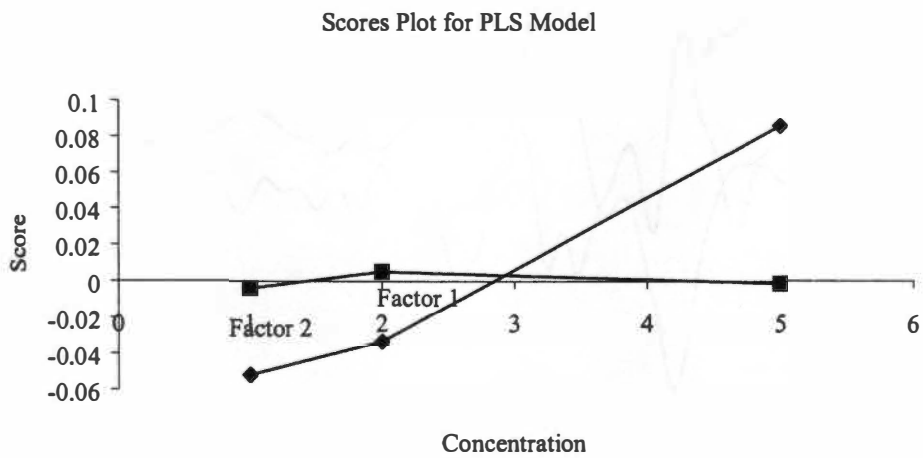


Figure 9.17 Scores plot for C-1 PLS model based on 1660 to 1900 nm for 1-5%

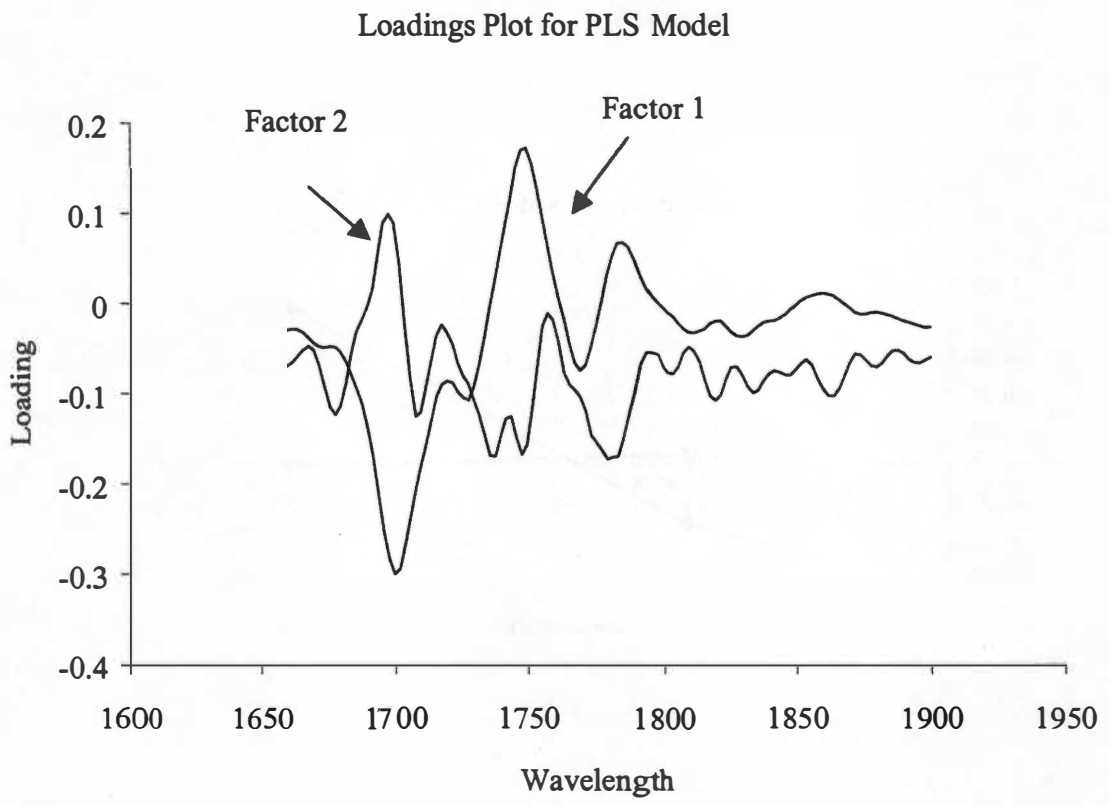


Figure 9.18 Loadings plot for C-1 PLS model based on 1660 to 1900 nm for 1-5%

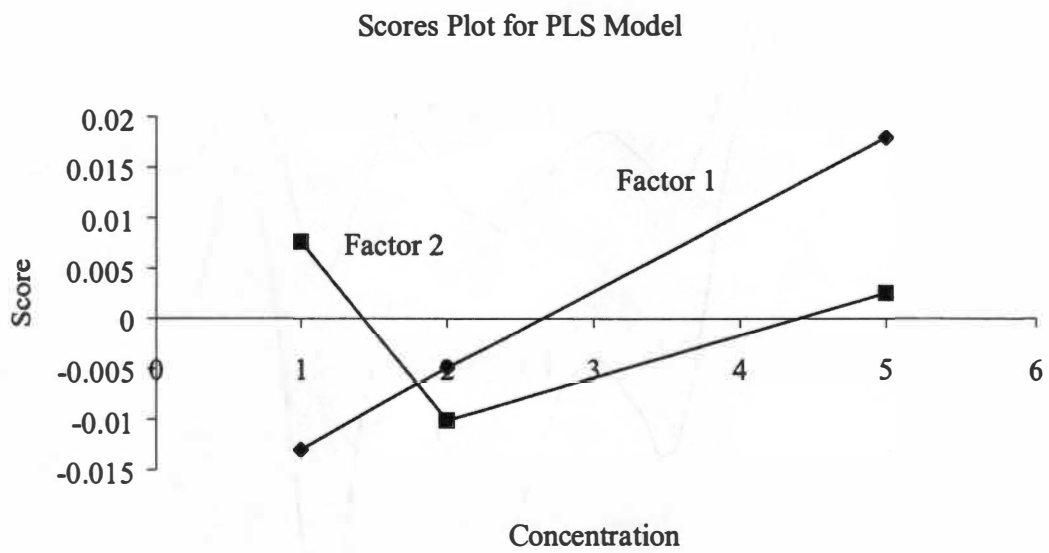


Figure 9.19 Scores plot for C-1 PLS model based on 1340 to 1424 nm for 1-5%

Loadings Plot for PLS Model

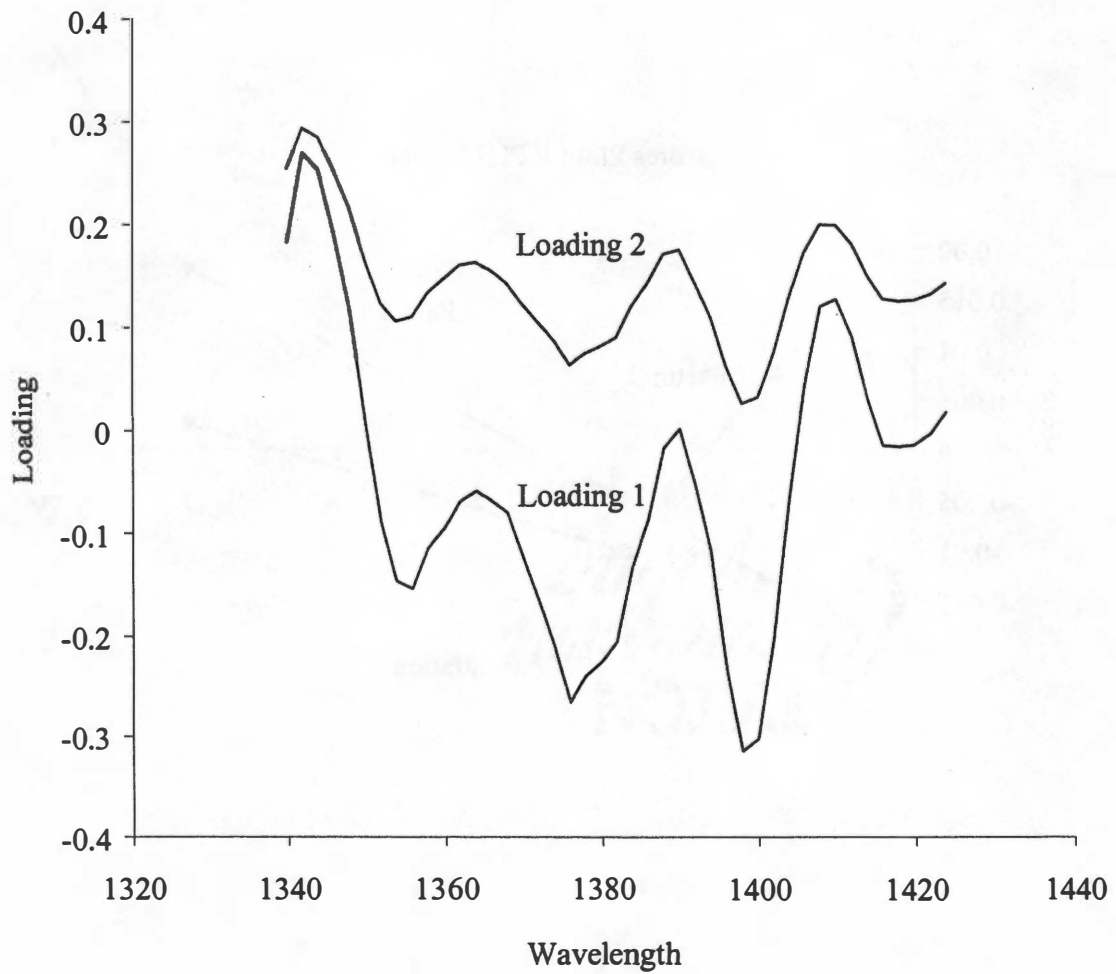


Figure 9.20 Loadings plot for C-1 PLS model based on 1340 to 1424 nm for 1-5%

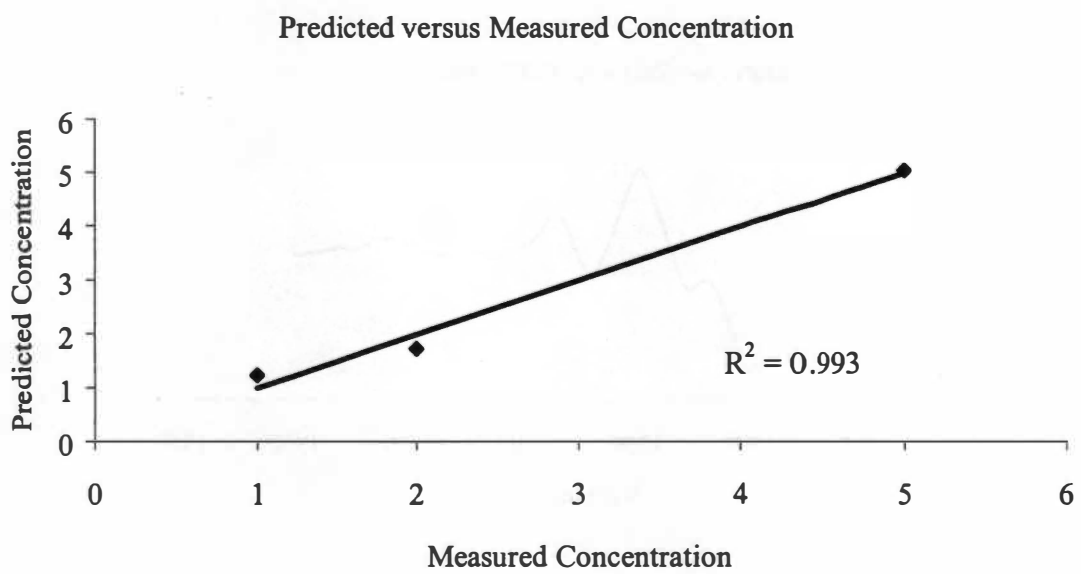


Figure 9.21 Predicted versus measured plot for C-1 PLS mode based on 1660 to 1900 nm for 1-5%

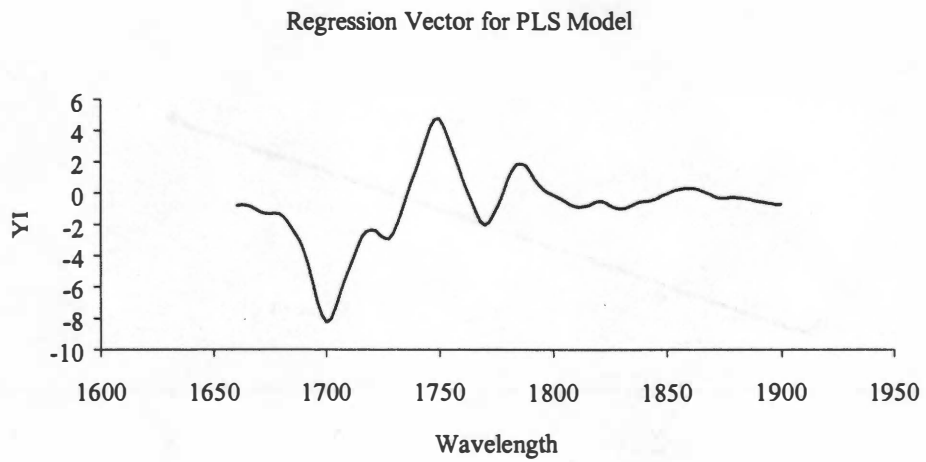


Figure 9.22 Regression vector plot for C-1 PLS model mode based on 1660 to 1900 nm for 1-5%

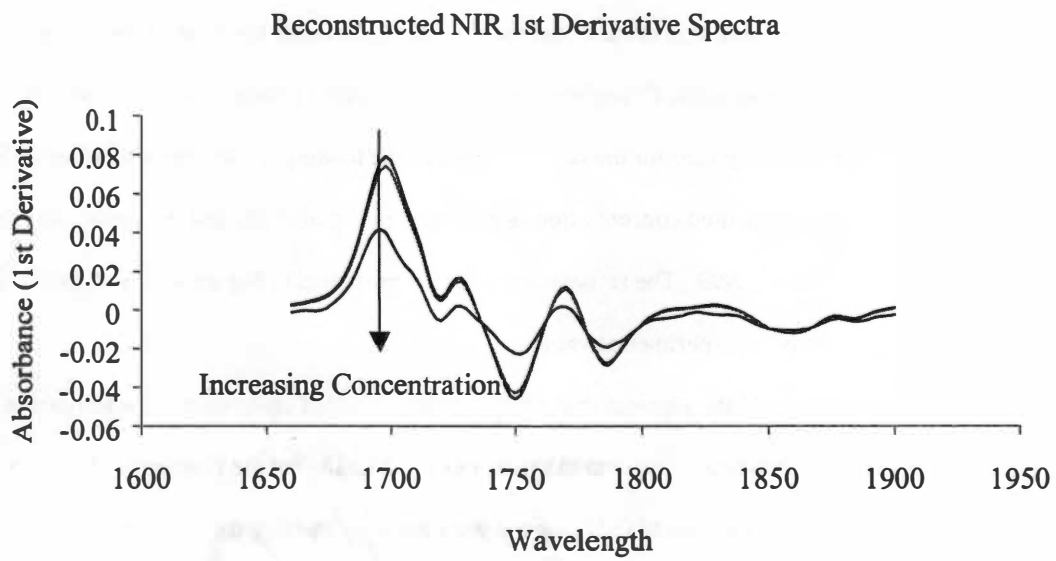


Figure 9.23 Reconstructed absorbance data from C-1 PLS model based on 1660 to 1900 nm for 1, 2, and 5%



show that there is an optimal peak to build a PLS model on, the scores and loadings plots are shown for two factors for the 1340-1424 nm range and the 1660-1900 nm range.

C-5 behaved in a similar manner to C-1 in the NIR region. Five separate regions were identified as containing useful spectroscopic information. In the case of this pigment, all of the models were practically identical with one factor accounting for more than 99% of the variance with the actual value ranging from 99.4 to 99.9%. The SEC values for each model were found to be centered around 0.5. A summary of these results is contained in Table 9.4 with the detailed plots of the 1660 to 1720 nm range model presented in Figures 9.24 to 9.30.

Figure 9.25 shows a plot of the SEV versus the number of factors. From this plot, it is evident that the inclusion of two factors reduces the error to approximately 0%. Comparison of this plot to Figure 9.26, which shows the values of the scores, it is evident that the first factor accounts for most of the change in concentration and has an increasing value throughout the range of interest. Examination of the second factor shows that it is approximately zero for the range. A plot of the loadings plot is shown in Figure 9.27. A plot of the predicted versus measured concentration is presented in Figure 9.28, and the model does fit the data well with an  $R^2$  value of 0.999. The reconstructed data is presented in Figure 9.30 and shows that the model does work well with the experimental values.

Once the concentration of the pigment in the melt can be predicted using an on-line technique, a LAS PLS model can be built on the color space strength numbers if the quality of the pigment's chemistry and dispersion level is the same. For the case of C-5, plaques were made by melting formulations from 1 to 5% pigment in the 12 melt polypropylene and the color strength measurements were made on a Hunter Color Systems Lab Scan color computer. These strengths were referenced to the 1% C-5 sample, setting it to 100% by definition. The regression technique used was identical to measuring the concentration of the pigment in the melt, except the Y vector consisted of the strength and not the concentration. The spectra used for this calibration was the 1660 to 1720 nm data. Performing this regression, a one-factor model was built with a SEC of 39.7% for a range of strengths from 100% to 319% strength. The summary of this regression is shown in Table 9.5.

Table 9.4 PLS models for various NIR regions for 1-5% C-5 in polypropylene

Range (nm)	# of Factors	Variance	Percent	Cumulative	SEC	Press Cal	r Cal
1660-1720	Factor1	0.017648	99.95488	99.95488	0.51974	0.270129	0.984292
	Factor2	0.000008	0.045111	99.99999	0	0	1
1720-1750	Factor1	0.003346	99.41765	99.41765	0.5113	0.261428	0.984802
	Factor2	0.00002	0.58235	100	0	0	1
1750-1780	Factor1	0.002892	99.65208	99.65208	0.571119	0.326176	0.981002
	Factor2	0.00001	0.347904	99.99999	0	0	1
1660-1780	Factor1	0.023031	99.84032	99.84032	0.522916	0.273441	0.984098
	Factor2	0.000037	0.159687	100	0	0	1
1660-1750	Factor1	0.020865	99.87165	99.87165	0.51977	0.27016	0.98429
	Factor2	0.000027	0.128351	100	0	0	1

### 1st Derivative NIR Absorbance Spectra C-5

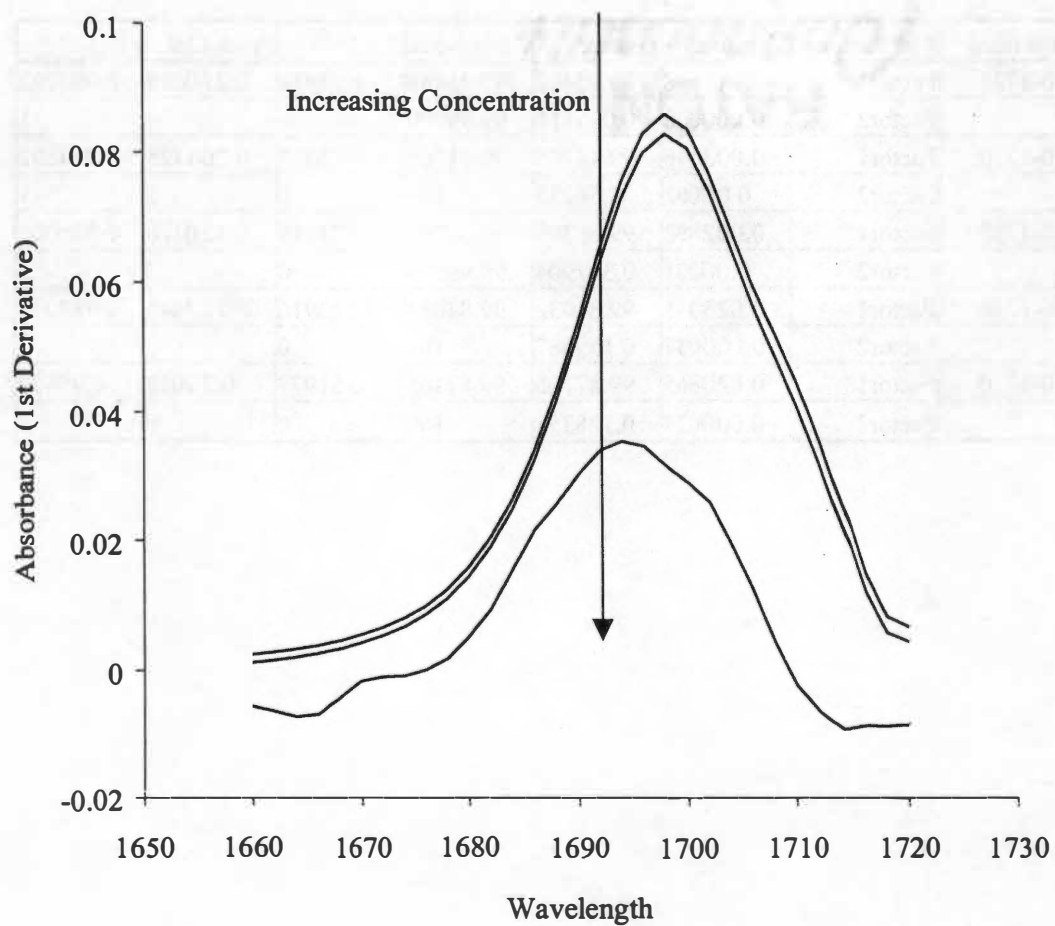


Figure 9.24 First derivative NIR absorbance spectra for 12, and 5% C-5 in polypropylene 1660 to 1720 nm

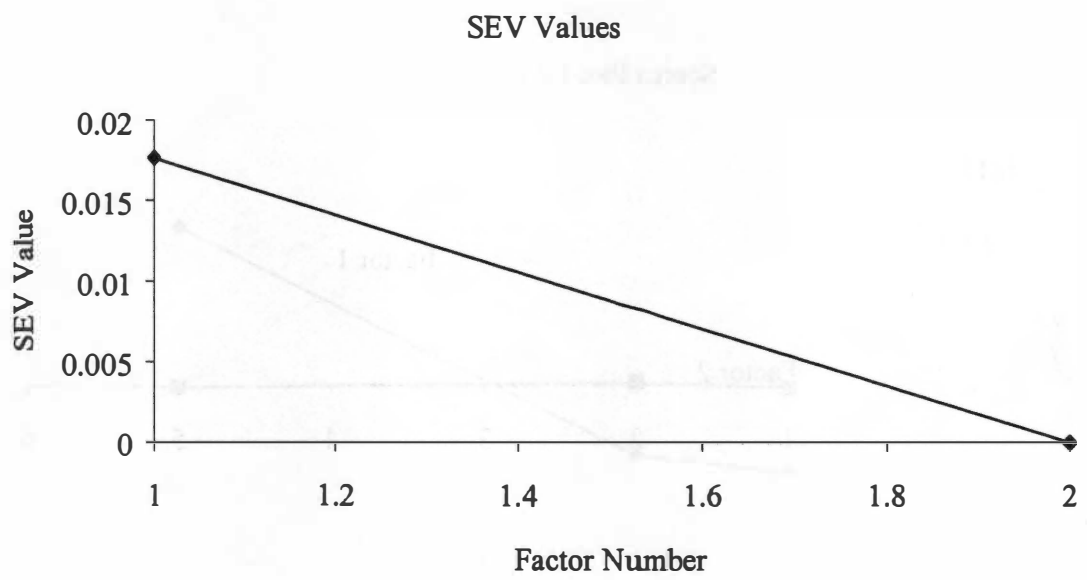


Figure 9.25 SEV values for 1-5% C-5 in polypropylene 1660 to 1720 nm

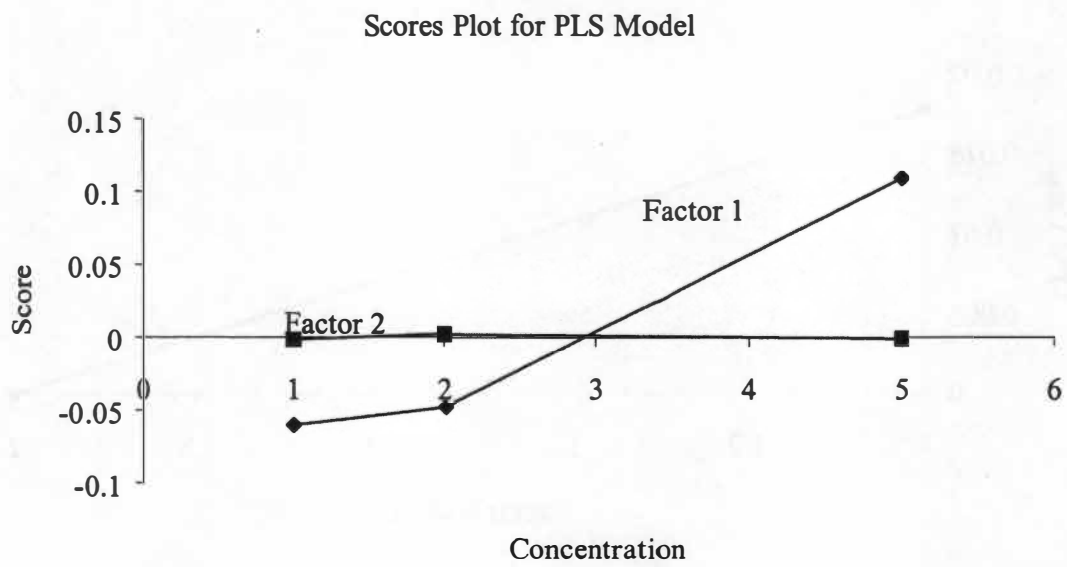


Figure 9.26 Scores plot for PLS model for 1-5% C-5 in polypropylene 1660 to 1720 nm

### Loadings Plot for PLS Model

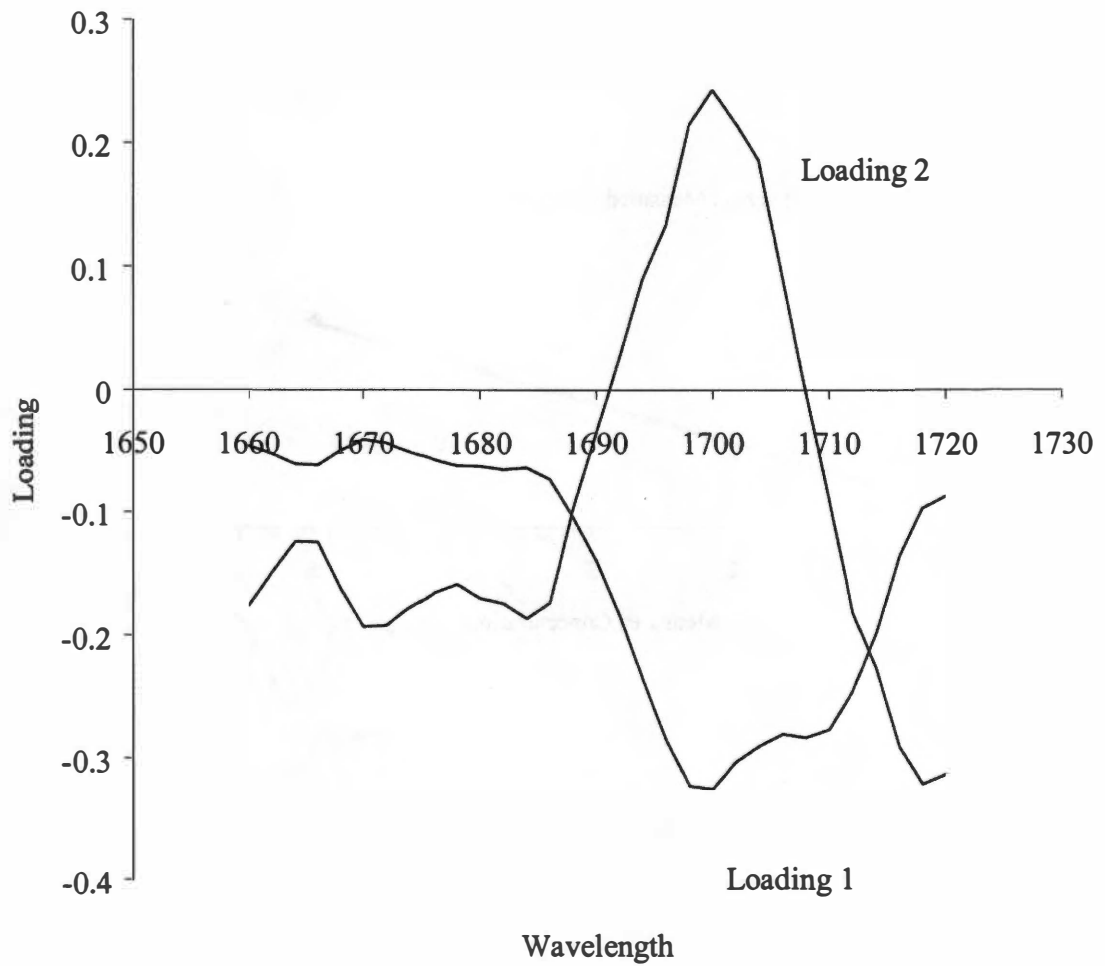


Figure 9.27 Loadings plot for PLS model for 1-5% C-5 in polypropylene 1660 to 1720 nm

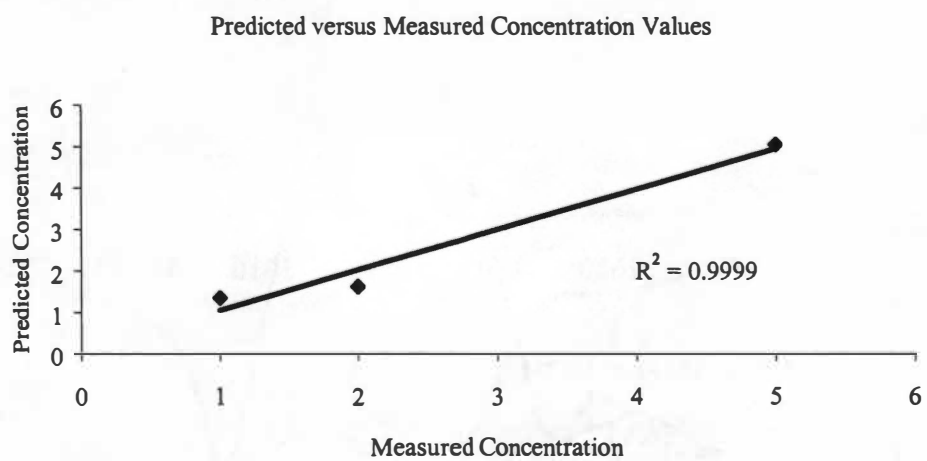


Figure 9.28 Predicted versus measured plot for PLS model for 1-5% C-5 in polypropylene 1660 to 1720 nm

Regression Vector Plot

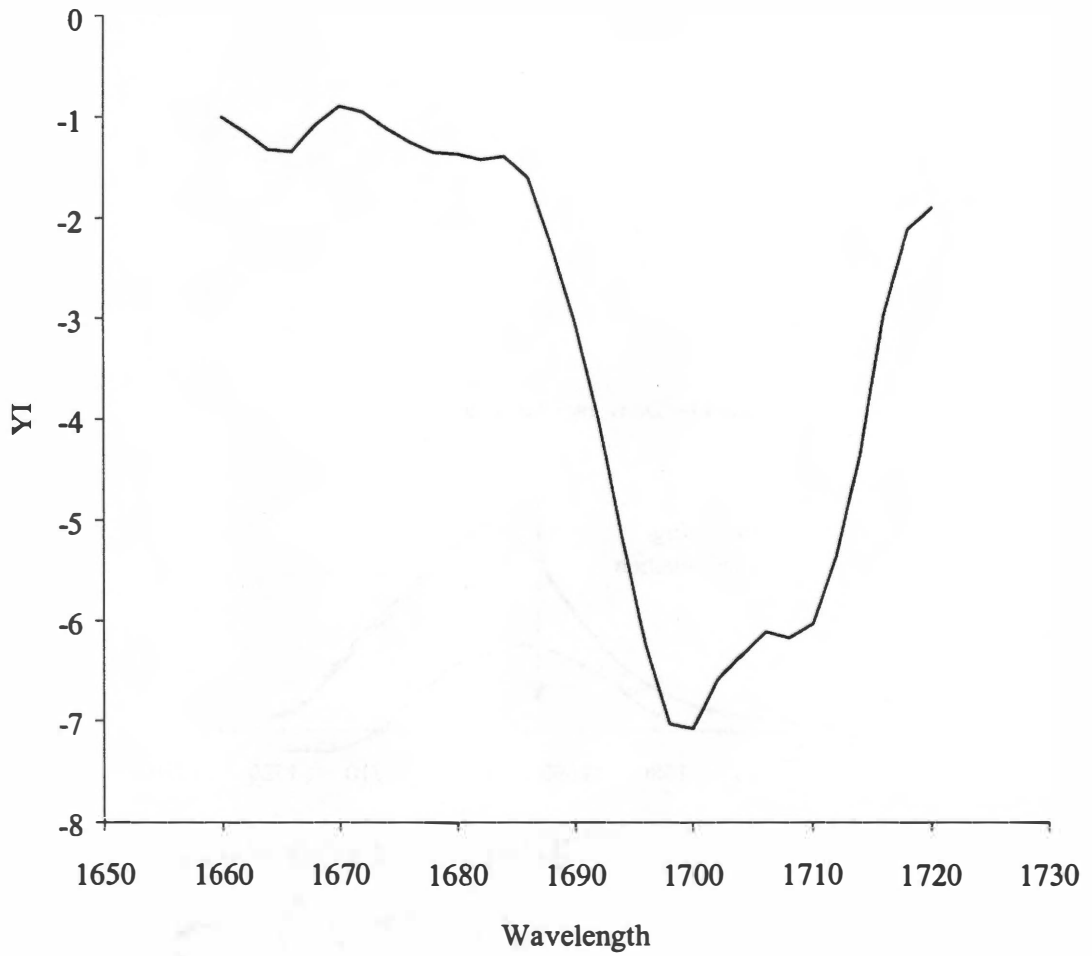


Figure 9.29 Regression vector plot for PLS model for 1-5% C-5 in polypropylene 1660 to 1720 nm



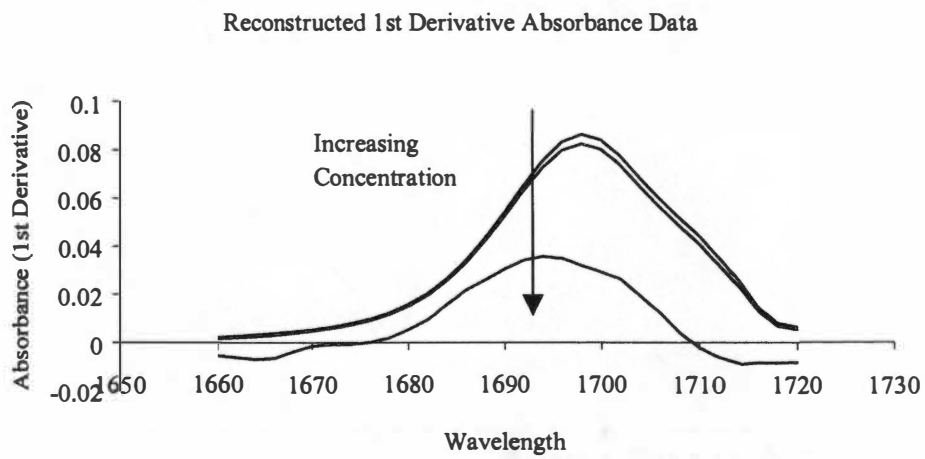


Figure 9.30 Reconstructed absorbance data from PLS model for 1, 2, and 5% C-5 in polypropylene 1660 to 1720 nm

Table 9.5 PLS model for strength values for 1-5% C-5 in polypropylene

Range (nm)	# of Factors	Variance	Percent	Cumulative	SEC	Press Cal	r Cal
1660-1720	Factor1	0.023030	99.834908	99.834908	39.770264	1581.673828	0.967877
	Factor2	0.000038	0.165094	100.000000	0.000000	0.000000	1.000000

## 9.4 EXPERIMENTAL LIMITATIONS

The experimental limitations for these experiments are similar to those in the additive studies, mainly the inherent concerns with the instrument and the sampling technique and the human error in the production of the samples. There is an additional limitation with the investigation of colorants. The spectroscopic measurements are looking for populations of certain chemical species, not the crystalline structure. It is from the crystalline properties of these materials that the quality of the coloration is determined. These pigments are sensitive to heat and shear effects and more work needs to be done to determine a technique to determine the quality of the pigment, not just the concentration level. Future work should be conducted determining absorbance changes due to changes in pigment quality.

The major limitation of course is the opacity of the melt itself. Because the instrument is limited to a 3 mm path length, only concentrations that allow for the light to be transmitted through the flow cell can be measured. In this case, three of the pigments did not allow for any light transmission and the other two were limited below 5% by mass. This limitation would be common for strand cut pellet compounding, but the technique could be useful for other operations such as cast or blow film where the working diameter of the melt is much lower.

## 9.5 CONCLUSIONS

From the preliminary experiments conducted on the C-1 sample using FTIR, it is possible to see that the use of spectroscopic techniques to measure pigment concentration has merit. The scans demonstrated that the concentration of pigment not only had a response in this region, but that the absorption was a function of the pigment concentration.

The resulting spectra were not regressed to build complex mathematical models to predict the loading of the pigment, but rather the spectra were obtained to show proof of concept. This was due to the samples being in a thin film and not in a melt stream. What this does represent is that on-line spectroscopy can be used on an industrial film line, blown or cast, and that measurements relating to concentration can be made.

The experiments using on-line spectroscopy represent some of the first work conducted in the field using these techniques. Results utilizing UV spectroscopy showed conclusively that it should not be used

for the spectroscopic study of highly concentrated pigmented polymer systems. The opacity issues due to the pigment not being soluble in the melt disallow light transmission through the flow cell. The spectra that are collected from these trials show limited information.

NIR spectroscopy was demonstrated to be better suited for these studies, but is still limited to concentrations below 5% by weight and only effective for some pigments. This should not be dismissed from the view that the study did not work for the initial concentrations of interest. However, the concentration limitations that were demonstrated are still useful for current commercial products in the fiber master batch market. Models can be constructed for these systems with a degree of accuracy that would allow for their use in a quality control application. LAS-PLS models were constructed for both pigment C-1 and C-5 using NIR spectroscopy. From this technique, models based on multiple spectral regions were able to quantify the concentration in a range of 1% to 5%, by mass, pigment in polypropylene. These models had SEC values of approximately 0.3 for the C-1 data and 0.5 for the C-5 pigment data. While these values are not spectacular, they do represent the first critical work using a transmission spectroscopic technique to quantify pigment concentration.

Models can also be generated that correlate the color space behavior of the concentrate to the absorbance spectra. As was demonstrated within the confines of this work, the color strength of the resulting plaques can be regressed against the melt spectroscopic data and result in calibration models with a useful degree of accuracy. In the case of the model constructed for the C-5 data, the error over the entire range was +/- 10%, which is useful for quality control monitoring. Future work should be devoted to correlating the color space CIELab numbers of these pigments with the low concentration melt spectra. The conclusions that were reached for the additive sample set hold true here as well. The development of on-line spectroscopy measurement instrumentation will prove to be a valuable tool in the polymer processing industry.

## CHAPTER 10

### ESTIMATION OF PIGMENT DISPERSION IN POLYMERS

#### INTRODUCTION

As has been previously reported, the final product application determines the amount of pigment dispersion that is needed before the final manufacturing step. Due to the small diameter of the actual fiber, all spinning operations require the highest level of pigment dispersion. Presence of large non-dispersed pigment material can cause the fiber to break during any one of many processing steps. This will lead to downtime being incurred by the end user. The other situation that can occur is a visible change in color of the spun fiber. This can lead to wide product variation when looking at a large lot of material being produced during one production run. A device to indicate a Boolean “go/no-go” level of dispersion would be a valuable addition to the arsenal of instrumentation available to the polymer processing industry.

#### 10.1 THEORY

The dispersion of a pigment in a polymer system is dependent on numerous factors. As was explained earlier, proper pigment dispersion is required for proper part color appearance. Industrial pigments are most commonly sold as agglomerates. These materials need to be properly incorporated into the resin matrix and reduced in particle size simultaneously. The ease of pigment dispersion is related back to the mechanical forces required to disperse the material [132]. The effect of dispersion of the pigment is equivalent to reducing the average particle size of the pigment. This will have the effect of increasing the tinting strength (more exposed pigment particles per unit volume), changing the shade (higher number of exposed pigment particle sides increases the surfaces that can scatter light), reduce the opacity (the smaller agglomerates will make the field appear “cleaner”, increase gloss (more surfaces to reflect light), increase the viscosity (more polymer will be between pigment particles), and logically reduce the amount of pigment required for appearance requirements. Shearing forces are required to overcome the surface forces in the pigment molecule that hold the agglomerates together. These forces are dependent on such factors as the pigment related issues (chemical composition, crystal structure, particle size distribution, etc...), polymer related issues (polarity, molecular weight distribution, viscosity, etc...), additives in the

pigmented system, interactions between the pigment and the polymer, presence and activity of a dispersing agent, and any pretreatment activities.

Dispersion in general is based on four objectives [133], all relating back to final product quality. The first objective is reduction of agglomeration of the pigment. This usually occurs through mechanical forces including reduction between two solid surfaces, grinding actions, thermal crushing or impingement. Most commonly, pigments are crushed through some process. Care must be applied so that the properties that give the color characteristics to the pigment itself are not destroyed in this process. The second objective in pigment dispersion is to wet the pigment surface. This is done so that the pigment is linked to the binder or other components of the medium. The amount of energy required to wet out the pigment will depend on the interaction between the pigment and the binder, the kinetics and mass transfer coefficients of the process, the size and geometry of the components and the rheology of the medium. This field has been extensively studied.

The third objective in dispersion is the distribution of the wetted pigment particles throughout the polymer medium. This objective is accomplished using a variety of equipment and techniques depending on the process chosen. Equipment varies in form from various speed mixers, extruders of several different configurations and other blending equipment that can impart mechanical energy to the pigmented system via shear forces. The final objective of the dispersion process is generating a dispersed polymer system that is stable. Re-agglomeration and flocculation are to be avoided in all instances. Stability itself is dependent on numerous factors including the chemical composition of the system, the chemical and physical features of all of the components, and the rheology of the mixture. Several research projects have investigated this area of concern.

The dispersion of pigmented systems is measured in a variety of ways in the polymer processing industry. The most basic testing routine involves the pigmented polymer system being reduced to its final pigment concentration via the addition of resin and having a film blown of this material. Sections of a pre-determined size are analyzed for clumping or dark spots in the film. When viewed on a light box, an agglomeration of particles will appear as a dark spot. The spot frequency and their relative size are

recorded and a qualitative measure of the dispersion can be obtained. Other presently employed techniques are based on microscopy and other visible-optical techniques.

Due to the sensitive nature of most pigment particles, there is a limit to the amount of shear forces that can be applied to an individual pigment particle before irreversible damage is done to the colorant properties of the particle. Additionally, there is an ultimate tinctorial strength for a particular pigment in a particular carrier resin. The dispersion of a material will reach a maximum depth of shade asymptotically with the dispersion time.

Determining the level of dispersion of pigments in polyolefins is a critical quality control issue in the production of color concentrates. Historically, dispersion is measure via a blown film analysis on a diluted pigmented polymer or the color concentrate is passed through a fine screen pack and the pressure rise across the pack is recorded. For more instantaneous measurement of dispersion in the pigmented concentrate, confocal laser scanning microscopy (CLSM) can be used to identify the presence of agglomerates in the pellet form rather than diluting the material and blowing a film. This technique requires minimal sample preparation and is non-destructive in nature. Micrographic images can be correlated with traditional dispersion tests to develop a repeatable protocol.

The concept of confocal laser scanning microscopy was introduced in the late 1950's, but only recently have advances in optics, lasers, and image processing allowed for more practical uses including biological research, material science, and chemical analysis. In LSCM, a laser beam with wavelengths of either 488 nm or 512 nm is first expanded and then converted to a scanning beam by an x-y deflection mechanism. This beam can then be focused on the sample, with the reflected and emitted fluorescent light following the reverse optical path where it is focused on a photomultiplier via a dichroic mirror. A confocal aperture is located before the photomultiplier to screen out the fluorescent light that is not in the focal plane of the sample. Using this technique it is possible to focus at various depths of the sample even in thick samples. The sample point of interest is the confocal spot. A two dimensional image of the focal depth can be produced by first performing a raster sweep and then using an imaging routine to convert the digital signal into a pixel based image. Z-direction sweeps can be done in increments as small as 0.1micron. A schematic of the principle is shown in Figure 10.1 and 10.2. The physical layout of the

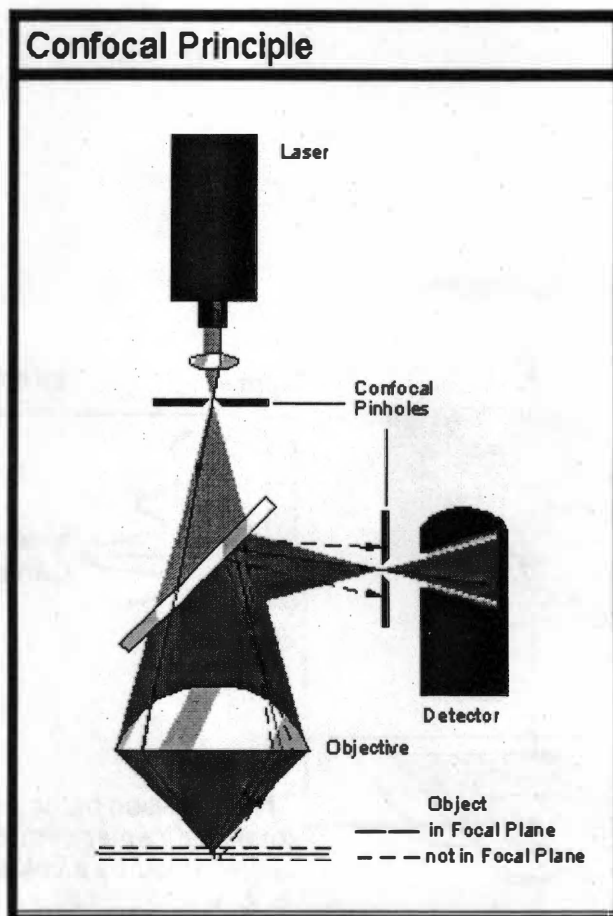


Figure 10.1 Schematic of confocal laser scanning microscopy principle



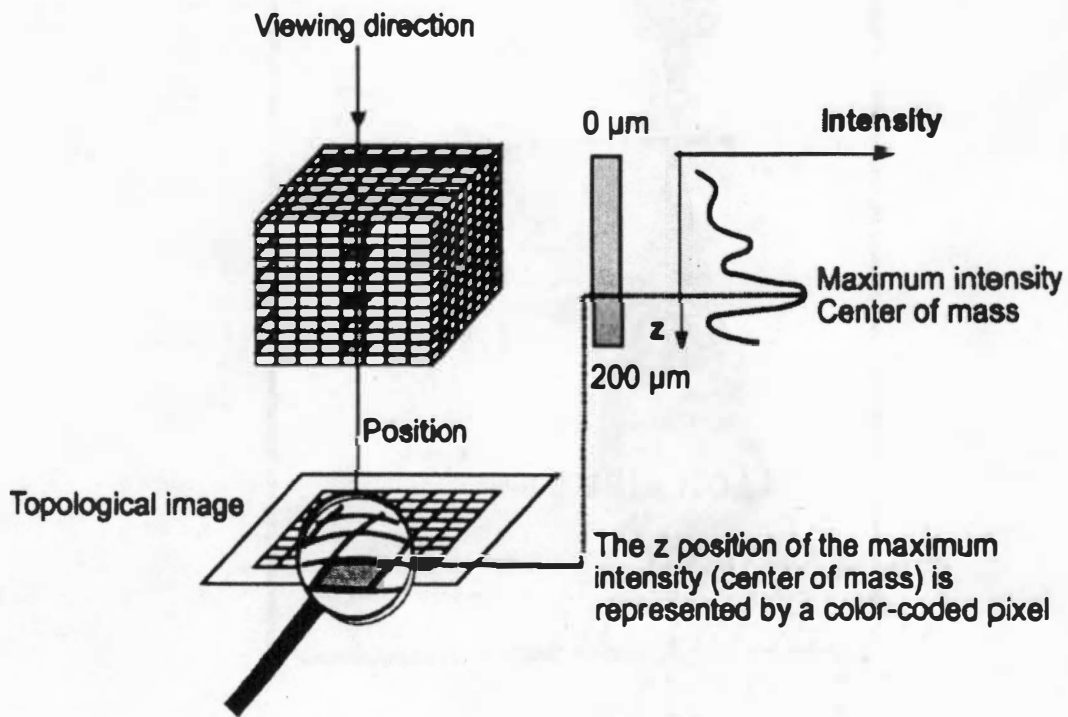


Figure 10.2 Schematic of data generation for confocal laser scanning microscopy

instrument is shown in Figure 10.3. In this experimental set up, there are three main components. The microscope is located on the left of the picture with the laser apparatus on the top of it. This microscope can also be used for normal microscopic studies without the use of the confocal apparatus. The computer screen in the middle is the users control information with the knobs allowing adjustment of the system. The screen on the right is the output of the CLSM microscope.

This technique has the following advantages over conventional microscopy: exclusion of light from outside the confocal spot, optical sectioning rather than defocusing, allowance for three dimensional imaging, ability to scan from multiple directions (not only the z dimension), and minimization of operator error in interpretation of focus limitations.

It is the goal of this section of research to find a spectroscopic technique to locate a point in which the dispersion of the pigment in the polymer carrier is adequate for the final application. The spectra of the melt will be compared with the results from the CLSM micrographs as well as blown film that is traditionally used as the dispersion test.

## 10.2 EXPERIMENTAL

Preliminary work focused on a single sample set of C-3. This particular sample had poor dispersion during its production process and was at the limit for acceptability in a stringent application such as fiber. The pigment was compounded and blown into a 1-mil thick film. FTIR was used to investigate single large agglomerates in the film.

Because the minimum path length of the spectroscopic techniques was 3.0 mm, determination of the degree of dispersion would not be possible using one of these techniques. This is the result of a large volume being studied instantaneously. To resolve this problem and develop a technique that was not as labor intensive as blowing film, the use of CLSM was evaluated for this application.

To further investigate differences in dispersion, the pigments chosen for this study were compounded in four different manners. The first three samples were compounded with a 1.5% pigment concentration on a 34 mm Leistritz co-rotating twin-screw extruder and pelletized using a Conair-Jetro 304 pelletizer. They differed in the pretreatment of the raw materials. The first was a true two-step dispersion



Figure 10.3 Physical layout of confocal laser scanning microscopy used in this study

process as would be typical of a fiber grade quality. The second was intensive mixing of the raw materials in a dry form. The third was dry color extrusion where the raw materials are fed directly into the feed throat of the extruder. The fourth sample was prepared by dry mixing of the raw materials and compounding on a single screw Killion 1" extruder, followed by pelletizing using a Conair-Jetro 304 pelletizer. The samples were evaluated in pellet form using a Leica TCS NT E microscope at a depth of 2000  $\mu\text{m}$ . By using these different techniques, gross changes in dispersion level are visible to even the untrained eye. Only the samples prepared using the first technique would be suitable for commercialization. The other techniques could only be used for lower quality thick section molded or blown parts where dispersion is not as critical.

### 10.3 MICROSCOPIC AND SPECTROSCOPIC RESULTS

Preliminary FTIR spectra for the C-3 dispersion sample are shown in Figure 10.4. For this pigment, a peak at  $2350\text{ cm}^{-1}$  varies with concentration. By measuring the absorbance at this frequency, generalizations about the level of dispersion in the mixture can be made. This narrow region is shown in Figure 10.5. The experiment looked at two separate points on the film. The first was a low concentration of C-3 in a polyethylene film. The second was an agglomerate of pigment less than 0.25 mm in diameter. The laser on the FTIR unit has an actual diameter of roughly twice this amount so a significant amount of light was able to reach the detector. This approach to measuring the dispersion is the same as measuring the concentration of differently loaded samples in Chapter 9. These spectra are not investigating the more difficult problem of characterizing changes of the crystal structure or chemical changes of the end groups of the individual molecules because the laser is actually measuring the absorbance for a volume that includes the large agglomerate, properly dispersed pigment particles and the carrier resin.

To study the capabilities of CLSM, samples of the red pigment (C-2) pellets were supplied at concentrations of 0.15%, 0.3%, 1.2%, and 3.0% pigment loadings. This micrograph series shows the increase in concentration quite dramatically, but at a loading of 3.0%, the pigment particles at this resolution are so close to one another that they are hard to distinguish as separate entities and the photomultiplier voltage needed to be reduced because of flare off of the sample. These micrographs are shown in Figures 10.6 through 10.9. Because of this, 3% pigment loading was set as the maximum.

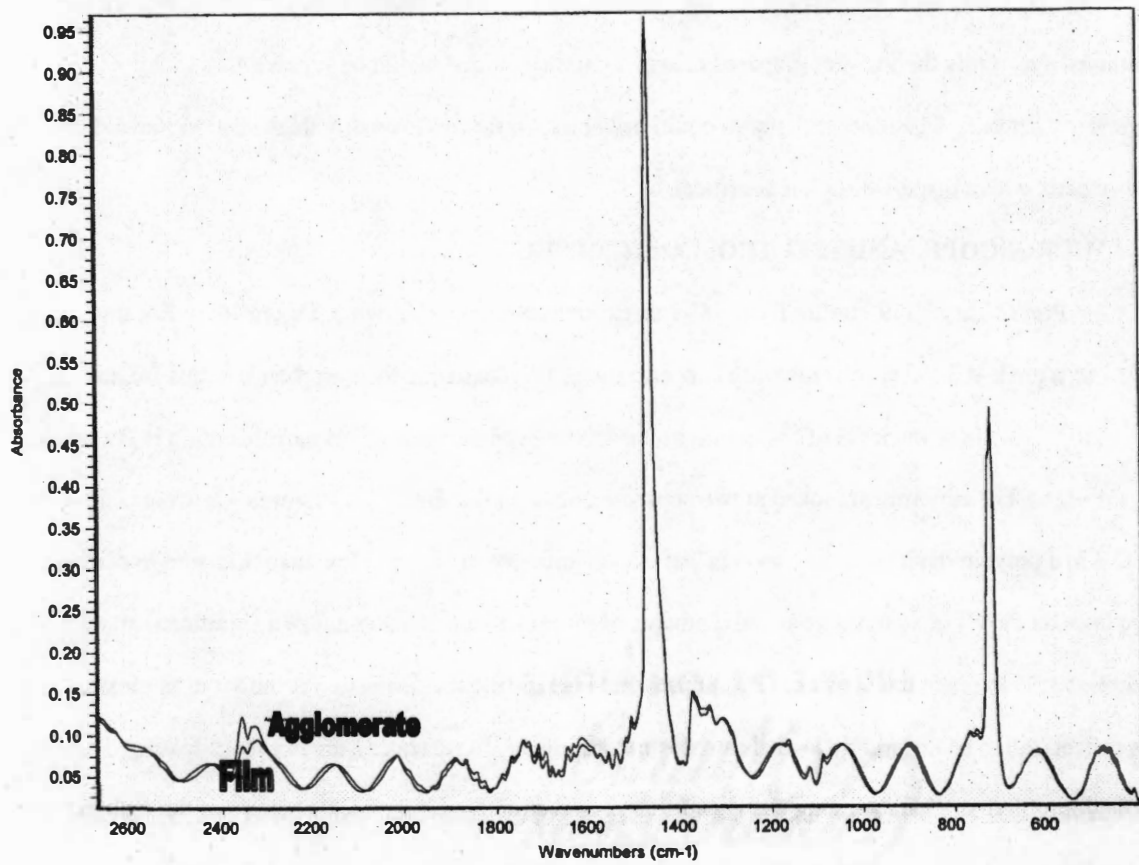


Figure 10.4 FTIR spectra of blown film of C-3 in polyethylene, background film and agglomerate

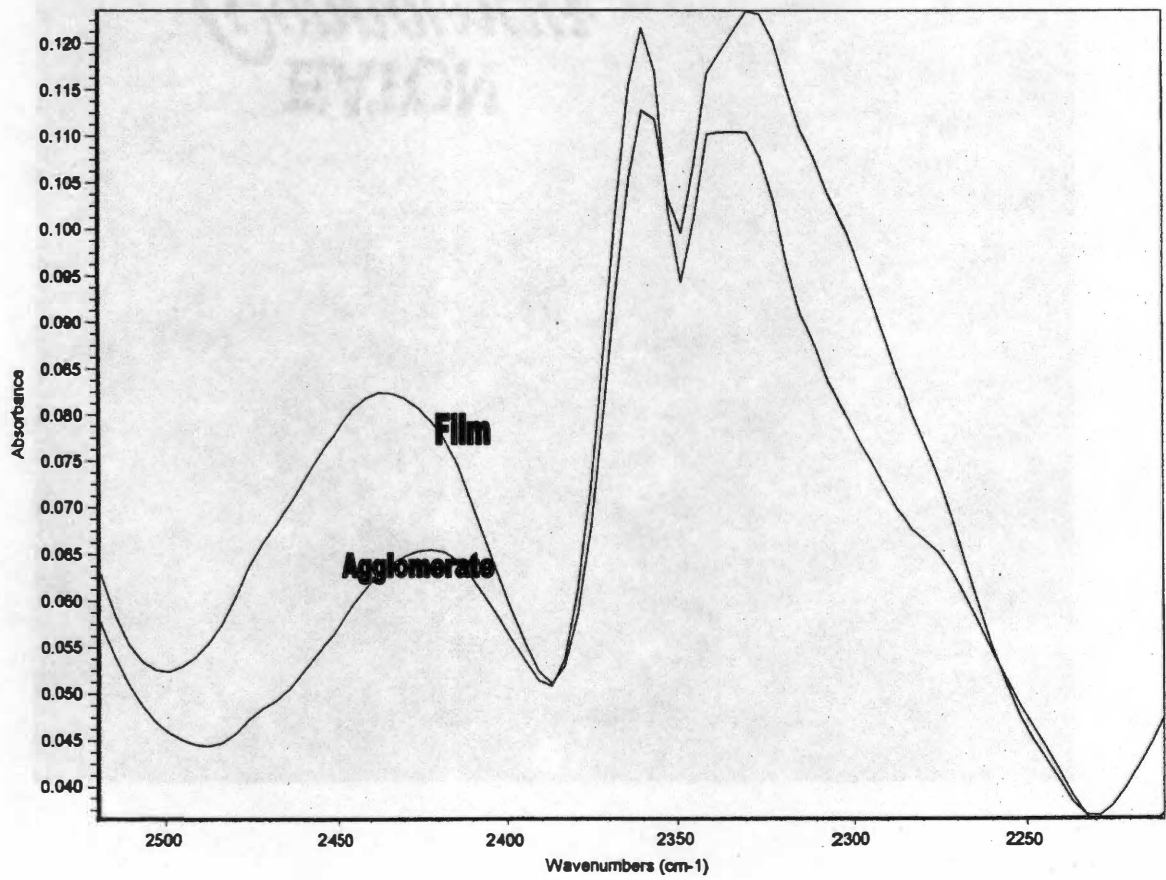


Figure 10.5 Detailed FTIR spectra of blown film of C-3 in polyethylene, background film and agglomerate for the 2250 to 2500  $\text{cm}^{-1}$  region

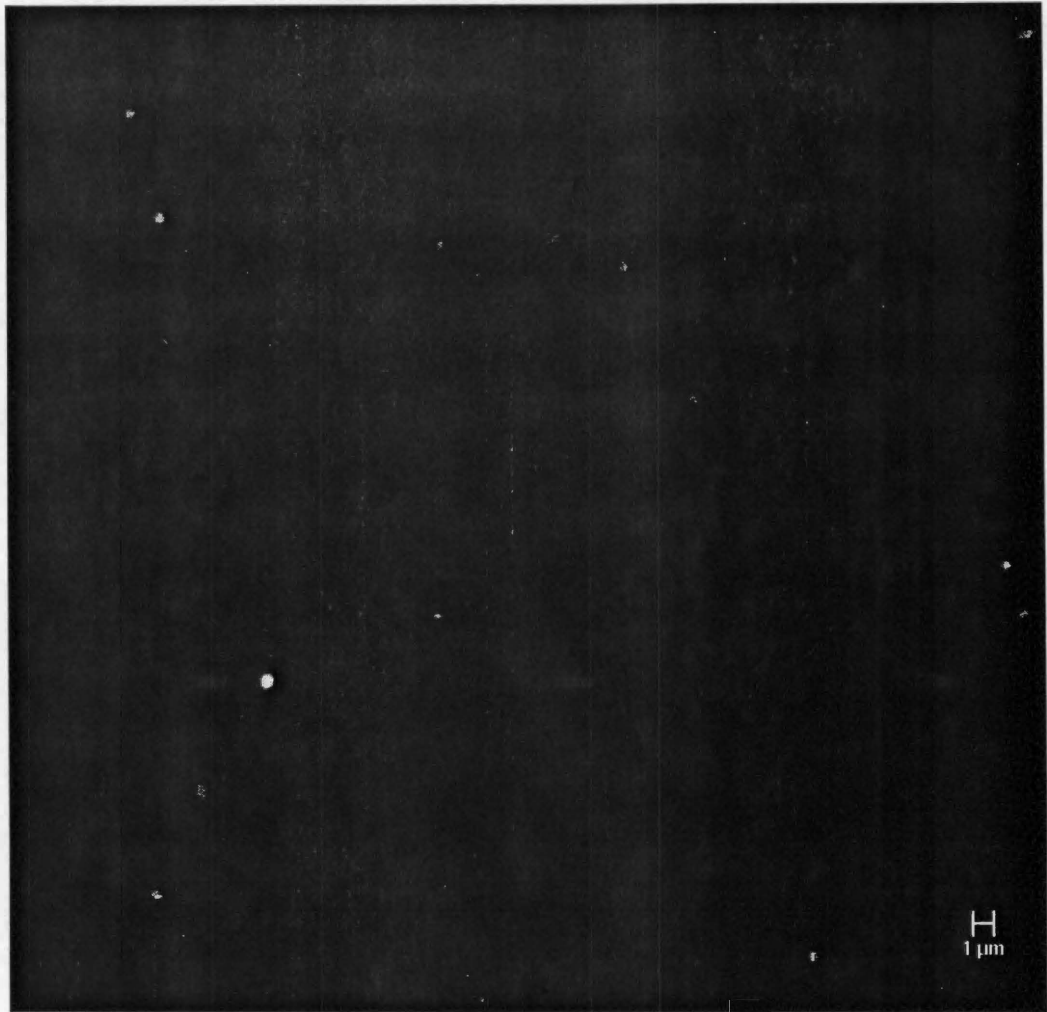


Figure 10.6 CLSM micrograph of C-2 at 0.15% loading in polypropylene

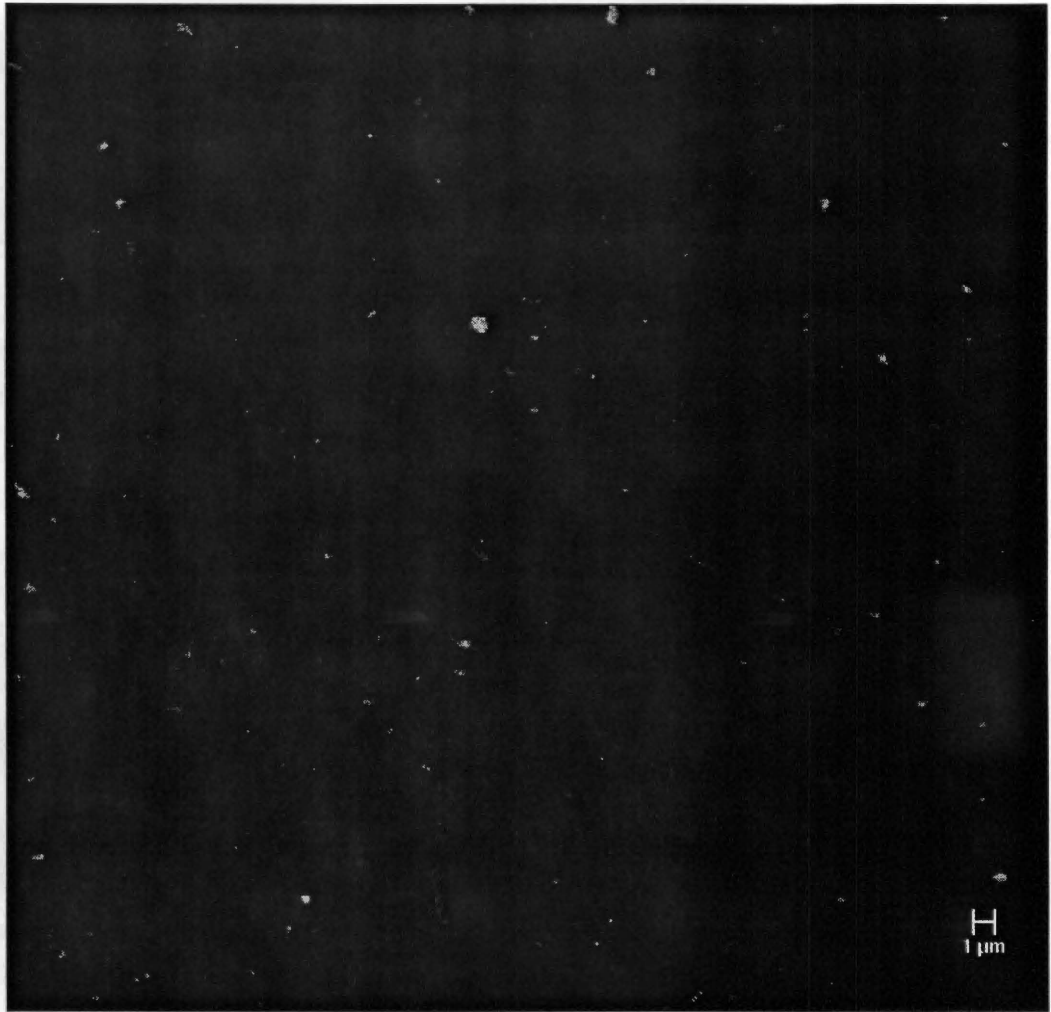


Figure 10.7 CLSM micrograph of C-2 at 0.3% loading in polypropylene





Figure 10.8 CLSM micrograph of C-2 at 1.2% loading in polypropylene

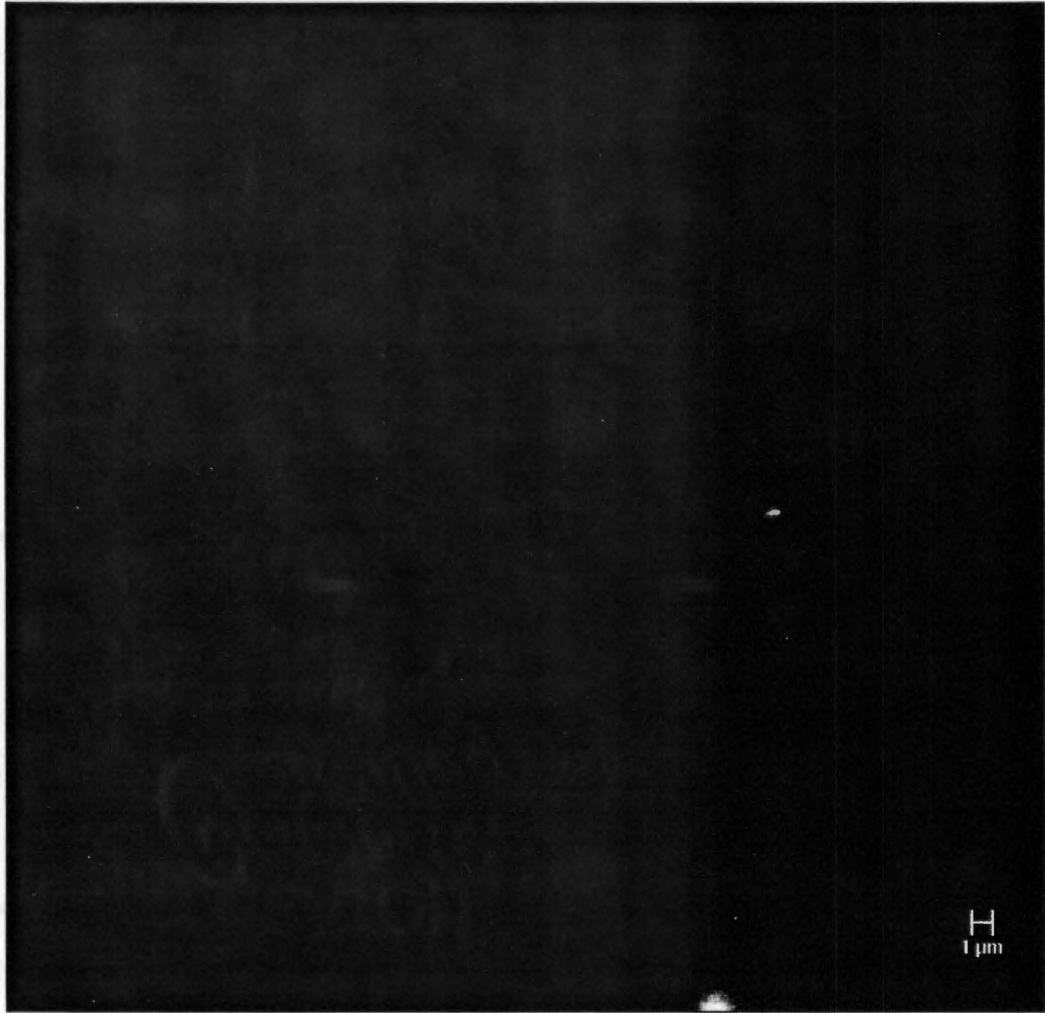


Figure 10.9 CLSM micrograph of C-2 at 3.0% loading in polypropylene

To make a comparison of the varying degrees of dispersion that is possible, blown film samples were produced utilizing pigment C-4 that were dispersed using three different preparation techniques. The first preparation used a pre-dispersed pigment preparation followed by twin screw compounding. This sample was then dry blended with polyethylene resin and a blown film sample at 2 mil thickness was produced. The resulting film is shown in Figure 10.10 with a ruler added for scale. This film shows uniform color development, no streaking, and no visible agglomerates at this magnification. The second sample was produced by mixing dry pigment and resin together on a pellet melter, granulating the solidified mixture and then preparing a blown film as previously described. This film is shown in Figure 10.11, also with a ruler for scale. This film presents some of the problems with not properly dispersing the pigment and reducing the agglomerates. The film is shows no-uniform color development, streaking and the presence of visible agglomerates. The third preparation is similar to the second, except that the dry pigment and resin were combined using heated two-roll mill. This film is shown in Figure 10.12 with a ruler added for scale. This film also shows color development that is better than the second film, but not as high in quality as the first, some streaking due to pigment agglomerates becoming trapped on the die surface and visible agglomerates within the field. These techniques were found to give sufficiently different levels of dispersion of the pigment particles. The samples were then characterized by counting the visible pigment agglomerations on a 8 ½" by 11" sample and averaged over four film sections. The results were as follows: two step method – 4 specs/film, two roll mill – 60 specs/film and pellet melter – 49 specs/film.

The second set of experiments utilizing the Leica CLSM microscopy to probe the master batch in a pelletized form using various levels of dispersion. It was discovered that the phthalo green sample (C-4) fluoresced intensely at 488 nm and 512 nm and could not be investigated using this technique. All of the samples contained 1.5% pigment concentration in a 12 melt polypropylene carrier. Figure 10.13 presents the CLSM micrograph for C-1 prepared by single screw extrusion of a dry color pre mix. In this micrograph, the pigment particles appear to be rather dispersed, but not all of uniform size or shape. There is a large agglomerate that appearing in the lower left side of the micrograph. Figure 10.14 shows pigment C-5 after a two-step dispersion process. In this micrograph, the pigment agglomerates are all of similar size



Figure 10.10 Blown film sample of two-step dispersion process (ruler added for scale)

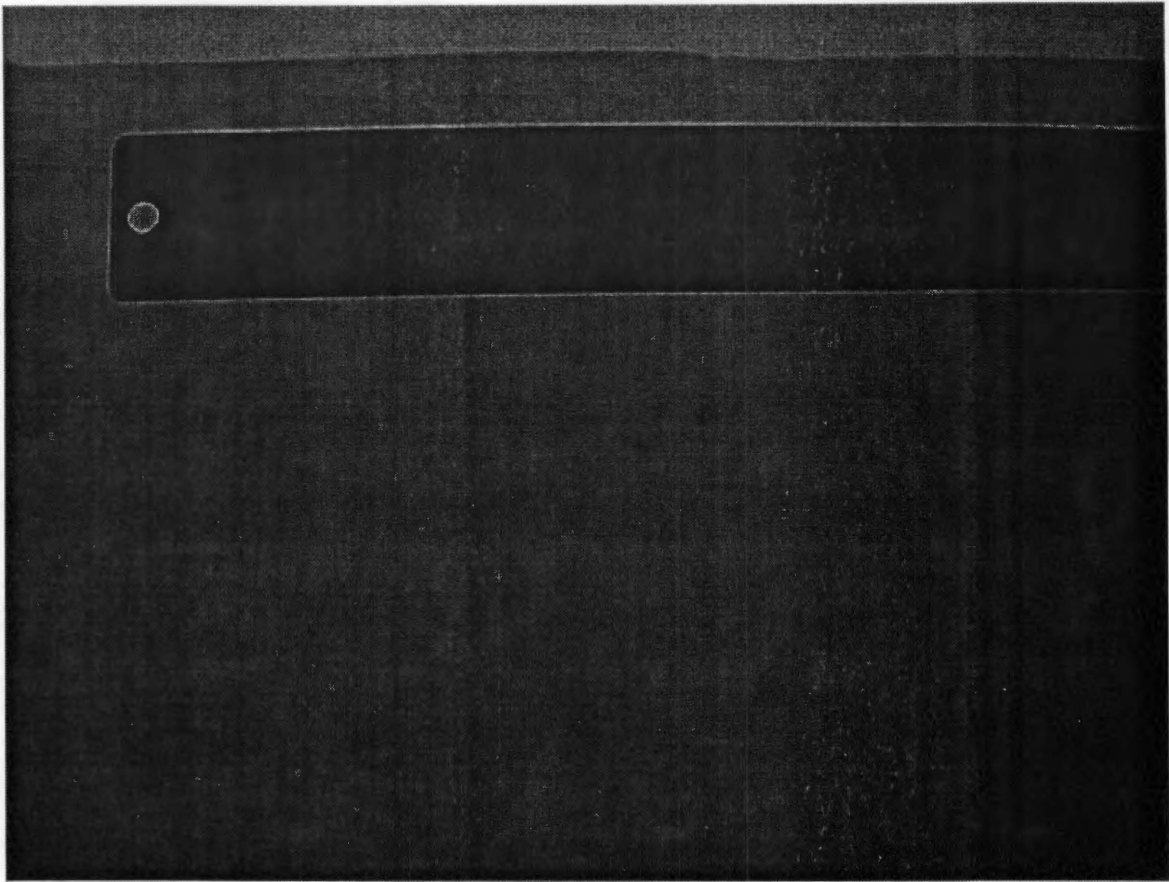


Figure 10.11 Blown film sample of pellet melter dispersion process (ruler added for scale)

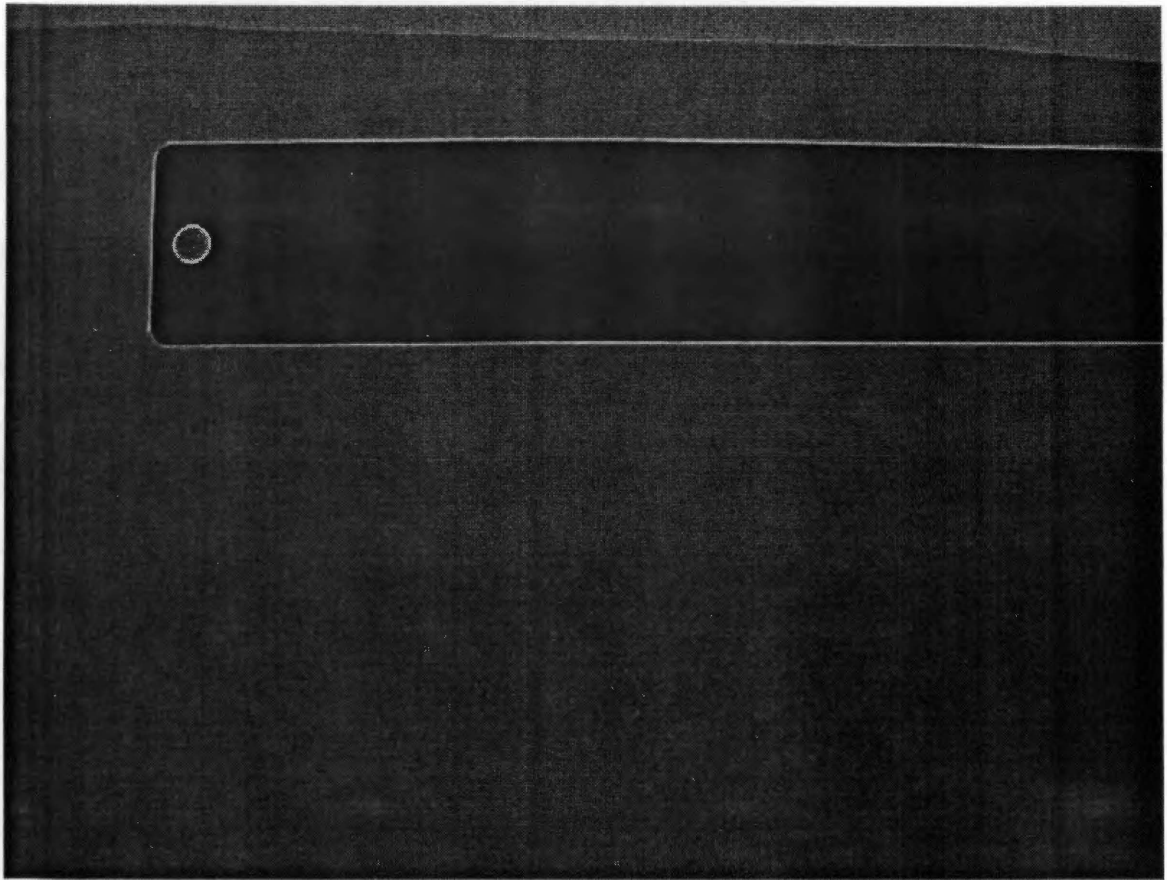


Figure 10.12 Blown film sample of Brabender dispersion process (ruler added for scale)

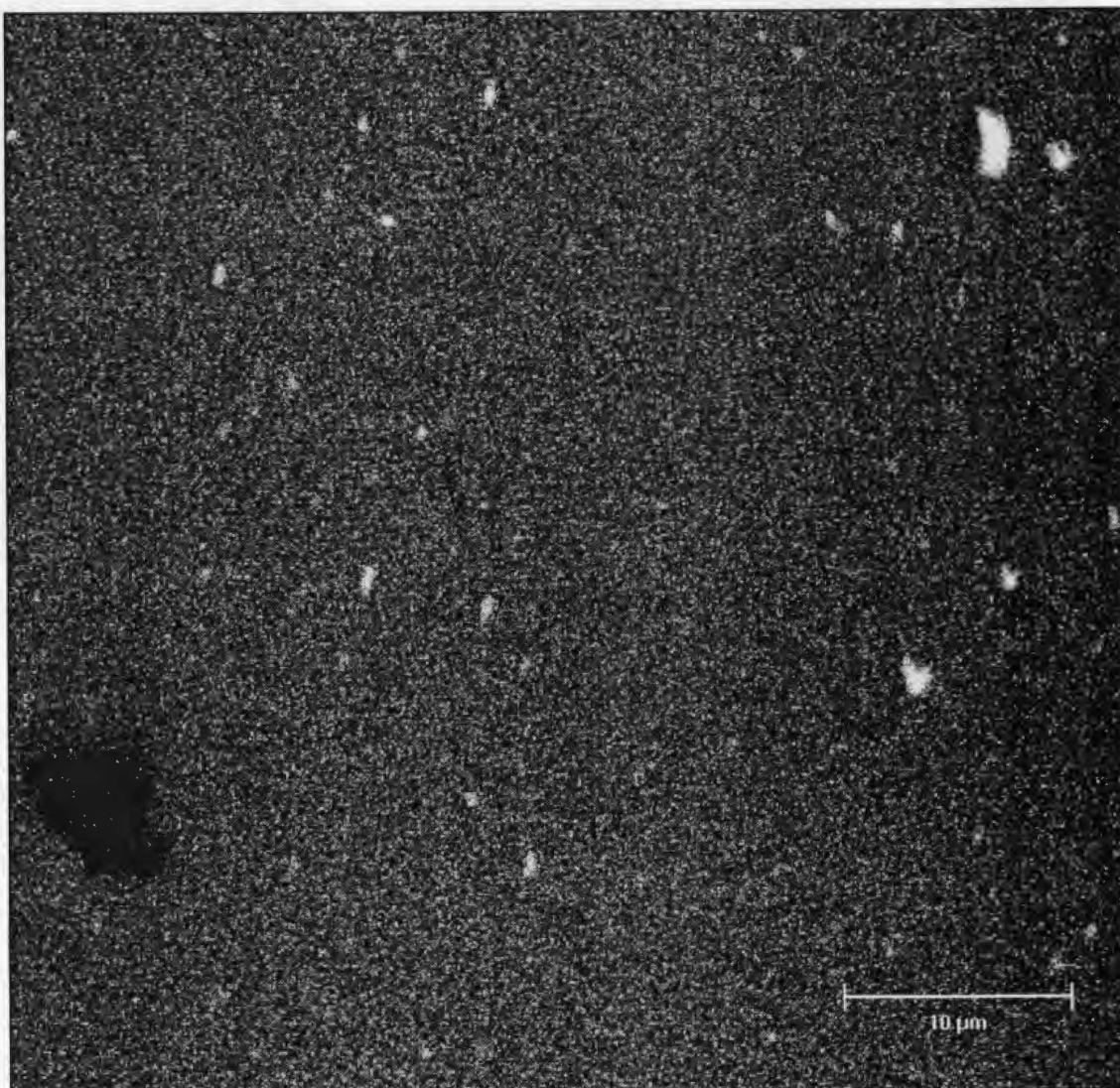


Figure 10.13 CLSM micrograph of crocody yellow (C-1, dry color, single screw extrusion)

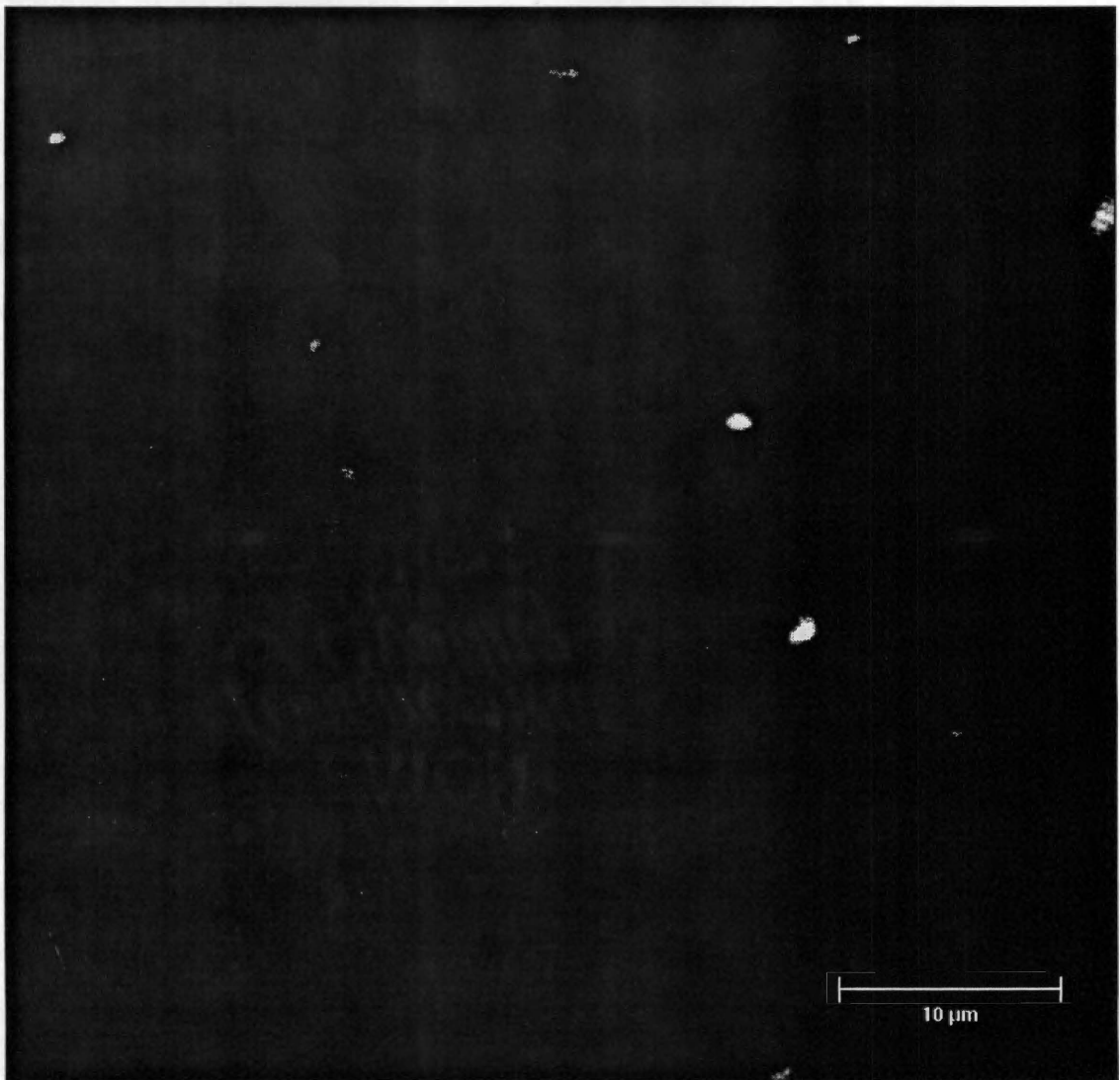


Figure 10.14 CLSM micrograph of diazo condensate yellow (C-5, two step dispersion)



and shape as well as evenly distributed throughout the field of view. The quality of dispersion can be readily compared with the C-1 sample in the previous micrograph.

Figure 10.15 is the CLSM micrograph of pigment C-2 with an intensive mix step before twin screw extrusion. In this micrograph, the pigment particles are uniformly distributed throughout the field and are of similar size and shape. However, it should be noted that the agglomerates are larger in diameter than those found in Figure 10.14, indicating a lower quality of dispersion. Figure 10.16 is a CLSM micrograph of pigment C-3 that was prepared with by dry color, twin-screw extrusion. The pigment was hand mixed with the resin prior to extrusion. This micrograph shows that the pigment particles are not evenly distributed throughout the polymer, and they are not uniform in size or shape. The quality is similar to that found in the micrograph of the C-1 sample (Figure 10.13). From these micrographs, it is possible to characterize the number and size of the agglomerates, demonstrating that this technique can be used for determination of dispersion quality.

#### **10.4 EXPERIMENTAL LIMITATIONS**

There are several limitations that occur when trying to measure the dispersion of a pigment in this manner. The preliminary experiments were conducted with a film. Most industries measure the dispersion in a film form, but measure the number of agglomerates, which appear a spots, per sheet. Measuring the dispersion in this manner is not a quantitative characterization of the dispersion. A count of the specs is given, but the difference between a quality product and an off specification product is a subjective call. The use of CLSM had several limitations as demonstrated in these trials. The first of which is the problem in dealing with pigment master batches of high concentrations. This technique is limited to pigment levels below 3.0% in polypropylene. This is similar to the order of magnitude limitations pointed out in Chapter 9 for the determination of pigment concentrations using on-line spectroscopy. The other limitation of this technique was found with the fluorescing of the pigment C-4 sample from the excitation wavelength of the laser. Each pigment would have to be screened for this phenomena prior to a dispersion routine being developed. The third limitation is similar to the subjective call mentioned in the measurement of film quality. It is operator dependant to determine the difference between a quality product and an off specification product.

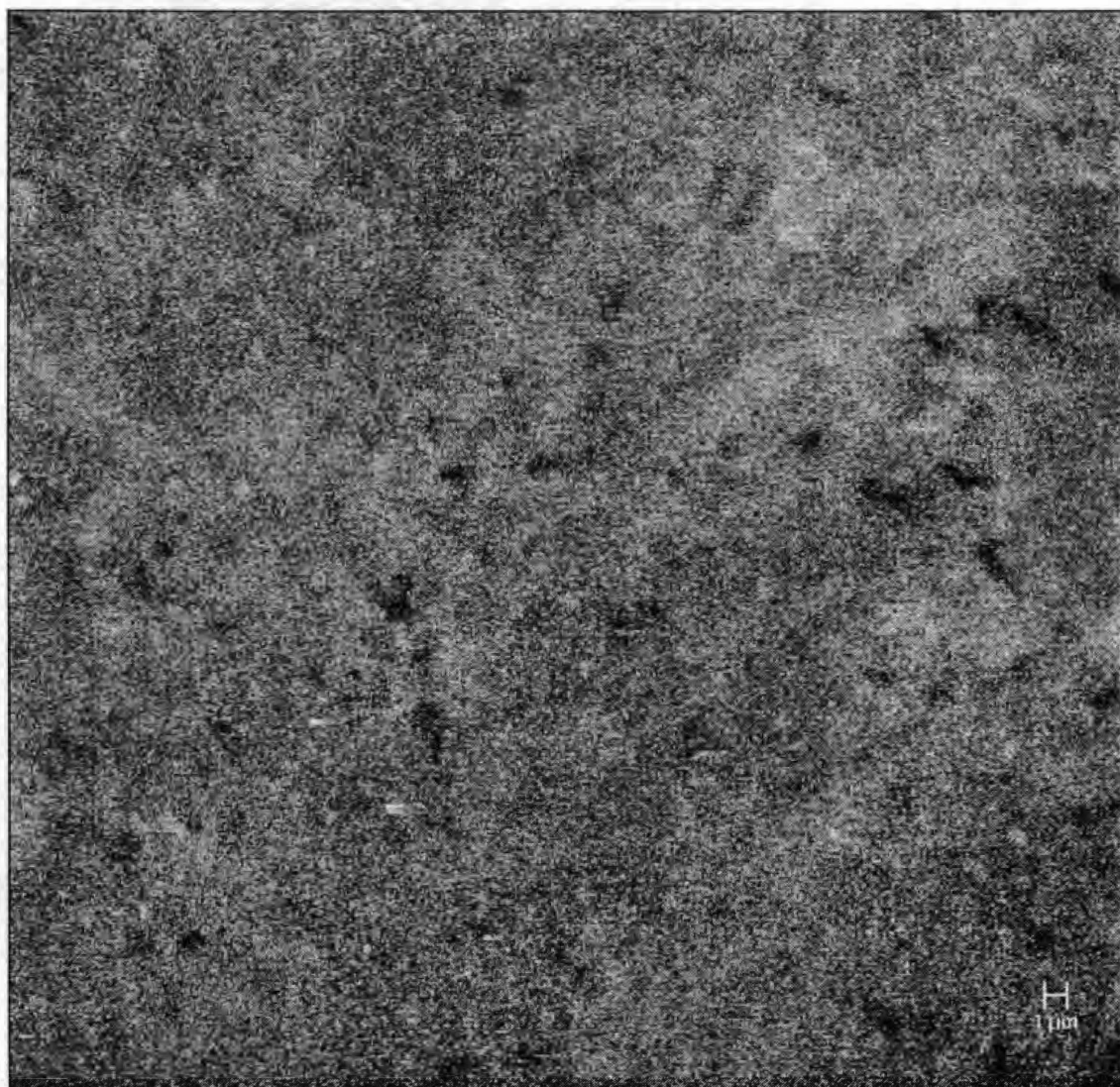


Figure 10.15 CLSM micrograph of cromo red (C-2, intensive mixing, twin screw extrusion)



Figure 10.16 CLSM micrograph of phthalo blue red shade (C-3, dry color, twin screw extrusion)

Due to the opacity of the melt, it was impossible to gather data for dispersion using an on-line spectroscopic measurement technique. Because of this, the use of another technique had to be developed to characterize the dispersion of pigment agglomerates and particles in polypropylene. The study conducted on the pigmented systems by use of CLSM was the first detailed study presented in the open literature.

Limitations also result on the capability of the instrument in measuring thick samples or molten samples. The film blown for these experiments was rather thin and was the reason that a transmission FTIR instrument could be used. When dealing with thicker samples, Beer-Lambert's Law will come into effect and will skew any concentration measurements. It is not known what effect an agglomerate of pigment material will have on a thick or molten sample.

To eliminate these problems, this type of technique could be applied to different polymer processing applications where the flow field of the melt is more contained to a narrower cross section, such as blown or cast film. In these cases, the concentration of the pigment in the path length is not only lower were it can be accurately measured, the mass flow rate of material is also lower which will allow for more instantaneous measurements to be made.

## 10.5 CONCLUSIONS

While the results of this study were not what were initially expected, they do consist of useful information in that they have identified the limitation of certain experimental apparatuses currently available. The use of CLSM contained in this work was the first attempt of determining the capabilities of this instrument to determine the quality of pigment dispersion in polymeric materials. As can be seen in the micrographs, the highly concentrated samples seem to be evenly dispersed, but when a gradual increase of pigment concentration is studied, the fact that the field of view is blurred becomes obvious and that no realistic information is available at levels above 3%. At these levels, the pigment particles become indistinguishable from one another.

CLSM was demonstrated to be a useful tool in the quantification of pigment dispersion. By using this method, it was possible to distinguish between four different types of pigment dispersion techniques. These trials required no sample preparation and could be conducted in a much more time efficient manner

than current commercial techniques, greatly reducing the cycle time on quality control measurements.

While this is not instantaneous or on-line capable, its use in an industrial setting would be beneficial.

Although these experiments were conducted to only show that this approach is based on fundamental concepts, visible evidence of measuring dispersion via concentration should be practical. On-line measurements will have to be conducted with short sampling times to get any useful information of the instantaneous concentration. These experiments have shown that dispersion will effect the local concentration of pigment in the material. Future work needs to be conducted on looking at not only the presence of agglomerates, but physical changes in the pigment itself, either changes in the crystal nature or physiochemical changes on the functional end groups.

Future work should also be focused on the use of visual spectroscopy of the extrudate. This would allow for correlation of pigment concentration with the color space properties of the given pigment in a resin system. This approach could also be more readily implemented with polymer processing equipment in that the operating temperatures and pressures are considerably lower downstream from the extruder's die head. In these cases, the measurement would be conducted at room temperature and pressure in an open environment.

## CHAPTER 11

### COMPLEX VISCOSITY MEASUREMENTS OF POLYMER MELTS

#### INTRODUCTION

Rheology is the study of material flow characteristics [166]. Depending on a liquid's behavior, it can be classified as a Newtonian or non-Newtonian fluid [167]. Newtonian fluids have a viscosity that is independent of an applied stress, but is only a function of temperature and pressure. Non-Newtonian fluids have a viscosity that is a function of applied stress and strain as well as temperature and pressure. Polymeric materials exhibit the characteristics of non-Newtonian fluids. One phenomena of a Non-Newtonian fluid is a shear thinning behavior. In this behavior, the material's viscosity decreases with increasing shear rate. This is due to the variation of polymer chain disentanglement rate with increasing strain rate. This phenomenon is important in industrial polymer processing, and therefore a practical on-line measurement technique is beneficial. This section will outline a mathematical relationship between the spectral intensity and the rheological behavior of the molten polymer and the prediction of the polymer's viscosity from spectroscopic data.

#### 11.1 THEORY

Rheometers are the most commonly used instrument to measure viscosity of molten polymers [166]. Several different configurations, such as extensional rheometers, drag flow rheometers, and pressure driven rheometers, have been developed to quantify different physical properties. A melt indexer is the most commonly used rheometer used in industry. It is pressure driven in design and has been standardized internationally. The indexer measures the behavior of the material as the grams of material that flow through the die in a 10 minute time period. An indexer is depicted in Figure 11.1[166].

Polymeric materials show a wide range of mechanical behaviors. At low temperatures and high strain rates, most materials behave as an elastic solid, but at high temperatures and low strain rates, the behavior is similar to a fluid. This behavior is referred to as viscoelasticity [167]. When a sinusoidal stress is applied to an ideal elastic solid, the resulting shear strain will be in phase with the stress. When a sinusoidal stress is applied to an ideal viscous liquid, the resulting shear strain will be 90° out of phase with the stress. Thus, viscoelastic materials will be in the 0° to 90° range. The response can then be

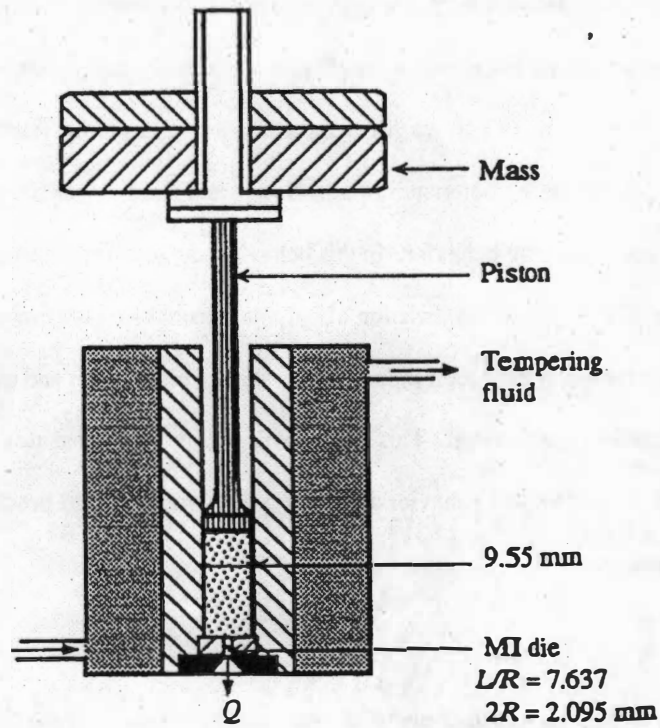


Figure 11.1 Schematic of an ASTM standardized melt index (MI) measurement apparatus  
 [Source: C. W. Macosko, *Rheology – Principles, Measurements, and Applications* (VCH Publishers, Inc. New York, 1994)]

characterized as an elastic (storage) modulus component that is the in phase component, and the viscous (loss) modulus component, the out of phase part. If the material has a sinusoidal stress applied to it, the relationship between stress and strain are given by the following [166].

$$\text{Strain: } \gamma = \gamma_0 \sin(\omega t) \quad (11.1)$$

$$\text{Stress: } \tau = \tau_0 \sin(\omega t + \delta) \quad (11.2)$$

$$\tau = \tau_0 \sin(\omega t) \cos(\delta) + \tau_0 \cos(\omega t) \sin(\delta) \quad (11.3)$$

$$\tau = \tau' \sin(\omega t) + \tau'' \cos(\omega t) \quad (11.4)$$

$$\text{Elastic modulus: } G' = \tau'/\gamma \quad (11.5)$$

$$\text{Viscous modulus: } G'' = \tau''/\gamma \quad (11.6)$$

$$\text{Complex viscosity: } |\eta^*(\omega)| = (\eta'^2 + \eta''^2)^{1/2} \quad (11.7)$$

$$|\eta^*(\omega)| = [(G'/\omega)^2 + (G''/\omega)^2]^{1/2} \quad (11.8)$$

where  $\omega$  = angular frequency

$\eta'$  = dynamic viscosity

$\eta''$  = elastic component of the complex viscosity

Drag flow rheometers are the most commonly used device to measure viscoelastic properties in the polymer industry. This instrument measures the velocity of the moving surface and the forces on one of the surfaces. Most of these instruments operate on rotary motion and usually contain one of three different types of geometry: parallel disks, cone and plate, or concentric cylinder. A schematic of a cone and plate rheometer was presented in Figure 7.10. This device is capable of measuring the storage modulus, loss modulus, and complex viscosity as a function of angular frequency for a specified stress and temperature. Rheological flow behavior of polymers is anisotropic during an extrusion process. The extent of the anisotropy is dictated by the molecular orientation during processing. Under typical processing conditions, the anisotropic effects can be correlated strongly with the molecular weight distribution, chain length, and extent of branching, all of which can effect the spectroscopic results. Most spectroscopic techniques will be more strongly affected by chemical changes than by these rheological properties and therefore the effects are independent of each other. Addition of additives or pigments to a polymer system can also



affect the viscosity of the resulting mixture [168]. The opportunity to de-couple these phenomena should not be overlooked.

It is rare that a product made of polymeric materials is produced without the addition of colorants or additives to improve appearance or physical properties. The addition of these materials can have a tremendous effect on the flow characteristics as compared to the base resin [169]. These effects manifest themselves as such properties as melt strength and processibility as a result of the rheology of the material being affected. The majority of additives used in the polymer processing industry are melt blendable, and, therefore, the resulting rheology of the system is a combination of the two materials. Pigments, on the other hand, are not soluble in the melt and, therefore, are crystalline particulates in the polymer matrix. The effect of these pigments is dependent on the particle size, shape and distribution. At low concentrations, the resultant behavior of the relative viscosity can be characterized by Einstein's relation [170, 171].

$$\mu_r = \frac{\mu}{\mu_o} = (1 + 2.5\phi) \quad (11.9)$$

where  $\mu$  and  $\mu_o$  are the viscosity of the mixture and the pure melt respectively and  $\phi$  is the volume fraction of the particle. Several studies have focused on such systems as talc filled polypropylene [172, 173], carbon black filled polyolefins [174, 175] and fumed silica PDMS systems [176-179]. It is important to determine the location at which this relationship is not valid.

## 11.2 EXPERIMENTAL

There are several samples that will be investigated in this portion of the research endeavor. The additive sample spectra that were produced in Chapter 8 were reinvestigated to locate possible band locations that could be correlated with either complex viscosity or melt index. As well as the additive samples, the pigment samples were also revisited to make determinations of the interaction of pigment loading with the material's melt index and complex viscosity. The melt index data for all samples was generated during the samples' initial production and subsequent models incorporated this information. Data concerning the complex viscosity was obtained using a cone and plate drag flow rheometer and producing thin sections of virgin sample material on a Carver press. Comparisons were also made at the

initial melt index upon completion of the manufacturing step and after processing during spectroscopic analysis.

### 11.3 RESULTS AND DISCUSSION

Data concerning the complex viscosity was obtained using a Rheometrics cone and plate drag flow rheometer. Concentrates of the sample materials were compounded on a 34 mm twin screw extruder, and sample plaques were prepared utilizing a Carver press. Complex viscosity data was collected over a frequency of 0.1 to 500 radians per seconds. Samples were investigated at 230 °C with an applied stress of 2500 dyne/cm<sup>2</sup>. These conditions simulate the shear that would be typical in the die section of a compounding extruder.

Figures 11.2 through 11.8 show the resulting complex viscosity for the ultraviolet stabilizers used in this study. As is evident, at low concentrations these materials behave similarly and the complex viscosity of each is in the same order of magnitude. All of these melt additives exhibit a maximum in the complex viscosity under 10 % additive concentration. These materials all have melting temperatures well below that of the polymer and have effectively thinned out at the processing temperature. The additive actually dissolving into the polymer before the polymer melts can explain this phenomenon. The point at which the maximum occurs would be the solubility limit for that additive in the polymer.

For UV-4 (Figure 11.3), the maximum viscosity occurs at 1% loading by mass. The viscosity then decreases in a linear manner as a function of concentration. UV-7 (Figure 11.4) exhibits a great increase in complex viscosity at 5% loading with a linear drop from 10 to 50%. UV-1 (Figure 11.5) has a gradual viscosity change with a maximum occurring at 5%. UV-2 (Figure 11.6) is a low melting temperature additive and, as a result, loses a great deal of its viscosity as its concentration is increased. UV-6 (Figure 11.7) displays the same behavior as is seen in the other additives, but the viscosity of the mixture exhibits a tremendous increase as the concentration exceeds 25%. This can be explained by inadequate dispersion and a two-phase material with highly loaded polymer regions and melted additive regions. UV-3 (Figure 11.8) and UV-5 (Figure 11.9) both display the same trend with maximum complex viscosity occurring at 2% and 1%, respectively.

# UV 4 in PP

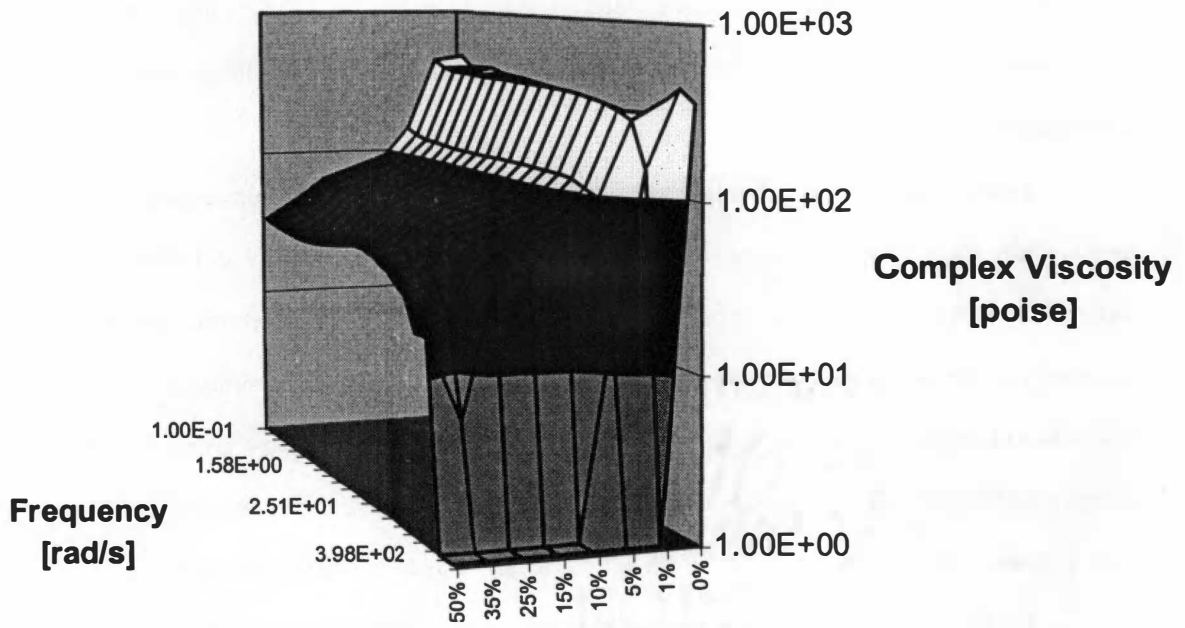


Figure 11.2 Complex viscosity measurements of UV-4 in PP at 230 °C and strain rate of 2500 dyne/cm<sup>2</sup>.

# UV 7 in PP

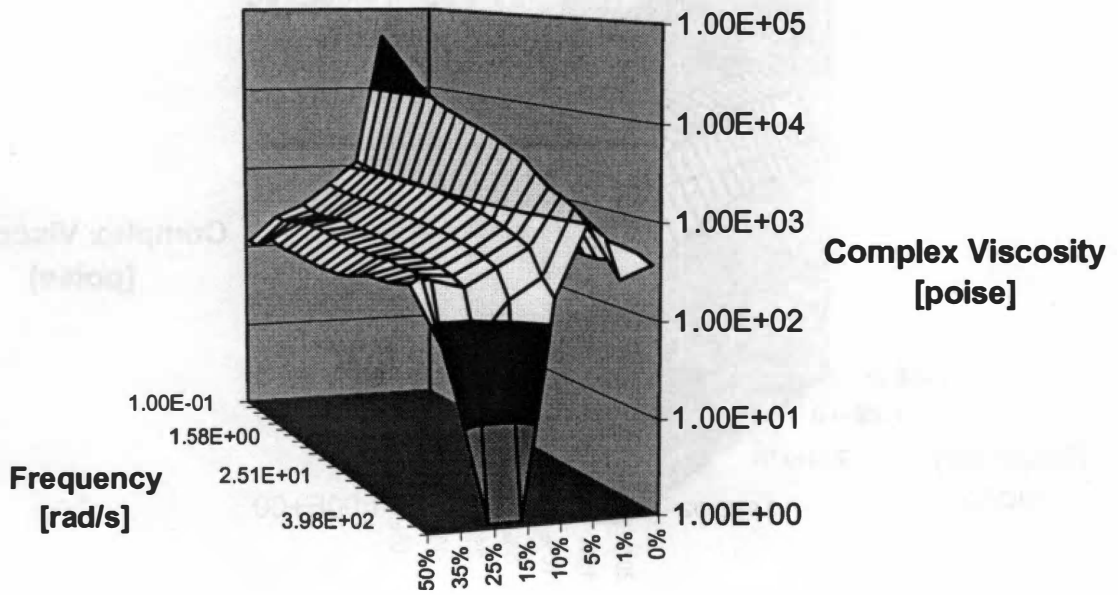


Figure 11.3 Complex viscosity measurements of UV 7 in PP at 230 °C and strain rate of 2500 dyne/cm<sup>2</sup>.

# UV 1 in PP

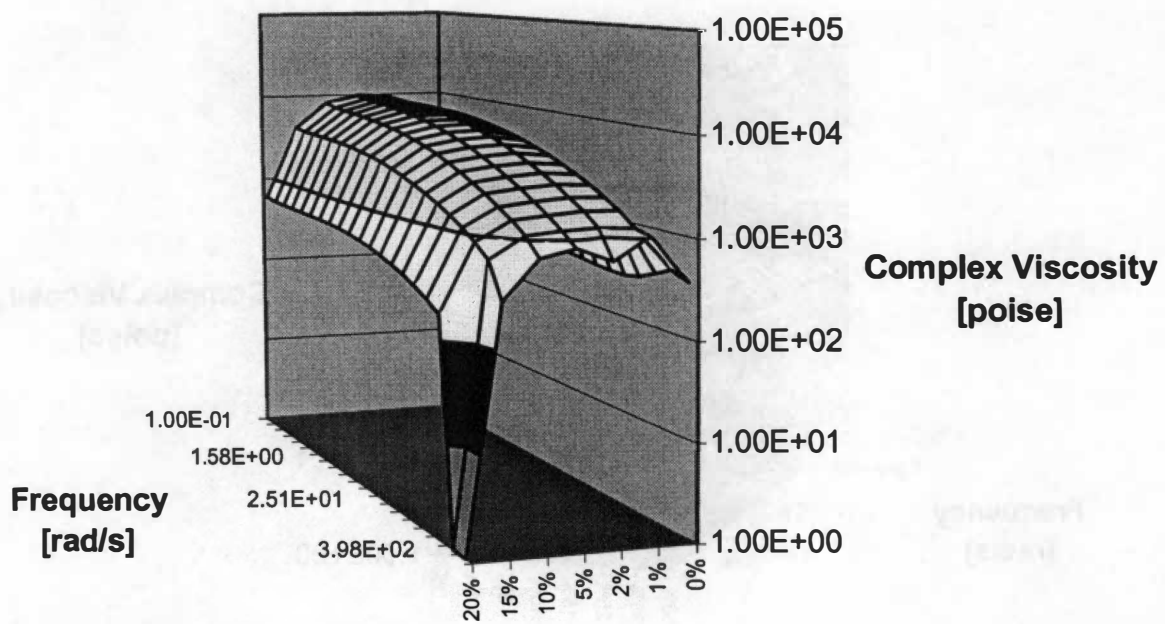


Figure 11.4 Complex viscosity measurements of UV 1 in PP at 230 °C and strain rate of 2500 dyne/cm<sup>2</sup>.

# UV 2 in PP

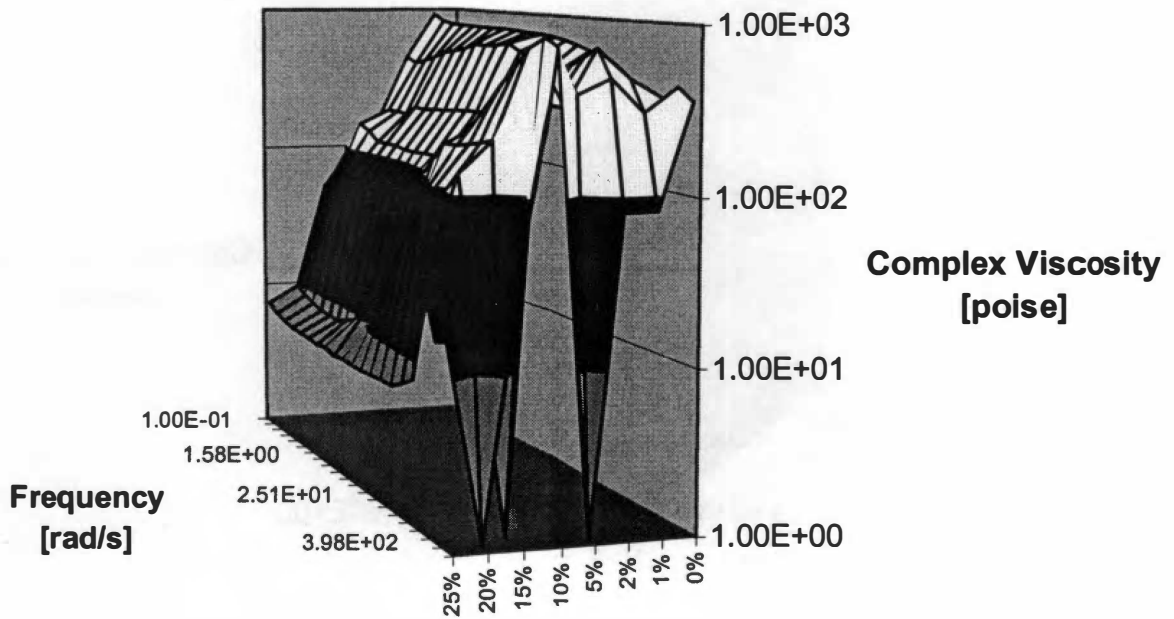


Figure 115 Complex viscosity measurements of UV 2 in PP at 230 °C and strain rate of 2500 dyne/cm<sup>2</sup>.

# UV 6 in PP

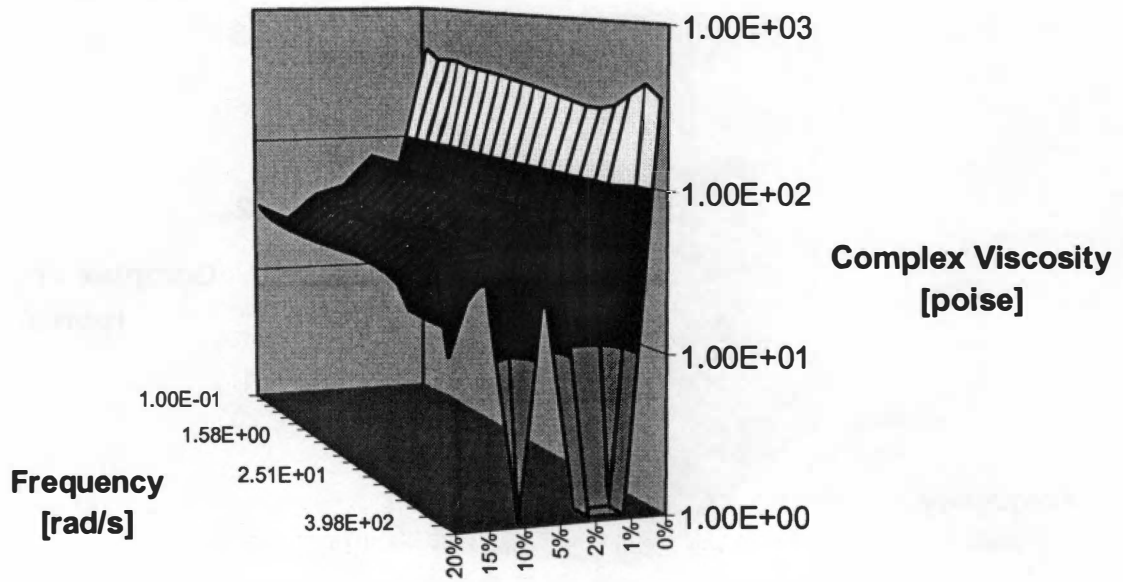


Figure 11.6 Complex viscosity measurements of UV 6 in PP at 230 °C and strain rate of 2500 dyne/cm<sup>2</sup>.

# UV 3 in PP

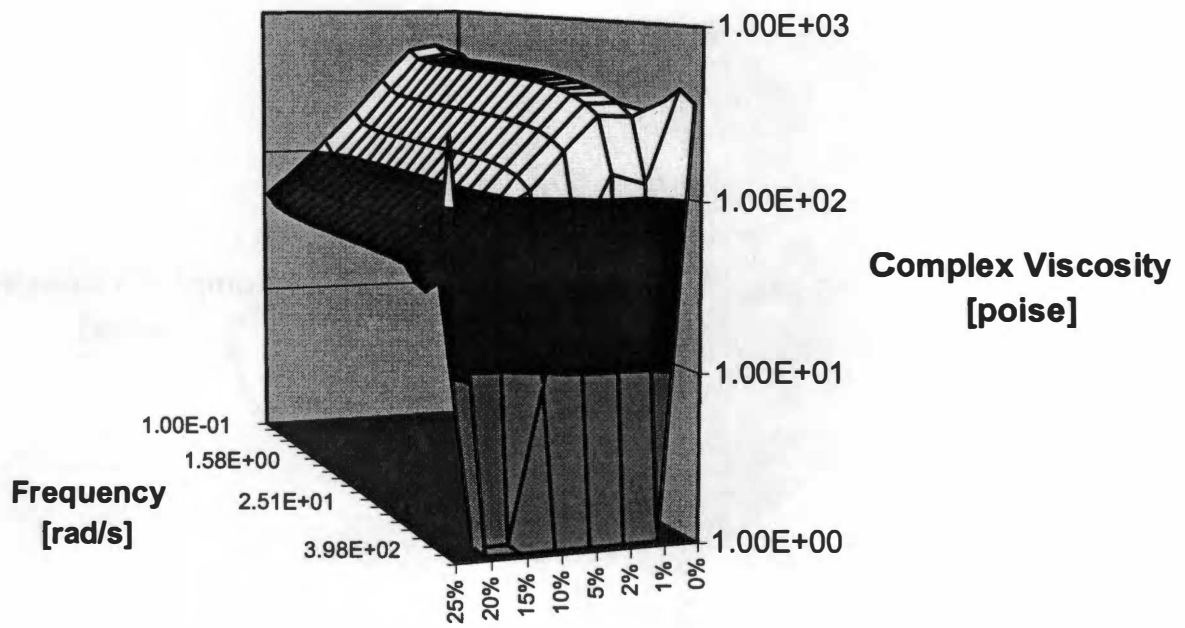


Figure 117

Complex viscosity measurements of UV 3 in PP at 230 °C and strain rate of 2500 dyne/cm<sup>2</sup>.



# UV 5 in PP

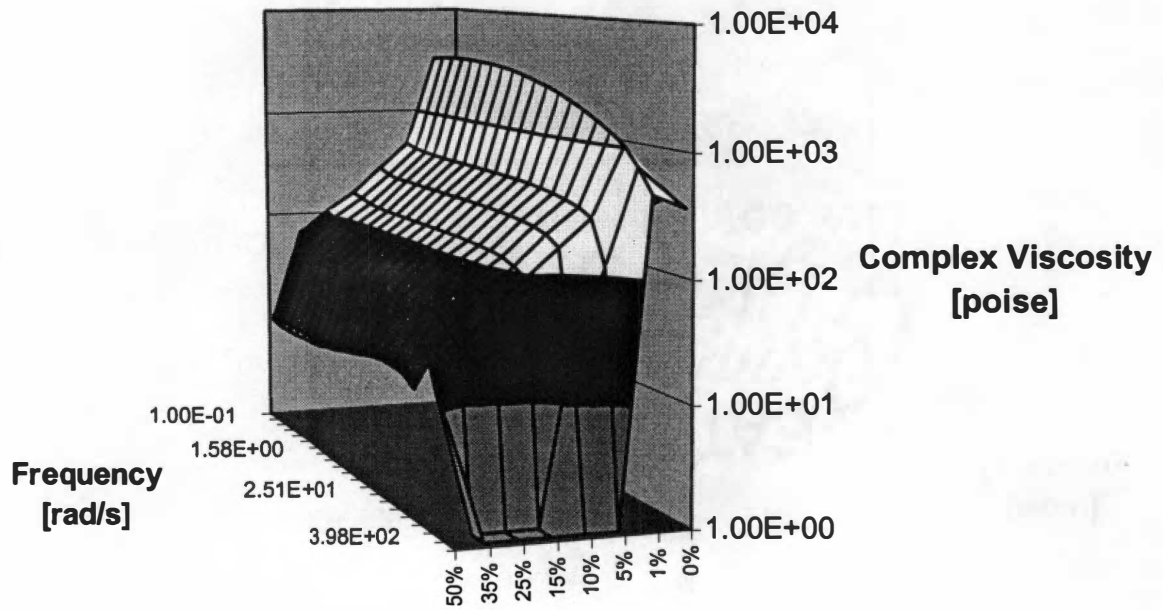


Figure 11.8 Complex viscosity measurements of UV 5 in PP at 230 °C and strain rate of 2500 dyne/cm<sup>2</sup>.

As should be expected, the antioxidant additives (Figures 11.9-13) in the study all follow the same behavior as the ultraviolet stabilizers, because all of the additives chosen for this study are all melt blendable with melting points in the 100 to 180 °C region. The initial peak in viscosity occurs for all of these materials at concentrations around 1% additive. With the exception of AO-4 (Figure 11.10), the effect of additive loading does not have a dramatic effect on the complex viscosity.

The pigments chosen for this study (Figures 10.14-10.18) are typical colorants used for the production of custom colors in the fiber spinning industry and are commonly used in the production of carpet. These pigments can exhibit dye-like behavior at low concentrations because of solubility issues, but at loadings above 5% should follow the Einstein model. The deviation from the model can be explained by the difficulty in obtaining highly concentrated single pigment dispersions. At high concentrations, the pigment crystals can agglomerate because of the lack of polymer to wet out the particles. Because of this, there are now large agglomerates in the melt and not discrete particles.

Pigment C-1 (Figure 11.14) shows a solubility limit at 1%. There is some indication of an decrease in viscosity with concentration. The results can be skewed some by the presence of low melting compatibilizers at higher concentrations. These additives are included into the system to wet out the pigment particles as well as hinder agglomerate formation. Pigment C-5 (Figure 11.15) shows similar effects on complex viscosity with a more pronounced increase at a concentration of 25%. Pigment C-2 (Figure 11.16) shows both the solubility at 1% and the linear increase in complex viscosity at concentrations greater than 5%. Pigment C-3 (Figure 11.17) and Pigment C-4 (Figure 11.18) both exhibit this behavior as well.

For the prediction of complex viscosity from spectroscopic information, it would be possible to build a PLS calibration model for each angular frequency by correlating the complex viscosity data with the corresponding NIR or UV spectral data. The sheer number of calculations to build these models would be enormous. In previous research, Vedula [2] and Li [46], both found that PCA analysis could be used to extract most of the information about the complex viscosity through the first principal component, thereby making the complex viscosity being able to be modeled as the product of a scores and loading plot.

# AO 4 in PP

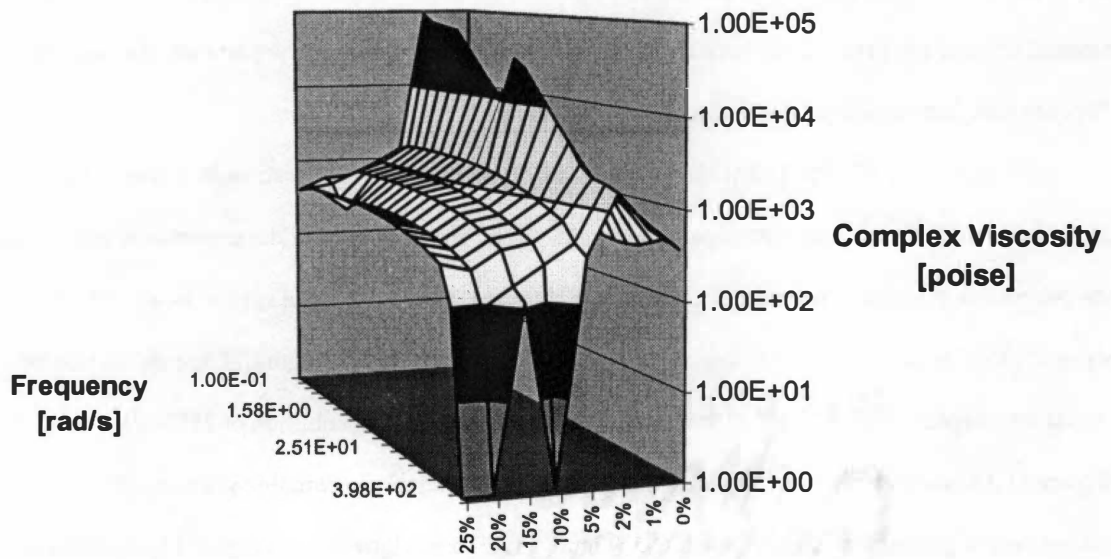


Figure 11.9 Complex viscosity measurements of AO 4 in PP at 230 °C and strain rate of 2500  $\text{dyn}/\text{cm}^2$ .

# AO 5 in PP

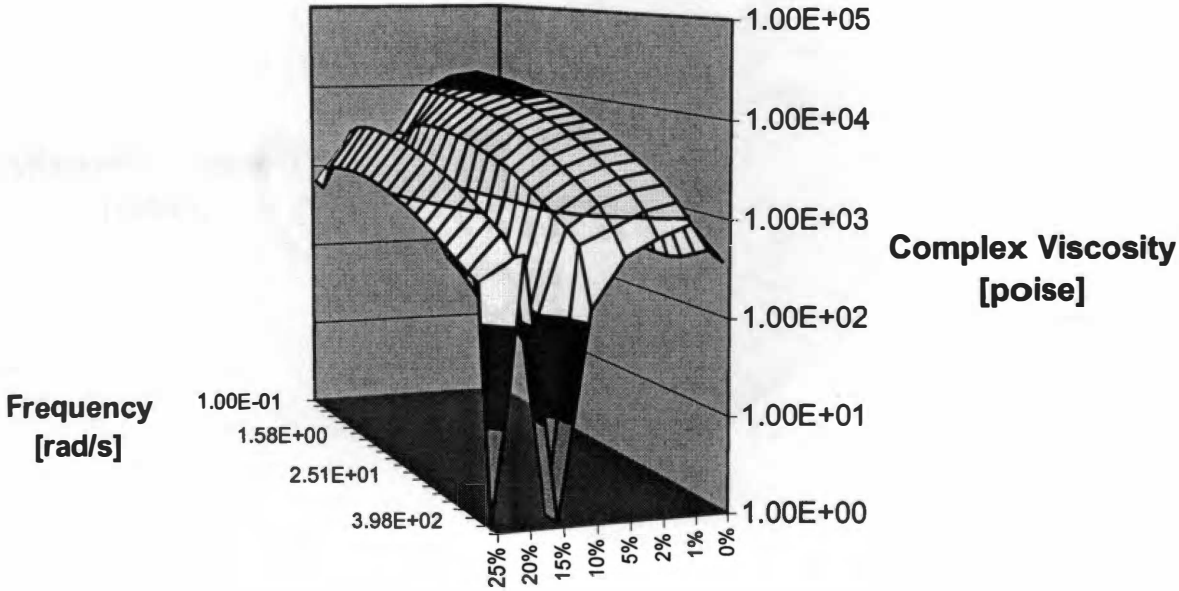


Figure 11.10 Complex viscosity measurements of AO 5 in PP at 230 °C and strain rate of 2500 dyne/cm<sup>2</sup>.

# AO 1 in PP

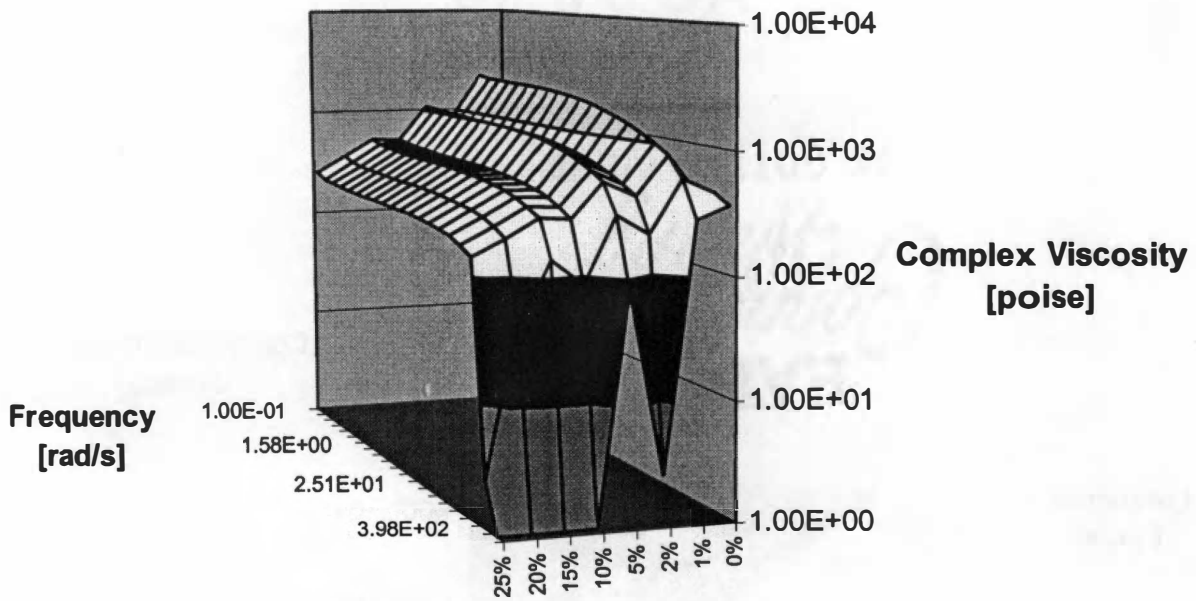


Figure 11.11 Complex viscosity measurements of AO 1 in PP at 230 °C and strain rate of 2500 dyne/cm<sup>2</sup>.

## AO 3 in PP

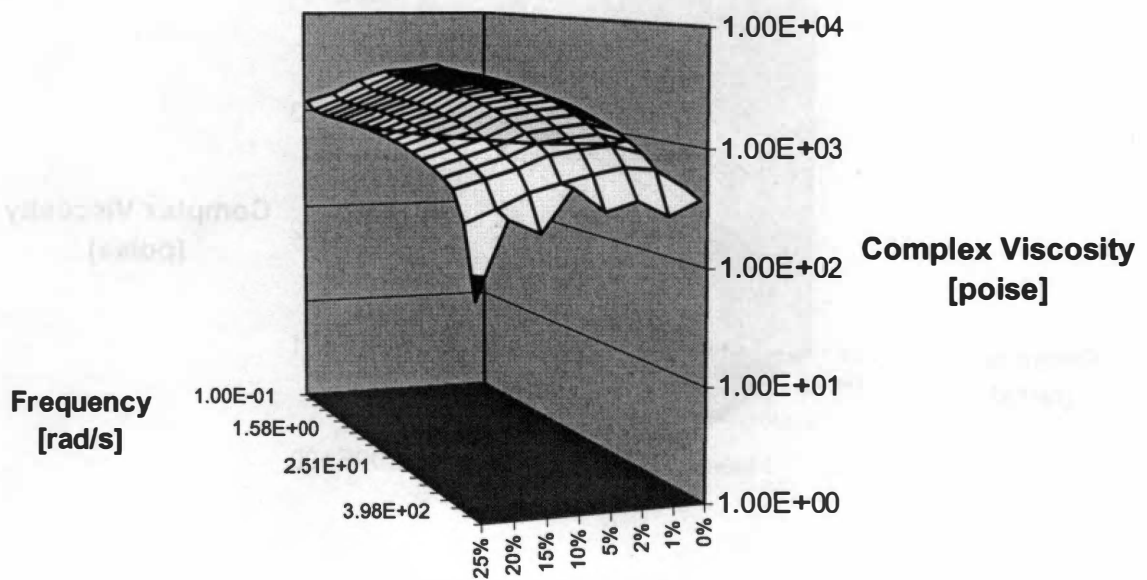


Figure 11.12 Complex viscosity measurements of AO 3 in PP at 230 °C and strain rate of 2500 dyne/cm<sup>2</sup>.

## AO 2 in PP

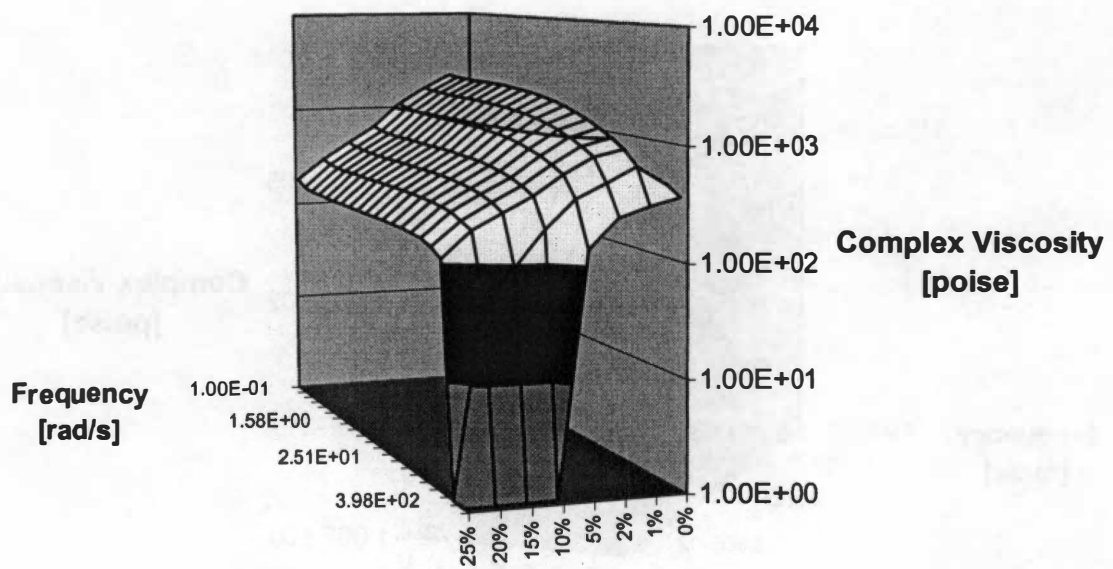


Figure 11.13 Complex viscosity measurements of AO 2 in PP at 230 °C and strain rate of 2500 dyne/cm<sup>2</sup>.

# C-1 in PP

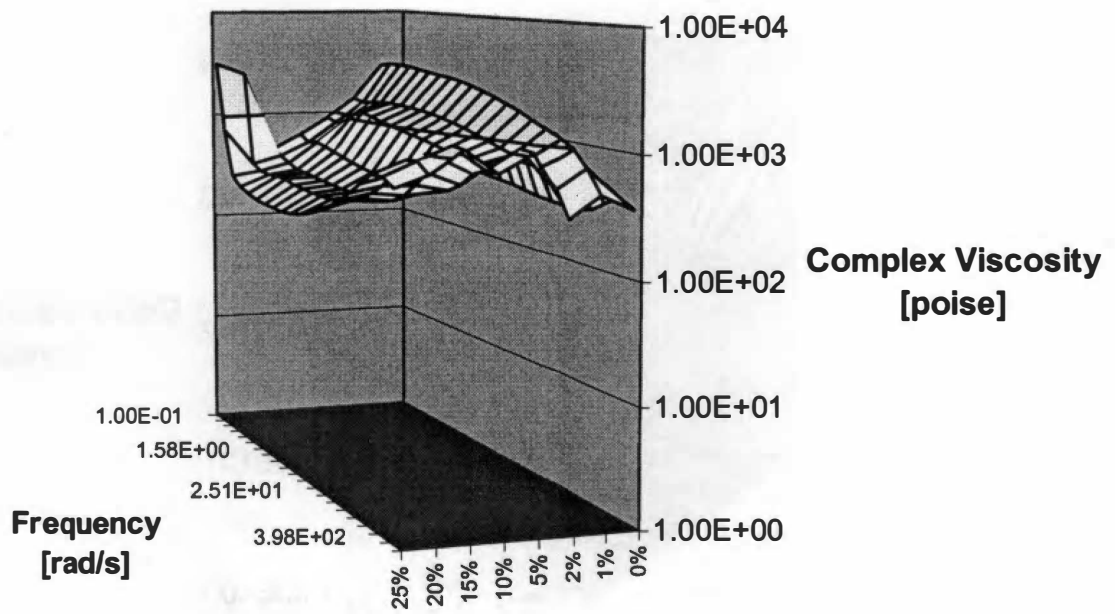


Figure 11.14 Complex viscosity measurements of C-1 in PP at 230 °C and strain rate of 2500 dyne/cm<sup>2</sup>.



# C-5 in PP

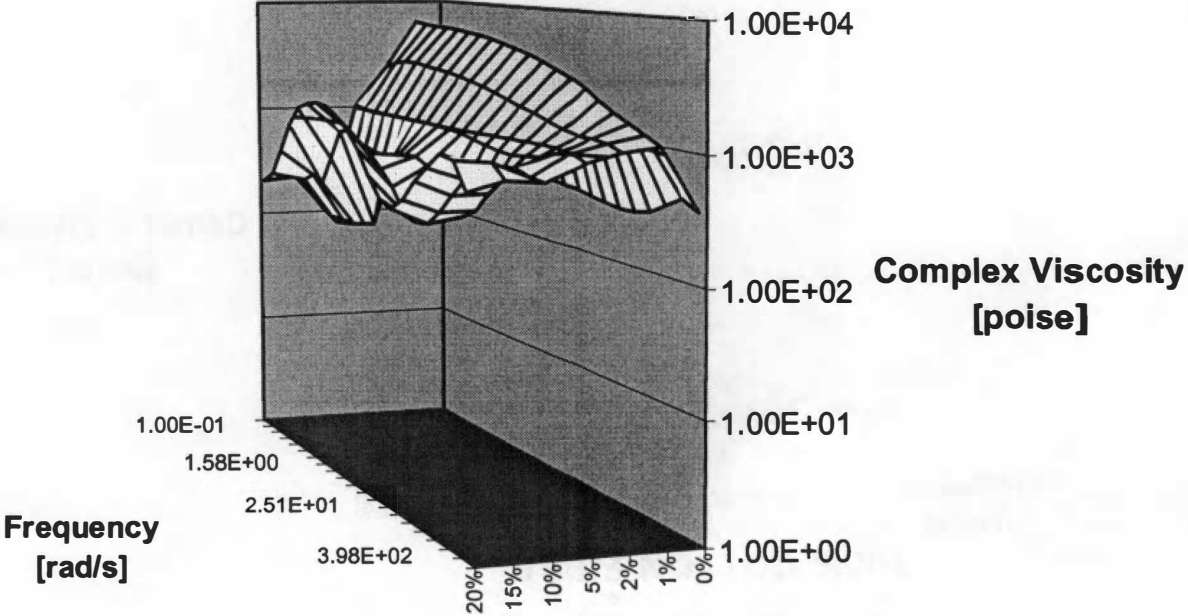


Figure 11.15 Complex viscosity measurements of C-5 in PP at 230 °C and strain rate of 2500 dyne/cm<sup>2</sup>.

## C-2 in PP

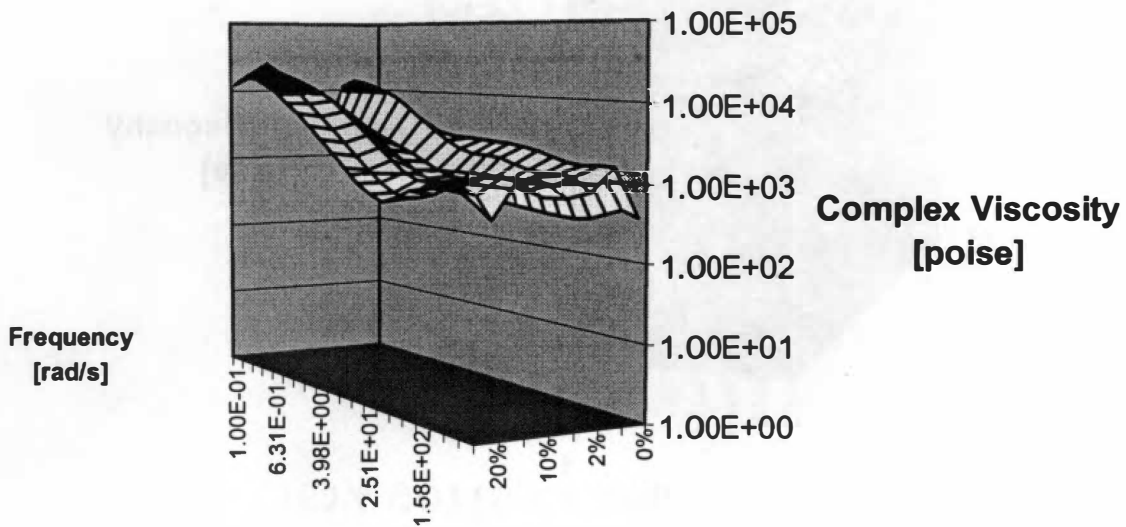


Figure 11.16 Complex viscosity measurements of C-2 in PP at 230 °C and strain rate of 2500 dyne/cm<sup>2</sup>.

# C-3 in PP

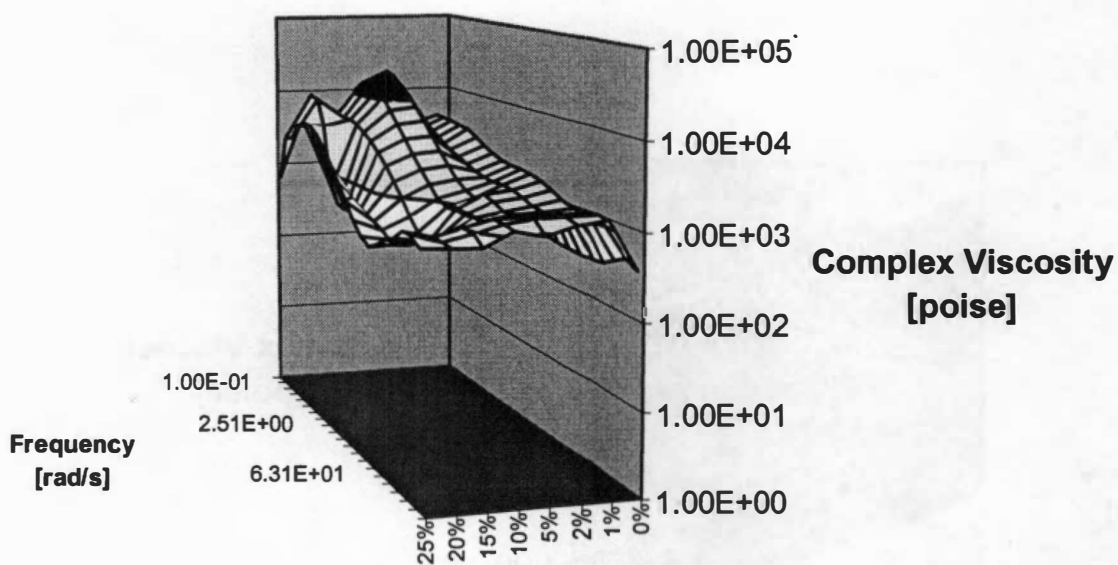


Figure 11.17 Complex viscosity measurements of C-3 in PP at 230 °C and strain rate of 2500 dyne/cm<sup>2</sup>.

# C-4 in PP

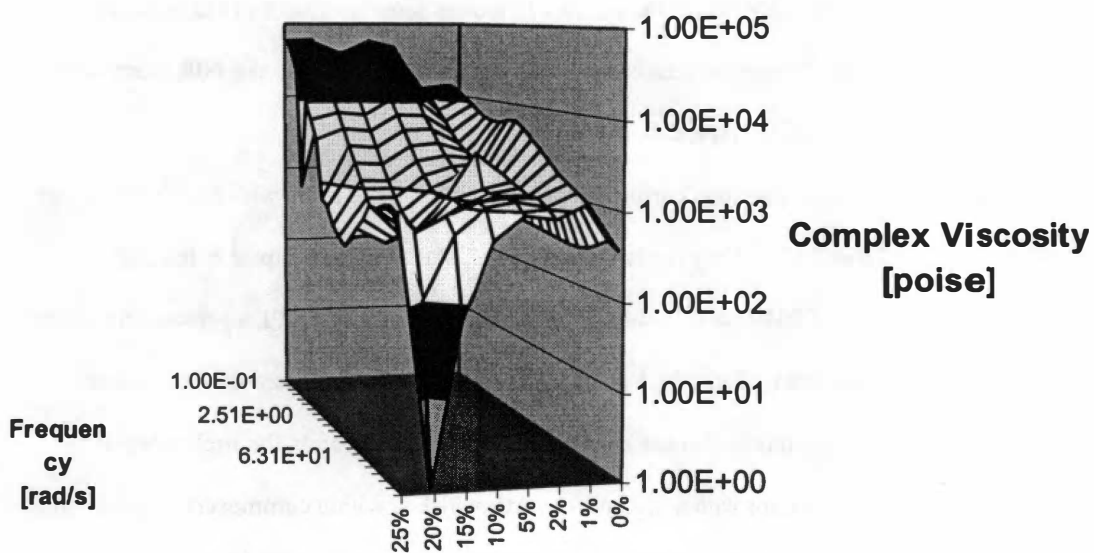


Figure 11.18 Complex viscosity measurements of C-4 in PP at 230 °C and strain rate of 2500 dyne/cm<sup>2</sup>.

For an intensive study of this concept, rheological data was collected for AO-2 for a range of 0.1 to 500 rad/s with 20 equally spaced data points. This complex viscosity data was then regressed using PLS with LAS cross validation against the NIR spectral response in the 2040 to 2200 range that were found to be the best in correlating the concentrations. To show that most of the information is indeed in the first factor of the regression, the scores and loadings plots for the 0.1 rad/s data are shown in Figures 11.19 and 11.20. Table 11.1 presents the variance explained by PLS analysis of the data for each factor. As can be seen, the majority of the information is contained in the first factor. Figure 11.21 presents a plot of SEV versus factor number to further demonstrate this point.

As can be seen from these plots, the first loading vector does approximate the curvature of the complex viscosity. The plot of the SEV versus the number of factors show that most of the information is in the first factor. Knowing this, detailed models can be built for any data set where the NIR spectroscopy delivers meaningful spectra and the rheological properties are known.

More detailed rheological work was performed on the AO-2 sample set in which melt index data was available as shown in Table 11.2. Using the same procedure as outlined in Chapter 8, the first derivative spectra for the range of 2040 nm to 2400 nm were regressed using LAS PLS regression against the experimental values of melt index. Table 11.3 gives all of the necessary information about this model. Following the same analysis of the model that has been conducted in this research, the melt index of the mixture can be modeled with one factor with a SEC of 0.14 MI, which is within commercial control limits. By using this model, the on-line data for the concentration analysis for 8% can be reanalyzed and compared with the measured MI of 13.2. As is seen in Figure 11.22, the data fits well within the control limits.

#### **11.4 EXPERIMENTAL LIMITATIONS**

There are several limitations with this approach of rheological characterization. Complex viscosity measurements are usually not conducted in practical applications due to the level of involvement required in the preparation of the sample and the long experimental time. Melt index measurements are usually the only rheological measurement made and are done less frequently during the production of that particular product. The complex viscosity also varies on the shear applied to the material. Due to the complex flow pattern in the cell, there will be a distribution of shear rates throughout the molten material.

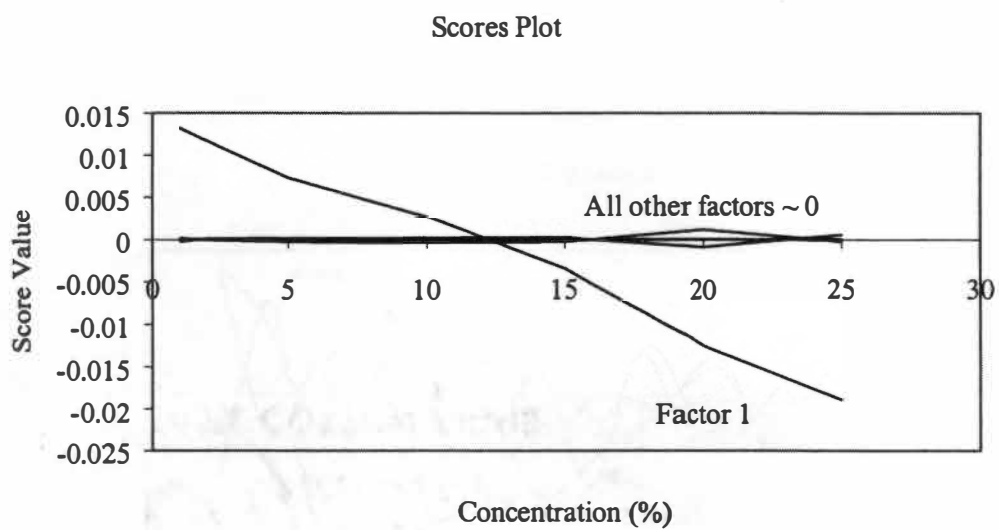


Figure 11.19 Scoresplot for PLS regression of AO-2 complex viscosity at 0.1 rad/s

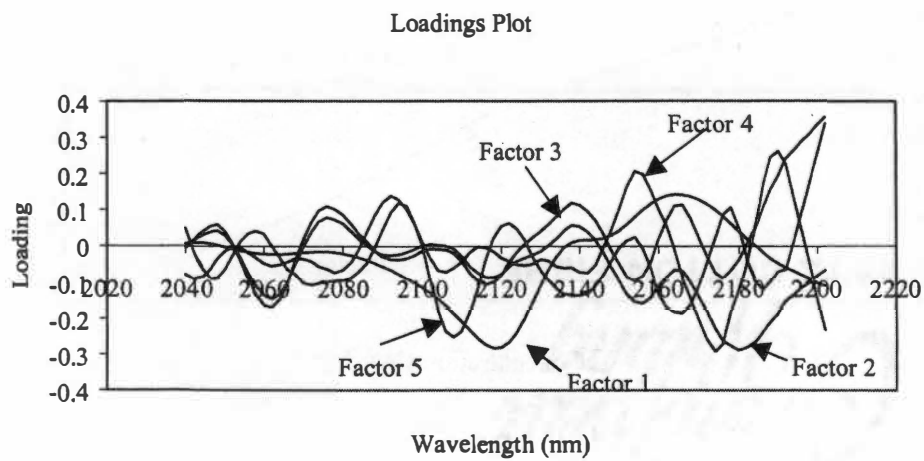


Figure 11.20 Loadings plot for PLS regression of AO-2 complex viscosity at 0.1 rad/s

Table 11.1 Overall variance explained by PLS analysis of complex viscosity matrix

Factor Number	Variance explained by this factor (%)	Overall variance explained (%)
1	99.650	99.650
2	0.199	99.849
3	0.143	99.992
4	0.003	99.996
5	0.002	99.998



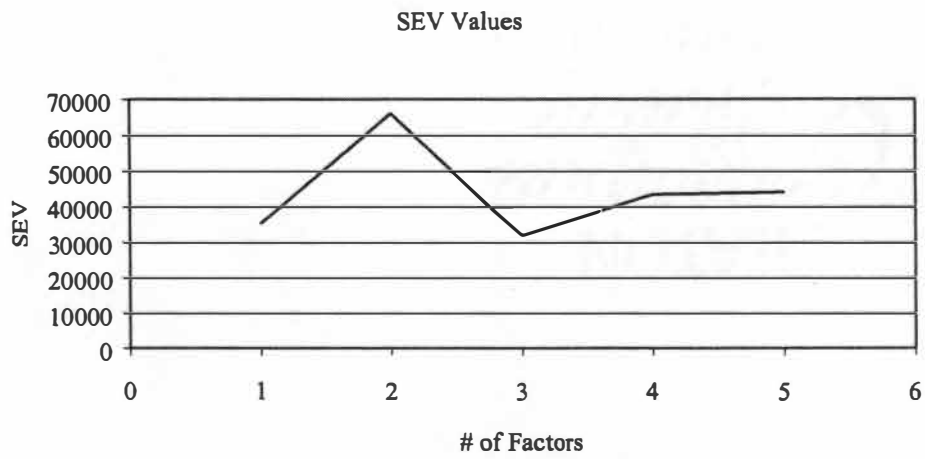


Figure 11.21 SEV values for PLS model

Table 11.2 Melt index values for AO-2 in polypropylene

Concentration (%)	Melt Index
1	11.8
2	12.1
5	12.4
8	13.2
10	13.4
15	14.4
20	15.6
25	16.5

Table 11.3 PLS regression model information for AO-2 melt index

Factor #	Percent	Cumulative	SEV	Press Val	r Val	SEC	Press Cal	r Cal
Factor1	99.6646	99.6646	0.1578	0.1743	0.9956	0.1465	0.1074	0.9973
Factor2	0.0095	99.6741	0.4422	1.3685	0.9822	0.1458	0.0850	0.9979
Factor3	0.3154	99.9895	0.3293	0.7591	0.9899	0.0780	0.0183	0.9995
Factor4	0.0062	99.9957	0.3030	0.6429	0.9901	0.0115	0.0003	1.0000
Factor5	0.0017	99.9973	0.3000	0.6298	0.9904	0.0061	0.0000	1.0000

### Real Time MI Prediction

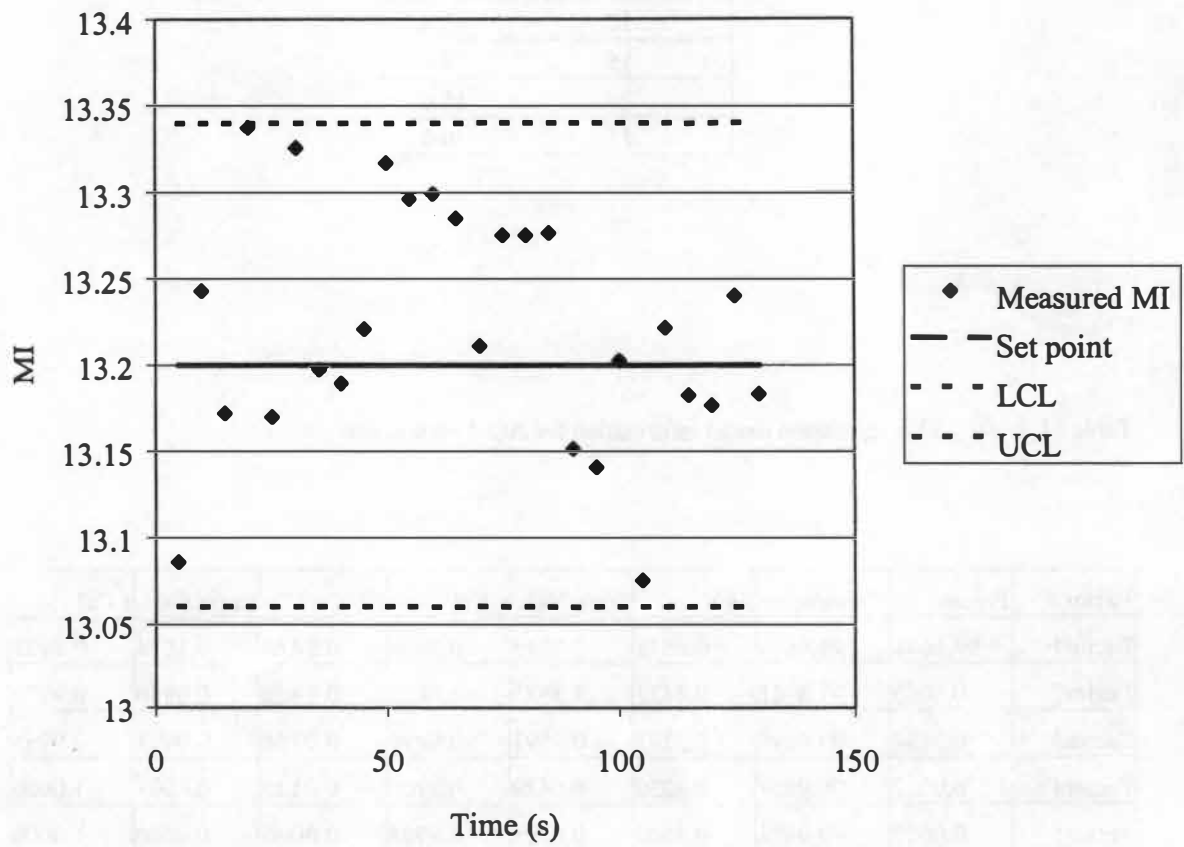


Figure 11.22 Real time prediction of melt index of AO-2 using on-line spectroscopy

For the use of NIR or UV spectroscopy to determine the rheological properties, analysis of the raw rheological data must be made before a proper correlation can be made. The data for AO-2 seems to follow a very predictable path with concentration, but some of the other samples do not due to thermodynamic considerations. Eventually a concentration of additive or pigment will be reached where there will be two separate regions and not a continuum. This is similar to the problems that were observed for the use of on-line spectroscopy for highly loaded systems. The measured rheological properties will not be representative of the two separate phases. This method should only be attempted on ideally behaving materials.

## 11.5 CONCLUSIONS

From the preliminary results, it is evident that there is a difference in the rheological behaviors of the materials due to changes in concentration of the additives and pigments. While these differences are small in magnitude, the application of linear algebra based regression techniques should allow for the development of robust mathematical prediction algorithms. The use of on-line spectroscopic techniques to measure rheological properties will also benefit the instantaneous measurement of dispersion since the quality of the dispersion is based on the actual amount of work done to the material by shear forces.

NIR spectroscopy can be used to correlate the rheological properties of a molten polymer system. PLS calibration models were successfully constructed for a given value of  $\omega$  with the spectral characteristics of the material. These models were found to behave as theorized and studied in prior work. NIR spectroscopy can also be used with multivariate analysis to predict the melt index behavior of AO-2 in polypropylene. The calibration model formed from the concentration spectral data was found to be reliable by using a concentration different from the calibration set.

## CHAPTER 12

### CONCLUSIONS AND FUTURE WORK

As has been demonstrated, the spectroscopic techniques that are currently available have not reached their full application potential for the polymer process industry. The ability to measure additive and pigment loadings in a plant environment are a requirement for the next generation of process control to be developed for the compounding of polymeric systems via extrusion. Typical compounding still relies on the art rather than science side of polymer engineering. By obtaining a more detailed understanding of the fundamental processes, a more complete picture of compounding can be envisioned.

The sheer number of potential applications in an industrial setting for NIR and UV spectroscopic techniques is to the point of being so revolutionary that some industries have hesitations to start implementing the technology. By taking a systematic approach to screening the various techniques, this research has demonstrated that so long as a logical methodology is developed, the appropriate technique for the measurement goal will be located.

Additive and pigment concentrations have been measured utilizing fiber optic NIR and UV spectroscopy. The measurements were carried out in molten polypropylene streams whose composition was similar to products in the market for the production of carpet grade fibers. From mathematical techniques including multivariate analysis, it was demonstrated that real time concentration measurements could be made. The calibration measurements were tested for robustness, and shown to be adequate for on-line monitoring. These measurements can be incorporated into routine quality control reporting techniques without difficulty. Additives and pigments were screened utilizing the two spectroscopic techniques, and suitability and detection limits were determined. Components in the formulation can be measured based on their individual chemistries. Due to the great spectroscopic interaction of common additives, care must be used in the production of calibration data and the resultant optimal prediction model.

By using UV spectroscopy, calibration models were built to determine the concentration levels of two different antioxidants (FS 410FF and Cyanox<sup>®</sup> 1790) and four different ultraviolet stabilizers (Cyasorb<sup>®</sup> 1164, Tinuvin<sup>®</sup> 234 and 783, and Uvinol<sup>®</sup> 5050H). The models built from the spectra could be used for a range of concentrations that have commercial significance.

The use of NIR spectroscopy allowed for the concentration determination limits of the additives studied using UV spectroscopy to be expanded and also include three other antioxidants (Irgafos<sup>®</sup> 168, XP 60 and XP 620) and three different ultraviolet stabilizers (Chimassorb<sup>®</sup> 119 and 944 and Tinuvin<sup>®</sup> 783 FB). These models were demonstrated to be useful to the higher levels of concentration found in the production of commercial master batches. The calibration models and analysis were proved to be robust based on the results from the prediction of independent samples. It was found that the absorption regions that allow for spectroscopic measurement depend on the chemical structure of the additive. Because NIR is dependant on secondary and combination effects, it can be used to measure higher concentrations of additives. In this case, concentrations of 50% by mass were demonstrated to be measured.

Care must be used in the selection of the fiber optic system to be employed. The main issues to be addressed are what measurements will lead to meaningful understanding of the process of interest, and what are the characteristics of the process that can affect its measurement. The first issue is focused on determining if the chemical constituents will have a spectroscopic response given the light source that will excite the molecules, and whether the detector is capable of measuring that response. The second issue is focused on the nature of the measurement material. As was demonstrated in this research, the opacity caused by turbidity can negate the use of a transmission technique. Highly loaded systems can either absorb all of the available light, as was seen in the UV measurements, or can scatter all of the available light, as was seen in the NIR measurements. The main way to eliminate these problems is to reduce the total number of molecules that are being investigated. The most common way to do this is to reduce the path length in the flow cell, effectively reducing the control volume that is being analyzed. For this work, the path length was set at 3 mm, which constituted the minimum that could be used in compounding extruders allowing for no interference of the polymer flow characteristics.

The work utilizing a Killion 1" single screw extruder demonstrated that a practical in plant operation of on-line spectroscopy can be implemented in a harsh manufacturing environment and that realistic measurements can be made with this technology for extrusion operations. This represents the technical use that has been the ultimate goal of the entire research endeavor. This can also be taken as one further step down the manufacturing chain of polymers, in that it is no longer limited to large scale

operations producing a handful of products, rather it can now be used for smaller, more diverse lot monitoring.

The effects of polymer additives and pigments on polymer systems were also studied. Low melt additives were shown to be soluble at low concentrations and then affected the complex viscosity in a linear manner. Non-melting dispersed pigments were also shown to have a slight solubility and then increase the complex viscosity based on Einstein's model. Results demonstrate that it is possible to obtain the melt flow rate of the molten polymer using multivariate analysis of the sample spectra.

From the work done in this study, the use of on-line NIR instrumentation can be practically incorporated to polymer compounding equipment for concentration measurements. The hardware systems used in this study are durable enough for harsh industrial environments typical of this industry. The savings in both time and tightening of quality control limits will prove economically viable to the overall manufacturing cost of the product.

Confocal laser scanning microscopy was investigated and its limitations were discovered as related to determination of pigment dispersion in polymeric materials. These trials demonstrated that there can arise problems with fluorescence of the pigment itself and that the technique should only be used at concentrations lower than 3% pigment by weight. By using this method, it was possible to distinguish between four different types of pigment dispersion techniques on commercially useful pigments for polymer processing. These trials required no sample preparation and could be conducted in a much more time efficient manner than current commercial techniques, greatly reducing the cycle time on quality control measurements. While this is not instantaneous or on-line capable, its use in an industrial setting would be beneficial.

NIR spectroscopy was used to correlate the rheological properties of a molten polymer system. PLS calibration models were successfully constructed for a given value of  $\omega$  with the spectral characteristics of the material. Experimental results demonstrated that it is possible to simultaneously predict the concentration and a rheological property (melt index) of Irgafos<sup>®</sup> 168 in polypropylene. These models were found to behave as theorized and studied in prior work.

There are a number of directions that this work can be further developed and each has its own advantages and disadvantages. The first is the further development of this system of on-line fiber optic probes to measure pigment loadings in color compounding and additive levels in additive compounding. Now that the concentration measurements are known and can be monitored, this information can be used in feed back control with loss in weight feeders. Further development of the process would allow for statistical process control to be done on the various types of compounding processes. It is not a far stretch of the imagination to envision a reflectance probe of either near infrared or ultra violet light determining the proper dispersion of pigment the molten state in real time.

As was discovered from the work done on the highly loaded additive systems, opacity issues that arise from either the scattering properties of the additive, or its natural color greatly affect the upper concentration limit of measurement. By making a reflectance type measurement, the issue of path length is solved in that the instrument will rely on the scattering of light for the optical behavior of the melt. By using a reflectance type spectroscopic system, the actual hardware of the system in the plant environment is also reduced. The number of probes is reduced to one, allowing for the probe to be placed in tighter geometries within the system. This would allow for better placement within either the head of the extruder or the die face. By making the concentration measurements as far downstream as possible, the mixing and dispersion characteristics of the extruder can be studied. The variance of the degree of dispersion is eliminated in this case, as the melt has been cycled through the entire mixing process. This will allow for the establishment of tighter tolerances in statistical quality control and the display of real time information that will allow process changes to be evaluated readily. Overall, the change of spectroscopic response will address the problems associated with turbidity in the melt. For these reasons, the use of on-line fiber optic Raman spectroscopy should be further studied for polymer compounding applications.

Another significant direction that future work can proceed would be the combination of all of the techniques. Now that the majority of technical issues have been solved for the building of these systems, the evolution of the technology would be to construct a system that makes use of the different techniques. What can be envisioned is a multi-probe attachment on either the head of an extruder, or within the die itself. These probes could utilize either transmission or reflectance spectroscopy. Use of the first type



complicates the construction of the flow cell due to spacing limitations, but while these are technically challenging, they can be overcome. The combination of all of these spectroscopic techniques will allow for real time collection of a variety of information that could be useful for process monitoring and process control.

From the development of real time data, robust control models can be developed to greatly reduce the design time of compounded products. This field is currently based on tried and true techniques and the development of such a system will allow for more automation to occur. Research in the field of instrumentation shows a growing trend of chemical companies moving towards full automation of their facilities. To accomplish this goal, the necessary measurement instrumentation can be implemented from this technology. The control techniques have been studied for decades and the basic algorithms such as feedback and cascade methods are well understood.

There is still the opportunity to investigate other uses for the device rather than just pigment and additive loadings and dispersion. Most chemicals have a spectroscopic response in these regions. More and more of the technology used in the production of military satellites is becoming available to the public for commercial uses, including precision optics, CCD cameras, miniature lasers and high speed miniature computer chips. As advances in manufacturing technology have allowed components to become smaller and faster, developing a handheld spectroscopic device becomes increasingly possible. This device has a multitude of uses. Everything from determining chemical composition during a hazardous material spill to medical measurements of chemical concentrations in the blood, to the more mundane task of measuring chlorine concentrations in swimming pools can be made possible. The opportunity to develop such devices should not be overlooked.

As more sophisticated and lower cost optical components become available to the open market from sources in both the technology field as well as research in the area of national defense, more durable and robust systems can be constructed of various components to measure almost anything that has enough light throughput and a spectroscopic response compatible with the measuring device. The cost of these systems will continue to decrease, allowing for the use of these systems to be justified in more lower-

margin chemical and manufacturing processes. The applications of these systems are only limited by the imagination of the spectroscopist.

## REFERENCES

## REFERENCES

1. *Modern Plastics Encyclopedia Handbook* (McGraw-Hill, Inc. New York, 1994).
2. S. Vedula, *In-line Fiberoptic Spectroscopy: Applications to Polymer Process Monitoring*. Ph.D. Dissertation (1997). University of Tennessee, Knoxville.
3. A. S. Bonanno, J. M. Olinger, P. R. Griffiths, *Near Infrared Spectroscopy – Bridging the Gap between Data Analysis and NIR Applications* (Ellis Harwood, New York, 1992).
4. E. W. Ciurczak, *Handbook of Near-Infrared Analysis*, D. A. Burns and E. W. Ciurczak, Eds. (Marcel Dekker, Inc. New York, 1992).
5. W. F. McClure, *Analytical Chemistry* **66**, 43A (1994).
6. J. Lin, C. W. Brown, *Applied Spectroscopy* **47**, 62 (1993).
7. G. Lanchenal, *Vibrational Spectroscopy* **9**, 93 (1995).
8. M. G. Hansen, A. Khettry, *Polymer Engineering and Science* **34**, 1758 (1994).
9. A. Khettry, *In-line Monitoring of Molten Polymeric Processes*. Ph.D. Dissertation (1995). University of Tennessee, Knoxville.
10. H. L. McPeters, S. O. Williams, *Process Control and Quality* **3**, 75 (1992).
11. H. L. McPeters, *Analytica Chimica Acta* **238**, 83 (1990).
12. P. J. Brimmer, S. L. Monfre, F. A. DeThomas, *Making Light Work: Advances in Near-Infrared Spectroscopy*, I. A. Cowe and I. Murray, Eds. (VCH Publishers, New York, 1992).
13. R. P. Buaman, *Absorption Spectroscopy* (John Wiley & Sons, Inc. New York, 1962).
14. J. G. Calvert and J. N. Pitts. *Photochemistry* (Wiley, New York, 1967).
15. Y. B. Shilo and E. T. Denisov. *Vysokomo, Soedi, Ser. A* **16A** (10), 2313 (1974).
16. T. H. Gow, *Guide to Modern Methods of Instrumental Analysis* (Wiley-Interscience, New York, 1972).
17. C. E. Meloan, *Elementary Infrared Spectroscopy* (Macmillian, New York, 1963).
18. L. G. Weyer, *Applied Spectroscopy Reviews* **21**, 1 (1985).
19. P. W. Atkins, *Physical Chemistry*, 4<sup>th</sup> Edition (W. H. Freeman, New York, 1990).
20. I. Murray and P. C. Williams, *Near-Infrared Technology in the Agricultural and Food Industries* (American Association of Cereal Chemists, St. Paul, MN, 1987).
21. J. A. Dean, *Analytic Chemistry Handbook* (McGraw-Hill, New York, 1995).
22. N. B. Colthup, B. L. Daly, and S. E. Wiberly, *Introduction to Infrared and Raman Spectroscopy*, 3<sup>rd</sup> Edition (Academic, New York, 1990).

23. D. A. Skoog, J. J. Leary, *Principles of Instrumental Analysis* (Saunders College Publishing, 1992).
24. D. Lin-Vien, N. B. Colthup, W. G. Fateley, and J. G. Grasselli, *The Handbook of Infrared and Raman Characteristic Frequencies of Organic Molecules* (Academic, New York, 1991).
25. A. Khettry and M. G. Hansen, *Polymer Engineering and Science* **36**, 1232 (1996).
26. R. F. Goddu, *Advances in Analytic Chemistry and Instrumentation* **1**, 347 (1960).
27. C. E. Miller, and B. E. Eichinger, *Applied Spectroscopy* **44**, 887 (1990).
28. C. E. Miller, *Applied Spectroscopy Reviews* **26**, 275 (1991).
29. E. W. Crandall, *Journal of Applied Polymer Science* **19**, 987 (1975).
30. K. A. Bunding Lee, *Applied Spectroscopy Reviews* **28**, 231 (1993).
31. L. E. Skaare, P. Klæboe, C. J. Nielsen, *Vibrational Spectroscopy* **3**, 23 (1992).
32. K. A. Bunding Lee, R. W. Chylla, T. E. Janota, *Applied Spectroscopy* **47**, 94 (1993).
33. W. H. Grieve, D. D. Doepken, *Polymer Engineering and Science* **8**, 19 (1968).
34. T. Takeuchi, S. Tsuge, Y. Sugimura, *Analytical Chemistry* **41**, 184 (1969).
35. E. W. Crandall, A. N. Jagtap, *Journal of Applied Polymer Science* **21**, 449 (1977).
36. G. F. Kirkbright, K. R. Menon, *Analytica Chimica Acta* **136**, 373 (1982).
37. R. D. Driver, K. P. Gim, *Proceedings of SPIE, The International Society for Optical Engineering* **1243** (1998).
38. H. W. Siesler, *Makromol. Chem. Macromol. Symp.* **52**, 113 (1991).
39. R. Spatafore, L. McDermont, *PITCON Proceedings* **627**(1992).
40. J. Batra, *Polymer Engineering and Science* **34** (1994).
41. R. Schirmer, *Advances in Instrumentation* **41**, 1229 (1986).
42. S. Farquharson, P. B. Arnoudse, M. H. Wyckoff, P. T. Keillor III, *SPIE-Chemical, Biochemical, and Environmental Sensors* **1172**, 164 (1989).
43. M. Huehne, *SPIE-International Conference on Fourier Transform Spectroscopy* **1575**, 214 (1991).
44. N. Eisenreich, *ANTEC Proceedings* **3131** (1996).
45. E. E. Griesser, A. Sahagen, *SPE International Conference on Polyolefins, Houston, TX Proceedings*, (1995).
46. J. Li, *In-line Monitoring of Polymer Processing Using Fiber-optic Spectroscopy*. Ph.D. Dissertation (1999). University of Tennessee, Knoxville.

47. C. E. Miller, *Applications of NIR Spectroscopy to Polymers*. Ph.D. Dissertation (1989). University of Washington, Seattle.
48. D. Fisher, *Fresenius Journal of Analytical Chemistry* **359**, 74 (1997).
49. R. Reshadat, *SPE ANTEC Proceedings* 2057 (1995).
50. R. P. Hammond, *Measurement and Control* **28** (10), 232 (1995).
51. C. E. Miller, B. E. Eichinger, T. W. Gurley, J. G. Hermiller, *Analytical Chemistry* **62**, 1778 (1990).
52. C. E. Miller, T. Naes, *Applied Spectroscopy* **44**, 895 (1990).
53. E. Bouveresse, D. L. Massart, *Vibrational Spectroscopy* **11**, 3 (1996).
54. R. E. Dodd, *Chemical Spectroscopy* (Elsevier, New York, 1962).
55. G. W. King, *Spectroscopy and Molecular Structure* (Holt, Rinehart and Winston, New York, 1964).
56. E. I. Stearns, *Practice of Absorption Spectrometry* (Wiley, New York, 1969).
57. C. N. Banwell, *Fundamentals of Molecular Spectroscopy* (McGraw-Hill, New York, 1966).
58. R. P. Bauman, *Absorption Spectroscopy* (Wiley, New York, 1962).
59. H. H. Jaffe, M. Orchin, *Theory and Applications of Ultraviolet Spectroscopy* (Wiley, New York, 1962).
60. J. N. Murrell, *The Theory of the Electronic Spectra of Organic Molecules* (Methuen, London, 1963).
61. C. B. Johnson, *Proceedings of SPIE, The International Society for Optical Engineering* 1243 (1998).
62. A. H. Keough, *Tech. Pap. Soc. Mfg. Eng.* FC85-427, 18 (1985).
63. H. J. Paik, N. Sung, *Polymer Engineering Science* **34**, 1025 (1994).
64. W. Wang, N. Sung, *Polymer Engineering Science* **34**, 107 (1994).
65. B. J. Hunt, M. I. James, *Polymer Characterization* (Blackie Academic, London, 1993).
66. F. Scholl, *Atlas of Polymer and Plastic Analysis*, Vol. 3 (Hanser, Munich, 1981).
67. S. R. Epton, *Transactions of the Faraday Society* **44**, 226 (1948).
68. W. Freitag, O. John, *Angewandte Makromolekulare Chemie* **175**, 181 (1990).
69. R. Spatagore, *Proceedings of the 48<sup>th</sup> SPE-ANTEC* 23 (1998).
70. J. Yang, *Proceedings on the International Conference on Petroleum Refining and Petrochemical Processing* (1991).

71. R. E. Schirmer, A. G. Gargus, *American Laboratory* **11**, 123 (1986).
72. R. E. Schirmer, A. G. Gargus, *American Laboratory* **18** (12), 30 (1988).
73. R. E. Schirmer, *ISA Transactions* **28** (2), 65 (1989).
74. T. R. Crompton, *Chemical Analysis of Additives in Plastics* (Pergamon Press, Oxford, 1971).
75. J. Haslam, H. A. Willis, D. C. Squirrel, *Identification and Analysis of Plastics*, 2<sup>nd</sup> Ed. (Iliffe Books, London, 1984).
76. K. S. Anseth, T. A. Walker, C. N. Bowman in *Multidimensional Spectroscopy of Polymers, Vibrational, NMR, and Fluorescence Techniques*, M. W. Urban, T. Provder Eds. (ACS, Washington D.C., 1995).
77. K. S. Anseth, M. D. Rothenberg, C. N. Bowman, *Macromolecules* **27**, 2890 (1994).
78. M. W. Urban, T. Provder, *Multidimensional Spectroscopy of Polymers, Vibrational, NMR, and Fluorescence Techniques* (ACS, Washington D.C., 1995).
79. D. J. Gardiner, P. R. Graves, *Practical Raman Spectroscopy*, (Springer-Verlag, Berlin, 1989).
80. C. V. Raman, *Nature* **121**, 501 (1928).
81. C. V. Raman, *Nature* **121**, 711 (1928).
82. A. Smekal, *Naturwiss* **11**, 873 (1923).
83. B. Schrader, *Infrared and Raman Spectroscopy, Methods and Applications* (VCH Publishers, Weinheim, 1995).
84. G. Placzek, E. Teller, *Z Phys* **81**, 209 (1933).
85. H. A. Szymanski, *Raman Spectroscopy, Theory and Practice* (Plenum Press, New York, 1967).
86. N. B. Colthup, L. H. Daly, S. E. Wiberley, *Introduction to Infrared and Raman Spectroscopy* (Academic Press, New York, 1964).
87. G. D. Ogilvie, L. Addyman, *L'Actualite Chimique*, Avril, 51 (1980).
88. J. D. Loudon, in *Multidimensional Spectroscopy of Polymers, Vibrational, NMR, and Fluorescence Techniques*, M. W. Urban, T. Provder Eds. (ACS, Washington D.C., 1995).
89. J. M. Chalmers, L. Croot, J. G. Eaves, N. Everall, W. F. Gaskin, J. Lumsdon, N. Moore, *Spectrosc. Int. J.* **8**, 1 (1990).
90. J. M. Pastor, *Makromol. Chem. Macromol. Symp.* **52**, 57 (1991).
91. N. Everall, *Spectroscopy World* **3**(4), 29 (1991).
92. T. Jawhari, J. M. Pastor, *Journal of Molecular Structure* **266**, 205 (1992).
93. B. Chu, G. Fytas, G. Zalczer, *Macromolecules* **14**, 395 (1981).

94. B. Chu, D. C. Lee, *Macromolecules* **17**, 926 (1984).
95. E. Gulari, K. McKeigue, K. S. Ng, *Macromolecules* **17**, 1822 (1984).
96. L. Feng, K. S. Ng, *Macromolecules* **23**, 1048 (1990).
97. D. C. Lee, J. R. Ford, G. Fytas, B. Chu, G. L. Hagnauer, *Macromolecules* **19**, 1586 (1986).
98. B. Chu, D. C. Lee, *Macromolecules* **19**, 1592 (1986).
99. J. Khorami, A. Lemieux, H. Menard, D. Nadeau, *ASTM Spec. Tech. Publ. STP 997*, 147 (1988).
100. A. Baruya, D. L. Gerrard, F. W. Maddams, *Macromolecules* **16**, 578 (1983).
101. H. A. Willis, J. H. van der Maas, R. G. Miller, *Laboratory Methods in Vibrational Spectroscopy*, 3<sup>rd</sup> Ed. (Wiley, Chichester, 1987).
102. H. J. Bowley, D. L. Gerrard, I. S. Biggin, *Polymer Degradation Stability* **20**, 257 (1988).
103. M. M. Coleman, G. T. Sivy, *Carbon* **19**, 123 (1981).
104. G. T. Sivy, M. M. Coleman, *Carbon* **19**, 127 (1981).
105. M. M. Coleman, G. T. Sivy, *Carbon* **19**, 133 (1981).
106. G. T. Sivy, M. M. Coleman, *Carbon* **19**, 137 (1981).
107. S. W. Cornell, J. L. Koenig, *Macromolecules* **2**, 546 (1969).
108. M. E. Robison, D. I. Bower, W. F. Maddams, *Polymer* **19**, 773 (1978).
109. M. C. Painter, M. M. Coleman, J. L. Koenig, *The Theory of Vibrational Spectroscopy and its Applications to Polymeric Materials*, 3<sup>rd</sup> Ed. (Wiley, New York, 1982).
110. M. Clark, *Proceedings of the 1997 55<sup>th</sup> Annual Technical Conference, Part 2* (SPE, New York, 1997).
111. K. J. Williams, N. J. Everall, *Journal of Raman Spectroscopy* **26**, 427 (1995).
112. L. A. Archer, *Journal of Rheology* **38** (4), 1101 (1994).
113. L. A. Archer, G. C. Fuller, *Macromolecules* **27**, 4359 (1994).
114. L. A. Hanna, *European Polymer Journal* **26**, 667 (1990).
115. T. Milio, F. Nobuhio, *Polymer* **22** (5), 317 (1985).
116. C. K. Chai, N. M. Dixon, *Polymer* **36** (3), 661 (1995).
117. R. J. Samuels, *Structured Polymer Properties* (Wiley, New York, 1974).
118. G. Wilkes, *Advanced Polymer Science* **8**, 91 (1971).



119. J. R. Scherer in *Analytical Raman Spectroscopy*, J. G. Grasselli, B. J. Bulkin (eds.) (Wiley, New York, 1987).
120. G. R. Strobl, W. Hagerdorn, *Journal of Polymer Science, Polymer Physics* **16**, 1181 (1978).
121. E. Foldes, G. Keresztury, M. Iring, F. Tudos, *Angew. Makromol. Chemie.* **187**, 87 (1985).
122. R. G. Alamo, *Macromolecules* **25**, 6381 (1992).
123. K. Itoh, M. Oya, *Polymer Journal* **8**, 837 (1986).
124. L. Mandelker, R. G. Almo, J. A. Haigh, *Polymer Preprints, American Chemical Society* **37** (2), 237 (1996).
125. F. N. Del, G. Zerbi, S. Radice, *Polymer* **38**, 2753 (1997).
126. H. Maeda, K. Matsukama, H. Inoue, M. Shirmoyama, *Vibrational Spectroscopy* **14**, 253 (1997).
127. J. L. Stanford, Y. F. Wang, R. J. Young, P. A. Lovell, *Macromolecules* **31**, 834 (1998).
128. J. L. Stanford, Y. F. Wang, R. J. Young, P. A. Lovell, *Macromolecules* **31**, 842 (1998).
129. D. I. Bower, *Journal of Polymer Science, Polymer Physics* **10**, 2135 (1972).
130. D. A. Jarvis, I. J. Hutchinson, D. I. Bower, I. M. Ward, *Polymer* **21**, 41 (1980).
131. J. M. Chalmers, L. Croot, J. G. Eaves, N. Everall, W. F. Gaskin, J. Lumsdon, N. Moore, *Spectrosc. Int. J.* **8**, 13 (1990).
132. P. A. Lewis, *Pigment Handbook, Volume 1*, 2<sup>nd</sup> Ed. (Wiley, New York, 1988).
133. W. Herbst, K. Hunger, *Industrial Organic Pigments, Production, Properties, Applications* (VCH, New York, 1993).
134. F. W. Billmeyer, M. Saltzman, *Principles of Color Technology*, 2<sup>nd</sup> Ed. (Wiley, New York, 1981).
135. R. S. Hunter, *The Measurement of Appearance* (Wiley, New York, 1975).
136. International Commission on Illumination, *Colorimetry: Official Recommendations of the International Commission on Illumination* (CIE, Paris, 1971).
137. H. Grassman, *Ann. Phys. Chem.* **89**, 69 (1853).
138. D. B. Judd, G. Wyszecki, *Color in Business, Science and Industry*, 3<sup>rd</sup> Ed. (Wiley, New York, 1975).
139. W. Ostwald, *Colour Science* (Winsor and Newton, London, 1931).
140. A. R. Robinson, *Color Resolution Applications* **2**, 7 (1977).
141. Society of Dyers and Colorists, *Colour Index*, 3<sup>rd</sup> Ed. (Society of Dyers and Colorists, Yorkshire, 1971).

142. International Commission on Illumination, *Recommendations on Uniform Color Spaces, Color Difference Equations, Psychometric Color Terms* (CIE, Paris, 1978).
143. H. Martens, T. Naes, *Multivariate Calibration* (Wiley, New York, 1989).
144. S. de Jong, *Chemometrics and Intelligent Laboratory Systems* **18**, 251 (1993).
145. S. D. Brown, *Applied Spectroscopy* **49**, 14A (1995).
146. A. Hoskuldsson, *Journal of Chemometrics* **2**, 211 (1988).
147. P. Geladi, B. R. Kowalski, *Analytica Chimica Acta* **185**, 1 (1986).
148. I. S. Helland, *Communications in Statistics-Simulation and Computation* **17**, 581 (1988).
149. K. R. Beebe, B. R. Kowalski, *Analytical Chemistry* **59**, 1007A (1987).
150. A. Hoskuldsson, *Journal of Chemometrics* **9**, 91 (1995).
151. S. Wold, K. Ebersen, P. Geladi, *Chemometrics and Intelligent Laboratory Systems* **2**, 37 (1987).
152. E. V. Thomas, *Analytical Chemistry* **66**, 795A (1994).
153. B. Everett, *Cluster Analysis* (Wiley, New York, 1974).
154. M. Meloun, J. Militky, M. Forina, *Chemometrics for Analytical Chemistry* (Ellis Horwood, New York, 1992).
155. K.R. Beebe, R. J. Pell, M. B. Seasholtz, *Chemometrics, a Practical Guide* (Wiley, New York, 1998).
156. B. R. Kowalski, C. F. Bender, *Journal of the American Chemical Society* **94**, 5632 (1972).
157. B. R. Kowalski, T. F. Schatzki, F. H. Stross, *Analytical Chemistry* **44**, 2176 (1972).
158. G. Strang, *Linear Algebra and its Applications* (Harcourt Brace Jovanovich, San Diego, 1988).
159. T. W. Wang, A. Khettry, M. Berry, J. Batra, *First International Chemometrics Internet Conference, INCINC'94* (1994).
160. D. M. Haaland, E. V. Thomas, *Analytical Chemistry* **60**, 1193 (1988).
161. D. M. Haaland, E. V. Thomas, *Analytical Chemistry* **60**, 1202 (1988).
162. J. M. Sutter, J. H. Kalivas, *Journal of Chemometrics* **6**, 217 (1992).
163. D. M. Haaland, *SPIE – 8<sup>th</sup> International Conference on Fourier Transform Spectroscopy* **1575**, 87 (1991).
164. T. Isaksson, T. Naes, *Applied Spectroscopy* **44**, 1152 (1990).
165. P. C. Painter, M. M. Coleman, *Fundamentals of Polymer Science* (Technomic Publishing, Lancaster, 1997).

166. C. W. Macosko, *Rheology – Principles, Measurements, and Applications* (VCH Publishers, Inc. New York, 1994).
167. H. A. Barnes, J. F. Hutton, K. Walters, *An Introduction to Rheology* (Elsevier, New York, 1989).
168. Lodge, A. S. *Elastic Liquids* (Academic Press, London, 1964).
169. Warriar, V. B., Todd, D. B., *SPE ANTEC*, 1047 (2000).
170. Einstein, A., *Ann. Phys.*, **19**, 298 (1906).
171. Einstein, A., *Ann. Phys*, **34**, 591 (1911).
172. Chapman, F. M., Lee, T. S., *SPE ANTEC*, 293 (1970).
173. Suh, C. H., White, J. L., *J. Non-Newtonian Fluid Mech.*, **62**, 175 (1996).
174. Payne, A. R., Whittaker, R. E., *J. Appl. Ploy. Sci.*, **16**, 1191 (1972).
175. Vinogradov, G. V., Malkin, A. Y., Plotnikova, O. Y., Nikolayeva, N. E., *Int. J. Poly. Mat.* **2**, 1 (1972).
176. Kosniski, L. E., Caruthers, J. M., *Rheol. Acta.*, **25**, 153 (1986).
177. Kosniski, L. E., Caruthers, J. M., *J. Non-Newtonian Fluid Mech.*, **17**, 69 (1985)
178. Aranguren, M. I., Mora, E., DeGroot, J. V., Macosko, C. W., *J. Rheol.*, **36**, 1165 (1992).
179. Havet, G., Isayev, A. I., *SPE-ANTEC*, 1037 (2000).

## VITA

Erik C. Nielsen was born in Montreal, Quebec, Canada on January 13, 1974. In May 1992, he graduated from Farragut High School in Knoxville, Tennessee with Honors. He entered study at Auburn University in September of 1992 and graduated in August 1995 with a Bachelor of Chemical Engineering (Energy and Fuels) Degree. He entered graduate school at Auburn in September 1995 and received the Master of Science in Mechanical Engineering in December 1996 with his thesis entitled "Selection of Alternative Refrigerants for Industrial and Commercial Applications". He enrolled in the Ph.D. program in the Department of Chemical Engineering at the University of Tennessee, Knoxville in July 1996. During his studies at the University of Tennessee, he was inducted to the Phi Kappa Phi Honor Society. In May 1998, he joined Techmer PM in Clinton, TN as a process engineer in the manufacturing division. He also served as a product design engineer and R&D group leader for the Eastern Division. Mr. Nielsen left Techmer PM in June of 2001 and joined Engelhard Corporation's Environmental Technology Division as a process development engineer in January 2002. He received his Ph.D. in Chemical Engineering with a minor in Management in May 2003.